INTERNATIONAL RESEARCH AND REVIEWS IN ENGINEERING

VOLUME - 2

EDITOR

ASSOC. PROF. DR. SELAHATTİN BARDAK

SERÜVEN
YAYINEVİ

Genel Yayın Yönetmeni / Editor in Chief • C. Cansın Selin Temana

Kapak & İç Tasarım / Cover & Interior Design • Serüven Yayınevi

Birinci Basım / First Edition • © Aralık 2023

ISBN • 978-625-6644-07-6

Serüven Yayınevi / Serüven Publishing
Türkiye Adres / Turkey Address: Kızılay Mah. Fevzi Çakmak 1. Sokak
Ümit Apt No: 22/A Çankaya/ANKARA
Telefon / Phone: 05437675765
web: www.seruvenyayinevi.com
e-mail: seruvenyayinevi@gmail.com

Baskı & Cilt / Printing & Volume
Sertifika / Certificate No: 47083

INTERNATIONAL RESEARCH AND REVIEWS IN ENGINEERING

VOLUME 2

December 2023

Editor
Assoc. Prof. Dr. SELAHATTİN BARDAK

CONTENTS

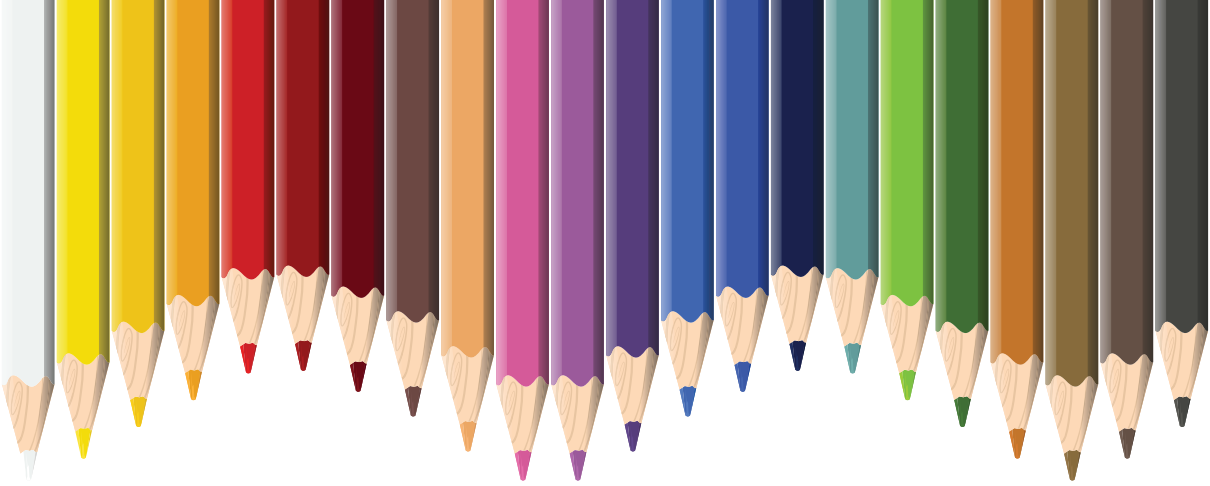

Chapter 1

PROCEDURES APPLIED IN THE REHABILITATION OF OPEN SOLID WASTE DUMPING AREAS IN TURKEY

Mirac Nur CINER[1]

1 Arş. Gör. Istanbul University-Cerrahpasa, Engineering Faculty, Department of Environmental Engineering, Avcilar, Istanbul-Turkey; mirac.ciner@iuc.edu.tr ORCID: 0000-0002-9920-928X

Introduction

In today's world, the increasing population and demands of modern living result in a significant amount of municipal solid waste (MSW) generation. If generated solid wastes are not disposed of in a manner consistent with engineering designs, they pose a significant risk to the environment and human health. Within the framework of the global sustainable development approach, strategies that transform waste from being a threat to the environment and human health into an input for the economy should be adopted (Saltabaş et al., 2009). The implementation of these strategies is only possible through the application of the waste management hierarchy. According to the waste management hierarchy, the first step is to prevent waste generation at the source. For wastes that cannot be prevented, the method should focus on reducing the amount of waste at the source (Öktem, 2016). These two management approaches should be the priority in the integrated management of wastes, both globally and in our country. The next management approach is the 3R method, which stands for reuse, recycle, and recover/energy recovery. After these steps, the final option is the disposal of solid wastes. Generated waste is rendered harmless to the environment and public health through various disposal methods, which are categorized into three main groups: sanitary landfilling, biological, and thermal processes (Arıkan et al., 2017). In less developed and developing countries, solid wastes are often haphazardly disposed of in open solid waste dumping areas, such as riverbanks, road edges, abandoned mines, riverbanks, and coastlines, away from residential areas (Ertürk and Görgün, 2011). In Turkey, this method has been historically used for many years for the disposal of solid wastes.

According to the 2020 MSW statistics of the Turkish Statistical Institute (TURKSTAT), among the 1389 municipalities in Turkey, 1387 municipalities providing waste services were determined to have collected 32.3 million tons of waste. Of the generated 32.3 million tons of waste, 69.4% is sent to sanitary landfill facilities. When looking at past years' waste statistics, an increase in the amount of waste going to sanitary landfilling is observed (TURKSTAT, 2020).

Additionally, according to the 2020 data, the per capita daily average waste collected in Turkey is 1.16 kg. Personal preferences, influenced by factors such as income level, sociocultural structure, population growth, and geographical location, contribute to the variation in the amount of generated waste (Mahees et al., 2011; Akintayo et al., 2023). In the three major cities of Turkey, the per capita daily average waste generation is determined to be 1.233 kg for Istanbul, 1.031 kg for Ankara, and 1.458 kg for Izmir (TURKSTAT, 2020). According to this statistic, only Izmir is among the top 20 cities with the highest waste production per capita among major cities (Table 1).

Table 1. The ranking of the top 20 cities with the highest per capita average waste generation

(TURKSTAT, 2020)

Number	Province	Collected Waste Quantity (tons)	Average Amount of Waste per Person (2020) (Kg/ Person-day)	Number	Province	Collected Waste Quantity (tons)	Average Amount of Waste per Person (2020) (Kg/ Person-day)
1	Bartın	77522.6	2.056	**11**	Yalova	133298.6	1.48
2	Kilis	79403	1.985	**12**	İzmir	2336954	1.458
3	Kars	99666	1.887	**13**	Antalya	1318612	1.429
4	Muğla	676811.4043	1.86	**14**	Çankırı	71344.41	1.404
5	Çanakkale	256572.837	1.849	**15**	Sinop	67009.05	1.373
6	Ardahan	26596	1.782	**16**	Karabük	94476.36	1.354
7	Burdur	122906.35	1.747	**17**	Edirne	155208.8	1.332
8	Ağrı	176084	1.514	**18**	Uşak	138188.2	1.307
9	Artvin	58062.09	1.489	**19**	Bolu	111319	1.302
10	Şırnak	211676	1.486	**20**	Van	542750.8	1.301

The Current Situation in Municipal Solid Waste Disposal

As of the year 2020, 69.41% of the collected 32.3 million tons of waste is directed to sanitary landfill facilities. However, a significant percentage, around 17%, is disposed of in municipal dumpsites. Despite the increasing awareness of waste recycling and reuse globally with the concept of 'cradle-to-cradle,' open dumping is still employed in the disposal of generated solid waste.

Figure 1 illustrates the distribution of waste quantities according to waste disposal methods in Turkey between the years 2012 and 2020. These methods include disposal in MSW landfills, sending to recycling facilities, and other disposal methods (open burning, burying, dumping into rivers and land). In 2012, 37.81% of the generated waste was dumped into MSW landfills, while this ratio decreased to 17% in the year 2020. Meanwhile, the quantity of waste sent to sanitary landfills and recycling facilities has increased from 2012 to 2018. However, in our country, especially in small settlements that are still inaccessible to municipalities, methods such as burning waste, dumping into rivers, streams, and land, and sending it to municipal landfills continued in 2020.

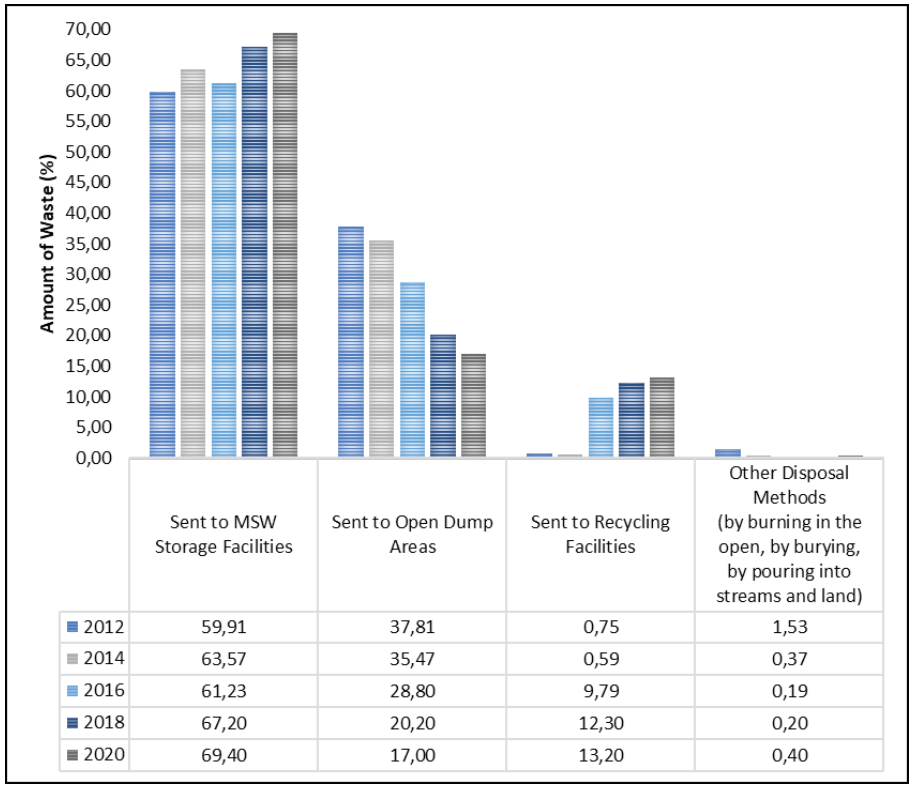

	Sent to MSW Storage Facilities	Sent to Open Dump Areas	Sent to Recycling Facilities	Other Disposal Methods (by burning in the open, by burying, by pouring into streams and land)
2012	59,91	37,81	0,75	1,53
2014	63,57	35,47	0,59	0,37
2016	61,23	28,80	9,79	0,19
2018	67,20	20,20	12,30	0,20
2020	69,40	17,00	13,20	0,40

Figure 1. MSW quantity and disposal methods collected annually over the years (TURKSTAT, 2020)

The Environmental Impacts of Open Dumping Areas

Open dumping is not a ultimate disposal method and brings along many environmental problems. Foremost among these are the inability to control leachate, the release of accumulated landfill gas into the atmosphere, the growth of pests threatening human health, and odor problems.

The leachate from solid waste, not subject to any containment system in open dump areas, contaminates both underground and surface waters. Leachate contains high concentrations of inorganic and organic pollutants and adversely affects the quality of the water sources it travels through (Bayhan & Özbek, 2015). Rainwater that falls onto irregular disposal sites, along with the inorganic and organic substances present in solid waste, dissolves through various reactions and permeates into leachate. The content of leachate is subject to various factors, including the proximity of solid waste to the surface, the content of solid waste, environmental interactions of leachate, landfill age, pH, climatic conditions, and waste age (Kadılar, 2021). The age of the landfill,

a parameter closely influencing leachate composition, results in a high proportion of biodegradable volatile fatty acids in leachates from young landfill areas. As landfill age increases, biological decomposition is completed, and the quantity of easily decomposable organic matter in leachate gradually decreases. In 2-3 year-old landfill areas, organic matter, microorganism types, and inorganic pollution loads reach their maximum (URL 1). These pollutants, at high concentrations, mix with surface and groundwater through various transport mechanisms, contaminating clean water sources and increasing treatment costs. The transport of these pollutants depends on climate, meteorological conditions, geographical and geological factors, and reaches recipient environments through transformation reactions and complex transport (Haksevenler Gürsoy & Ayaz 2021). Particularly, the population living in settlements around open dumping areas, who try to obtain drinking and utility water from underground sources through wells, is at significant risk (URL 2). Given the increasing pressure on water resources today, preserving the quality and quantity of existing sources is crucial.

In addition, dust clouds and gases generated from expansive areas covered by solid waste contribute to air pollution. Failure to control the generated gases can lead to open-air fires and explosions. In open dumping areas, the anaerobic decomposition of biodegradable organic components results in the emission of various gases such as methane, carbon dioxide, and hydrogen sulfide (Samarahan, 2020). The majority of landfill gases consist of approximately 40-60% carbon dioxide and 45-60% methane, with trace amounts of other gases also observed (Efe, 2022).

CO_2 is one of the significant greenhouse gases that play a role in the global energy balance and is anthropogenically released into the atmosphere through waste decomposition. Carbon dioxide accounts for approximately 76% of global anthropogenic greenhouse gas emissions, while methane contributes to about 16% (Aydın et al., 2011). When looking at the sectoral distribution of total greenhouse gas emissions, energy ranks first with 278.33 million tons of CO_2 equivalent (75.3%), followed by waste with 33.93 million tons of CO_2 equivalent (9.2%). The Industrial Processes sector follows with 31.69 million tons of CO_2 equivalent (8.6%), and agriculture with 25.7 million tons of CO_2 equivalent (7.0%) (Figure 2) (URL 3). The prevention of emissions of CH_4 and CO_2 gases, which have a high greenhouse effect and pose threats to the environment and public health, is only possible through the proper disposal of waste. These gases generated in landfill areas have a high energy potential and are of significant importance to the economies of countries.

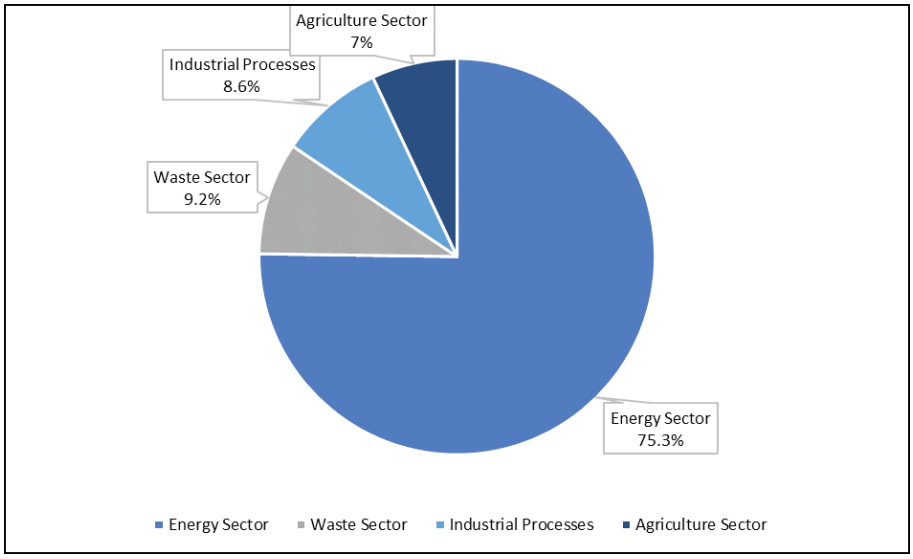

Figure 2. Sectoral distribution of total greenhouse gas emissions (URL 3)

Republic of Turkey Ministry of Energy and Natural Resources announced in June 2022 that the installed capacity based on biomass and waste heat energy was 2,172 MW (URL 4). The biomass source here includes municipal waste, sewage sludge, excreta from large and small livestock, poultry manure, slaughterhouse waste, forestry and forestry industry waste and residues, oilseeds, sugar and starch plants, fiber crops, and plant residues. Biomass is utilized to obtain energy through methods such as direct combustion, gasification, pyrolysis, fermentation, and biomethanization (Srivastava et al., 2020). Waste-to-energy facilities hold a 2.14% share nationwide, which is approximately 10 times the installed capacity in 2011 (Figure 3) (URL 4).

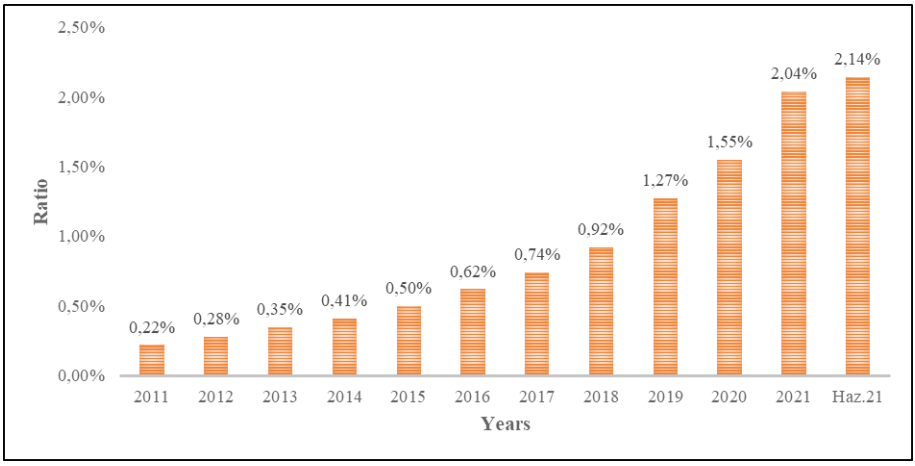

Figure 3. Proportion of biomass and waste heat energy within the total installed capacity (URL 4)

Besides global warming, the gases generated in open dumping areas pose risks of poisoning, explosion, and fire, threatening both the environment and public health. Especially during the summer months, fires can spread to forest areas at high wind speeds, causing destruction. An example of this is the fire that occurred in the Bayraklı Area within Burgazada boundaries. The fire, which broke out on October 6, 2003, in the Bayraklı Area, quickly spread to many points due to high wind speed. The fire, which was brought under control after 8 hours, resulted in the destruction of approximately 11 houses and 40 hectares of land (Kılıç, 2017).

Rehabilitation of Open Dumping Areas

Slope Regulations

In the initial stage, it is crucial to ensure the slope stability of the waste mass to achieve a well-defined geometry (Ertürk and Görgün, 2011). The maximum and minimum slopes on the upper layer are calculated, taking into account future settlements and surface water drainage. At this stage, the primary goal is to prevent rainwater from penetrating into the waste, minimizing the contact of water with pollutants. To achieve this, the upper surface of the waste dumping area is leveled and brought to the same grade. Subsequently, to enhance stability and create a foundation for other layers, a pre-fill layer with a thickness of approximately 50 cm should be placed on top of the leveled waste surface. Unless there are regional geotechnical constraints, the waste slope should not exceed 1 in 3 (33% slope), and the upper slopes should not exceed 20 in 1 (5% slope) (Rushbrook & WHO, 2001).

Gas Drainage Layer

The collection of landfill gas generated in open dumping sites and its disposal in a manner that poses no risk is essential. The gas drainage layer, approximately 30 cm thick and placed on top of the initial fill layer, serves to distribute pressure and protects the mineral impermeable layer from gas pressure (Öztürk, 2015). Typically, gravel with a permeability of around $1x10^{-3}$ m/s is used in this layer. In areas where the waste depth exceeds 7m, vertical gas wells (with a diameter of approximately 1m) are drilled, while in areas with a depth less than 7m, horizontal drainage can be employed (Gökçe & Hasanoğlu, 2015). Landfill gases can be collected using passive or active systems (Duan et al., 2021). Passive systems rely on the principle of utilizing the diffusion movement of gas within the landfill area, while active gas collection systems involve removing the gas through a vacuum collection system. Passive systems are more economical and require less maintenance compared to active gas collection systems. However, in these systems, creating a pressure gradient in the gas extraction wells and trenches is necessary. If an insufficient

pressure gradient is established, the desired level of gas emission cannot be achieved. In such cases, air may infiltrate the solid waste masses, disrupting anaerobic treatment. Additionally, the direct release of collected gas into the atmosphere and the absence of energy recovery are among the disadvantages of this method. In active methods, the extracted gas is burned to generate energy. It is recommended to use hybrid systems that combine both active and passive collection methods in landfill sites.

Impermeable Layer

The impermeable layer generally consists of two compacted clay layers with a permeability of less than $1x10^{-8}$ m/s each. In places where obtaining clay is challenging, a geomembrane can be used (Sarptaş et al., 2006). When there are clay deposits in the vicinity, a natural clay layer is preferred over a geomembrane due to its natural origin. Cost-benefit analysis is considered in the selection process.

The Water Drainage Layer

The layer located above the impermeable zone is the water drainage layer. This layer facilitates the drainage of rainwater and surface water. It is composed of low-lime, high-permeability gravel or sand with a permeability greater than $1x10^{-3}$ m/s (Sarptaş et al., 2006). This layer allows the drainage of precipitation and surface waters without infiltrating into the solid waste. In open dump areas, the management of two different water characterizations is necessary: surface water due to rainfall and leachate water.

In the drainage of surface waters, the establishment of two sub-systems is mandatory. The first system is designed for the collection of rainfall directly onto the waste disposal site, ensuring the collection of surface runoff and its diversion outside the open dump area without causing damage to the cover. The water seeping from the upper soil layer is collected through drainage pipes in the gravel layer placed on the clay layer and directed outside the site. The second system aims to collect the flow from the water collection basin above the site before it enters the field. For this purpose, water diversion trenches are excavated around the site, designed based on precipitation data obtained from the General Directorate of Meteorology to determine the amount of surface runoff (Gökçe & Hasanoğlu, 2015).

Final Cover Formation

Lastly, agricultural soil is spread on top for the vegetation of the landfill. This layer varies in thickness, depending on the root depth of the selected plants, and should be at least 1 meter thick. When choosing plants, short-rooted species that do not harm the impermeable layer and drainage layer with their roots should be selected. Additionally, the chosen plant species should be resistant to

landfill gases. A list of some species that can be used as cover plants in landfill areas is provided in Table 2 (Gökçe & Hasanoğlu, 2015). In the 4th section of the Directive on Solid Waste Landfill Management published in 1993, possible alternatives for the 'Upper Surface Impermeability System' given in the 'Principles of Rehabilitation of Unregulated Old Landfills' are provided. In this context, a layer containing natural and artificial impermeable materials is selected based on the proximity to resources and cost considerations. In open dumping areas where the final cover layer is applied, significant settling can be observed after 15-20 years. Therefore, before the closure process, it should be determined that there is no risk of settlement or sliding in the area.

Table 2. Some plant species that can be used in the final cover formation (Gökçe & Hasanoğlu, 2015)

Latin Name
Astragalus hamosus
Sarothamnus scoparius
Trifolium arvense
Lotus ornithopodioides
Medicago lupilina
Trifolium lappaceum
Onobrycis vicieafolia
Medicago disciformis
Trifolium campestre

In a study by Sağlık et al. (2021), the environmental issues arising from the increase in global population and consumption habits led to an increase in MSW generation. Focusing on the rehabilitation of the former landfill near the Çanakkale Onsekiz Mart University Terzioğlu Campus, the study emphasizes its visual significance. The historical use and current status of the former landfill are examined, and post-rehabilitation plant recommendations are provided to make the area suitable for landscape design. It is concluded that these recommendations will enhance urban life quality by increasing green space and eliminating visual pollution while contributing significantly to the fight against environmental pollution. The study highlights that completed rehabilitation and landscape design efforts will eliminate the hazardous image in the perception of users, creating a safe environment and providing an effective solution to environmental problems (Sağlık et al., 2021).

In their study conducted in 2006, they identified the potential issues related to open dump areas and their environmental impacts that Turkey may encounter during the integration process with the European Union (EU). Mea-

sures to be taken for the rehabilitation of open dump areas and the necessary legal regulations for this process are examined, with a particular focus on the open dump area of Kuşadası Municipality. In the context of Turkey's harmonization process with the EU Environmental Acquis, the rehabilitation of existing open dump areas emerges as an inevitable step. In this regard, general tasks such as the assessment of the current situation in the area, the planning of the cover layer and upper use, and the design of the gas collection system and leakage water are listed. As part of the study, a specific preliminary study conducted on the open dump area of Kuşadası Municipality details the rehabilitation-related tasks, aiming to guide decision-makers with similar examples during Turkey's EU harmonization process (Sarptaş et al., 2006).

The study (2006) provides strategic information and recommendations for the landscape restoration and improvement of existing open dump areas based on a sampling conducted at the Tuzluçayır-Mamak open dump area. This study emphasizes that the proposed landscape restoration highlights the need to cease disposal activities at the current Tuzluçayır-Mamak open dump area and rehabilitate the area. At the same time, it emphasizes that the Tuzlucayır-Mamak illegal dump is in Ankara's watershed and is a key part of Ankara's Open-Green Area System. This suggests that a method should be used that protects the environment and provides recreational benefits (Dilek, 2006).

A study conducted in (2007), investigated the vegetation initiatives implemented at the Adana-Sofulu Landfill in the Mediterranean Region for the improvement of Solid Waste Disposal Areas. Selected plants, including Althea rosea, Cynodon dactylon, Inula viscosa, Melilotus officinalis, and Thymbra spicata var. spicata, were irrigated with leachate from the landfill, and their development under adverse conditions in the landfill area was evaluated. The findings indicate that Althea rosea, Cynodon dactylon, and Melilotus officinalis can thrive successfully in landfill areas, while Inula viscosa and Thymbra spicata var. spicata are comparatively less effective in terms of biological remediation. Additionally, the study examined the effectiveness of planting urban landfill areas and irrigating the plants with leachate and tap water, determining that the plants exhibited better growth in the landfill area. The study emphasizes that increasing plant diversity through irrigation could contribute to faunal enrichment and underscores the importance of monitoring microbial activities in landfill areas (Erdogan & Uzun, 2007).

Maintaining and Monitoring the Rehabilitated Area

After the open dump area is rehabilitated, it is essential to monitor whether there are any ongoing risks to the environment and public health. Additionally, regular area monitoring should be conducted, and maintenance procedures should be applied when necessary. The monitored parameters and control intervals are provided in Table 3.

Table 3. Maintenance and monitoring intervals for rehabilitated wild landfill sites (URL 2)

Control Point	Potential Problems	Check Frequency
Top cover	Erosion and abrasion on the soil surface	Once a year and after heavy rain
Surface Drainage	Accumulation of soil in the surface drainage layer, control of drain pipes	Four times a year and heavy rainfall after that
Groundwater Monitoring	Groundwater pollution	Twice a year
Landfill Gas Monitoring	Odor, broken gas chimneys, compressors and flare equipment	Regularly
Flora	Vitality level	Four times a year

Conclusion

After the solid wastes generated in our country are collected in accordance with the Solid Waste Control Regulation, the necessary obligations and responsibilities are fulfilled during disposal in a manner that does not pose a threat to the environment and human health. According to TURKSTAT data, in 2012, there were a total of 672 facilities, including 83 waste disposal facilities and 589 recycling facilities, in operation. As of 2020, the number of sanitary landfill facilities has increased to 174. These facilities serve a population of 78.92 million in 1389 municipalities.

The management of solid waste is an international issue that encompasses various environmental, financial, and social aspects. Therefore, approaches to waste management should be steadfast and continuous, considering these reasons. Ensuring the systematic disposal of waste is essential for the improvement of a country's welfare. In our country, according to the National Waste Management and Action Plan, it is targeted that 35% of the waste generated in 2023 will be recycled, and 65% will be disposed of by sanitary landfill. Within the framework of this goal, it is imperative to develop policies that minimize the quantity of waste sent to municipal landfills and disposed of through other methods.

REFERENCES

Akintayo, T., Hämäläinen, J., Pasanen, P., & John, I. (2023). A rapid review of socio-cultural dimensions in Nigeria's solid waste management approach. *International Journal of Environmental Research and Public Health*, *20*(13), 6245.

Arıkan, E., Şimşit-Kalender, Z. T., & Vayvay, Ö. (2017). Solid waste disposal methodology selection using multi-criteria decision making methods and an application in Turkey. *Journal of Cleaner Production*, *142*, 403-412.

Aydın, G., Karakurt, İ., & Aydıner, K. (2011). Antropojenik metan emisyonlarinin sektörel analizi. *TÜBAV Bilim Dergisi*, *4*(1), 42-51 *(in Turkish)*.

Bayhan, Y. K., & Özbek, S. (2015). Formation of Leachates in the Landfills, Their Charecteristics and Investigation of Effects on the Groundwaters. *Kastamonu University Journal of Engineering and Sciences*, *1*(2), 53-59.

Dilek, E. F. (2006). Tuzluçayır-Mamak Düzensiz Depolama Alanı İçin Peyzaj Onarımının Önemi ve Gereği *(in Turkish*). *Journal of Agricultural Sciences*, *12*(04), 323-332.

Duan, Z., Scheutz, C., & Kjeldsen, P. (2021). Trace gas emissions from municipal solid waste landfills: A review. *Waste Management*, *119*, 39-62.

Erdoğan, R., & Uzun, G. (2007). Katı Atık Depolama Alanlarının Bitkisel Islahına Bir Örnek: Adana-Sofulu Çöp Depolama Alanı *(in Turkish*). *Akdeniz University Journal of the Faculty of Agriculture*, *20*(1), 71-82.

Ertürk, M. C., & Görgün, E. (2011). An Actual Example for Rehabilitation of Open Dump Areas in Turkey: Rehabilitation of Mersin Çavuşlu Open Dump Area. *Journal of Engineering and Natural Sciences*. *Sigma*, *3*, 200-208.

Gökçe, G., & Hasanoğlu, P. (2015). Katı Atık Düzenli Depolama Sahalarının ve Vahşi Depolama Alanlarının Islahı ve Bitkilendirilmesi. *Düzce Üniversitesi Bilim ve Teknoloji Dergisi*, *3*(1), 258-271 *(in Turkish)*.

Haksevenler, B. H. G., & Selma, A. (2021). Noktasal ve yayılı kirletici kaynaklarının yüzeysel su kalitesi üzerinde etkisi, Alaşehir Çayı alt havzası örneği. *Gümüşhane Üniversitesi Fen Bilimleri Dergisi*, *11*(4), 1258-1268 *(in Turkish).*

Kadılar, G. (2021). *Ünye ilçesi vahşi depolama alanının ıslahı ve düzenli depolama alanının araştırılması* (Master's thesis, Konya Teknik Üniversitesi) *(in Turkish)*.

Kılıç, A. (2017). Çöplük Yangınları ve Etkileri. *Yangın ve Güvenlik • Mayıs / Haziran 2017 (in Turkish)*.

Mahees, M. T. M., Sivayoganathan, C., & Basnayake, B. F. A. (2011). Consumption, solid waste generation and water pollution in Pinga Oya catchment area.

Öktem, B. (2016). Atık yönetiminde entegre uygulama. *Batman Üniversitesi Yaşam Bilimleri Dergisi*, *6*(2/1), 135-147 *(in Turkish).*

Öztürk, İ. (2015). Katı Atık Yönetimi ve AB Uyumlu Uygulamaları *(in Turkish*).

ISTAC Technical Book Series. Istanbul, Turkey.

Rushbrook, P., & World Health Organization (WHO). (2001). Guidance on minimum approaches for improvements to existing municipal waste dumpsites.

Sağlık, A., Domaç, Y. S., Reyhan, Ş. N., Furkan, A. V. C. I., Kartal, F., & Şenkuş, D. (2021). Katı Atık Depolama Alanlarının Islahı ve Analizi Çanakkale Onsekiz Mart Üniversitesi Örneği. *Akademia Doğa ve İnsan Bilimleri Dergisi*, *7*(1), 105-125 *(in Turkish*).

Saltabaş, F., Soysal, Y., Yıldız, Ş., & Balahorli, V. (2009). Evsel katı atık termal bertaraf yöntemleri ve İstanbul'a uygulanabilirliği. *Türkiye'de Katı Atık Yönetimi Sempozyumu'nda sunulan bildiri, Yıldız Teknik Üniversitesi, İstanbul, Türkiye*, 15-17 *(in Turkish)*.

Samarahan, K. (2020). Landfill Methane Emissions. *Handbook Of Environment And Waste Management-Volume 3: Acid Rain And Greenhouse Gas Pollution Control*, *3*, 397.

Sarptaş, H., Gündüz, O., Dölgen, D., & Alpaslan, N. (2006). Düzensiz Çöp Depolama Sahalarının Rehabilitasyonu: Kuşadası Örneği. *Katı Atık ve Çevre (in Turkish*).

Srivastava, R. K., Shetti, N. P., Reddy, K. R., & Aminabhavi, T. M. (2020). Sustainable energy from waste organic matters via efficient microbial processes. *science of the total environment*, *722*, 137927.

Şükran, E. (2022). Günümüzün Sürdürülebilir Enerjisi Kentsel Katı Atıklar ve Türkiye Potansiyeli *(in Turkish)*. *Journal of the Institute of Science and Technology*, *12*(4), 2396-2407.

Türkiye İstatistik Kurumu (TUİK). (2020). Atık İstatistikleri (*in Turkish)*. URL: https://data.tuik.gov.tr/Bulten/Index?p=Atik-Istatistikleri-2020-37198

URL 1 (2010) T.C. Çevre, Şehircilik ve İklim Değişikliği Bakanlığı Sızıntı Suyu Yönetimi İhtisas Komisyonu Taslak Çalışma Raporu (*in Turkish*) Website [Online]. https://webdosya.csb.gov.tr/db/cygm/editordosya/sizintisuyuyontaslak.pdf

URL 2 (2009) T.C. Çevre, Şehircilik ve İklim Değişikliği Bakanlığı Vahşi Depolama Alanlarının Islahı Kılavuzu (*in Turkish*)

Website [Online]. *https://cevresehiriklimkutuphanesi.csb.gov.tr/ShowPDF/e0c2fba3-3889-4815-9471-a93c3a8e3823*

URL 3 (2013) T.C. Çevre, Şehircilik ve İklim Değişikliği Bakanlığı 5. Bildirimi (*in Turkish*) Website [Online]. https://webdosya.csb.gov.tr/db/iklim/banner/banner595.pdf

URL 4 (2022) T.C. Enerji ve Tabii Kaynaklar Bakanlığı Biyokütle (*in Turkish*) Website [Online]. https://enerji.gov.tr/eigm-yenilenebilir-enerji-kaynaklar-biyokutle

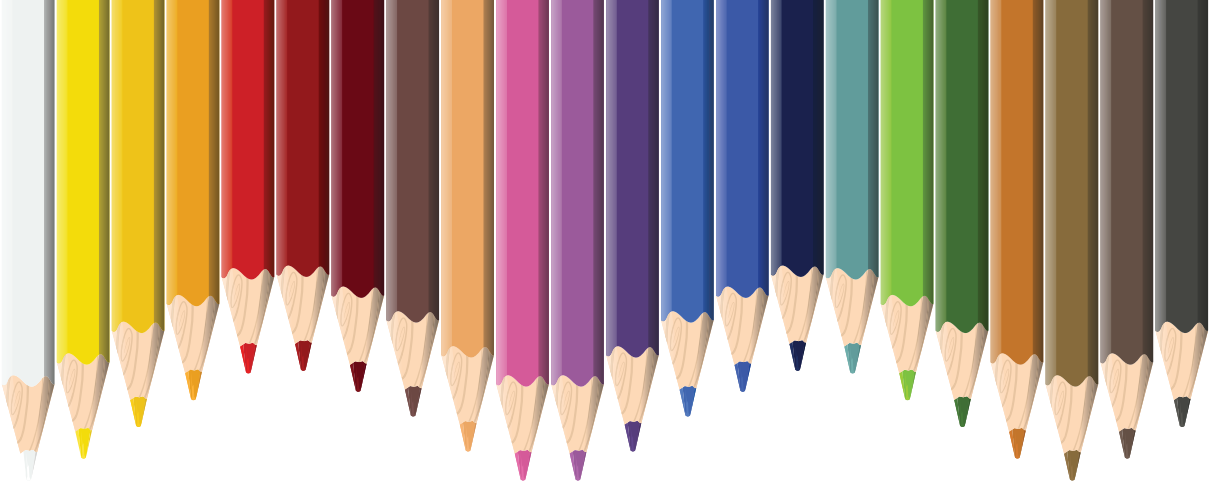

Chapter 2

UNDERSTANDING EXTREME RAINFALL UNDER CLIMATE CHANGE USING CMIP6 CLIMATE MODELS OVER TÜRKIYE

Sertac ORUC[1]

1 Assoc. Prof. Dr. Department of Civil Engineering, Çankırı Karatekin University, 18100 Çankırı, Türkiye https://orcid.org/0000-0003-2906-0771 sertacoruc@karatekin.edu.tr

INTRODUCTION

A projected increase in the frequency and intensity of extreme precipitation occurrences is among the most significant effects of a forthcoming warmer climate. It is possible to observe this rising trend of extreme precipitation in both climate model projections and observation records (Martel et al., 2021). Climate incidents such as fires, floods, heatwaves, and droughts have been recorded as caused by climate change and global warming (AghaKouchak et al., 2014; Roshani et al., 2020; Kim et al., 2020; Brás et al., 2021; Carnicer et al., 2022; Cavus et al., 2023) The scientific community generally affirms the fact that global warming and climate change exacerbate extreme events with regard to their duration, frequency, or intensity. Accordingly, numerous socio-economic sectors are unfavorably affected by these events all around the world (Iyakaremye et al., 2021; IPCC, 2021; Chiang et al., 2021; Baghel et al., 2022). Furthermore, these extreme events are more likely to be sensitive to climate change than the average climate, portraying them as a notorious global hazard (Guan et al., 2022). Based on CRED (2021), bringing forth 13% of disaster-associated casualties over the last twenty years, worldwide human mortality is seriously impacted by severe temperature incidents. In addition to that, a shocking 1.65 billion people have been impacted by floods, while 1.45 billion have been affected by droughts, as stated by Baghel et al. (2022).

Previous studies have shown that the frequency and intensity of climate extremes have risen on a global scale, and this pattern is expected to persist in the future (Donat et al., 2016; Myhre et al., 2019; Papalexiou & Montanari, 2019; Guan et al., 2022). Also, in conformity with the conclusions of Kouman et al. (2022), the current climate trends are predicted to last in the 21st century, as the results of both suggested high- and moderate-emission scenarios suggest. Because of the widespread implications they can have, the investigation of climate extremes, their variations, and their impacts on socioeconomic factors is of great importance (AghaKouchak et al., 2014; Moazenzadeh et al., 2018). The coupled effects of climate change, land use and land cover alterations, population increase, and unplanned urbanization provoke the negative impacts of such extremes even more severe (Kourtis and Tsihrintzis, 2022). Thus, it is key to meticulously investigate the changes in climate extremes on a global, regional, and local scale (Wang et al., 2022; Wudineh et al., 2022).

Considering the changing climate, extreme precipitation characteristics are most important in determining drainage, irrigation, and infrastructure designs effectively. These characteristics, which give an overview of the return level of extreme precipitation for return periods and extreme precipitation duration, are frequently used in hydrological infrastructure design and engineering applications (Quali et al., 2018). To ensure their relevance and efficiency in infrastructure development and flood risk management, extreme precipitation characteristics must be updated, considering ongoing climate change and

anthropogenic activities that are changing precipitation patterns. Engineers and planners can strengthen the resilience of critical infrastructure and adapt to changing climate patterns by integrating up-to-date rainfall estimates, protecting populations from the negative impacts of extreme rainfall events in the future (Panos et al., 2021).

In climate science, general circulation models (GCMs) are crucial since they offer important insights into future climate data (Randall et al., 2007). GCMs mimic complex interactions between climate factors and provide projections on regional and global scales by mathematically simulating Earth's atmosphere, oceans, and historical climate data. The Coupled Model Intercomparison Project (CMIP) brings together many GCMs from research centers around the world. This lets us compare and evaluate model performance in a structured way and gives us a solid set of projections (Pierce et al. 2009).

Modern climate models from leading research institutions worldwide are used in CMIP6, the sixth phase of the CMIP. With the advent of CMIP6 models, precipitation pattern simulation and its implications for future climate scenarios have advanced significantly (Bağcaci et al., 2021; Eyring et al., 2016). Its main goal is to improve projections for numerous variables, including precipitation, and expand our understanding of climate processes. CMIP6 builds on the strengths of its predecessors by adding improvements such as better representation of physical processes, higher spatial resolutions, and better initialization techniques. These all help make simulations of changes in precipitation more accurate on a global and regional level (Eyring et al., 2016; Wyeser et al., 2020). Including Shared Socioeconomic Pathways (SSPs), which cover a variety of potential future socioeconomic growth scenarios, is a noteworthy improvement in CMIP6 (O'Neil et al., 2016). The alternative narratives presented by these SSPs illustrate alternate societal and economic pathways, enabling an examination of diverse greenhouse gas emission trajectories and their associated climate impacts. The intricate interactions between human activities, including population expansion, technological improvements, energy consumption, and their influence on future precipitation patterns, are better understood by researchers by linking CMIP6 models with SSPs.

While GCMs are the main resource for future climate data, their resolution is generally coarse, particularly for regional and local studies. The resolution required to represent localized extreme weather phenomena needs to be improved in global climate models, even though they offer vital information about large-scale climate patterns (Dulière et al., 2011; Roberts et al., 2018). In contrast, downscaling techniques make it possible to convert coarse global climate model results into fine-scale regional assessments, allowing for a more precise and detailed projection of extreme rainfall occurrences (Teutschbein et al., 2012; Liang et al., 2008; Done et al., 2015). Quantile Delta Mapping (QDM) is a statistical downscaling technique that has drawn interest and

shown promise in this setting (Cannon et al., 2015). QDM is a powerful method that bridges the gap between fine-scale regional assessments and coarse-scale global climate models. It does this by keeping the statistical features of precipitation, like extreme quantiles. This method checks the differences in precipitation quantiles between what a climate model says and a historical climate dataset (reference data). It then uses those differences to change the model's predictions for the future. In addition to handling non-stationarity in the relationship between global climatic variables and local precipitation, QDM has many advantages over conventional approaches (Kim et al., 2021). Working directly with quantiles allows QDM to capture changes in the precipitation distribution, which is particularly important when estimating extreme values essential for building infrastructure and creating climate adaptation plans. Nevertheless, it should be noted that extreme precipitation events do not display spatial uniformity and instead demonstrate significant spatial variability.

The study aims to achieve several objectives, to estimate and intercompare the change in future extreme rainfall characteristics over Türkiye using the QDM downscaling approach and CMIP6 global climate models. The study also seeks to discuss the impact of climate change on the frequency of extreme rainfall, how temporally and spatially daily extremes change, and the need for updated information. The findings of this research have the potential to significantly improve Turkey's preparedness and response to climate change, promote sustainable urban development, and protect community well-being in the face of evolving environmental uncertainties. In the following sections, the study's methodology will be explained, including the use of reference data, climate models, frequency analysis, and the QDM downscaling approach. Accordingly, extreme precipitation patterns over Türkiye in the future will be calculated using CMIP6 models. The paper will conclude with a summary of key findings and some final remarks.

STUDY AREA, DATA and METHODOLOGY

2.1. Study Area

The location of Türkiye is mainly on the Anatolian Plateau in Western Asia, which has the coordinates 36° and 42° north latitude and 26° and 45° east longitude (Figure 1). The country has borders with the Black Sea in its north, the Aegean Sea in its west and the Mediterranean Sea in its south. It has a total land area of 783.562 km². A mild Mediterranean climate is mostly dominant in the Türkiye, yet due to its complex topography, mountainous regions, and being impacted by the sea, other climate conditions such as temperate continental, oceanic, and dry mid-latitude steppes are also seen. While milder conditions are experienced in the coastal areas, mountains like Taurus and

Northern Anatolia located parallel to the sea blocks the diffusion of marine effects towards the inland parts (Oruc, 2022). This leads to limited precipitation and continental climatic conditions for the inner parts of the country with hot, dry summers and cold winters (Amjad et al. 2020). Temperature and rainfall patterns display diverse features in Türkiye as well. The Central Anatolia region gets around 400 mm of yearly precipitation while the Black Sea region gets over 2200 mm, making it the highest amount in the country.

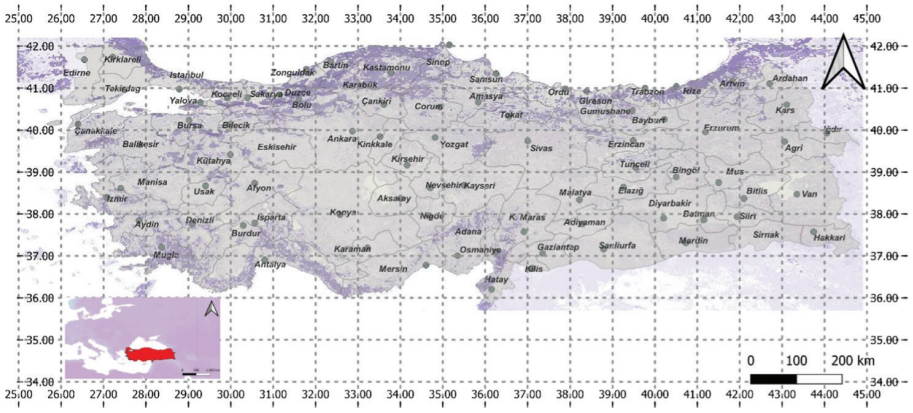

Figure 1. Study area (Oruc, 2022)

2.2. Data

2.2.1. Reference Data ERA5-Land

The ERA5-Land data from the European Centre for Medium-Range Weather Forecasts (ECMWF) were used in this work to downscale and correct biases in the CMIP6 global climate models and to evaluate the performance of the bias-corrected and downscaled data. ERA5-Land, as detailed by (Muñoz-Sabater et al., 2021), offers an open-access data set that extends from 1950 to approximately 2-3 months prior to the present, delivering high-resolution hourly information on surface variables. This dataset, which has an approximate grid spacing of 9 km, is the outcome of reprocessing the land component of the ERA5 climate reanalysis with a more precise spatial resolution. The ability to operate at more exact scales thanks to the horizontal resolution of 0.10° x 0.10° instead of 0.25°x0.25° is the main difference between this set and its original.

2.2.2. CMIP6 Global Climate Models

In this study, the CMIP6 global climate models were used as the source of future projections. The6th edition of the Coupled Model Comparison Project,

(CMIP6), (Eyring et al., 2016; O'Neill et al., 2016), is understood to have performed better compared to its predecessor CMIP5. Although the CMIP 6 data is relatively new, there appears to be a growing interest in the implementation of the latest projections.

Moreover, Bagçaci et al. (2021) stated that CMIP6 products in Turkey performed better than CMIP5 for precipitation and temperature, and therefore the results of climate change impact studies should be updated with the latest data. Therefore, CMIP6 models are not only the most up-to-date climate models, but also perform better on Turkey than the previous version of CMIP5 models. Table 1 lists the top ten CMIP6 models that demonstrate enhanced performance over Turkey, as identified by Bagçaci et al. (2021), while Figure 2 graphically presents the SSPs, outlining them as prospective future scenarios.

Table 1. Top 10 CMIP6 climate models over Türkiye used in the study (Precipitation and Temperature) (Bagcaci et al. (2021)

Rank	Precipitation	Temperature
	CMIP 6 GCM	**CMIP 6 GCM**
1	HadGEM3-GC31-MM	MPI-ESM1–2-HR
2	GFDL-ESM4	CNRM-ESM2–1
3	ACCESS-CM2	NorESM2-MM
4	EC-Earth3	MRI-ESM2–0
5	CNRM-CM6–1-HR	EC-Earth3-Veg
6	MRI-ESM2–0	CESM2
7	EC-Earth3-Veg	HadGEM3-GC31-MM
8	HadGEM3-GC31-LL	CNRM-CM6–1
9	MIROC6	CESM2-WACCM
10	UKESM1–0-LL	BCC-CSM2-MR

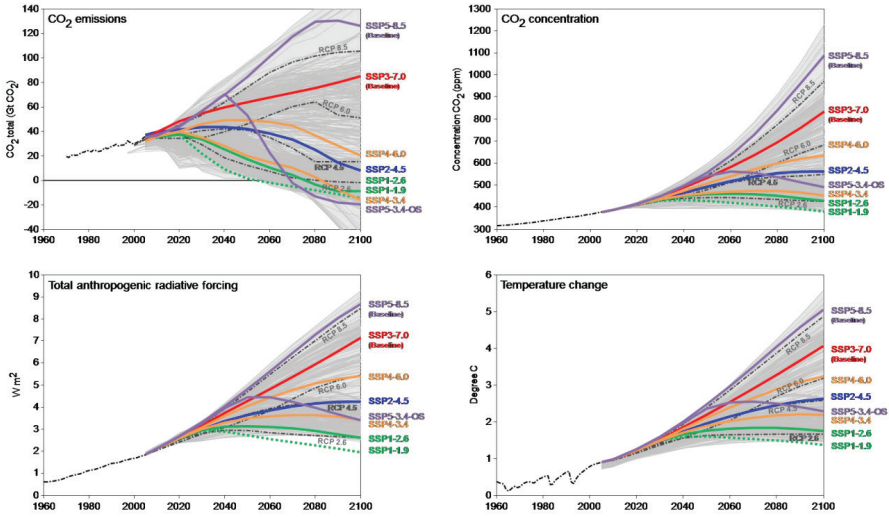

Figure 2. *CMIP6 Global Climate Model Future Scenarios (O'Neill et al, 2016)*

2.3. Method

2.3.1. Bias Correction

The quantile delta mapping method (QDM) has been developed to eliminate systematic biases in model outputs, while simultaneously preserving the relative changes observed within the quantiles of the models' variable under scrutiny (Cannon et al., 2015). A relative change term taken from the model data and a bias-corrected value obtained using reference data make up the core equation of the quantile delta mapping approach. This method differs from the detrended quantile mapping approach in that it takes into account all modeled quantiles in addition to the modeled mean. (Cannon et al., 2015; Gumus et al., 2023).

$$\hat{x}_{m,p}(t) = \hat{x}_{o:m,h:p}(t) * \Delta_m(t)$$
$$\hat{x}_{o:m,h:p}(t) = F_{o,h}^{-1}\{F_{m,p}[x_{m,p}(t)]\} \quad (1)$$
$$\Delta_m(t) = \frac{x_{m,p}(t)}{F_{m,h}^{-1}[F_{m,p}^{(t)}\{x_{m,p}(t)\}]}$$

$\hat{x}_{o:m,h:p}(t)$ is the bias corrected reference period data, $\Delta_m(t)$ is the

relative change in the model data over the reference and projection periods.

2.3.2. Multi-model ensemble average

In climate modeling research, the multi-model ensemble average (MMEA) is frequently employed to account for the biases and uncertainties introduced by GCMs (Kim et al., 2016, Ahmed et al., 2019). In this approach predictions of different models utilized to produce a single yet more accurate predictions. The idea behind this approach is that combining the strengths of multiple models will create a more robust and accurate predictive model that any single model cannot achieve individually. Using an ensemble average, in which the individual model predictions are averaged together to get a final output, is one method of combining the predictions of multiple models. On the other hand, it should not be forgotten that this may not always be the optimal method, However, it can be a straightforward and simple way to combine the predictions of different models. R software version 4.2.2 was used to conduct the analysis.

2.3.3. Extreme Value Analyses

For researching meteorological extremes, extreme value analysis (EVA) is often utilized (Oruc, 2021). Extreme value theory (EVT) focuses on analyzing the statistical characteristics of the extreme values (tails) of distributions and provides methodologies for assessing the extremes of a time series (Coles, 2001). EVT utilizes probability distribution functions such as the Generalized Extreme Value (GEV) or Generalized Logistic (GL) to model annual block maximum (A(B)M) series, or the Generalized Pareto Distribution (GPD) for peak-over-threshold (POT) series (Oruc, 2021). This theory is extensively employed in engineering disciplines to address extreme environmental conditions (Coles, 2001; Coles and Sparks 2006).

According to Gilleland and Katz (2016) the GEV distribution is considered capable of fitting block maxima (BM) of datasets **()**. It is characterized by three parameters, which are provided in the following equation (2), location (μ), scale (σ), and shape (ξ) parameters.

$$G(z) = \exp\left(-\left\{1 + \xi\left(\frac{z-\mu}{\sigma}\right)\right\}_{+}^{-1/\xi}\right), \quad (2)$$

where $z_{+} = \max\{z, 0\}$, $\sigma > 0$, and $-\infty < \mu, \xi < \infty$ (Coles 2001).

The BM method seeks to characterize the probability distribution of a block's maxima. The BM technique selects blocks of equal length and deter-

mines the maximum values from each block. Subsequently the GEV distribution is fitted to the acquired maximum series to estimate the return level, return period and the probability of exceedance. The block size holds significance as the convergence of the parent distribution's maximum series to the GEV distribution, as anticipated in the Block Maxima (BM) approach, may be hindered due to the limited number of blocks and biases and errors induced by the limited block size (Oruc, 2021).

GEV models were built using a BM method for this investigation, and distribution parameters were evaluated using MLE. According to Roslan et al. (2020), MLE is adaptive to model modifications and is often used to estimate GEV distribution parameters due to its beneficial asymptotic features. Model parameters were chosen in this manner because they optimize the likelihood function, allowing for the optimal distribution to describe the observed data (Mahmoodian, 2018).

RESULTS

For the projection of extreme precipitation events, an ensemble of 10 CMIP6 models was made to examine the alterations in extreme precipitation across Türkiye. To determine the return levels with different return periods, annual daily maximum precipitation data were employed with the Generalized Extreme Value (GEV) distribution, a method widely recognized as the most suitable for fitting extreme precipitation data, as evidenced by various global studies**.** Both SSP2-4.5 and SSP5-8.5 scenarios were used considering the near-mid-far future 24-hour (daily) return level values for 20-50-100 years return periods.

The daily annual maximum precipitation based on downscaled CMIP6 models for the grids covering Türkiye are used to derive return level values of various return periods and compared with the ERA5-Land values during the reference period by calculating the 20-50-100 years return levels.

The spatial and temporal distribution of magnitudes and relative changes of R20, R50, R100 for both scenarios are given in Figure 3, 4, and 5. The similarity between the ERA5-Land values and the downscaled GCM ensemble shows the success of bias correction and downscaling algorithm. In the case of 20-year return level values (Figure 3), lowest values are observed in the Central Anatolia Region and some parts of the Eastern Anatolia Region, where values vary around 40mm. Meanwhile, the highest values are observed in eastern coasts of Black Sea Region and western Mediterranean Region where return levels are over 100 mm. Although both scenarios projected an increase in 20-year return levels, the increase under the SSP5-8.5 scenario is more critical. By the end of the century, this scenario projects that historical highest return levels will be experienced across most of the Aegean, Mediterranean and Marmara coast.

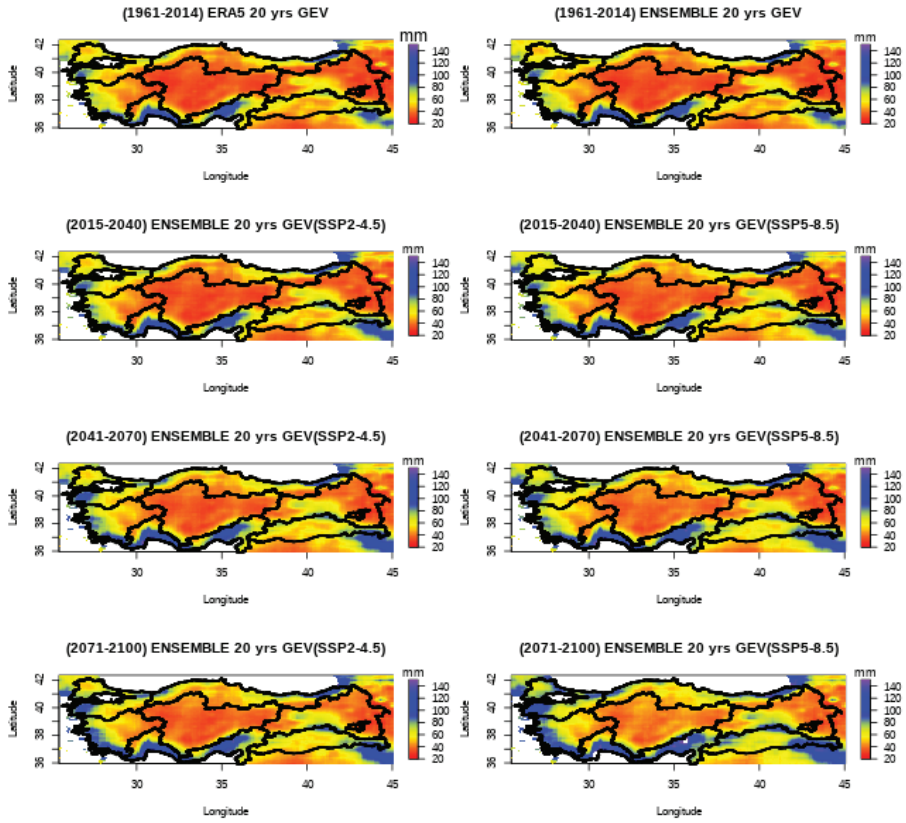

Figure 3. *20 years return level.*

When the historical results for 50 year return levels are investigated (Figure 4) the values are generally around 50 mm in the Central Anatolia region and most parts of the Eastern Anatolia Region. Meanwhile, values up to 150 mm is observed in eastern Black Sea and Mediterrenean Regions. Similar to 20 year return levels, a gradual increase in the entire Türkiye is projected under both scenarios. However, the highest increases are projected by the end of the century under SSP 5-8.5 scenario for the Mediterrenean and Aegean coasts. Altough the eastern Black Sea is a historical hotspot, it is relatively less effected by the changes in extreme precipitation.

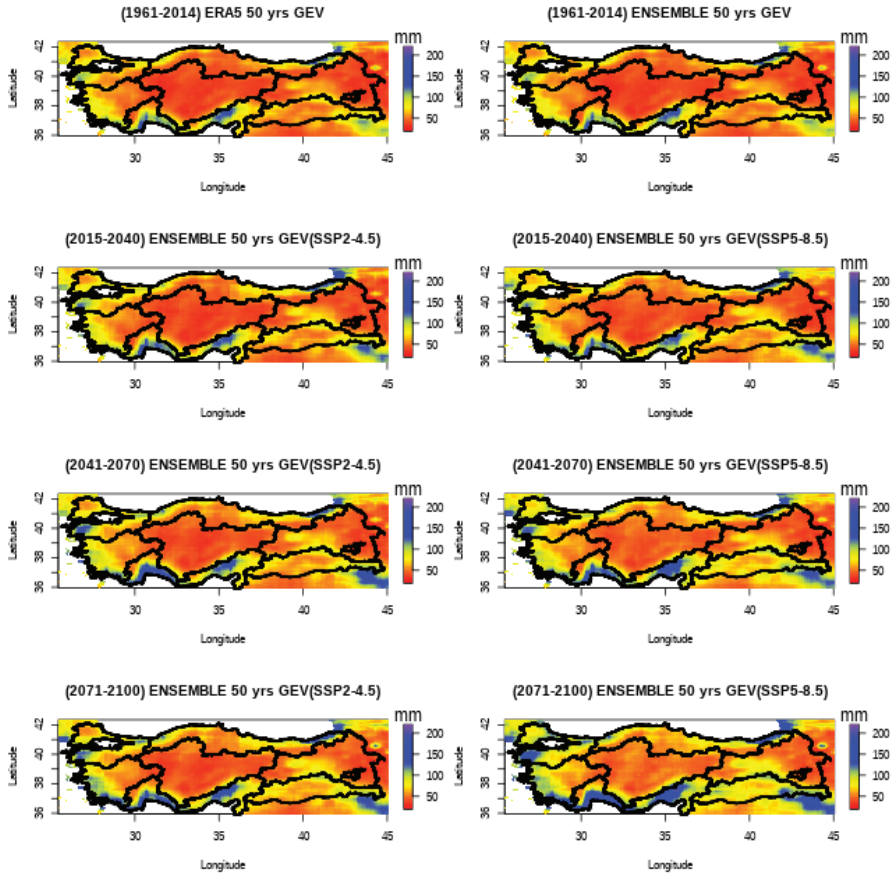

Figure 4. *50 years return level.*

Finally, 100 year return level values (Figure 5) show that historically the eastern coasts of the Black Sea Region and the Mediterrenean Region shows the highest values with up to 200 mm. On the other hand, values in the Centreal Anatolia and Eastern Anatolia regions does not exceed 70 mm. Apart from the coast and eastern parts, the Black Sea region also experiences relatively smaller return levels. However, in the future periods the values are expected to increase in all regions. Under SSP5-8.5 scenario values up to 100 mm could be experienced by the end of the century in the Central and Eastern Anatolia regions. In the Mediterrenean region where the highest increase is expected, values may rise up to 250 mm in some locations. Eastern parts of the Black Sea regions relatively less affected while the increases in the Mediterrenean and Marmara regions also show significant increases.

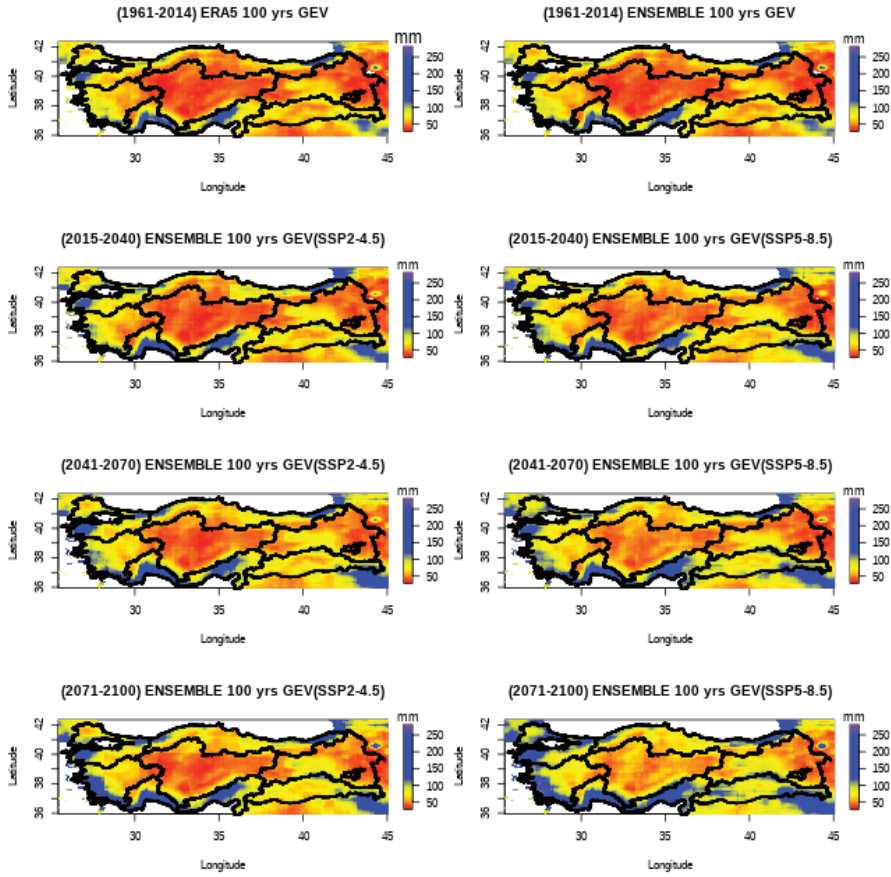

Figure 5. *100 years return level.*

All results indicate that gradual increases in return levels are expected. Even though increases under SSP5-8.5 are more drastic, SSP2-4.5 is also projects significant increases by the end of the century, especially around Mediterranean and Aegean coasts. The differences between scenarios are relatively small for the near future period (2015-2040), however after mid-century, the diverge becomes more evident. It is also observed that the difference between mid-century (2041-2070) and late-century (2071-2100) is more significant under SSP5-8.5 unlike SSP2-4.5 scenario where extremes are more stable.

CONCLUSIONS

The objective of this research was to examine the projected alterations in extreme precipitation over Türkiye as a consequence of climate change throughout the twenty-first century. The study employed Coupled Model Intercomparison Project Phase 6 (CMIP6) models in accordance with the Shared

Socio-Economic Pathways (SSP)5-8.5 and SSP2-4.5, utilizing a three-tiered future framework (near [2015-2040], middle [2041-2070], and far [2071-2100]). As a statistical downscaling technique, the Quantile Delta Mapping (QDM) method was applied to improve the spatial accuracy of low-resolution global climate models (GCMs). For this purpose, the fifth-generation reanalysis (ERA5-Land) dataset from the European Centre for Medium-Range Weather Forecasts (ECMWF) was utilized. The dataset has a spatial resolution of 0.1° × 0.1° (equivalent to approximately 9km).

Climate change is expected to affect precipitation patterns globally, and Turkey is no exception. The region's climate is influenced by its unique geography, which includes coastal areas, inland regions, and mountainous terrain. The impacts of climate change on precipitation are not uniform across Turkey. Different regions may experience varying changes due to local climate influences. For instance, coastal areas might see different changes compared to central or eastern parts of the country. With an increase in extreme precipitation events, the risk of flash flooding may rise, particularly in urban areas with inadequate drainage or in regions where the natural landscape has been significantly altered.

After performing an evaluation of the findings, it was determined that both the SSP2-4.5 and SSP5-8.5 scenarios account for significant changes in extreme precipitation over the course of the century in the studied area. However, SSP 5-8.5 scenario indicates a more dominant increase by the end of the century, according to the analyses results especially for the longer return periods. In the context of extreme precipitation, both scenarios suggest an intensification of the severity of heavy precipitation events. In conclusion, the results indicate that climate change will contribute to an intensification in both the severity and the recurrence rate of extreme climate conditions over Türkiye.

However, this study also has its own limitations. Firstly, the accuracy of the findings is dependent on the quality of the reference dataset used, which in this case is the ERA5-Land reanalysis data. It is acknowledged that reanalysis data may not often yield the extreme values when compared with the station observations. Additionally, the number of models used is expected to affect the results; increasing the number of models and/or employing a different ensemble method, such as a weighted average of models employed, is likely to enhance the accuracy of the findings.

Acknowledgement

This work is conducted as a part of the "High-Resolution Assessment of the Climate Change Impacts over Extreme Precipitation in Turkey using State of the Art Climate (CMIP6) Models" project supported by The Scientific and Technological Research Council of Türkiye (Grant No: 122Y259).

REFERENCES

1. AghaKouchak, A.; Cheng, L.; Mazdiyasni, O.; Farahmand, A. (2014). Global warming and changes in risk of concurrent climate extremes: Insights from the 2014 California drought. Geophys. Res. Lett., 41, 8847–8852.
2. Ahmed, K.; Sachindra, D.A.; Shahid, S.; Demirel, M.C.; Chung, E.S. (2019). Selection of multi-model ensemble of general circulation models for the simulation of precipitation and maximum and minimum temperature based on spatial assessment metrics. Hydrol. Earth Syst. Sci., 23, 4803–4824.
3. Amjad, M.R.; Yilmaz, M.T.; Yucel, I.; Yilmaz, K.K. (2020). Performance evaluation of satellite- and model-based precipitation products over varying climate and complex topography. J. Hydrol., 584, 124707.
4. Baghel, T.; Babel, M.S.; Shrestha, S.; Salin, K.R.; Virdis, S.G.; Shinde, V. (2022). A generalized methodology for ranking climate models based on climate indices for sector-specific studies: An application to the Mekong sub-basin. Sci. Total Environ., 829, 154551.
5. Bağçaci, S. Ç., Yucel, I., Duzenli, E., & Yilmaz, M. T. (2021). Intercomparison of the expected change in the temperature and the precipitation retrieved from CMIP6 and CMIP5 climate projections: A Mediterranean hot spot case, Turkey. Atmospheric Research, 256, 105576.
6. Brás, T.A.; Seixas, J.; Carvalhais, N.; Jägermeyr, J. (2021). Severity of drought and heatwave crop losses tripled over the last five decades in Europe. Environ. Res. Lett., 16, 65012.
7. Cannon, A.J.; Sobie, S.R.; Murdock, T.Q. (2015). Bias Correction of GCM Precipitation by Quantile Mapping: How Well Do Methods Preserve Changes in Quantiles and Extremes? J. Clim., 28, 6938–6959.
8. Carnicer, J.; Alegria, A.; Giannakopoulos, C.; Di Giuseppe, F.; Karali, A.; Koutsias, N.; Lionello, P.; Parrington, M.; Vitolo, C. (2022). Global warming is shifting the relationships between fire weather and realized fire-induced CO2 emissions in Europe. Sci. Rep., 12, 10365.
9. Cavus, Y., Stahl, K., and Aksoy, H. (2023). Drought intensity-duration-frequency curves based on deficit in precipitation and streamflow for water resources management, Hydrol. Earth Syst. Sci. Discuss. [preprint], https://doi.org/10.5194/hess-2023-107, in review.
10. Chiang, F.; Mazdiyasni, O.; AghaKouchak, A. (2021). Evidence of anthropogenic impacts on global drought frequency, duration, and intensity. Nat. Commun., 12, 2754.
11. Coles S (2001) An introduction to statistical modeling of extreme values. Springer, London
12. Coles SG, Sparks RSJ (2006) Extreme value methods for modelling historical series of large volcanic magnitudes. Statistics in Volcanology, H. M. Mader, S. G. Coles, C. B. Connor, L. J. Connor

13. CRED. Disasters in Numbers 2021; Centre for Research on the Epidemiology of Disasters (CRED): Brussels, Belgium, 2021.

14. Donat, M.G.; Lowry, A.L.; Alexander, L.V.; O'Gorman, P.A.; Maher, N. (2016). More extreme precipitation in the world's dry and wet regions. Nat. Clim. Chang., 6, 508–513.

15. Done, J. M., Holland, G. J., Bruyère, C. L., Leung, L. R., & Suzuki-Parker, A. (2015). Modeling high-impact weather and climate: lessons from a tropical cyclone perspective. Climatic Change, 129, 381-395

16. Dulière, V., Zhang, Y., & Salathe, E. (2011). Extreme Precipitation and Temperature over the U.S. Pacific Northwest: A Comparison between Observations, Reanalysis Data, and Regional Models. Journal of Climate, 24, 1950-1964. https://doi.org/10.1175/2010JCLI3224.1.

17. Eyring, V., Bony, S., Meehl, G. A., Senior, C. A., Stevens, B., Stouffer, R. J., & Taylor, K. E. (2016). Overview of the Coupled Model Intercomparison Project Phase 6 (CMIP6) experimental design and organization. Geoscientific Model Development, 9(5), 1937-1958.

18. Gilleland E, Katz R (2016) extRemes 2.0: an extreme value analysis package in R. J Stat Softw 72:1–39. https://doi.org/10.18637/jss.v072.i08

19. Guan, J.; Yao, J.; Li, M.; Li, D.; Zheng, J. (2022). Historical changes and projected trends of extreme climate events in Xinjiang, China. Clim. Dyn., 59, 1753–1774.

20. Gumus, B.; Oruc, S.; Yucel, I.; Yilmaz, M.T. (2023). Impacts of Climate Change on Extreme Climate Indices in Türkiye Driven by High Resolution Downscaled CMIP6 Climate Models. Sustainability, 15, 7202.

21. IPCC. IPCC Climate Change 2021: The Physical Science Basis: Working Group I Contribution to the Sixth Assessment Report of the Intergovernmental Panel on Climate Change; Cambridge University Press: Cambridge, UK, 2021.

22. Iyakaremye, V.; Zeng, G.; Zhang, G. (2021). Changes in extreme temperature events over Africa under 1.5 and 2.0 °C global warming scenarios. Int. J. Clim., 41, 1506–1524.

23. Kim, J.; Ivanov, V.Y.; Fatichi, S. (2016). Climate change and uncertainty assessment over a hydroclimatic transect of Michigan. Stoch. Environ. Res. Risk Assess., 30, 923–944.

24. Kim, S., Joo, K., Kim, H., Shin, J. Y., & Heo, J. H. (2021). Regional quantile delta mapping method using regional frequency analysis for regional climate model precipitation. Journal of hydrology, 596, 125685.

25. Kim, Y.H.; Min, S.K.; Zhang, X.; Sillmann, J.; Sandstad, M. (2020). Evaluation of the CMIP6 multi-model ensemble for climate extreme indices. Weather. Clim. Extrem., 29, 100269.

26. Kouman, K. D., Kabo-bah, A. T., Kouadio, B. H., & Akpoti, K. (2022). Spatio-temporal trends of precipitation and temperature extremes across the

North-East Region of Cote d'Ivoire over the period 1981–2020. Climate, 10(5), 74

27. Kourtis, I.M., & Tsihrintzis, V.A. (2022). Update of intensity-duration-frequency (IDF) curves under climate change: a review. Water Supply. 2 (5): 4951–4974. doi: https://doi.org/10.2166/ws.2022.152

28. Liang, X. Z., Kunkel, K. E., Meehl, G. A., Jones, R. G., & Wang, J. X. (2008). Regional climate models downscaling analysis of general circulation models present climate biases propagation into future change projections. Geophysical research letters, 35(8).

29. Mahmoodian M (2018) Chapter 4: time-dependent reliability analysis. Reliability and Maintainability of In-service Pipelines. 103–117

30. Martel, J.L., Brissette, F.P., Lucas-Picher, P., Troin, M., & Arsenault, R. (2021). Climate change and rainfall intensity-duration-frequency curves: Overview of science and guidelines for adaptation. Journal of Hydrologic Engineering, 26, 03121001.

31. Moazenzadeh, R.; Mohammadi, B.; Shamshirband, S.; Chau, K. (2018). Coupling a firefly algorithm with support vector regression to predict evaporation in northern Iran. Eng. Appl. Comput. Fluid Mech., 12, 584–597. https://doi.org/10.1080/19942060.2018.1482476.

32. Muñoz-Sabater, J.; Dutra, E.; Agustí-Panareda, A.; Albergel, C.; Arduini, G.; Balsamo, G.; Boussetta, S.; Choulga, M.; Harrigan, S.; Hersbach, H.; et al. (2021). ERA5-Land: A state-of-the-art global reanalysis dataset for land applications. Earth Syst. Sci. Data, 13, 4349–4383.

33. Myhre, G.; Alterskjær, K.; Stjern, C.W.; Hodnebrog, Ø.; Marelle, L.; Samset, B.H.; Stohl, A. (2019). Frequency of extreme precipitation increases extensively with event rareness under global warming. Sci. Rep., 9, 16063.

34. O'Neill, B. C., Tebaldi, C., Van Vuuren, D. P., Eyring, V., Friedlingstein, P., Hurtt, G., ... & Sanderson, B. M. (2016). The scenario model intercomparison project (ScenarioMIP) for CMIP6. Geoscientific Model Development, 9(9), 3461-3482.

35. Oruc, S. (2022). Performance of bias corrected monthly CMIP6 climate projections with different reference period data in Turkey. Acta Geophys., 70, 777–789.

36. Oruc, S. (2021). Trend and nonstationary relation of extreme rainfall: Central Anatolia, Turkey. Acta Geophys. 69, 243–255. https://doi.org/10.1007/s11600-020-00518-w

37. Ouali, D., Cannon, A.J. (2018). Estimating rainfall intensity–duration–frequency curves at ungauged locations using quantile regression methods. Stoch Environ Res Risk Assess 32, 2821–2836. https://doi.org/10.1007/s00477-018-1564-7

38. Panos, C.L., Wolfand, J.M., & Hogue, T.S. (2021). Assessing resilience of a dual

drainage urban system to redevelopment and climate change. *Journal of Hydrology, 596*, 126101. https://doi.org/10.1016/j.jhydrol.2021.126101

39. Papalexiou, S.M.; Montanari, A. (2019). Global and regional increase of precipitation extremes under global warming. Water Resour. Res., 55, 4901–4914.

40. Pierce, D.W., T.P. Barnett, B.D. Santer, and P.J. Gleckler. (2009). Selecting global climate models for regional climate change studies. Proc. Natl. Acad. Sci. U.S.A., 106(21), 8441-8446.

41. Randall, D. A., Wood, R. A., Bony, S., Colman, R., Fichefet, T., Fyfe, J., ... & Taylor, K. E. (2007). Climate models and their evaluation. In Climate change 2007: The physical science basis. Contribution of Working Group I to the Fourth Assessment Report of the IPCC (FAR) (pp. 589-662). Cambridge University Press

42. Roberts, M., Vidale, P., Senior, C., Hewitt, H., Bates, C., Berthou, S., Chang, P., Christensen, H., Danilov, S., Demory, M., Griffies, S., Haarsma, R., Jung, T., Martin, G., Minobe, S., Ringler, T., Satoh, M., Schiemann, R., Scoccimarro, E., Stephens, G., & Wehner, M. (2018). The Benefits of Global High Resolution for Climate Simulation: Process Understanding and the Enabling of Stakeholder Decisions at the Regional Scale. Bulletin of the American Meteorological Society. https://doi.org/10.1175/BAMS-D-15-00320.1

43. Roshani, A.; Parak, F.; Esmaili, H. (2020). Trend analysis of climate change compound indices in Iran. J. Water Clim. Chang., 12, 801–816.

44. Roslan RA, Na CS, Gabda D (2020) Parameter estimations of the generalized extreme value distributions for small sample size. Math Stat 8(2A):47–51.

45. Teutschbein, C., & Seibert, J. (2012). Bias correction of regional climate model simulations for hydrological climate-change impact studies: Review and evaluation of different methods. Journal of hydrology, 456, 12-29.

46. Wang, L.; Li, Y.; Li, M.; Li, L.; Liu, F.; Liu, D.L.; Pulatov, B. (2022). Projection of precipitation extremes in China's mainland based on the statistical downscaled data from 27 GCMs in CMIP6. Atmos. Res., 280, 106462.

47. Wudineh, F.A.; Moges, S.; Kidanewold, B.B. (2022). Detecting Hydrological Variability in Precipitation Extremes: Application of Reanalysis Climate Product in Data-Scarce Wabi Shebele Basin of Ethiopia. J. Hydrol. Eng., 27, 5021035.

48. Wyser, K., Kjellström, E., Koenigk, T., Martins, H., & Döscher, R. (2020). Warmer climate projections in EC-Earth3-Veg: the role of changes in the greenhouse gas concentrations from CMIP5 to CMIP6. Environmental Research Letters, 15(5), 054020.

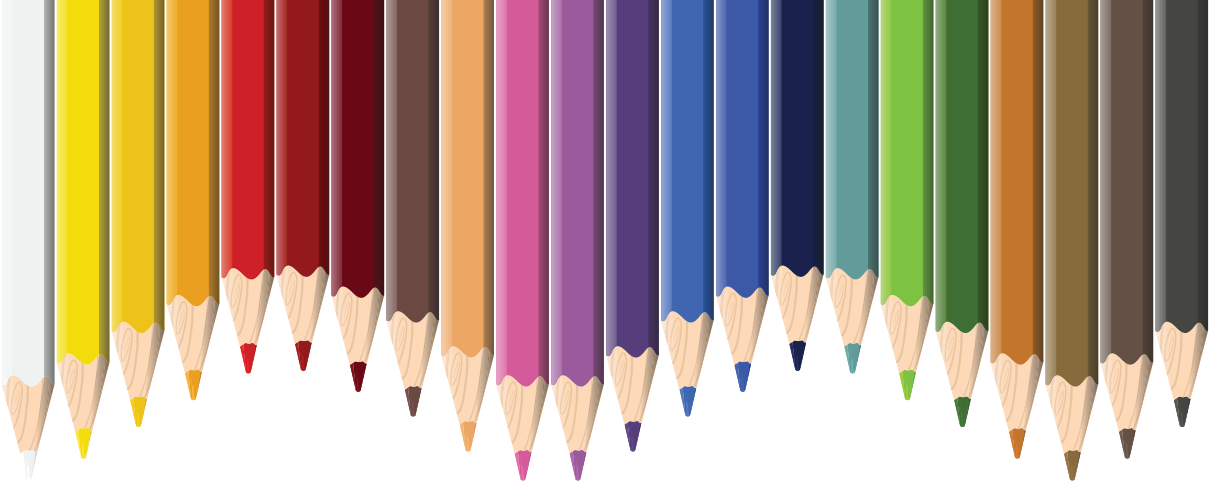

Chapter 3

ELECTROMAGNETIC THRUSTERS

Hakan BUCAK [1]

1 Asst. Prof. Tarsus University, Faculty of Aeronautics and Astronautics, Aerospace Engineering, Tarsus, Mersin - Türkiye; hakanbucak@tarsus.edu.tr ORCID: 0000-0002-6696-326X

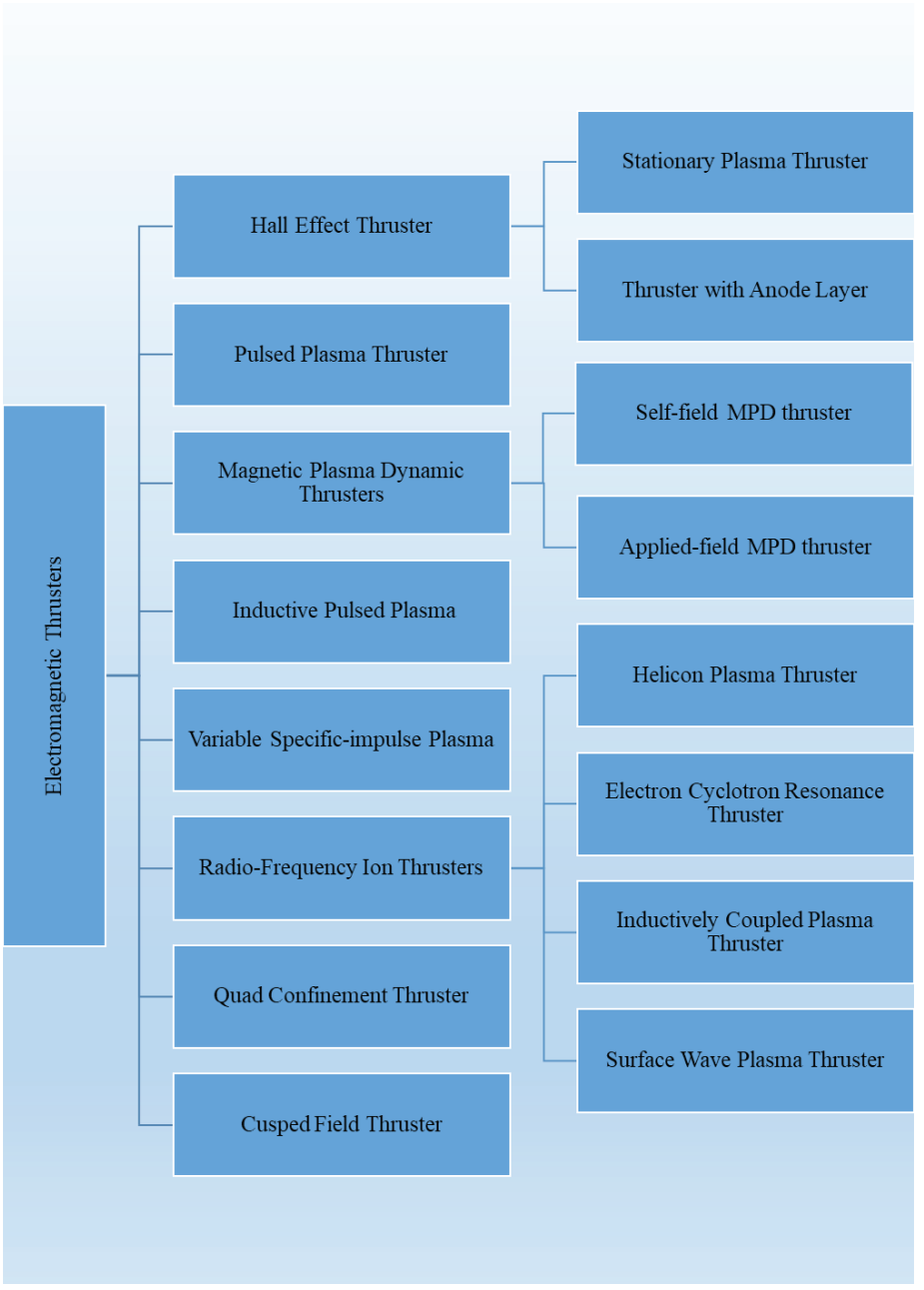

Figure 1. Electromagnetic thrusters

Electromagnetic propulsion represents the third category within electric propulsion, with a primary focus on propelling highly charged plasmas through the utilization of currents and magnetic fields. In contrast to electrostatic engines, electromagnetic engines demonstrate a notably high thrust density, ranging from 10 to 100 times that of ion engines, and produce a neutral exhaust beam, obviating the necessity for an ion neutralizer. The interaction of electric and magnetic fields, perpendicular to each other, facilitates the acceleration of plasmas.

Electromagnetic thrusters employ various methods to ionize propellant and propel it using an electromagnetic field, combining elevated specific impulses with the capacity to handle exceptionally high power levels. This category of electric propulsion engines can achieve significantly greater thrust levels (N-kN) in comparison to electrostatic thrusters (Tajmar 2003).

Electromagnetic techniques offer a noteworthy advantage over electrostatic counterparts as they can confine and direct plasmas characterized by higher temperature and density. This results in increased exhaust velocities, leading to a more efficient utilization of propellant mass (Jordan 2000).

Electromagnetic thrusters propel ionized gas flow without being constrained by electric space charge, distinguishing them from gridded ion thrusters. Various types include pulsed thrusters, magnetoplasmadynamic (MPD) thrusters, and helicon thrusters. MPD thrusters, in particular, have the potential to generate substantial thrust at high power levels, making them suitable for missions related to cargo and personal transportation to Mars (Levchenko et al., 2022).

The operation of electromagnetic thrusters involves the acceleration of ionized gas flow through the interaction of electric current and a magnetic field, which can either be externally applied or self-generated through significant current flow. These thrusters can function in pulsed mode or as steady-state devices (Beattie & Penn, 1989).

1. Hall Effect Thruster

Hall-effect thrusters leverage the Hall current and its interaction with a magnetic field to produce thrust. In situations characterized by low-density plasmas and elevated magnetic fields, the Hall-effect electric field becomes prominent, yielding advantageous outcomes. The Hall current induces an orbital motion of electrons around a central guide, and with the application of a radial magnetic field, the flow spirals outward, resulting in acceleration.

In the case of Hall thrusters, a process involves introducing gas (typically xenon) into an annular space through an anode. Electrons flowing in the opposite direction, derived from an external hollow cathode current, ionize the

gas. Ions then accelerate under the influence of the electrostatic field generated by the negative cathode, while electrons undergo an azimuthal drift (Hall current). Thrust is transferred to magnetic coils through interaction with the electron Hall current. Hall thrusters fall under the category of electrostatic ion accelerators, and their exhaust plume is highly ionized, exhibiting efficiencies within the 45–55% range, which increase with voltage (Martinez-Sanchez & Pollard, 1998).

Effective control of Hall thrusters entails managing low flow rates, typically a few milligrams per second, achieved by either thermally adjusting gas viscosity or employing precision electromechanical valves. Variables such as thrust, specific impulse, and power can be regulated through voltage, with additional control possible through manipulation of the magnetic field. The power-processing unit for Hall thrusters is intricate and weighty, designed to accommodate plasma fluctuations and coordinate magnet current and flow controls. Two competing designs, namely the ceramic-lined stationary plasma thruster (SPT) type and the 'thruster with an anode layer' (TAL) type, are discussed in the literature (Martinez-Sanchez & Pollard, 1998).

Researchers have conducted analytical studies on oscillation phenomena in Hall thrusters, observing discharge current oscillations, referred to as ionization oscillations, occurring at frequencies ranging from 10 to 100 kHz. A one-dimensional discharge model, incorporating conservation equations for ions and neutrals and considering spatially sinusoidal fluctuations of densities along the channel, accurately predicted oscillation frequencies consistent with experimental observations (Tahara & Nishida, 1999).

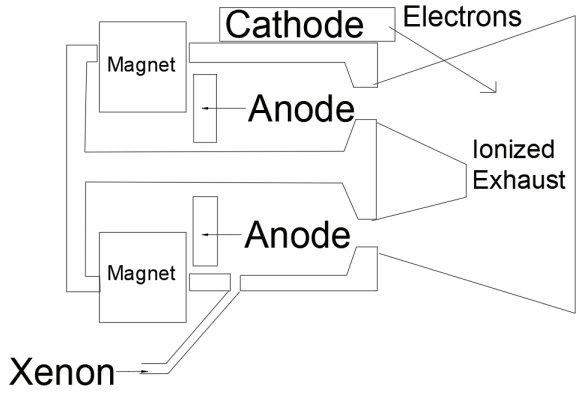

Figure 2. Hall effect thruster

1.1. Stationary Plasma Thruster

In the early 1960s, the Kurchatov Institute of Atomic Energy (KIAE) in Russia, led by Professor Alexey Morozov, designed the initial laborato-

ry models of Stationary Plasma Thrusters (SPTs). By the late 1960s, these thrusters, operating with gaseous propellant at power levels in the hundreds of Watts, demonstrated a thrust efficiency ranging from 0.2 to 0.35 and specific impulses varying from 1000 to 2000 seconds. The quasi-electrostatic ion acceleration in SPTs enabled higher ion current density without being restricted by space charge limitations. Initial tests involved the correction of the orbit of the "Meteor" satellite, highlighting the practicality and compatibility of SPTs with satellite subsystems (Kim & Popov, 2001).

In the SPT configuration, a DC electric field is established along the axis of the thruster, with the anode positioned at the non-exhaust end and the cathode either externally or at the exhaust end of the ionization chamber. Electrons emitted from the cathode are attracted into the chamber by the electric field, and their circulation lifetimes are prolonged through E x B drift, assisting in the ionization process. Subsequently, the electrostatic field accelerates ions into the exhaust flow. The applied voltage difference, typically around 300 V, generates an accelerating electric field, while a radial magnetic field confines electron flow, concentrating the voltage difference for efficient ion acceleration. Notably, Russian-built Fakel SPTs have accumulated over 10,000 hours of space operation (Jordan 2000) (Stephenson 1995).

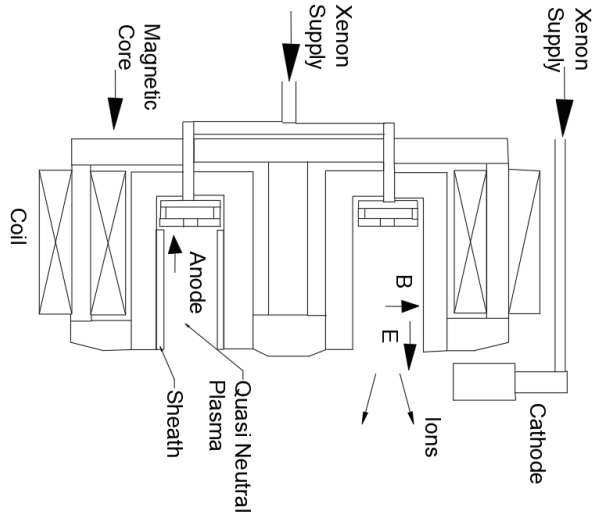

Figure 3. Stationary plasma thruster

1.2. Thruster with Anode Layer

Hall thrusters featuring an anode layer, also known as "thrusters with anode layer" or "thrusters with external layer" differ in configuration from Stationary Plasma Thrusters (SPTs). In this design, anodes are positioned down-

stream, and the ion production region is situated more externally compared to SPT units. Hall thrusters of the TAL type typically have smaller dimensions and lower erosion rates. Significantly, TAL thrusters generally exhibit twice the thrust-to-power ratio of ion-bombardment electrostatic systems, requiring electric field potentials of only 300-400 V.

Over several decades, the USSR extensively employed both SPTs and TALs, incorporating them into Meteor weather satellites, military surveillance platforms, and Express telecommunication satellites. Even following the end of the Cold War, Russian Hall thrusters found applications in U.S. military research initiatives, such as STEX, launched in October 1998. Through a successful marketing campaign, conducted in collaboration with U.S. companies, the reach and utilization of these advanced propulsion systems have been further expanded (Jordan 2000).

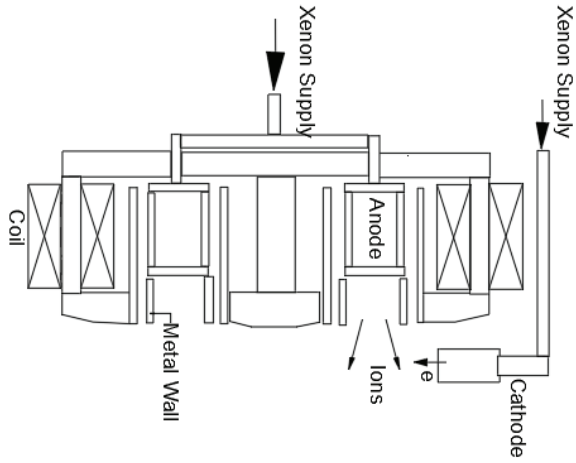

Figure 4. Thruster with anode layer

2. Pulsed Plasma Thruster

Pulsed Plasma Thrusters (PPTs) stand out in the realm of electric propulsion due to their unique operation in short pulses, typically around 10 milliseconds, and their utilization of solid propellants such as Teflon. The propulsion process involves charging a capacitor, applying 1–2 kilovolts across the Teflon surface, initiating a discharge through a spark plug, and ionizing, evaporating, and predominantly ionizing a small quantity of material. The instantaneous current, reaching tens of kiloamperes, generates a magnetic field that accelerates the gas slug to speeds nearing the 'critical Alfven velocity,' resulting in specific impulses of 1000–1500 seconds or higher at very high power (Martinez-Sanchez & Pollard, 1998).

PPTs excel in tasks requiring precision orbital or attitude control and have been utilized on satellites like LES-6 and the U.S. Navy's NOVA constellation since the late 1960s. However, challenges include modest efficiency (8–13%) and significant mass. Ongoing research aims to enhance efficiency through pulse tailoring, nozzle recovery, and increased instantaneous power. Despite these challenges, PPTs continue to be a favourable choice for light propulsion applications that demand reliability and precise control (Martinez-Sanchez & Pollard, 1998).

The Tokyo Metropolitan Institute of Technology (TMIT) collaborates with NASDA in PPT research, focusing on evaluating the feasibility of attitude control, de-orbit manoeuvres, and formation flight for small satellites like μ-LabSat II. The advantages of PPTs for small satellites, stemming from their compact size and reduced weight, make them an attractive option, and ongoing research strives to improve their performance, reliability, and feasibility (Tahara 2003).

Comprehending the intricacies of PPTs involves delving into electromagnetic and electrothermal processes. The ignition of the discharge, often initiated by a spark plug, plays a pivotal role. Numerical simulations contribute to modeling PPT behavior, offering insights into factors influencing thrust variations from one shot to another. The 35-year development history covers fundamental physics, diverse PPT types, performance evaluations in both flight and laboratory settings, theoretical advancements, and modeling breakthroughs (Burton & Turchi, 1998) (Pottinger & Scharlemann, 2007).

The propulsion mechanism of a PPT involves a propellant bar positioned between two electrodes connected to a capacitor bank. An ignition spark triggers an electric discharge along the propellant surface, leading to heat-induced ablation and ionization of the propellant. The ionized propellant is then accelerated by electromagnetic fields, akin to Magnetoplasmadynamic (MPD) thrusters. A simple spring facilitates the axial advancement of the bar, enabling propellant replenishment (Mickelsen 1967).

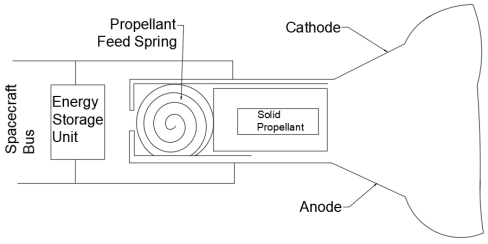

Figure 5. Pulsed plasma thruster

3. Magnetic Plasma Dynamic Thrusters

Magnetoplasmadynamic (MPD) Thrusters typically achieve higher power densities in plasmas through magnetic interactions rather than electrostatic interactions. The self-field MPD thruster generates an azimuthal magnetic field and corresponding magnetic pressure by directing a robust radial current between concentric electrodes. The thrust produced is directly proportional to the magnetic pressure, and the back electromotive force (EMF) scales as $I^{3/mc}$.

MPD thrusters utilizing noble gases have demonstrated efficiencies of up to 35%. Even when operating at megawatt power levels, greater efficiencies are observed when employing hydrogen at higher specific impulses. Challenges for MPD thrusters persist, particularly in terms of high-power requirements and addressing the development of a robust plasma pinching force (Martinez-Sanchez & Pollard, 1998).

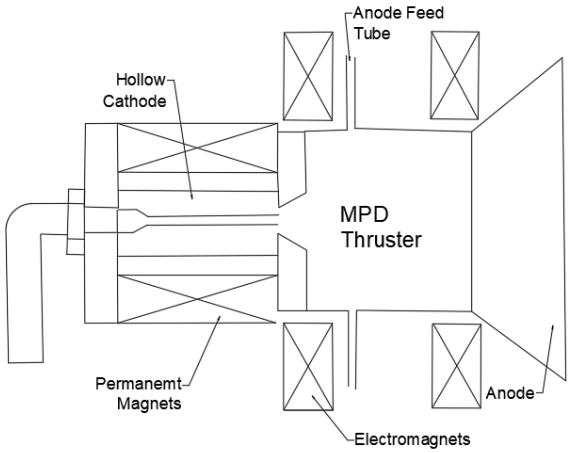

Figure 6. Magnetic plasma dynamic thrusters

3.1. Self-field MPD Thruster

Various self-field Magnetoplasmadynamic (MPD) thrusters, operating within the high-power range of 100 kW to 1 MW, have been subject to scrutiny in recent decades, all functioning in steady-state mode. Different geometries have been explored in various studies, a few of which are outlined below.

The ZT-thrusters, characterized by a cylindrical design, underwent investigation at power levels reaching 350 kW and currents up to 15 kA. These thrusters encountered limitations not intrinsic to the thruster itself but rather due to inadequate cooling of the vacuum chamber. Extensive plasma diagnostics, involving emission spectroscopy and electrostatic probes, along with an analysis of temperature distribution on the cathode surface, were conducted and compared with numerical computations (Schmidt 2005).

Researches (Herdrich et al., 2009) explored the performance of nozzle-type Magnetoplasmadynamic (MPD) thrusters employing argon as a propellant. These thrusters demonstrated thrust values reaching up to 25 N with a thrust efficiency of approximately 10%. Featuring a coaxial geometry, the cathode positioned upstream on the center axis and the anode downstream formed the nozzle, incorporating neutral segments in the nozzle throat for a gradual reduction in potential difference. Hybrid approaches, such as DT and HAT/CAT geometries, blending thermal expansion and magnetic acceleration, achieved thrust values of 27 N at power levels up to 550 kW, current levels up to 8000 A, and thrust efficiencies up to 27%. However, challenges included constrained current levels due to voltage oscillations and the onset of arc phenomena at the anode. The study integrates experimental work with numerical codes for theoretical calculations, providing a comprehensive understanding of MPD thruster dynamics.

This extensive research, coupled with optical diagnostics and theoretical investigations into the onset of instabilities, suggests that these phenomena may be attributed to charged particle depletion in the anode boundary layer. The HAT thruster, specifically designed to investigate the influence of the hot anode surface on instabilities, is detailed in a particular study (Herdrich et al., 2009).

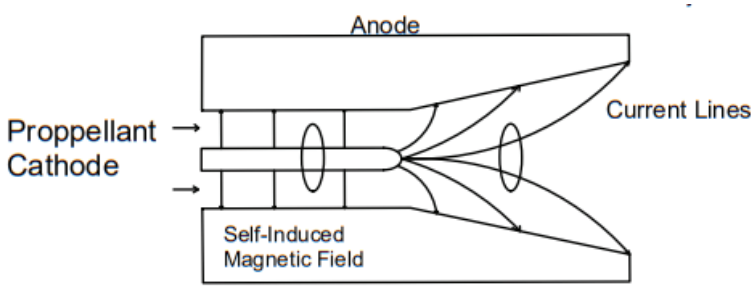

Figure 7. Self-field MPD thruster

3.2. Applied-field MPD Thruster

The applied field MPD thruster, also known as a "Lorentz Force Accelerator," features an axisymmetric chamber with a cathode running along its length, carrying a substantial current. The ionization of inflowing neutral gas occurs due to the potential difference, and the plasma experiences acceleration through both Joule heating and electrodynamic forces. The dominant acceleration mechanism is provided by the Lorentz force, generated by the interaction of the current-carrying plasma with a magnetic field. There are two methods of magnetic field production: self-field and applied field. The applied field approach incorporates an external solenoidal magnetic field to enhance acceleration and plasma confinement. MPD thrusters can operate in

quasi-steady state or pulsed modes, with efficiency being dependent on power input. Steady-state units have not yet been flown due to higher power requirements. The Japanese ISAS satellite SFU tested the general operation of quasi-steady-state MPD thrusters (Jordan 2000).

In the power range of 5-100 kW, Stationary Applied Field Magnetoplasmadynamic (AF-MPD) thrusters are undergoing experimental investigations aimed at determining their operational and performance parameters, along with the characterization of their plume. The primary objective is to assess the laboratory thruster's quality and validate the numerical simulation program SAMSA. Thruster characterization involves varying the applied magnetic field strength up to 0.5 T on the axis of symmetry and axial variation of the magnetic coil. The spatial distribution of the magnetic flux density is measured using a Hall probe, showing good agreement between measured magnetic field and numerical results. The influence of mass flow rate, as well as arc current and voltage, is also under investigation. Thrust measurement is facilitated by assembling the laboratory thruster on a thrust balance, and plume characterization involves electrostatic probe measurements. The modular assembly of the thruster allows for changes in electrode geometry and magnetic field configuration based on numerical or experimental results. The radiation-cooled design not only simplifies the thruster's structure but also facilitates further development toward a flight model, and the IRS laboratory thruster has demonstrated successful engagement (Herdrich et al., 2009).

Regarding the effects of applied field strength and shape on performance, various investigations have been conducted. Generally, efficiency, specific impulse, and voltage show linear increases with applied field strength for $\bar{B} >> 1$. Operation without an applied field at powers less than 100 kW tends to result in a diffuse beam, while the addition of an applied field produces characteristic cathode and anode jets extending downstream of the anode. Myers observed that, as the applied magnetic field strength increased (100 kW, cylindrical anode, $\bar{B} = 1$ to 9), a larger fraction of the input power was deposited in the plasma, making it available for conversion to thrust power (Kodys & Choueiri, 2005).

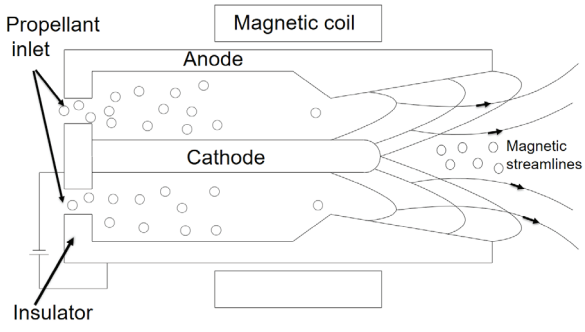

Figure 8. Applied-field MPD thruster

4. Inductive Pulsed Plasma

There is not very much information about this type of thruster. One study is given below.

In a pulsed inductive thruster, a cluster of high-voltage capacitors, approximately 10 kV, discharges into a flat induction coil strip encircling a cylindrical chamber. Just prior to the discharge, a rapid valving system introduces neutral propellant into the chamber. Before the propellant has a chance to disperse through diffusion, the discharge pulse generates a robust magnetic field within the chamber. This magnetic field both ionizes and propels the plasma away from the coil. As the chamber is sealed at one end, the propellant plasma is contained and expelled from the exhaust end of the chamber (Jordan 2000).

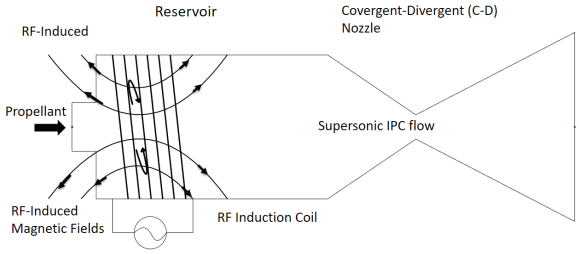

Figure 9. Inductive pulsed plasma

5. Variable specific-impulse plasma

The variable specific impulse plasma thruster operates with an electrodeless cylindrical chamber, performing ionization, plasma heating, and conversion to directed exhaust. In the forward section of the chamber, hydrogen is introduced and undergoes ionization. The resulting ions disperse into the mid-section, where additional heating occurs through electron and ion cyclotron heating, as well as whistler wave heating. Progressing downstream, the plasma enters the nozzle section, where the shape, field strength, and configuration transform the thermal energy of the plasma into kinetic energy for propulsion.

To mitigate elevated temperatures of the chamber walls, neutral hydrogen is injected radially near the nozzle. This injection serves the dual purpose of cooling the walls and disrupting the connection between the plasma and the enclosed magnetic field, particularly at low specific impulse values where plasma densities are high. Alternatively, at higher specific impulses, a high-frequency AC ripple field is employed to disrupt the magnetic field-plasma connection. Currently, the variable specific impulse plasma thruster is undergoing laboratory testing and development phases. The Johnson Space Center is actively exploring a version suitable for manned space missions, known as VASIMR (Jordan 2000).

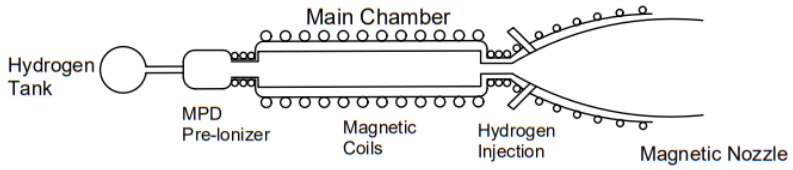

Figure 10. Variable specific-impulse plasma

6. Radio-Frequency Ion Thrusters

Radiofrequency ion thrusters operate by ionizing a propellant gas within an insulated discharge chamber using radio frequency (RF) radiation. Subsequently, ions are extracted through an accelerator grid, mirroring the mechanism found in gridded electrostatic propulsion systems. Like other charged plasma ejection systems, an external neutralizer cathode is used to maintain current balance in the exhaust. Demonstrations involving the RIT-10, an RF thruster developed through collaboration between the University of Giessen and Daimler-Benz Aerospace, have shown thrust levels in the range of tens of milliNewtons. This thruster was utilized on the EURECA test satellite in 1993, and larger variants featuring 15-cm and 35-cm grids have also been developed.

Within the realm of RF thrusters, as an alternative to the electron-bombardment approach, the propellant gas is ionized through MHz frequency excitation facilitated by free electrons. This concept, credited to Prof. Loeb of Giessen University in Germany, involves an extractor grid (+1.5 kV) redirecting ions into the discharge chamber. The accelerator grid (-1.5 kV) and deaccelerator grid (around ground potential) are designed in a manner similar to electron bombardment thrusters. Despite design advantages, such as the absence of a hollow cathode in the main discharge chamber, the efficiency of the RF thruster is slightly lower than that of Kaufman engines using the RF plasma process. Astrium in Germany markets the RIT-XX thruster series (RF Ion Thruster), with the RIT-10, generating 10 milliNewtons of thrust, being flight-qualified on the EURECA mission in 1993. The RIT thruster is also employed on the ARTEMIS satellite in conjunction with the UK thruster (Tajmar 2003).

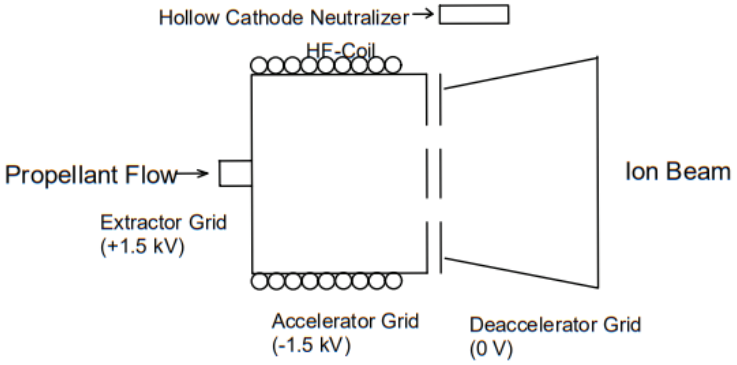

Figure 11. Radio-Frequency ion thrusters

6.1. Helicon plasma Thruster

Helicon Plasma, similar to pulsed plasma thrusters, utilizes Lorentz force interaction for plasma acceleration. It employs a helicon tube to generate a traveling electromagnetic wave along the centre of the plasma chamber, maintaining high magnetic field strengths. Helicons have been proposed for use in various electromagnetic thrusters and have gained attention in applications such as the variable specific impulse plasma thruster (Jordan 2000).

A study in literature focuses on measuring thrust in a permanent magnet helicon double layer thruster through direct experimentation using a pendulum thrust balance and a highly sensitive laser displacement sensor. Operating at low pressures (0.08 Pa), downstream ion beams were detected, revealing a maximum thrust force of around 3 millinewtons for argon at an RF input power of approximately 700 watts. The measured thrust was found to be directly proportional to the upstream plasma density, aligning closely with theoretical thrust calculations based on the maximum upstream electron pressure. These findings offer valuable insights into the performance and alignment of experimental results with theoretical predictions in the context of permanent magnet helicon double layer thrusters. (Takahashi et al., 2011).

Recent discoveries of current-free double layers (DLs) in RF plasmas and the formation of ion beams in such systems have renewed interest in plasma expansion studies, particularly in the context of propulsion. Plasma thrusters, unlike conventional electrostatic acceleration thrusters, utilize bipolar electric fields or DLs to achieve supersonic ion speeds. These systems involve an insulating source tube, a magnetic field for plasma confinement and expansion, and an RF antenna for plasma generation. Importantly, no biased electrodes are required, reducing erosion of system components. The study of plasma thrusters has focused on fundamental DL physics, various propellant gases, helicon wave characterization, and the use of permanent magnets. Experimen-

tal research, including thrust measurements for the permanent magnet helicon double layer thruster, contributes to the understanding of plasma thruster performance (Takahashi et al., 2011).

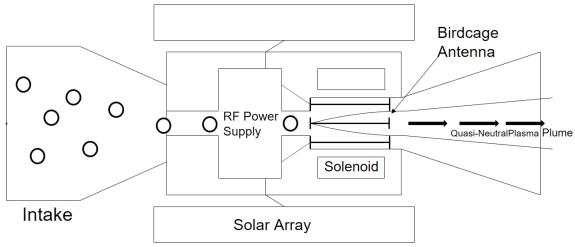

Figure 12. Helicon plasma thruster

6.2. Electron Cyclotron Resonance Thruster

Electron Cyclotron Resonance (ECR) employs an electrodeless technique that utilizes a microwave waveguide for gas ionization. In this process, circularly polarized transverse-electric mode radiation is absorbed by a limited population of free electrons moving in cyclotronic paths within a plasma chamber. The plasma chamber is surrounded by an externally generated magnetic field from a solenoid. Gas ionization occurs due to collisions between circulating electrons and neutral gas atoms. These circulating electrons align their magnetic dipoles opposite to the externally applied magnetic field. As the solenoid field diverges toward the exhaust port, it accelerates the plasma to high velocity. A unit, having successfully passed an 18,000-hour life test in its engineering model, is scheduled for launch post-2002 as part of the Japanese asteroid sample return mission MUSES-C (Jordan 2000).

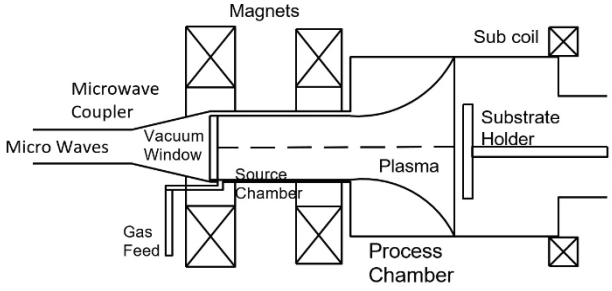

Figure 13. Electron cyclotron resonance thruster

6.3. Inductively Coupled Plasma Thruster

In the realm of inductively coupled plasmas (ICP), the process involves passing initially ionized argon gas through a quartz torch positioned inside a copper coil connected to a commercial radio frequency (RF) generator operating at 27.1 MHz with up to 3 kW forward power. The copper coil generates

high-frequency currents that produce oscillating magnetic fields, resulting in closed elliptical paths outside the coil. Electrons and ions experiencing the oscillating electromagnetic field undergo high acceleration rates, causing electron acceleration during each half cycle. Collisions between accelerated electrons and ions, along with subsequent ionization of unionized argon gas, contribute to further ionization (Soltanpour et al., 2018).

Noble gases like argon commonly fuel inductively coupled plasmas, facilitating efficient vaporization, dissociation, atomization, excitation, and final ionization of sample constituents. This high-temperature process induces complete fragmentation of sample molecules, leaving only detectable atomic constituents—metals, metalloids, or heteroatoms. These atomic constituents can serve as surrogates for detecting complex molecules such as proteins, nucleic acids, or small organic molecules. ICP-mass spectrometry (ICP-MS) stands out due to its high sensitivity, a wide linear dynamic detection range (up to nine orders of magnitude), and specificity for accurate detection and quantification of various elements, including metals, metalloids, and heteroelements (Pröfrock & Prange, 2012).

ICP-MS, with a plasma temperature exceeding 7000 K, is well-suited for liquid samples when coupled with techniques like flow-injection analysis, high-performance liquid chromatography, or capillary electrophoresis. Gaseous or solid samples can be analyzed using gas chromatography (GC) or laser ablation (LA) as sample introduction techniques, respectively. ICP-MS can provide precise isotope ratio information for elements featuring multiple stable isotopes, making isotope dilution analysis the preferred method for accurate quantitative results. Despite its versatility, ICP-MS is often perceived only as a “metal” detector, and efforts are underway to change this perception (Pröfrock & Prange, 2012).

In a pulsed inductive thruster, a bank of high-voltage capacitors (around 10 kV) discharges into a flat induction coil strip surrounding a cylindrical chamber. Preceding the discharge, a fast valving system injects neutral propellant into the chamber. The discharge pulse generates a high magnetic field within the chamber, ionizing and accelerating the plasma away from the coil. As the chamber is closed on one end, the propellant plasma is confined and expelled from the exhaust end. However, challenges may arise regarding shielding transient magnetic and electric fields. Thompson Ramo Wooldridge Inc. has conducted development work, but no space tests have been executed (Pröfrock & Prange, 2012).

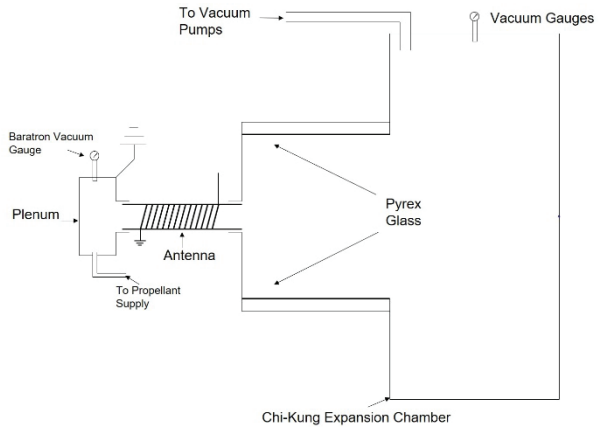

Figure 14. Inductively coupled plasma thruster

6.4. Surface Wave Plasma Thruster

Researchers are looking into new ways to create large-diameter, high-density microwave plasmas (bigger than 30 cm) without using an external magnetic field and at low pressures (less than 20 mTorr). This technology has potential uses in the next-gen super-small computer chips and flat panel displays. To make this work well, it's super important to really understand how the plasma behaves. The study digs into the details of what happens when you use microwave energy to create waves on a flat plasma surface. They found specific wave patterns using optical and microwave measurements, and their analysis explains how these waves work. They also figured out that the plasma could absorb these waves in a special way, which they call collisionless absorption. The study introduces tools that use these waves, some of which you can actually buy. If you are curious about why this matters for making better high-density plasma sources, the study has all the details (Sugai et al., 1998).

Comparing surface wave plasma (SWP) and inductively coupled plasma (ICP) reactors, which are high plasma density, unmagnetized sources, reveals their potential in next-generation etching processes (Kokura et al., 1999).

In comparing the 2.45 GHz SWP and the 13.56 MHz ICP concerning radical composition in C4F8/Ar discharges and the electron energy distribution function (EEDF), notable distinctions emerged from a study conducted in an identical plasma vessel with the same wall temperature. The ICP demonstrated a higher dissociation degree of C4F8 at an equivalent electron density compared to the SWP. Conversely, the SWP exhibited significantly higher neutral radical densities (CF3, CF2) at the same electron density, while the ICP showed an elevated F radical density. In terms of ionic composition, the ICP contained more Ar+ ions and fewer fluorocarbon ions (CmF+n), whereas the SWP featured large molecular ions (C2F+4, C3F+3, C3F+). In conclusion, the ICP was found

to be more dissociative than the SWP at the same electron density, tentatively attributed to differences in their EEDFs (Kokura et al., 1999).

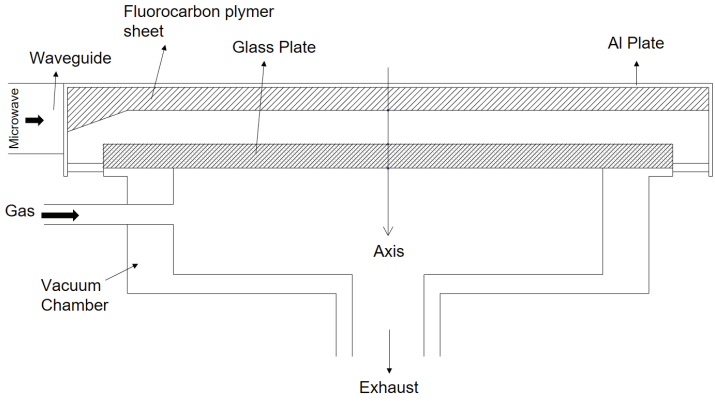

Figure 15. Surface wave plasma thruster

7. Quad Confinement Thruster

The Quad Confinement Thruster (QCT) is an innovative electric propulsion device designed to generate thrust and vector it without the need for additional pointing mechanisms. First developed in 2010 by researchers at the Surrey Space Centre, the thruster has undergone various stages of development, including the launch of a flight demonstration unit on Surrey Satellite Technology Ltd's NovaSAR-1 satellite in 2018 (Rosati Azevedo et al., 2021).

Despite these advancements, the QCT faces challenges in commercial development due to its limited thrust efficiency, demonstrated to be no more than 6%. This efficiency is notably lower compared to Hall Effect thrusters (HET), which routinely achieve over 40% thrust efficiencies, even at the low power levels required by small satellite platforms (Rosati Azevedo et al., 2021).

The Quad Confinement Thruster (QCT) utilizes a concept similar to the Hall effect thruster (HET), employing a magnetic field between an anode and an external hollow cathode neutralizer. An electric field within the magnetic barrier accelerates ion beams, and thrust vectoring is achieved by manipulating the magnetic field's topology. This magnetic barrier is established by a quadrupole arrangement of eight electromagnets positioned around the thruster's periphery. The magnetic structure allows for thrust vector control, akin to traditional electric thruster gimbal mechanisms, providing a significant advantage by eliminating the need for a gimbal mechanism. This design has the potential for mass and complexity savings (Knoll et al., 2015).

Approximately 50% of the QCT's overall mass (4.4 kg) is attributed to its electromagnets and supporting structure, generating a relatively weak magnetic field (maximum <250 G). The observed beam vectoring is speculated to

be linked to an electrostatic interaction of ions rather than a direct interaction with the magnetic field. Langmuir probe measurements in the near-field region indicate a repositionable magnetic null point within the channel, allowing for a sustained electric field component perpendicular to the device's axis, contributing to the observed beam vectoring (Knoll et al., 2015).

The Quad Confinement Thruster, conceived in 2009 through collaborative efforts between the Surrey Space Centre, SSTL, and Airbus Defence and Space, underwent iterative experiments before transitioning into an industrialization phase in 2013. This initiative sought to create a standardized, flight-worthy iteration specifically designed for small satellites (Lane & Knoll, 2015).

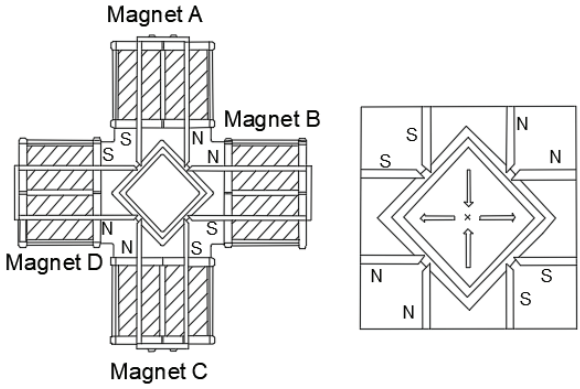

Figure 16. Quad confinement thruster

8. Cusped Field Thruster

The cusped field thruster (CFT) stands out as an innovative electric propulsion concept, offering advantages such as an extended lifespan, simple structure, easy integration, low mass, and high reliability. This thruster type has captured considerable attention in aerospace research, leading to the design and experimental testing of several cusped field thrusters by the Harbin Institute of Technology (HIT) and Beijing Institute of Control Engineering (BICE). In tandem, particle-in-cell (PIC) simulation models were developed to uncover the underlying principles.

A study (Yongjie et al., 2018) introduces the Variable Magnet Length Cylindrical Hall Thruster (VML-CFT) as a noteworthy iteration to assess the impact of diverse magnet lengths on thruster performance. The investigation underscores that thrusters featuring an extended middle stage, reduced magnetic interface angle, and diminished cusp field intensity at the exit exhibit superior thrust and efficiency. Comprehensive simulations highlight the substantial influence of magnetic field topology on plasma distribution within the primary ionization region. The VML-CFT showcases outstanding performance met-

rics, achieving 107.5 millinewtons in thrust, 38% efficiency, and 2232 seconds in specific impulse, all while operating at a power consumption level of 3037 watts. Notable achievements include effective control of plume divergence to less than 20° and anode xenon flow reaching 50 standard cubic centimeters per minute (sccm). This study represents a significant advancement in optimizing cylindrical Hall thrusters for enhanced space propulsion applications.

Experimental work revealed two operating modes for the thrusters: low current mode and high current mode. Typically operating in the high current mode when the mass flow rate is high and anode voltage is low, the central leak path inside the channel played a significant role in forming a potential drop near the channel exit, hindering the establishment of a strong electric field. A fluid model was designed based on the study of electron transfer paths in the channel, outlining two electron transfer paths.

The study (Yongjie et al., 2018) presents experimental findings investigating the influence of magnetic field strength in the channel under different discharge voltage conditions. The results reveal a notable trend, wherein weaker magnetic fields correspond to higher efficiency and thrust. Additionally, variations in plume shape observed across different anode voltage conditions are attributed to ion adjustments, providing valuable insights into the intricacies of electric propulsion systems.

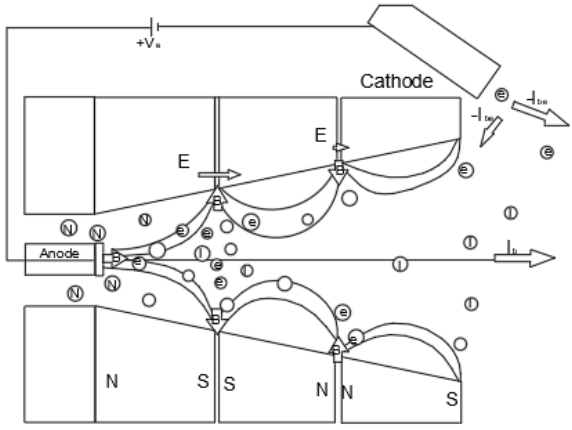

Figure 17. Cusped field thruster

REFERENCES

Beattie, J., & Penn, J. (1989). Electric Propulsion - A national capability. 25th Joint Propulsion Conference. doi:10.2514/6.1989-2490

Burton, R. L., & Turchi, P. J. (1998). Pulsed plasma thruster. Journal of Propulsion and Power, 14(5), 716–735. doi:10.2514/2.5334

Herdrich, G., Bauder, U., Bock, D., Eichhron, C., Haag, D., & Lau, M. (2009). Activities in electric propulsion development at IRS. Transactıons Of The Japan Socıety For Aeronautıcal And Space Scıences, Space Technology Japan, 7(ists26). doi:10.2322/tstj.7.tb_5

Jordan, I. J. E. (2000). Electric Propulsion: Which One For My Spacecraft? In V. Pisacane (Ed.), Space Systems I (pp. 744). Submitted December 6, 2000, as part of requirements for 744 Space Systems I course at JHU, Whiting School of Engineering.

Kim, V., & Popov, G. (2001). Electric Propulsion Activity in Russia. Research Institute of Applied Mechanics and Electrodynamics of Moscow Aviation Institute (RIAME MAI), 2. Leningradskoye shosse, P.O.box 43, Moscow 125080, Russia.

Knoll, A., Lamprou, D., Lappas, V., Pollard, M., & Bianco, P. (2015). Thrust Balance Characterization of a 200 W quad confinement thruster for high thrust regimes. IEEE Transactions on Plasma Science, 43(1), 185–189. doi:10.1109/tps.2014.2323417

Kodys, A., & Choueiri, E. (2005). A critical review of the state-of-the-art in the performance of applied-field magnetoplasmadynamic thrusters. 41st AIAA/ASME/SAE/ASEE Joint Propulsion Conference &Amp; Exhibit. doi:10.2514/6.2005-4247

Kokura, H., Yoneda, S., Nakamura, K., Mitsuhira, N., Nakamura, M., & Sugai, H. (1999a). Diagnostic of surface wave plasma for oxide etching in comparison with inductive RF plasma. Japanese Journal of Applied Physics, 38(9R), 5256. doi:10.1143/jjap.38.5256

Lane, O., & Knoll, A. K. (2015, July). Quad confinement thruster–industrialisation & flight integration. In 34th International Electric Propulsion Conference Proceedings.

Levchenko, I., Goebel, D. M., & Bazaka, K. (2022). Electric propulsion of spacecraft. Physics Today, 75(9), 38–44. doi:10.1063/pt.3.5081

Martinez-Sanchez, M., & Pollard, J. E. (1998). Spacecraft Electric Propulsion-an overview. Journal of Propulsion and Power, 14(5), 688–699. doi:10.2514/2.5331

Mickelsen, W. R. (1967). Auxiliary and primary electric propulsion - present and future. Journal of Spacecraft and Rockets, 4(11), 1409–1423. doi:10.2514/3.29107

Pottinger, S. J., & Scharlemann, C. A. (2007, September). Micro pulsed plasma thruster development. In Proceedings of the 30th International Electric Propulsion

Conference, Florence, Italy (pp. 17-20).

Pröfrock, D., & Prange, A. (2012a). Inductively coupled plasma–mass spectrometry (ICP-MS) for Quantitative Analysis in Environmental and Life Sciences: A Review of Challenges, solutions, and Trends. Applied Spectroscopy, 66(8), 843–868. doi:10.1366/12-06681

Rosati Azevedo, E., Tirila, V. G., Schwertheim, A., & Knoll, A. (2021, March 17–19). Magnetic Field Enhancement of the Quad Confinement Thruster (QCT): Design and Early Development of the QCT Phoenix. Presented at the Space Propulsion 2020, Estoril, Portugal.

Schmidt, T. D. (2005). Bemannte missionen zum Mars mit kontinuierlichen antrieben (Master's thesis). Institute of Space Systems (IRS), Stuttgart.

Soltanpour, P. N., Johnson, G. W., Workman, S. M., Jones, J. B., & Miller, R. O. (2018a). Inductively coupled plasma emission spectrometry and inductively coupled plasma-mass spectrometry. SSSA Book Series, 91–139. doi:10.2136/sssabookser5.3.c5

Stephenson, R. R. (1995, September). Electric propulsion development and application in the United States. In Proceedings of the 24th International Electric Propulsion Conference, Moscow (Vol. 1, pp. 95-1).

Sugai, H., Ghanashev, I., & Nagatsu, M. (1998a). High-density flat plasma production based on Surface Waves. Plasma Sources Science and Technology, 7(2), 192–205. doi:10.1088/0963-0252/7/2/014

Tahara, H., & Nishida, M. (1999). Overview of electric propulsion activity in Japan. 35th Joint Propulsion Conference and Exhibit. doi:10.2514/6.1999-2159

Tahara, H. (2003). An Overview of Electric Propulsion Activities in Japan. In 28th International Electric Propulsion Conference, Toulouse.

Tajmar, M. (2003). Electric Propulsion Systems. Advanced Space Propulsion Systems, 73–98. doi:10.1007/978-3-7091-0547-4_6

Takahashi, K., Lafleur, T., Charles, C., Alexander, P., Boswell, R. W., Perren, M., … Lamprou, D. (2011). Direct thrust measurement of a permanent magnet Helicon Double Layer Thruster. Applied Physics Letters, 98(14). doi:10.1063/1.3577608

Yongjie, D., Hong, L., Liqiu, W., Yanlin, H., Yan, S., Hui, L., … Daren, Y. (2018). Overview of hall electric propulsion in China. IEEE Transactions on Plasma Science, 46(2), 263–282. doi:10.1109/tps.2017.2776257

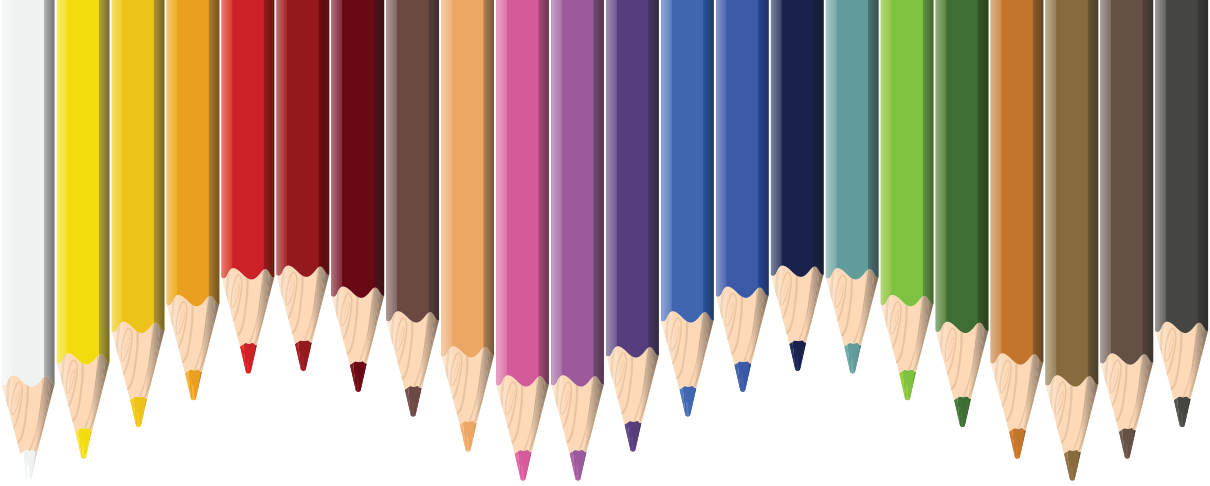

Chapter 4

BASICS OF LAB-ON-A-CHIP

Emrah KAPLAN[1]

1 Dr. ,Gümüşhane Üniversitesi, Mühendislik ve Doğa Bilimleri Fakültesi, Elektrik- Elektronik Mühendisliği Bölümü, ekaplan@gumushane.edu.tr, Orcid no: 0000-0002-2350-7424

1. INTRODUCTION

The point of care (POC) concept refers to medical diagnostic tests performed where patients receive care (Jung et al., 2015). These tests are usually performed using simple and easy-to-use devices that provide fast results. Lab-on-a-Chip (LoC) technologies play an important role in the implementation of the POC approach. For example, POC devices developed using LoC technologies can provide faster, more sensitive, cheaper, more comfortable for the patient, and more efficient diagnosis and treatment results compared to traditional laboratory tests. This further increases the advantages of the POC approach.

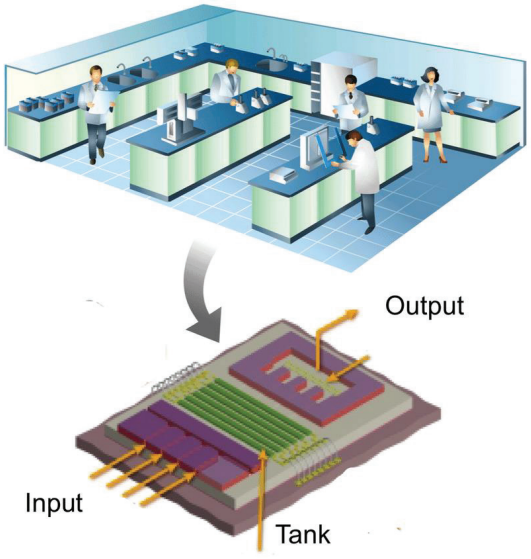

Figure 1. Figural description of LoC format. Thanks to advances in the LoC format, the need for classical laboratories at least one room in size with desktop or larger-sized devices will decrease in the future and living comfort will increase (Salmon, 2014).

Technological advances in micro- and nanofabrication steps have led to the development of impressive, miniaturized technologies for personalized care and health management. These developments have led to the emergence of various miniaturization technologies reported worldwide, especially in the fields of health, environmental protection, and food safety, and have enabled the production of more efficient and miniaturized sensors. The growth of the biosensor industry has increased the demand for devices that offer rapid detection, especially in accordance with the POC concept, and can be applied in environments close to the end user. This increase in demand has greatly affected the market attractiveness of sensing devices worldwide. In

this context, LoC devices have started a new era in the practical applications of miniaturized sensors with their portable size and fast analysis capabilities. When these sensors are integrated into LoC devices, they can facilitate testing and provide fast and effective health, environmental and process monitoring solutions. This integration transforms approaches to diagnosis and monitoring, both in laboratory environments and in the field, and enables it to reach a wide range of users. The current shape and future potential of the biosensor market will play a role in increasing the evolution of LoC technologies and the demand for these innovative devices from healthcare and other sectors.

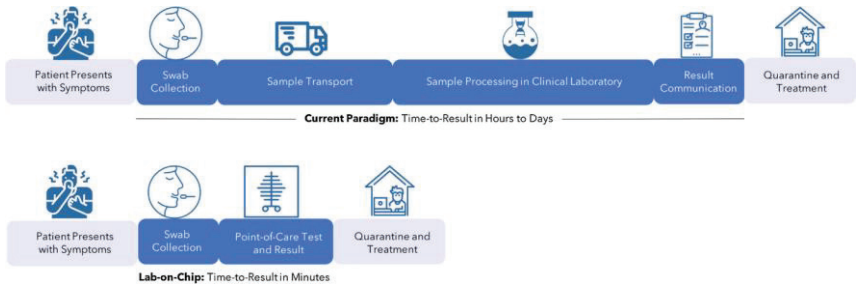

Figure 2. How might a LoC diagnosis impact a patient's workflow? Current classic diagnostic workflows include collecting samples, transporting them, processing them, and delivering the results to the patient. (Bottom) LOC technologies enable on-chip POC tests with results in minutes (Carly Tymm et al., 2020).

This book chapter discusses the basic concepts, working mechanisms and applications of LoC technologies. In particular, a comprehensive review has been conducted regarding how microfluidic systems can be used (Whitesides, 2006), various types of sensors and detectors, and examination of various materials and fabrication methods. Additionally, it focuses on how these technologies can create change in areas such as health, environmental analysis and biological research.

1.1. LoC and Historical Development

Another name for LoC devices is Micro-total analytical systems (μ-TAS) (Hanke & Dittrich, 2012). LoC technology aims to perform different laboratory functions on a single chip and on a much smaller scale. This technology was developed to speed up, simplify, reduce product and personnel costs, and use fewer samples and reagents. LoC devices generally use microfluidic systems to direct liquids in microliter volumes and then perform biological and chemical analyzes with the measurement systems inside.

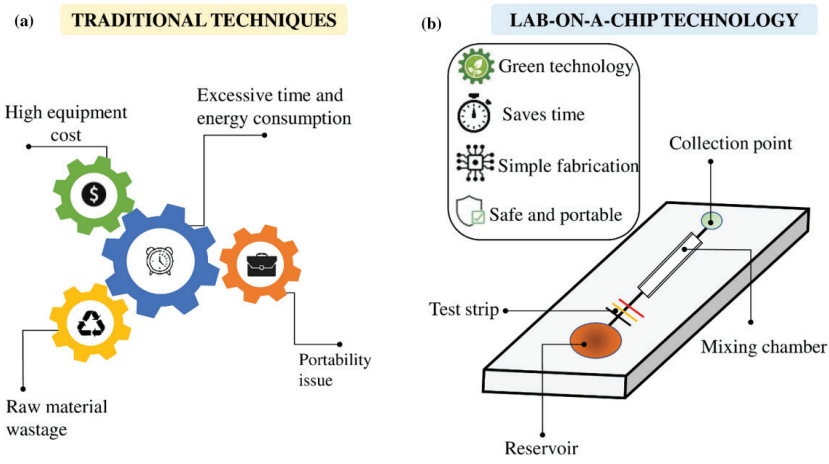

Figure 3. What are the differences between traditional techniques and LoC technology? LoC technology is the name given to miniature devices that perform multiple laboratory tasks on a single platform. LoC devices suitable for use in many sectors such as healthcare, agriculture and food can be developed and used in areas such as precise liquid guidance, intensified processing, and analytics. Thanks to LoC, it is possible to benefit from the advantages shown in the picture such as time saving, money saving, less waste and portability (Adithya Sridhar et al., 2021).

In the late 1980s, silicon-based micromachining techniques began to be adapted from the electronics industry to biological and chemical sensor applications (van Lintel et al., 1988). This process led to the development of the first MEMS (Micro Electromechanical Systems) and subsequently the first products of the LoC concept. In the 1990s, with the development of microfluidic systems, the first microliter volume liquid control was achieved, and LoC technology began to gain momentum. Ten years later, LoC devices began to be used in biological and chemical tests such as DNA analysis, protein analysis, cell culture and pathogen detection. In the next stage, with the process of automating the devices, the need for an experienced operator was eliminated and multiple operations could be performed on a single device. Nowadays, with the application of artificial intelligence to LoC technology, new areas of work have emerged on targets such as the production of personalized devices and faster diagnosis.

Advances in LoC technology have allowed to produce more efficient devices and greater testing opportunities. These innovations have significantly improved people's quality of life because costs have decreased, the need for professional operators has decreased, and thanks to the POC concept, people can now perform some health tests more frequently and in the comfort of their home. In the future, this technology will continue to further improve people's living comfort by revolutionizing personalized

medicine and rapid diagnosis. Additionally, these advances in the LoC concept will continue to provide significant efficiency gains in the food security, environmental research, and defence sectors.

1.2. Basic Principles and Working Mechanisms

LoC technology is produced and used to perform laboratory functions on a micro-scale platform, where operators work, and large-sized devices are used. This technology is used primarily in biological and chemical analysis. LoC has advantages such as less reagent and sample usage, faster processing times and portability.

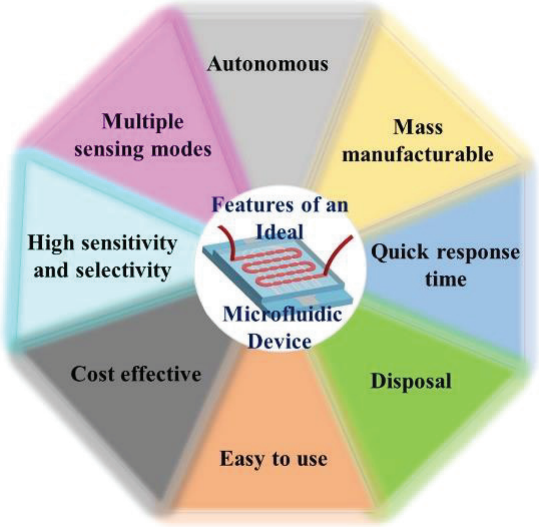

Figure 4. The desired features of an ideal LoC device are presented together in the picture. Being disposable can provide an additional advantage (Aralekallu et al., 2023).

Microfluidics is the most fundamental factor in this type of devices. It covers the processes of directing small volumes of liquids at the level of micrometres or nano filters on the chip and testing them in analysis units produced on the chip. Miniaturization and integration are an important step in laboratory devices. Various laboratory functions are integrated on a single microchip. These functions may include liquid transport, mixing, heating, cooling, performing reactions, separation, and sensing. LoC devices include one or more of a variety of sensors used to detect chemical or biological components of liquids, measuring physical parameters such as temperature or pH. To minimize user intervention, increase the precision of processes, and minimize contamination, LoCs can be supplemented with electronic systems to automatically control the flow of liquids and other processes

(Ahaitouf et al., 2021). The design and LoC operation processes of microchannels are also being developed to reduce the risk of cross-contamination.

The behaviour of liquids in microchannels is different from water flowing in pipes encountered in daily life. Parameters such as surface tension and viscosity become more influential at the microscale and can easily change the flow characteristics. When selecting the materials used in the production of LoC devices (silicon, glass, plastics, etc.), the chemical compatibility, biocompatibility, mechanical properties, and production costs of the device should be considered.

The advantages that make LoC devices special are as follows: Thanks to the use of reagents and samples at very small scales, costs are reduced, the amount of waste is reduced, and experimental results are obtained faster.

To decrease the both the waste level and the cost, LoC devices enable the use of reagents and samples on a very small scale. This also increases the test speed. The ability to automatically perform multiple analytical operations simultaneously increases the efficiency of LoC devices in a shorter tie period. Highly skilled LoC designs can produce results without even needing an expert operator. These principles and advantages enable LoC technology to be used effectively in a wide range of applications. The concept has a potential to revolutionize medical diagnostics, biological research and environmental analysis.

2. BASIC COMPONENTS AND DESIGN

LoC devices basically consist of fluid transducers and sensor parts. There are also micro channels or environments that allow fluid movement that connect these two systems.

2.1. Liquid Displacement Systems

Microfluidic movement is generally accomplished for two main goals which are mixing and manipulating the liquid (Kaplan et al., 2017). The chart below explains about general types of small volume liquids manipulations. Microfluidic fluid manipulation are important parts of the processes, which can be divided into continuous flow microfluidics and digital microfluidics. Mixing and separation (Chia-Fu Chou & Zenhausern, 2003) are two common fluid handling techniques in continuous flow microfluidics. Droplet based and liquid bead based digital microfluidic technologies are used to process individual droplets sepaately (Curtis D. Chin et al., 2012; Mark et al., 2010).

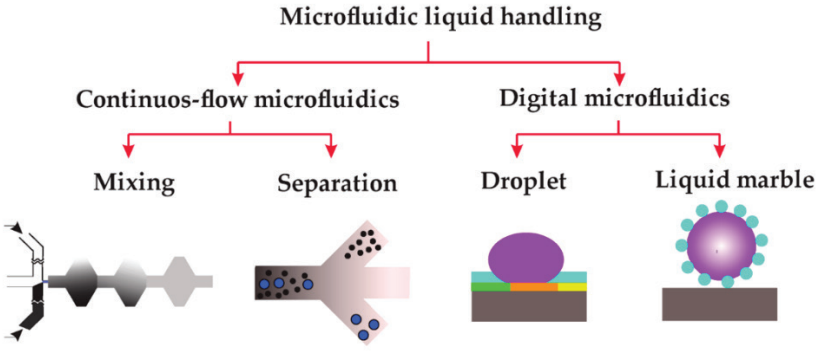

Figure 5. There are two main types of microfluidics: digital microfluidics and continuous-flow microfluidics. Both are used to handle liquids in biological processes. In continuous-flow microfluidics, two common ways to handle liquids are mixing and separating. For manipulating single droplets, droplet-based and liquid-marble-based digital microfluidic technologies are used (Nguyen et al., 2017).

In LoC systems, fluid manipulation occurs through pumps that move the fluid in microchannels and valves that direct the fluid. It is possible to group the fluid translation mechanisms of microfluidic systems by sorting them according to their similar properties to see their relationships. We can divide pressure-driven flow methods into two classes. "Pressure Driven Flow", where micropump like external pressure sources are used to move liquids in the system (Huo et al., 2020), and "Centrifugal Microfluidics", where a disc shaped platform is used to create a centrifugal force (Kimura et al., 2018). Electrical and electromechanical liquid translation methods can be divided into four main methods: electroosmosis, which moves charged particles with an electric field, electrokinetic, which controls liquid movement, electrowetting (Si Kuan Thio & Sung-Yong Park, 2022), which directs droplets by changing the surface tension, and linear actuator devices that push or pull liquid with mechanical actuators. Methods utilizing natural forces and physical principles consist of two main components: the capillary flow method, which is based on surface tension differences and does not require extra energy, and the acoustic wave method, which moves liquids on a microscale with ultrasonic waves (Kaplan et al., 2017a).

2.2. Sensors and Detectors

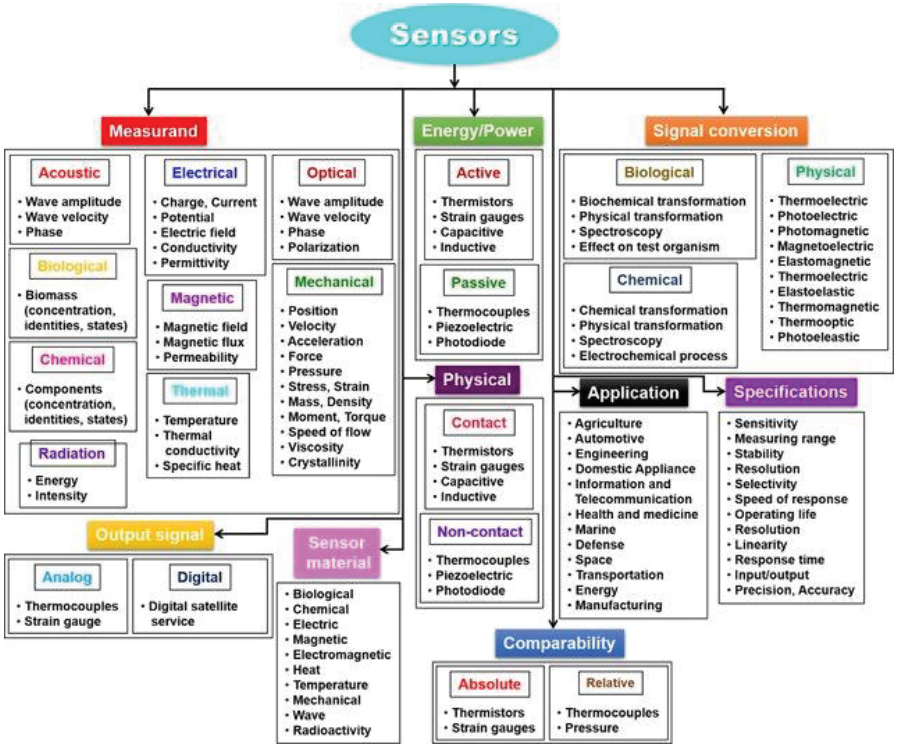

Figure 6. Classification of sensors based on measurement, energy/power, physical contact, signal conversion, output signal, comparability, sensor material, specification, and applications (Naresh & Lee, 2021).

The types of sensors used in LoC platforms are generally designed to detect a variety of biological, chemical and physical properties to make analytical detections and measurements (Arash Ghoorchian et al., 2022). These sensors provide precise and rapid analysis, which is one of the core functions of LoC devices.

Optical sensors are used to measure optical properties such as light absorption, fluorescence, bioluminescence, and phosphorescence. It is especially used to find biological molecules and measure their concentrations. Electrochemical sensors can identify chemical compounds by measuring current changes between electrodes (Kaplan, 2015). These sensors are used to examine pH, oxygen levels, metal ions, and some organic compounds. Thermalsensors are used to monitor biological processes such as temperature changes, enzymatic reactions, or microbial growth. Piezoelectric sensors detect mechanical stress or pressure changes. They measure physical

properties such as flow rate and liquid pressure. Capacitive sensors are used specifically in cellular analysis to detect changes in the electrical properties of the dielectric material (Moser et al., 2019). Sensors that use acoustic waves work using sound waves (specifically cell detection and fluid analysis). Flow rate, fluid pressure, and in some cases even the mechanical properties of the cell are measured by mechanical sensors. Biosensors detect specific biological interactions to identify pathogens, proteins, and other biological molecules (Sengupta et al., 2021). Chemical sensors are used for a range of chemical analysis to find specific chemical compounds or groups. Photonic crystal sensors measure light wavelength changes for very sensitive biological and chemical detections.

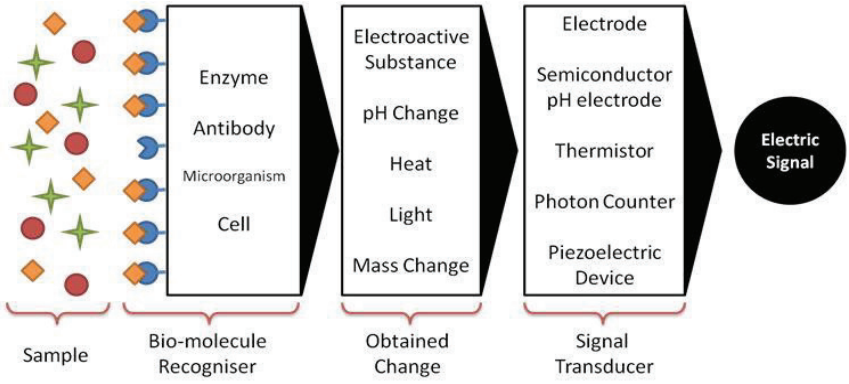

Figure 7. Biosensor components are shown according to the connection between each part of the sensors (Ghoshal et al., 2010).

All these sensors enable the use of LoC devices in a wide range of applications and offer fast, precise, and low-cost analysis in various fields. Each sensor type can be customized for specific types of analyses and applications.

2.3. Integration and Miniaturization

Integration and miniaturization techniques in LoC devices constitute the basic characteristics of these devices. LoC devices are microfluidic systems that perform laboratory operations on very small scales. There are steps to be considered in the process from the design to the production of these devices. First, it must be determined which microflow system will be applied. Material selection is made by looking at parameters such as biocompatibility and the type of chemicals to be used.

LoC devices can conduct complicated processes effectively because to the many functional components (such as sensors, pumps, and valves). To have a fully functional final product it is critical to pay attention to the

integration process during both the design and manufacturing phases. LoC devices may conduct a variety of laboratory activities such as DNA amplification, protein analysis, and cell culture. Extra structures that can conduct activities such as heating, cooling, and optical detection must be microfabricated in the LoC system in order to accomplish numerous operations on the same chip platform.

The required hardware and software must also be incorporated into the LoC system in order to export and analyse the data gathered from the measurements taken by the LoC (Kovarik et al., 2012). While these devices are generally produced by microfabrication methods such as photo lithography, stamping or injection, nanofabrication methods are also used depending on the situation. Proper application of all these systems and techniques increases the ease of use, efficiency, sensitivity, and versatility of LoC devices.

3. PRODUCTION TECHNIQUES AND MATERIALS OPTIONS

The production techniques used in LoC technology are named micro and nano, according to the minimum sizes that can be produced. Details and important features of these techniques are explained below.

3.1. Microfabrication Methods

Microfabrication involves a set of processes used to produce LoC and all other miniaturized devices. Microfabrication methods are generally applied in three different ways, but in recent years, a fourth method, 3D printer option, has been added to these. 3D printing is becoming an increasingly preferred method in prototyping processes of microfluidic devices. Increasing resolutions make it possible to print features at the level of hundreds of microns, and with the new filament types developed (such as COC filaments), results close to the currently used methods can be obtained.

3.1.1. Photolithography

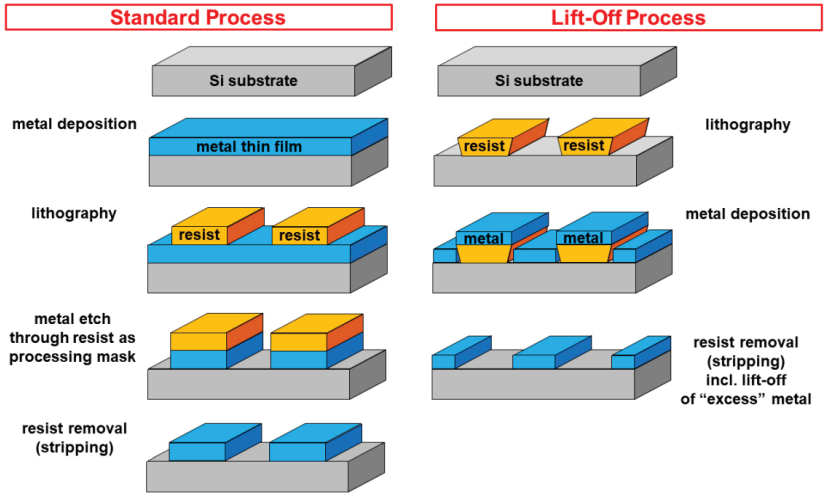

Figure 8. The image shows two photolithographic microfabrication processes. In the standard process (Left), when the Lift off process is applied (Right). The lift-off method is preferred when it is necessary to create more precise patterns(Atkinson et al., 2023).

Photoresists used in the photolithography process are light-sensitive materials and are very important for creating precise patterns in microfabrication processes. Since these polymer layers undergo chemical change under a certain light spectrum, their determined parts are made more rapidly soluble with the help of a mask and light (Qin et al., 2010). The transfer of micro-scale patterns to surfaces is achieved with the help of this logic.

The figure shows two photolithographic microfabrication processes. In the standard process (Left), metal is first deposited onto a silicon substrate, then coated with a lithographically engineered material (photo resist). The exposed metal is etched away to reveal the metal pattern and any remaining resist is removed. When the Lift-off process is applied (Right), first the resistor design and metal deposition occur, and then the resistor is removed by taking the metal on top of it. This leaves a clean pattern that does not need to be engraved. This process is very useful for creating precise patterns where etching may compromise precision (Lin Lin & Chen-Kuei Chung, 2021).

3.1.2.Soft Lithography

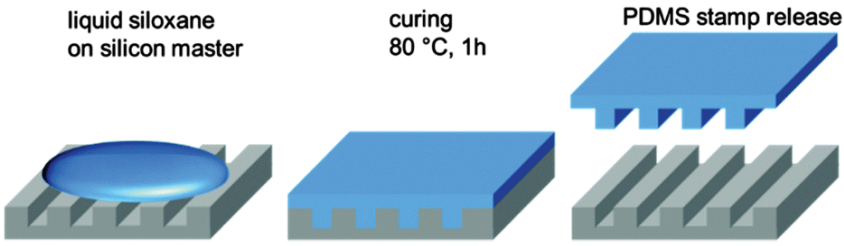

Figure 9. The process of creating a PDMS stamp consists of pouring siloxane oligomer liquid onto a patterned silicon wafer, thermally curing it, and then releasing it from the mould to obtain a flexible copy (M. Wisser et al., 2015).

Soft lithography, a technique pioneered in the early 90s, is a vital microfabrication method for creating micro- and nanoscale patterns, especially in the fields of biotechnology, nanotechnology, and microelectronics (Dkhar et al., 2023). Using elastomeric stamps, often made from materials such as PDMS, it copies patterns onto a variety of substrates, bypassing the complexity and high costs of traditional photolithography. It is widely used in the efficient fabrication of microfluidic devices, biosensors, and metal nanostructures in fields such as opto-electronics and plasmonics, favouring environmentally friendly bottom-up methods over top-down etching, especially where uniformity and precise alignment are less critical.

In the soft lithography process, a master mould with the desired pattern is created; an elastomeric material (usually PDMS) is poured onto it. It is hardened to form a solid yet flexible replica; this is then separated from the mould. The structures produced by this method are used as micro-channels or to transfer any material to another target surface.

3.1.3.Injection Moulding

Injection moulding is an optimal method for mass producing LoC devices owing to its cost-effectiveness and excellent efficiency. Initially, a mould is fabricated to correspond with the dimensions and characteristics of the LoC device under consideration.

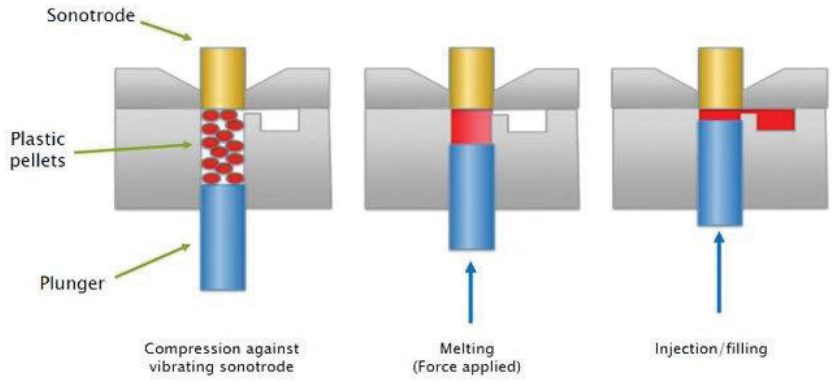

Figure 10. The steps applied in production with injection moulding are as follows. Mold design and production, polymer melting, injecting, cooling solidification and product removal. Thanks to the Sonotrode, which provides vibration during injection, all mould details are filled with molten polymer (Gülçür et al., 2018).

The cavities and chambers of the apparatus are precisely defined at the microscale within these metal moulds. The mould is inflated with high-pressure molten thermoplastic polymers that are suitable for the intended application of the LoC device. The molten polymer completely fills the mould components due to the application of pressure. Upon cooling and solidifying in the mould, every aspect of the LoC gadget becomes apparent. The finished product is extracted from the mould for a further processing or assembling on a specific location. Overall, this technique is well-suited for large-scale manufacturing of devices with detailed microfluidic structures with minimal mistake.

3.1.4.3D Fabrication

3D printer technology is increasing its popularity today and has even begun to be used at home. Different 3D fabrication technologies are available on the market, including stereolithography (SLA), digital micromirror device-based projection printing (DMD-PP), two-photon polymerization (2PP), fused filament fabrication (FFF), inkjet, and bioprinting (Dkhar et al., 2023). These technologies are especially suitable for LoC designs that have complex geometry and whose manufacturing process takes a lot of time with classical methods. Thanks to the use of various hydrophobic materials in printers, low-cost personalized LoC devices can be prototyped quickly and in a single step (Karayannis et al., 2019).

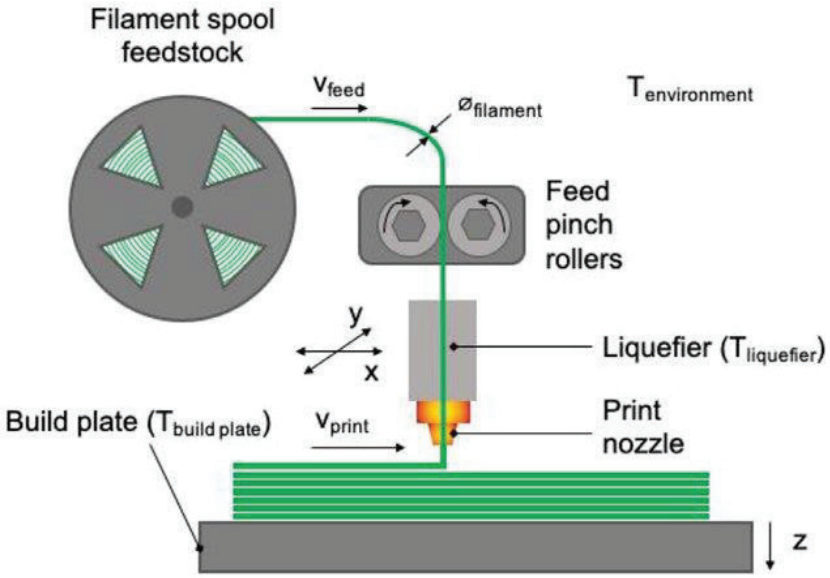

Figure 11. Schematic drawing of a 3D printer mechanism and its working logic. It fabricates structures with Fused Filament Fabrication (FFF) technique which has potential to be used for rapid LoC device prototyping (Vaes & Van Puyvelde, 2021).

Necessity of controlling optical characteristics and surface roughness is a drawback of 3D printing. It is crucial to control during the print in order not to have a failed product before wasting more time.

Health and safety issues, particularly ultrafine particle, and Volatile Organic Compound (VOC) emissions, are also important factors to consider. Researchers emphasize the importance of security and risk management in the early stages of device design and development for the safe production of LoC devices.

3.2. Nanofabrication (Electron Beam Lithography)

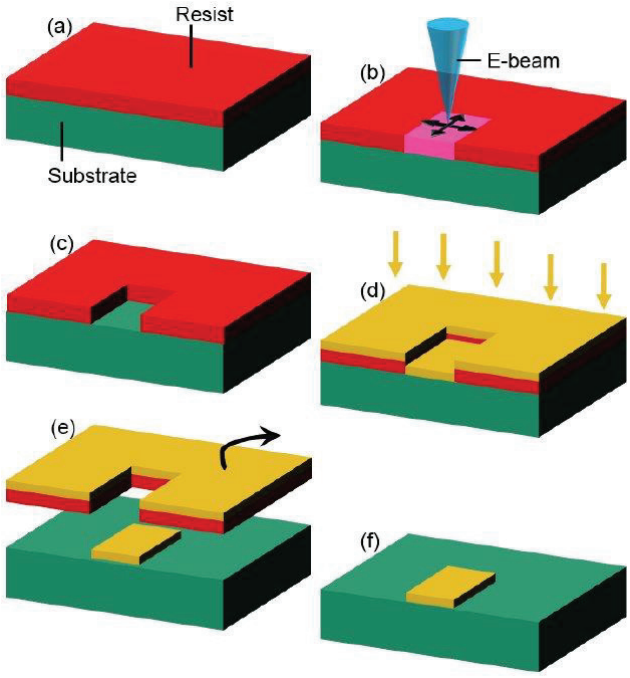

Figure 12. Major EBL steps (Bauman, 2015).

The Electron beam lithography (EBL) process has very similar application stages to photolithography method. However, since the wavelength of the electron beam is smaller than the UV beam, it can be reduced to nano sizes instead of micro. In other words, it allows creating higher resolution, smaller sized structures. EBL offers the advantage of creating custom patterns with exceptional precision by reaching sizes below 10 nanometres (Bauman, 2015).

EBL systems use electrostatic or magnetic lenses to concentrate the electron beam. The concentrated electron flow is passed over a special layer of electron-sensitive material called photoresist, creating detailed designs with high accuracy on this surface. The electron beam changes the resolution of the resist so that, after applying solvent liquid in the resist development process, specific regions are removed from the surface in accordance with the targeted pattern. Commercial EBL systems are expensive investments. However, for research purposes it is possible to convert the electron microscope to an EBL system at a lower cost.

3.3. Production Materials

Polydimethylsiloxane (PDMS) is widely used in microfluidic prototyping due to its ability to rapidly form fine surface features using cold casting. It has mechanical properties that make it unsuitable for commercial use and adsorbs small hydrophobic molecules (Lin Lin & Chen-Kuei Chung, 2021). In LoC production, glass appears as an alternative material in drums where optical transmittance, high strength, thermal and chemical stability are required (Howie, 2022). Newly developed thermoplastic soft elastomers are emerging as an alternative to PDMS. A variety of technical thermoplastic polymers can be used for LoC applications, such as PMMA, PS, PC and COC. They are chemically resistant, optically clear, and compatible with numerous manufacturing and connection methods, making them suitable. During the production processes, appropriate materials are selected by considering the thermal, mechanical, chemical, optical and biological requirements of the LoC device planned to be produced. Below are the advantages and disadvantages of these materials (Howie, 2022).

	COC	PMMA	Polystyrene	Polycarbonate
Mechanical properties	Good	Very Good High aspect ratio features possible.	Good	Good
Thermal properties	Very Good Certain grades can have a high glass transition temp.	Good	OK Low continuous service temperature relative to glass transition.	Very Good Can sustain temperatures close to glass transition temp for long periods.
Chemical resistance	Very Good Resistant to strong acids and bases. Dissolved by some hydrocarbons and aldehydes and ketones can cause swelling.	Good Weak acids and bases may cause swelling. Dissolved by some hydrocarbons including alcohols.	Good Resistant to weak acids and bases but dissolved by strong acids and some hydrocarbons.	OK Generally resistant to alcohols but other hydrocarbons and many bases can cause crystallization and cracking.
Optical properties	Very good High transmission and low autofluorescence. Very low haze.	Good High transmission and low autofluorescence in visible spectrum.	OK Good optical transmission but high autofluorescence typically peaking around ~500 nm.	OK Good optical transmission but high autofluorescence typically peaking around ~400 nm.

Table 1. Properties of engineering polymers commonly used in LoC devices (Howie, 2022).

In cases where chemical compatibility is required, glass and silicone can be preferred as alternatives to polymers; these materials can be processed

and patterned with wet or dry lithography techniques but are generally more costly than polymers.

Hydrogels are water-based hydrophilic polymer networks that resemble an extracellular matrix and are used as cell supports, but they offer less detailed microfabrication than other polymers due to their low density and strength.

While the paper used in microfluidic paper-based analytical devices offers an economical option as well as being flexible, cellulose-based, and biocompatible, it is a substrate suitable only for certain applications due to its weak mechanical properties and limited technological possibilities.

In Lab-on-Chip (LoC) devices, conductive materials are critical for signal transmission and sensor applications. In this field, obtaining surface modulation by methods such as compression and sintering of copper powders or electroless coating can offer innovative approaches in the development of electrode materials (Ekmekci et al., 2017; Ekmekci & Bülbül, 2015). Such methods have the potential to improve the performance and efficiency of LoC devices and can contribute to making the devices more effective and responsive.

As a result, it is stated that although glass and silicone are important materials, polymers have become the material of choice in this field, as well as research in microfluidic technology focusing on biological and medical applications. While PDMS continues to be widely used, R&D studies on new materials and composites with unusual properties continue.

3.4. LoC Challenges and Quality Control

The fabrication of LoC devices is fraught with unique challenges arising from the complexity of micro- and nanoscale manufacturing processes and the challenges of integrating different technologies. Manufacturing errors or a microscale dust particle that cannot be seen with the naked eye can cause devices to become unfunctional. In addition, high prototype production costs and durability and reliability problems of the devices are also important sources of concern.

Additionally, there are challenges in the prototype development process, such as lowering detection limits, increasing sensitivity and specificity, combining electronic and biological systems, and integrating functions such as sensing and liquid manipulation. As shown in the graph below, the low portability of some high-precision measurement methods is another factor that limits the effectiveness of these devices in field applications. This may impact the uses of LoC technologies, especially when combined with efforts to reduce the size of laboratory instruments and sample volumes. These

problems negatively affect the development and dissemination of LoC technologies.

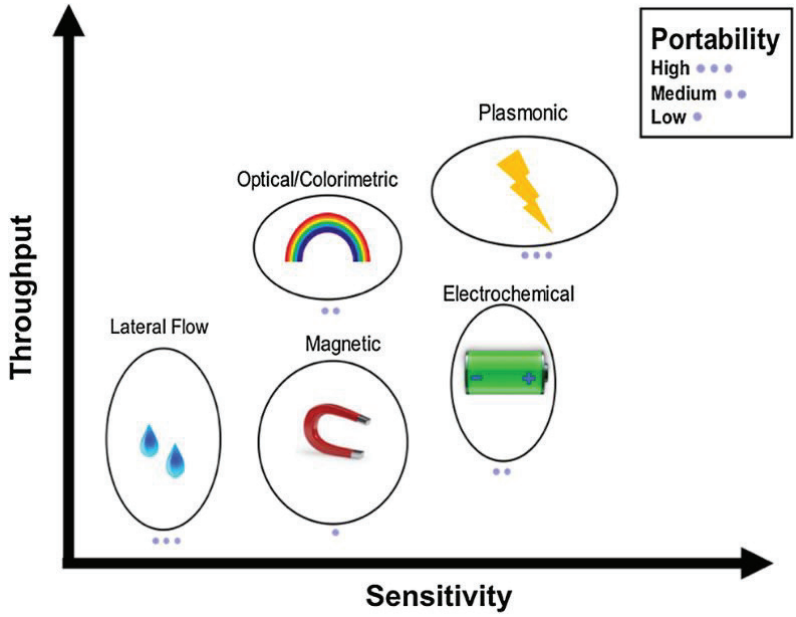

Figure 13. Technology Summary. Summary of nano-scale biosensing methods reviewed with comparison of throughout capability, sensitivity, and portability trends broadly estimated from literature on the axes (Carly Tymm et al., 2020).

LoC devices should be aimed to be produced as user-friendly concepts, but this alone will not be sufficient. To be able to fully trust the device results, users must be ensured to learn the correct use of the devices, the interpretation of the results and how to solve common problems.

Schematic drawings representing fabrication processes are helpful for visually understanding the complexity and detailed nature of these processes. However, each of these processes is highly technical and prone to problems. For example, even if you make the same production on a different device or in a different laboratory, you may need to update the parameters in your production recipe again. For this reason, patience, attention, and practical experience are required during the design and production to obtain accurate and quality production results.

The quality control processes of LoC devices ensure that the products are of high quality and meet all standards at every stage of production. Checking the quality of raw materials is the first step in this process. The

quality of intermediate products is constantly tested during the production process, so that possible errors can be quickly found and corrected. Functional tests ensure that the device performs as expected. These tests measure the reliability and performance of the device. It goes through a series of tests and inspections to ensure that the product meets all quality and performance standards. LoC devices can be certified, and conformance tested to ensure they comply with certain standards and rules. This rigorous procedure ensures that the device meets the highest quality and performance standards before reaching the customer.

Interdisciplinary collaboration, advanced sensor technologies, creative device design and high-precision manufacturing techniques are required to overcome the challenges. The development and implementation of LoC technology will be possible by integrating various technological fields and applying micro/nanoscale engineering approaches (Georgios Manessis et al., 2022).

4. CONCLUSION

LoC technologies have the potential to improve human comfort, highlight the importance of early diagnosis, and provide affordable healthcare solutions. Sensitive sensors can detect diseases in the early stages even with minimal sample quantities, thus significantly increasing the chances of treating serious diseases, especially cancer. With LoC, there may be an opportunity to increase access to health services and reduce health inequalities by making advanced health technologies available to wider audiences at affordable prices. All these technologies can improve the overall quality of human life by simplifying health monitoring and diagnostic processes.

Apart from healthcare and biotechnology, LoC technologies can also offer innovative solutions in sectors such as automotive and defence. In the automotive industry, protecting passenger health by monitoring in-vehicle air quality; In the field of defence, it can make contributions such as increasing security measures by quickly detecting biological and chemical threats. In addition, it can undertake important functions in the food industry such as performing contamination tests, constantly controlling the cold chain, ensuring food safety, and detecting environmental risks early by constantly monitoring water and air quality within the scope of environmental monitoring.

If LoC devices are supported by artificial intelligence and internet of things concepts, much more innovative results will emerge. Secondly, memristors are a new circuit element that is still being developed and can store information without requiring energy (Gul & Efeoglu, 2017). Thanks to

the energy efficiency feature of these components, it can be very advantageous to produce Lab-on-Chip (LoC) devices that are more efficient and consume less energy. Interdisciplinary collaboration and innovative design approaches are vital for the development of LoC technologies. However, policymakers can increase both scientific and societal benefits by making regulations and investments that will encourage the advancement of this technology. The development and dissemination of LoC technologies has the potential to create social and economic benefits by improving early diagnosis and disease management in healthcare, while providing innovative solutions in a wide range of areas, from automotive to defence. These technologies are critical for a healthier, safer, and more sustainable society.

As a result, LoC technologies can reach large audiences and make significant contributions to areas such as health, security, and environmental sustainability. Understanding the potential of these technologies and using them effectively will be possible with public awareness and the support of policy makers. Therefore, scientific fairs and events for the public can contribute to the development of these and similar critically important technologies and increase their social benefits.

5. REFERENCES

Adithya Sridhar, Kapoor, A., Kumar, P. S., Kumar, P. S., Muthamilselvi Ponnuchamy, Ponnuchamy, M., Sivasamy Balasubramanian, Sivasamy, B., Jang, H. W., & Vo, D.-V. N. (2021). Lab-on-a-chip technologies for food safety, processing, and packaging applications: A review. *Environmental Chemistry Letters*, 1–27. https://doi.org/10.1007/s10311-021-01342-4

Ahaitouf, A., Norshah Rizal Ali, Ahaitouf, A., Mohd Zaid Abdullah, Abdullah, M. Z., & Abdullah, M. Z. (2021). Irreversible bonding techniques for the fabrication of a leakage-free printed circuit board-based lab-on-chip in microfluidic platforms—A review. *Measurement Science and Technology*, *32*(5), 052001. https://doi.org/10.1088/1361-6501/abeb92

Aralekallu, S., Boddula, R., & Singh, V. (2023). Development of glass-based microfluidic devices: A review on its fabrication and biologic applications. *Materials & Design*, *225*, 111517. https://doi.org/10.1016/j.matdes.2022.111517

Arash Ghoorchian, Mahdie Kamalabadi, Mahdie Kamalabadi, Zahra Amouzegar, Nahid Rezvani Jalal, Hazem M. Abu Shawish, Hazem M. Abu Shawish, Salman M. Saadeh, Salman M. Saadeh, Abbas Afkhami, Tayyebeh Madrakian, Sabu Thomas, Tuan Anh Nguyen, & Mazaher Ahmadi. (2022). *Lab-on-a-chip miniaturized analytical devices*. 261–284. https://doi.org/10.1016/b978-0-12-823727-4.00003-1

Atkinson, N., Morhart, T. A., Wells, G., Flaman, G. T., Petro, E., Read, S., Rosendahl, S. M., Burgess, I. J., & Achenbach, S. (2023). Microfabrication Process Development for a Polymer-Based Lab-on-Chip Concept Applied in Attenuated Total Reflection Fourier Transform Infrared

Spectroelectrochemistry. *Sensors*, *23*(14), Article 14. https://doi.org/10.3390/s23146251

Bauman, S. (2015). *Fabrication of Sub-10 nm Metallic Structures via Nanomasking Technique for Plasmonic Enhancement Applications*.

Carly Tymm, Tymm, C. C., Junhu Zhou, Zhou, J., Tadimety, A., Burklund, A., & Zhang, J. X. J. (2020). Scalable COVID-19 Detection Enabled by Lab-on-Chip Biosensors. *Cellular and Molecular Bioengineering*, *13*(4), 1–17. https://doi.org/10.1007/s12195-020-00642-z

Chia-Fu Chou, & Zenhausern, F. (2003). Electrodeless dielectrophoresis for micro total analysis systems. *IEEE Engineering in Medicine and Biology Magazine*, *22*(6), 62–67. https://doi.org/10.1109/MEMB.2003.1266048

Curtis D. Chin, Chin, C. D., Linder, V., & Sia, S. K. (2012). Commercialization of microfluidic point-of-care diagnostic devices. *Lab on a Chip*, *12*(12), 2118–2134. https://doi.org/10.1039/c2lc21204h

Dkhar, D. S., Kumari, R., Malode, S. J., Shetti, N. P., & Chandra, P. (2023). Integrated lab-on-a-chip devices: Fabrication methodologies, transduction system for sensing purposes. *Journal of Pharmaceutical and Biomedical Analysis*, *223*, 115120. https://doi.org/10.1016/j.jpba.2022.115120

Ekmekci, D., & Bülbül, F. (2015). Preparation and characterization of electroless Ni–B/nano-SiO2, Al2O3, TiO2 and CuO composite coatings. *Bulletin of Materials Science*, *38*(3), 761–768. https://doi.org/10.1007/s12034-015-0912-1

Ekmekci, D., Yılmaz, F., Kölemen, U., & Cora, Ö. N. (2017). Microindentation on the porous copper surface modulations. *Applied Physics A*, *123*(11), 705. https://doi.org/10.1007/s00339-017-1327-1

Georgios Manessis, Gelasakis, A. I., & Ioannis Bossis. (2022). Point-Of-Care Diagnostics for Farm Animal Diseases: From Biosensors to Integrated Lab-On-Chip Devices. *Biosensors*, *12*(7), 455–455. https://doi.org/10.3390/bios12070455

Ghoshal, S., Mitra, D., Roy, S., & MAJUMDER, D. (2010). Biosensors and Biochips for Nanomedical Applications: A Review. *Sens. Transducers J.*, *113*, 1–17.

Gul, F., & Efeoglu, H. (2017). Bipolar resistive switching and conduction mechanism of an Al/ZnO/Al-based memristor. *Superlattices and Microstructures*, *101*, 172–179. https://doi.org/10.1016/j.spmi.2016.11.043

Gülçür, M., Whiteside, B., Nair, K., Babenko, M., & Coates, P. (2018). *Ultrasonic injection moulding of polypropylene and thermal visualisation of the process using a bespoke injection mould tool*.

Hanke, C., & Dittrich, P. S. (2012). Small – smaller – μTAS. *Analytical and Bioanalytical Chemistry*, *403*(1), 5–6. https://doi.org/10.1007/s00216-012-5855-4

Howie, A. N., Philip. (2022, September 20). *Lab-on-chip devices: Materials considerations*. Med-Tech Innovation. https://www.med-technews.com/api/content/960c5188-35d2-11ed-811e-12274efc5439/

Huo, C., Bai, C., & Zhang, P. (2020). Micropumps for Microfluidic Devices and BioMEMS. *Journal of Physics: Conference Series*, *1626*(1), 012040. https://doi.org/10.1088/1742-6596/1626/1/012040

Jung, W., Han, J., Choi, J.-W., & Ahn, C. H. (2015). Point-of-care testing (POCT) diagnostic systems using microfluidic lab-on-a-chip technologies.

Microelectronic Engineering, *132*(132), 46–57. https://doi.org/10.1016/j.mee.2014.09.024

Kaplan, E. (2015). *Surface acoustic wave enhanced electroanalytical sensors* [PhD Thesis, University of Glasgow]. https://theses.gla.ac.uk/6557/

Kaplan, E., Oğuz, Y., Gül, F., & Eroğlu, H. (2017a). *Highly Efficient Acoustic Micro-Actuators*. http://acikerisim.gumushane.edu.tr/xmlui/handle/20.500.12440/1897

Kaplan, E., Oğuz, Y., Gül, F., & Eroğlu, H. (2017b). *Reusable Micro-Mixers*. http://acikerisim.gumushane.edu.tr/xmlui/handle/20.500.12440/1898

Karayannis, P., Petrakli, F., Gkika, A., & Koumoulos, E. P. (2019). 3D-Printed Lab-on-a-Chip Diagnostic Systems-Developing a Safe-by-Design Manufacturing Approach. *Micromachines*, *10*(12), Article 12. https://doi.org/10.3390/mi10120825

Kimura, H., Sakai, Y., & Fujii, T. (2018). Organ/body-on-a-chip based on microfluidic technology for drug discovery. *Drug Metabolism and Pharmacokinetics*, *33*(1), 43–48. https://doi.org/10.1016/j.dmpk.2017.11.003

Kovarik, M. L., Gach, P. C., Gach, P., Ornoff, D. M., Yuli Wang, Wang, Y., Balowski, J., Lila Farrag, Farrag, L., & Allbritton, N. L. (2012). Micro total analysis systems for cell biology and biochemical assays. *Analytical Chemistry*, *84*(2), 516–540. https://doi.org/10.1021/ac202611x

Lin Lin & Chen-Kuei Chung. (2021). PDMS Microfabrication and Design for Microfluidics and Sustainable Energy Application: Review. *Micromachines*, *12*(11), 1350. https://doi.org/10.3390/mi12111350

Mark, D., Haeberle, S., Roth, G., Felix von Stetten, von Stetten, F., & Zengerle, R. (2010). Microfluidic lab-on-a-chip platforms: Requirements, characteristics and applications. *Chemical Society Reviews*, *39*(3), 1153–1182. https://doi.org/10.1039/b820557b

Moser, N., Keeble, L., Rodriguez-Manzano, J., & Georgiou, P. (2019). ISFET Arrays for Lab-on-Chip Technology: A Review. *International Conference on Electronics, Circuits, and Systems*, 57–60. https://doi.org/10.1109/icecs46596.2019.8965034

M. Wisser, F., Schumm, B., Mondin, G., Grothe, J., & Kaskel, S. (2015). Precursor strategies for metallic nano- and micropatterns using soft lithography. *Journal of Materials Chemistry C*, *3*(12), 2717–2731. https://doi.org/10.1039/C4TC02418D

Naresh, V., & Lee, N. (2021). A Review on Biosensors and Recent Development of Nanostructured Materials-Enabled Biosensors. *Sensors*, *21*(4), Article 4. https://doi.org/10.3390/s21041109

Nguyen, N.-T., Hejazian, M., Ooi, C. H., & Kashaninejad, N. (2017). Recent Advances and Future Perspectives on Microfluidic Liquid Handling. *Micromachines*, *8*(6), Article 6. https://doi.org/10.3390/mi8060186

Qin, D., Xia, Y., & Whitesides, G. M. (2010). Soft lithography for micro- and nanoscale patterning. *Nature Protocols*, *5*(3), Article 3. https://doi.org/10.1038/nprot.2009.234

Salmon, H. (2014). *Mobile Magnetic Microrobots Control and Study in Microfluidic Environment: New Tools for Biomedical Applications*.

Sengupta, J., Arpita Adhikari, Adhikari, A., & Hussain, C. M. (2021). Graphene-based analytical lab-on-chip devices for detection of viruses: A review. *Carbon Trends*, *4*, 100072. https://doi.org/10.1016/j.cartre.2021.100072

Si Kuan Thio & Sung-Yong Park. (2022). A review of optoelectrowetting (OEW): From fundamentals to lab-on-a-smartphone (LOS) applications to environmental sensors. *Lab on a Chip*. https://doi.org/10.1039/d2lc00372d

Vaes, D., & Van Puyvelde, P. (2021). Semi-crystalline feedstock for filament-based 3D printing of polymers. *Progress in Polymer Science*, *118*, 101411. https://doi.org/10.1016/j.progpolymsci.2021.101411

van Lintel, H. T. G., van de Pol, F. C. M., & Bouwstra, S. (1988). A piezoelectric micropump based on micromachining of silicon. *Sensors and Actuators*, *15*(2), 153–167. https://doi.org/10.1016/0250-6874(88)87005-7

Whitesides, G. M. (2006). The origins and the future of microfluidics. *Nature*, *442*(7101), 368–373. https://doi.org/10.1038/nature05058

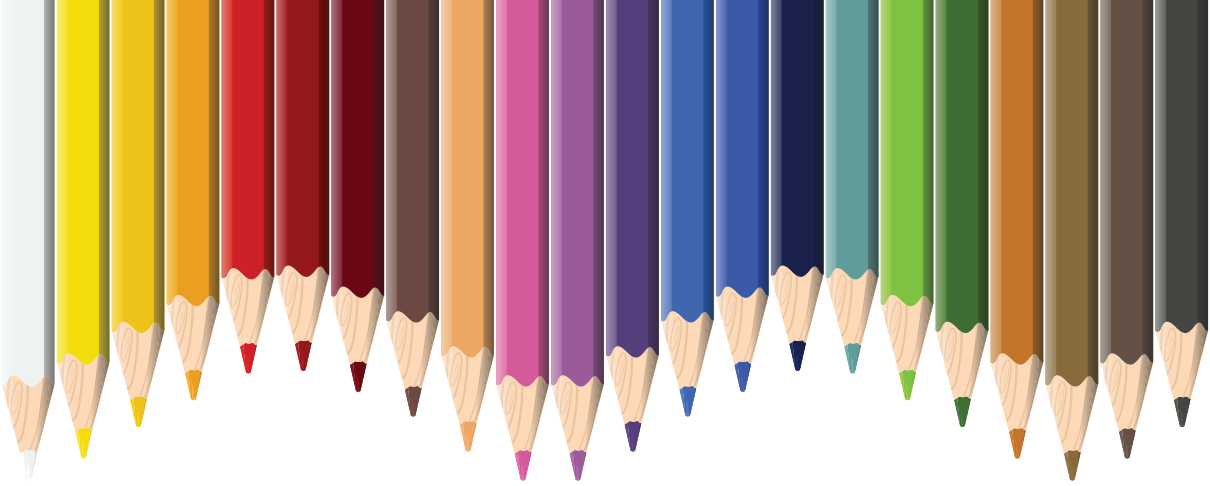

Chapter 5

GALVANIZED STEEL OF WELDING TECHNIQUE AND INDUSTRIAL APPLICATIONS

Ferit ARTKIN[1]

1 Lect. Dr., Kocaeli University, Hereke Asimkocabiyik Vocational School, ORCID: 0000-0002-8543-6334

Introduction

An essential natural tendency is suddenly reversed when iron is taken out of its ore. In most conditions, steel as well as iron will rust if left unprotected and eventually revert to their original state.

One of the most important aspects of using steel economically is preventing corrosion. The application of the proper protective coating can postpone the need for structural and equipment replacement, reduce or eliminate maintenance costs and interrupted service time, and result in significant economies of scale in the long run.

With much more advantages over painted or another coating technology, galvanizing is the finest option for preventing corrosion. In actuality, there is no comparison in terms of handling, robustness, coating thickness, application, and protection.

Galvanizing is a highly effective corrosion solution with a long, free of maintenance lifespan, which is why engineers and architects require it. Simply put, galvanized steel is regular steel that has been heavily zinc-coated. Not only does this barrier prevent corrosion, but it also effectively shields the steel from welding damage.

There are several reasons why you might wonder if it's possible to weld galvanized steel. The question is not whether you can do it or not. Large parts may require welding before galvanizing. Galvanized steel may be welded by us. On the other hand, welding may be more challenging with zinc-coated steel then it would ordinarily be with uncoated steel. Additionally, if any portions are left exposed or broken during welding, it may make the components susceptible. When welding galvanized steel, hazardous substances may be emitted during the heating process.

Although galvanized steel is still one of the most widely used constructing and manufacturing materials today, sustainable galvanized steel products are being made with ever-evolving technologies.

Galvanized Steel

Galvanised steel is a popular choice in industrial, agricultural, and construction projects. The main purpose of galvanisation is to protect the steel from corrosion, and this is achieved by applying a thin layer of zinc, either through a process of 'hot dip' galvanising, electro-galvanising, or metal spraying.

TFM - or Time to First Maintenance - is calculated according to the appearance of rust on five percent of the galvanised steel sheet surface. What this means is that five percent of the zinc coating has now eroded, exposing the steel to corrosion. It is at this stage that maintenance needs to be implemented

to protect the integrity of the steel and prolong its durability. TFM varies according to the atmospheric conditions of the structure. For example, in a dry, rural area with little rainfall and pollution, a TFM could be over 100 years, while in a more humid tropical environment, that TFM might reduce to about 70 years. By hot-dip galvanising a thin 6mm steel sheet, you are creating a zinc coating of 85 microns, which more than meets the corrosion performance required for many applications across the world.

Figure 1. Industrial Applications of Galvanized Steel for Pipelines (freepik.com, 2023).

Galvanized steel which has smooth finish, rust-free, and lowered maintenance costs a sheet of galvanised steel is smooth to the touch, making it easy to inspect. Being tough and durable, it is resistant to scratches and everyday damage. Any damage tends to occur through mishandling and untreated long-term wear and tear. Due to its smooth surface, should the galvanised steel sheet incur any damage, the integrity of the protection is compromised, making it prone to rusting. Fortunately, this makes it easily noticeable on regular inspection and therefore can be treated quickly and effectively. When it is damaged, it is the zinc that is in the first line of fire. That means that the steel underneath is protected and will only be affected if the blemish is left untreated. Protection from contamination the galvanisation process acts as a protective buffer against oxygen and moisture, resulting in a smooth, rust-free layer. As a result, the steel sheets are perfect for use in projects which require a clean, clinical environment, such as operating rooms and food preparation areas.

However, for long-term structural projects, the additional costs will more than pay for themselves in terms of longevity and reduction in maintenance over the years. Cheaper is never normally better.

White Rust for Galvanized Steel

The galvanisation process ensures that the steel sheet remains resistant to rust. However, you need to be aware of the presence of white rust, which can develop over time if the steel is exposed to moisture and not maintained.

White rust is a white chalky substance that can form on the surface of zinc due to moisture. It can cause significant damage to the galvanised coating and can ultimately compromise the durability of the zinc coating.

Otherwise known as zinc hydroxide, this white rust must be treated immediately to prevent it from spreading and reversing the effect of the galvanisation process as a whole. But prevention is better than cure, so ensure the following steps are taken to minimise the risk of white rust in the first place. Make sure the galvanised steel sheets are packed in a dry, moisture-free environment. Ensure that there is good air circulation between sheets. Store the sheets at a slight angle to ensure that any water or moisture can be drained away and not sit stagnant on the surface of the steel sheets. Make sure the surface of the zinc coating is treated with a barrier or water repellent coating to minimise any contact between water and the galvanised surface of the steel sheet. If your galvanised steel sheet has developed a white rust coating, then it can be treated. The treatment depends on the severity of the damage to date. If there is a light powdery residue, then it can usually be brushed off with no residual treatment required. However, the more established and severe the zinc oxidisation process, the more remedial treatment is required to ensure it does not compromise the long-term integrity of the galvanised coating.

Figure 2. Example of White Rust on Galvanized Steel in industry (metaldecking.com, 2023).

One of the commonly encountered problems with galvanized steel building products is the presence of wet storage stain – also known as white rust. This condition causes a significant, powdery deposit on the galvanized material's surface which can result in damage to the coating and is detrimental to the product's appearance. Galvanizing is a metallic layer of zinc which is specified in the weight of zinc per square foot. Zinc is durable and provides an excellent anti-corrosion performance for steel (rapidmetals.co.uk, 2023). The stable form of zinc oxide that provides galvanized coatings with their longer corrosion protection cannot develop without unrestricted ventilation and carbon dioxide. Simply put, white rust is the chemical combination zinc hydroxide that occurs when zinc comes into contact with moisture. Because the substance is not freely exposed to air that contains carbon dioxide, it does not transform into the zinc carbonate passive coating.

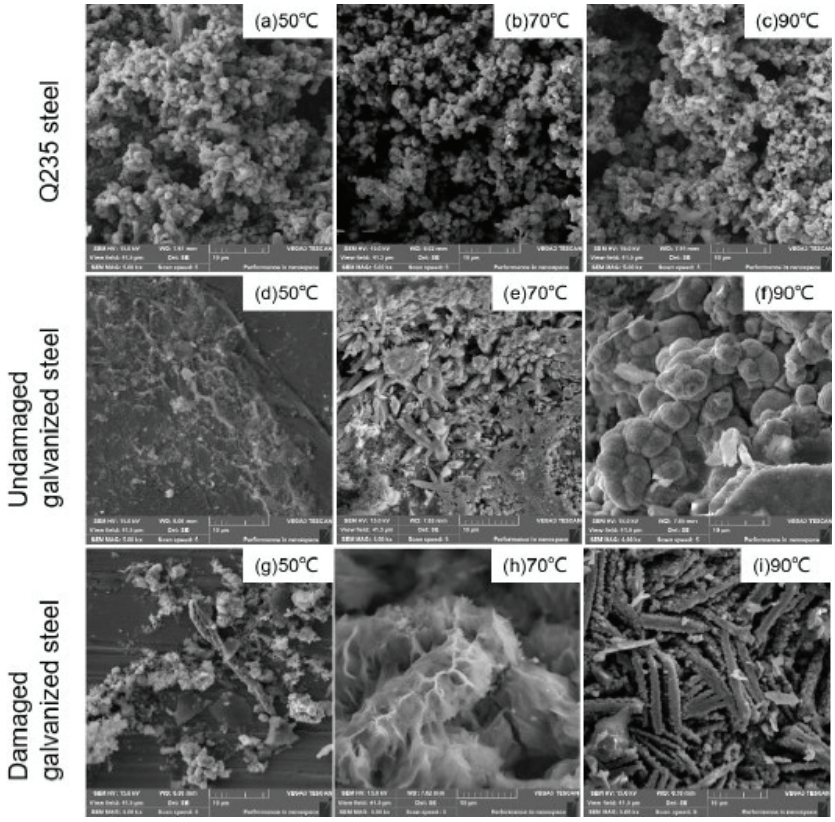

Figure 3. SEM photos of Q235 steel and undamaged-damaged galvanized steel (Yusong L., et al., 2023).

Zinc hydroxide (white rust) will continue to form as long as the surfaces are wet and starved of carbon dioxide. Once the wet material has been separated and allowed to dry the staining will remain, however, no further staining will occur.

Advantages of Galvanized Steel

Steel that has been coated with a coating of zinc to stop rust and corrosion is known as galvanized steel. This process makes steel significantly more durable and versatile, offering a variety of advantages over uncoated steel.

Durability, the zinc coating acts as a physical barrier between the steel and the elements, protecting it from rust, corrosion, and wear and tear. This can significantly extend the lifespan of steel structures and components, often lasting for decades with minimal maintenance. Low maintenance, unlike uncoated steel, which requires regular painting or other protective measures to prevent rust, galvanized steel is virtually maintenance-free. This can save

time and money in the long run, making it a cost-effective choice for many applications. Versatility, galvanized steel can be used in a wide variety of applications, both indoors and outdoors. It is commonly used in construction, infrastructure, agriculture, automotive, and other industries.

Conductivity: Galvanized steel is a good conductor of electricity, making it suitable for use in electrical applications. Aesthetics: Galvanized steel has a distinctive silver-gray appearance that can be left as-is or painted for a more customized look. Sustainability, galvanized steel is a recyclable material, making it an environmentally friendly choice. Fire resistance: Galvanized steel is fire-resistant, making it a safe choice for use in buildings and other structures.

Galvanized steel is simple to work with, easy to install, and can be shaped into a variety of forms and sizes by cutting and welding. Overall, galvanized steel is a versatile and durable material that offers a wide range of advantages over uncoated steel. It is a cost-effective choice for many applications and can help to extend the lifespan of steel structures and components.

Galvanized Steel in Welding Techniques

Closer control of welding conditions than for uncoated steel is usually necessary but procedures are simple and well established. This section details procedures for all suitable welding techniques for galvanized steel including GMA (gas metal arc), carbon arc, GTA (gas tungsten arc), manual arc, and oxyacetylene welding.

GMA (gas metal arc) welding, also known as CO_2 or MIG welding, is a versatile semi-automatic welding process which is convenient and easy to use. It is particularly suited to the welding of thinner materials. Welding galvanized steel vaporizes the zinc near the arc (zinc boils before steel melts). The zinc oxidises in the air to a fine white powder. In the GMA welding of galvanized steel, the presence of the zinc coating has no effect on weld properties although some weld spatter is produced. Arc stability is excellent and is not affected by the galvanized coating, although some reduction in welding speed is required.

The weld takes place in a protective gas shield. A small diameter consumable wire electrode of 0.8 mm to 1.6 mm is fed automatically to the weld torch. The high current density resulting from the small diameter of the wire is in the region of 200 A/mm^2. Gas metal arc welding, also known as Metal-Inert Gas (MIG) welding, is a versatile semi-automatic welding technique particularly suited for the welding of thinner materials (<1/2 [13 mm] thick.

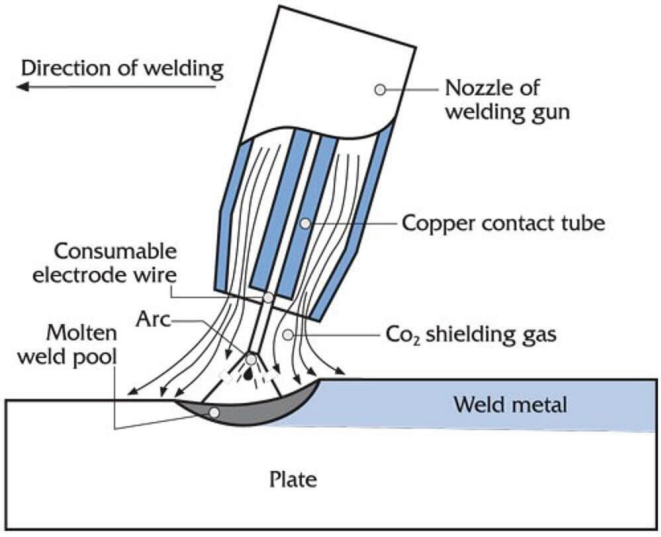

Figure 4. Gas Metal Arc Welding (GMAW) parts in ilustrated (galvanizeit.org, 2023).

Gas metal arc welding, also known as Metal-Inert Gas (MIG) welding, is a versatile semi-automatic welding technique particularly suited for the welding of thinner materials (<1/2 [13 mm] thick.

Welding speeds for GMAW are typically slower for galvanized surfaces. These reduced speeds allow longer time for the zinc to burn off at the front of the weld pool. Increasing the current supplied to the welding electrode may provide sufficient means to burn off zinc coatings of greater thickness.

Weld penetration depth is decreased when welding galvanized steel. When performing butt-welds, larger gaps must be provided. Consistent penetration is achieved by employing a side-to-side motion of the welding torch when butt-welding in the flat position. Spatter increases when welding galvanized steel using CO_2 shielding gas.

The formation of spatter particles is directly proportional to the thickness of the zinc coating. Therefore, spatter formation is greater for hot-dip galvanized steel than continuously galvanized (sheet) steel.

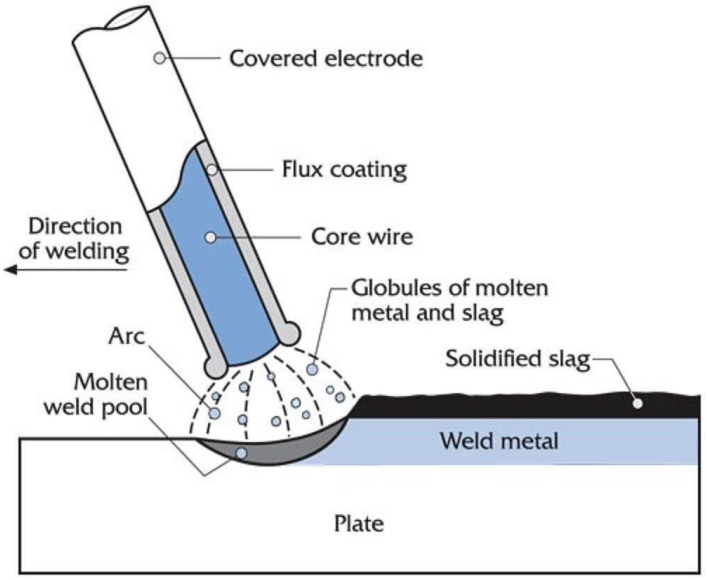

Figure 5. Shielded Metal Arc Welding (SMAW) parts in ilustrated (galvanizeit.org, 2023).

The most common arc welding process is shielded metal arc (SMAW) welding. SMAW welding is a process in which flux-covered electrodes ranging from 9 to 18 inches (23 to 46 cm) in length, and 1/16 to 5/16 inches (1.6mm to 8.0 mm) in diameter, are used.

Weld depth penetration is decreased in the SMAW welding of galvanized steel, as is the case for GMAW welding, the root opening for butt-welds must be increased from that of uncoated steel surfaces. However, it is possible to obtain full weld depth penetration by altering the normal weld techniques for uncoated steel. If the angle of the electrode is reduced from the normal 70º to 30º , and the weld speed is reduced significantly, normal weld depths can be achieved by moving the electrode back and forth in line with the joint.

Spatter formation also increases using SMAW welding. Generally, spatter formation does not increase to an extent where anti-spatter compounds are required. Slower welding speeds allow for more of the zinc coating to burn off and reduce the amount of spatter formation. As for GMAW welding, it is not usually necessary to increase the current to the electrode to increase the amount of zinc burned off.

Reducing the angle of the electrode and reducing the weld travel speed will significantly increase the quality of SMAW weld on the zinc-coated surface. Steels with thicknesses greater than 1/2 (13 mm) are recommended to be welded with SMAW.

Oxyacetylene Welding

All grades of hot-dip zinc coated steels can be welded by oxyacetylene fusion welding. Preparation for welding is similar to that for welding uncoated steel. Because low travel speed is necessary for this process, which is necessary to bring the joint edges to the fusion temperature, the extra heat causes the zinc coating to be affected over a much greater area than when using faster welding processes. Best results are obtained when the filler rod is moved back and forth, producing a ripple weld. Nozzle sizes similar to those used for welding uncoated steel of similar thickness should be used. Welds should not be remelted by a flame to improve their appearance; this will result in additional loss of the zinc coating.

Friction Welding

Flat-ended studs, whether uncoated or galvanized, cannot be welded to galvanized plate because the alloy layers in the zinc coating appear to act as a low friction-bearing surface and insufficient heat is developed for welding. Using pointed studs solves the problem with friction welding studs to galvanized surfaces. The best results are obtained on studs with a point having a 120º angle. The presence of zinc coating on the stud increases the time required for welding.

Resistance Welding of Zinc-Coated Steel

Resistance welding is generally used to join galvanized steel less than 1/4 inch thick and with a zinc coating lighter than 305 g/m^2. Coatings up to 460 g/m^2 have been successfully welded, but electrode life is much shorter than with lighter coatings. On heavier coatings, it is necessary to replace or redress worn electrodes more frequently. Sheet materials can be resistance welded without removal and with little damage to the zinc coating. Most after-fabrication galvanized coatings are thicker than recommended for resistance welding and become impractical to do so.

Conclusion

Beyond health dangers, there are additional issues that might arise from welding galvanized steel. The weld may be compromised by the zinc coating present in galvanized steels. The coating might result in impurities and porosity in a weld and makes penetration more challenging. It's also typical for there to be no fusion at the weld's tips. To reduce these dangers, welding procedures and technique must be followed correctly. Before welding, try to take off any zinc coating that may be around the weld region. If not, use a filler substance designed specifically for use on materials coated with zinc.

The variety of galvanizing procedure used to coat the steel is another aspect that will contribute to the quality of the welds.

Varying zinc layers over the steel surface are a result of different galvanizing techniques. The coatings on zinc electroplated steel are usually thinner than those on hot dipped galvanized and thermally sprayed steel. Choose zinc electroplated steel instead of thicker-coated hot-dipped or zinc thermal-sprayed steel to get a better weld. Once welding automation is taken into consideration, zinc plated and steel will also have a much more uniform coating.

Preserving corrosion resistance following welding is another challenge when welding galvanized steel. The region that is left uncoated and vulnerable following welding galvanized steel is caused by the zinc coating burning away surrounding the weld. Weld failure due to expediency may thus occur in the exposed, naked weld. A post-weld procedure, such as painting or re-galvanizing the material, must be employed if corrosion resistance is still needed after welding.

Galvanized steel may be securely and successfully welded, but there are several crucial precautions that need to be followed. Safety rules must be studied and understood in order to weld galvanized steel safely. Additionally, welders must wear the appropriate personal protective equipment to shield them from potentially harmful vapors. It's also critical to understand every detail of the application, including the kind of galvanizing technique being used, the environment in which the weldment will be placed, the welding procedure being followed, and the standards by which the weld will be judged.

References

Artkin, F., Evaluation of the Industrial Applications of Galvanized Coating, Platanus Publications, Academic Research and Reviews in Engineering Sciences, December, 2023.

D.Deacon, R.Hudson (2012), Steel Designer's Manual (7th Edition), Chapter 36 - Corrosion and corrosion prevention, The Steel Construction Institute.

Demirel, T., Bişkiner, E., Sahin, Z., Systematic Review on Research on Galvanized Coatings, Conference: Ases International Bandırma Scientific Studies Conference At: October 27-29, 2023, Balıkesir, Turkiye, p. 90-104.

https://designmanual.gaa.com.au/index.php/welding/welding-galvanizedsteel/#:~:-text=Galvanized%20steel%20is%20welded%20satisfactorily,release%20compound%20may%20be%20worthwhile.

https://galvanizeit.org/design-and-fabrication/fabrication-considerations/welding/welding-galvanized-steel Accessed 18 Dec., 2023.

https://metaldecking.com/news/white-rust-prevention-and-treatment/ Accessed 17 Dec., 2023.

https://www.freepik.com/premium-ai-image/industrial-pipeline-awaits-stack-galvanized-steel-aluminum-chrome-stainless-pipes-warehouse-shipment_61145589.htm, Accessed 15 Dec., 2023.

https://www.hobartbrothers.com/resources/technicalarticles/galvanizedsteelwelding/#:~:text=Galvanized%20steel's%20most%20positive%20attributes,-to%20defects%20when%20welded%20incorrectly Accessed 19 Dec., 2023.

https://www.neicorporation.com/self-healing-anti-corrosion-coating-for-zinc-plated-galvanized-steel/ Accessed 17 Dec., 2023.

https://www.rapidmetals.co.uk/pros-and-cons-of-galvanised-steel/#:~:text=Being%20tough%20and%20durable%2C%20it,making%20it%20prone%20to%20rusting Accessed 20 Dec., 2023.

J. Yahalom, Corrosion Protection Methods, Elsevier Encyclopedia of Materials: Science and Technology (Second Edition), 2001, Pages 1710-1713, https://doi.org/10.1016/B0-08-043152-6/00306-5.

S.J.Abbas, M.Alali, M.H.Abass, W.S.Abbas, Characterization of Galvanized Steel-low-alloy Steel Arc Stud Welded Joint, Journal of Achievements of Materials and Manufacturing Engineering 117(2):79-85, DOI: 10.5604/01.3001.0053.6707.

Yusong L., Bin He, Guo Fu, Shoujun Wu and Bin Fan, Effects of Ambient Temperature and State of GalvanizedLayer on Corrosion of Galvanized Steel in High-Humidity Neutral Atmosphere, May 2023, Materials, MDPI, 16 (10): 3656, DOI: 10.3390/ma16103656.

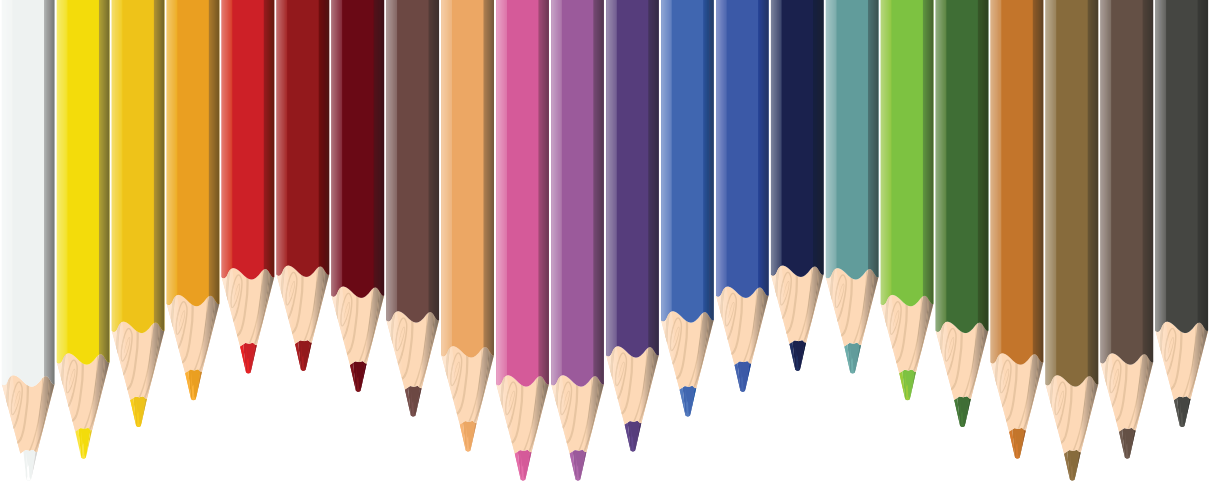

Chapter 6

CLASSIFICATION OF POLES USED IN ENERGY TRANSMISSION AND DISTRIBUTION

Hilmi ZENK[1]
Faruk GÜNER[2]

1 Ph.D., Assoc. Prof., Giresun University, 0000-0002-1653-8580
2 Ph.D., Assoc. Prof., Giresun University, 0000-0002-3438-0553

1. Introduction

In order for electrical energy to become usable, many systems in different disciplines must work together and smoothly from the point of physical production to the point of consumption. These systems can be briefly summarized as the systems required for the detection, extraction or control of the raw energy source, the systems required for the appropriate energy generation method, the systems that will ensure the regulation of energy and the standardization of electrical parameters such as current, voltage, frequency, the systems required for the transmission and distribution of energy and the systems required for the end user to use it safely.

In this study, poles are analyzed among the systems required for the transmission, distribution and utilization of energy in Turkey. Poles used in energy transmission and distribution in Turkey are generally designed for different purposes for power transmission lines and distribution networks. In the classification of these poles, factors such as the purpose of use, the type of material they are made of, the number of circuits they carry, and the voltage level are taken into account.

2. Standard Specifications for Poles

Before classifying electricity poles, some basic characteristics should be known. These properties can be defined as height, weight, peak force and peak width and foundation designs. The length of a pole can be defined as the length of the pole after it leaves the production, usually in mechanical calculations, the pole length is determined as the part coming out of the soil outside the foundation. The full length of poles defined as wooden poles varies between 9 and 15 meters and the top width varies between 16 and 19 cm. The material they are made of is concrete and the peak forces of the poles go up to 200 to 3500 kg. Iron poles, on the other hand, are made in various lengths by adding angle profile irons [1].

3. Classification of Poles

Electricity poles can be classified according to their intended use, the type of material they are made of, the number of circuits they carry and the voltage level.

3.1. Pole Types According to Purpose of Use

Poles are classified as stopper, corner stopper, carrier, corner carrier, end, branch, distribution and crossing poles according to their intended use.

3.1.1. Final (Last) Pillars

Used at the beginning and end of energy transmission lines. The aerial

line conductors are connected to the insulators with end ties, that is, they are strong poles that can withstand unilateral total tensile force. In the projects, the pole symbol is shown as a circle and the end poles are shown with the letter N as in Figure 1 [2].

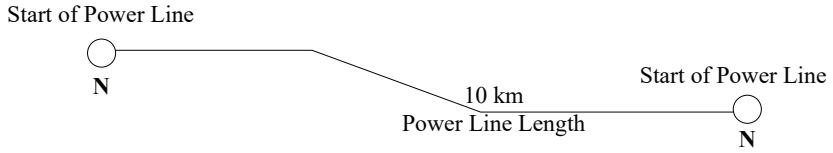

Figure 1. End posts

3.1.2. Supporting Poles

These are the poles used between the stopper poles in order to carry the conductor in the aerial lines, that is, to hold the weight of the conductor in the direction of the straight line on which the conductor is suspended, and shown in Figure 2 with the symbol T in the project.

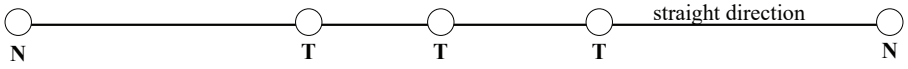

Figure 2. Supporting poles

3.1.3. Corner Support Poles

They are poles with mechanical strength that can change the direction of the linear line with small deviations (α_s). These **Corner Carrier** poles, where the conductors are connected to the insulators with a carrier bond, are shown in the project with KT as shown in Figure 3.

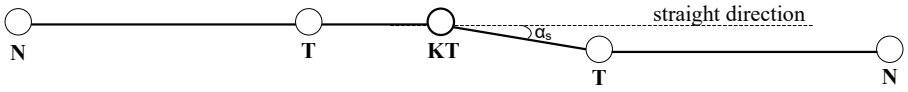

Figure 3. Supporting pole at the corner

3.1.4. Stopper Poles

In places where the power transmission lines where the carrier poles remain pass linearly, the line must be fixed to fixed and solid points at certain intervals along the route. Poles designed in such a way that the fixed points

can withstand the tensile force from the conductors are defined as stopper poles and denoted by the letter D. In energy transmission lines, it is appropriate to use stopper poles at certain intervals according to the conductor type. In case of problems such as wire breakage and pole overturning, the failure in question is limited between these stopper poles and does not affect other parts of the air line. In addition, as shown in Figure 4, the conductors on these poles are connected to the insulators with end ties in order to properly stretch the conductors to the insulators.

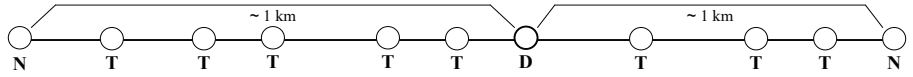

Figure 4. Stopper (D) pole

3.1.5. Corner Stop Posts

These are poles that are used at the corner points where the power transmission aerial lines going in straight direction need to change direction with large deviations (α_s) and at the same time act as astopper. The conductors in the Corner Stopper Poles are connected to the insulators with end ties and the project is indicated by the symbol KD as shown in Figure 5.

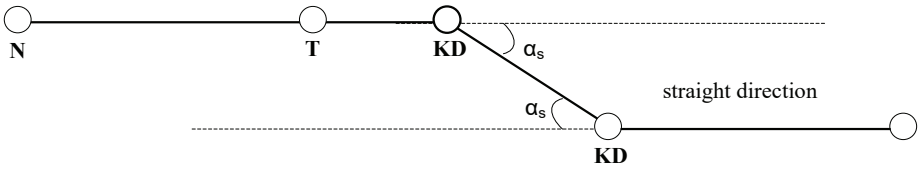

Figure 5. Corner stopper (KD) pole

3.1.6. Distribution (Branch) Poles

These poles are used where the air lines are divided into branches. These branch poles, which are indicated with B in the project as shown in Figure 6, may also have additional connecting facilities, switchgear elements such as disconnectors or breakers.

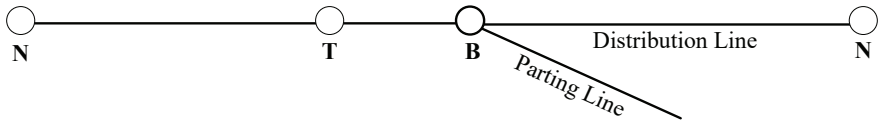

Figure 6. Distribution (B) pole

3.2. Types of Poles According to the Number of Circuits They Carry

3.2.1. Single Circuit Poles

These are poles with only one electrical circuit on the pole. This type of poles are installed as two-wire if they carry a single phase at Low Voltage level, four-wire if they carry three phases at Low Voltage level and three-wire if they carry three phases at High Voltage level. Single circuit poles are shown in Figure 7 [1].

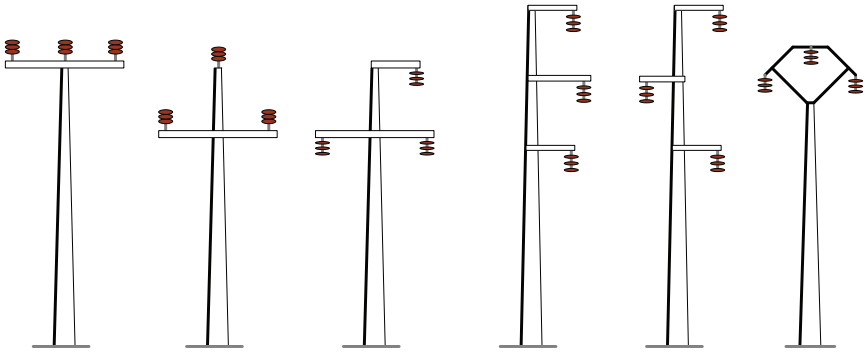

Figure 7. Single circuit pole designs

3.2.2. Multi-Circuit Poles

These are poles with only two, four and six separate electrical circuits on the pole. Depending on the design of this type of poles, the number of conductors can be very different as there may be an additional protection line conductor. Figure 8 shows the circuit designs on these poles.

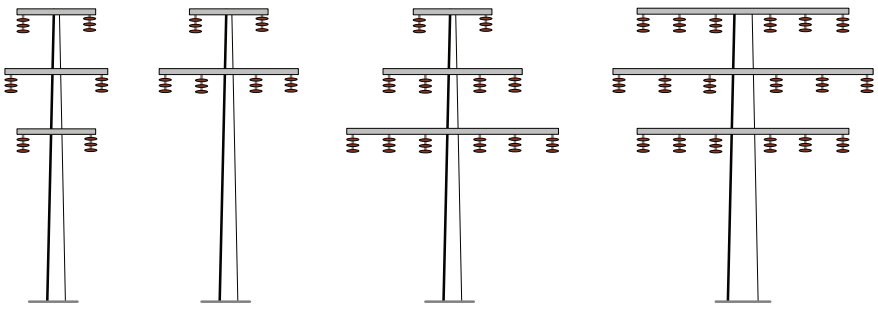

Figure 8. Multi-circuit pole designs

3.3. Types of Poles According to Voltages

According to international standards, voltage levels below 1 kV are defined as low voltage (LV - LV) and above 1 kV as high voltage (HV - HV). However, some countries have also leveled high voltage and defined intermediate voltages. For example, in Turkey, voltage levels are divided into low, medium (MV-LV), high (HV-HV) and very high voltage (MV-HV-VHV) and the poles carrying these voltages are divided into four as low, medium, high and very high voltage poles [4].

3.3.1. Poles used in Low Voltage

Up to 1000 volts, low voltage (LV) poles can be made of wood, iron or concrete. In some cases, both low voltage and medium voltage (MV) lines are installed on the same pole. A and K type poles are shown in Figure 9.

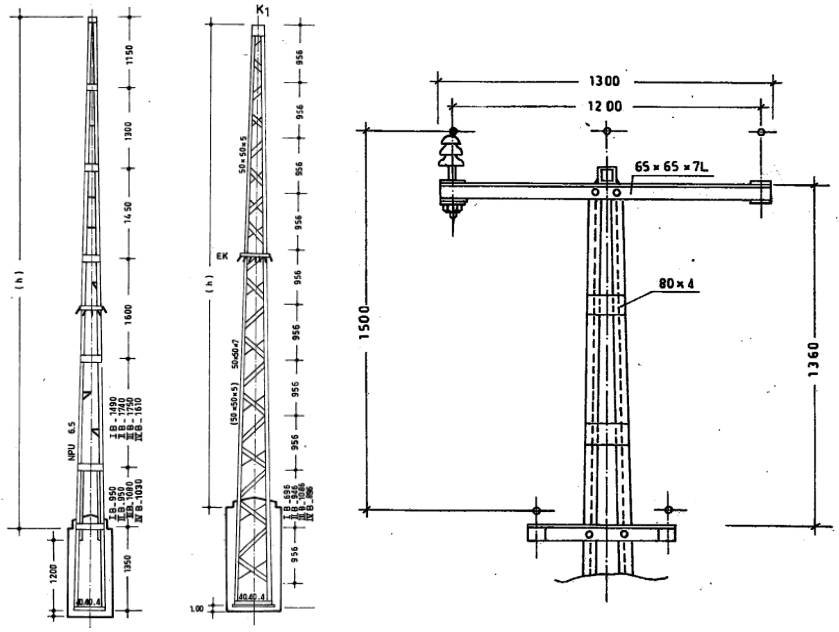

Figure 10. Detail of A and K type LV pole and A type poles carrying LV-MV common line [3]

3.3.2. Poles Used in Medium Voltage

They are poles used between 1kV - 36 kV. Their length varies between 9 m-25 m. They are manufactured as wood, concrete and iron poles. Concrete and iron poles are widely used in urban areas. In rural energy distribution and villages, wooden poles are only used as carrier poles in energy distribution lines carrying 3AWG (Swallow) conductors, and concrete and iron poles are

used as carrier (T), corner carrier (KT), stopper (D), corner stopper (KD), final (N) and branch (B) poles. Iron poles used in medium voltage are known by the name of the conductor they carry. MV iron poles are made of square section putrel iron. Concrete poles are manufactured at 1 meter intervals from 10 m to 26 m [5].

Figure 11. Galvanized bolted iron poles with 3/0 AWG (Pigeon) conductor used in MV

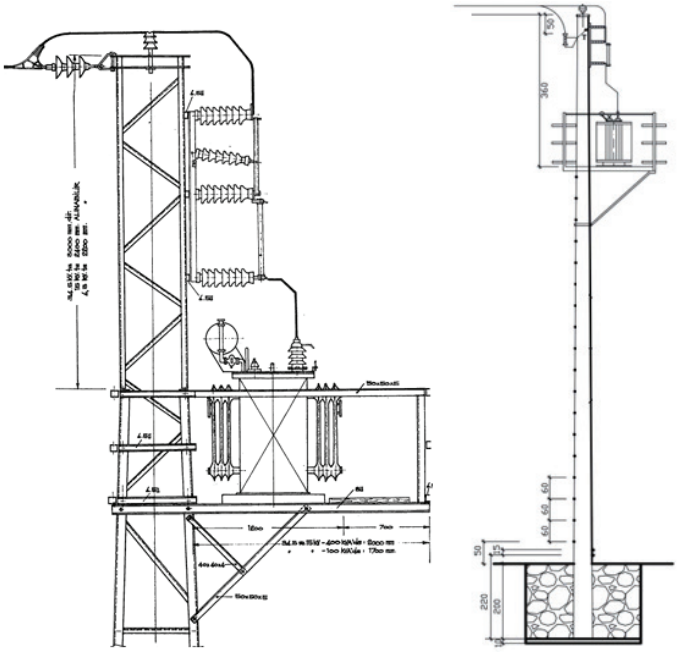

Figure 12. Technical drawing of MV concrete and iron transformer pole [6]

3.3.3. Poles Used in High Voltage

They are 60 kV poles made of painted-welded, galvanized-bolted, iron and concrete materials that carry power lines with voltage above kV. Painted-welded iron poles are coated with paint and protective layers to prevent them from being affected in all kinds of ambient conditions. The protective layers must be renewed at regular intervals. In addition, there are problems of transportation to points where there is no transportation. Due to these problems, painted-welded iron poles are replaced by galvanized-bolted iron poles. Pole designs, which vary according to the type of conductor, are designed in different types and lengths according to the various functions they will perform. The profiles in painted-welded iron poles are manufactured in pieces of 6 meters each on average and they are attached to each other with bolts.

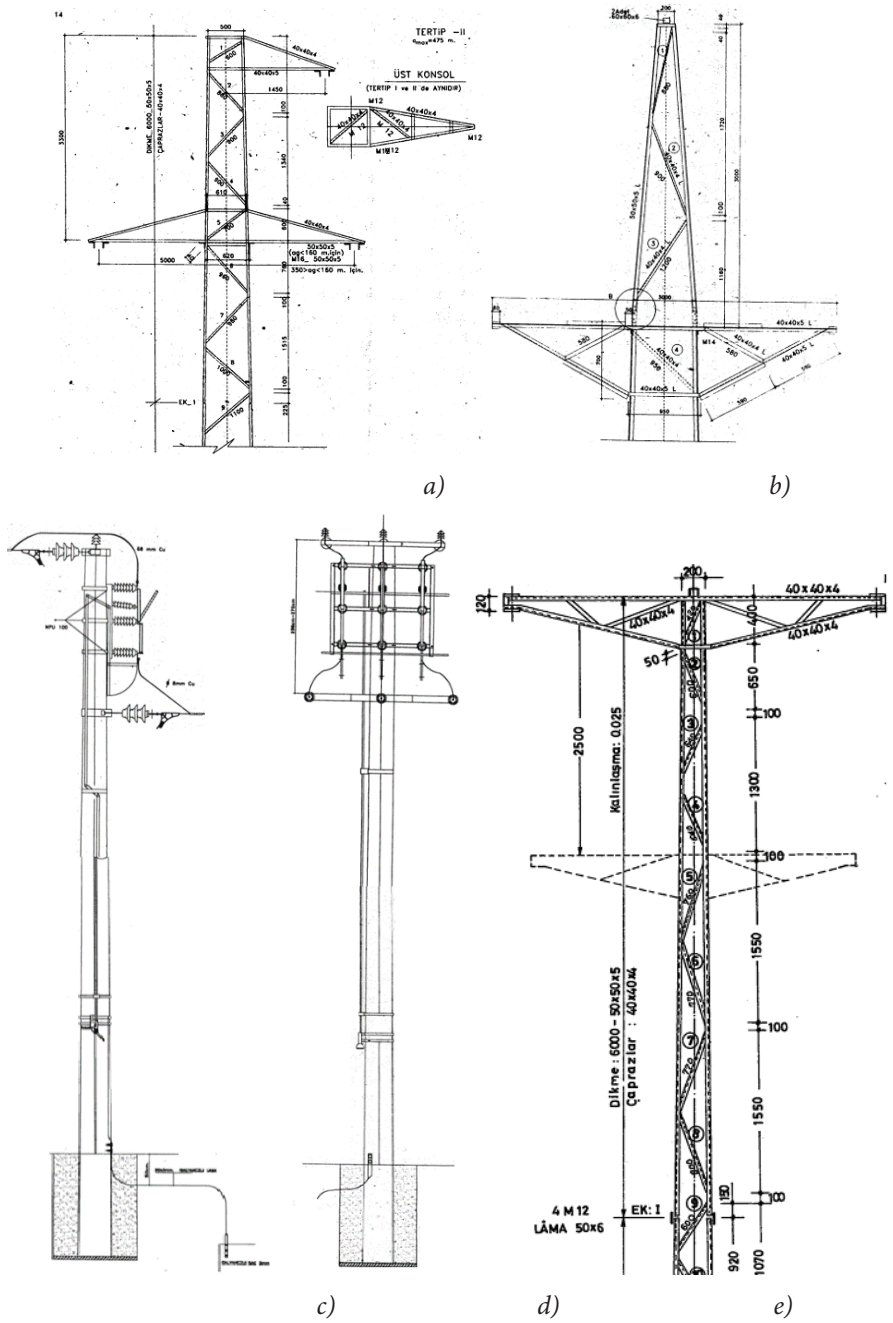

a) *b)*

c) *d)* *e)*

Figure 13. Some HV iron poles: a) Suspension Insulator Connected Carrier pole, b) Stopper pole, Sectionalizer System Connected pole c) Side View, d) Front View, e) Support Insulator Connected Carrier pole

3.4. Types of Poles According to Construction Materials

According to their construction materials (according to the material they are made of) poles are divided into three. These are iron poles, concrete poles and wooden poles. Iron poles are lighter than concrete poles and last longer than wooden poles. They can be transported in small pieces. Their cost is higher than wooden poles.

3.4.1. Tree Poles

It is a type of pole made from trees such as coniferous fir, juniper, larch, spruce. After the tree is cut, it is turned and subjected to special treatments as they are adversely affected by weather conditions and pests. These treatments include impregnating the wood pole with copper sulphate or tarring. Mechanical durability is limited for wooden poles. For this reason, the distance between the poles should be short.

After the foundation of the wooden poles is opened, after the fixing process, the foundation pit is filled by compacting the foundation with the excavation from the soil, stone and soil, and concrete is not poured. If concrete is poured into the foundation, the pole may break from the upper points of the foundation in the peak forces coming to the pole. In addition, the bottom of the pole may rot over time. To prevent this, the bottom of the pole (foundation) should be sprayed with injection. If concrete is poured on the base of the pole, it is not possible to open the base of the pole a little and spray it. Wooden poles are used as normal bearing and corner bearing poles. The top of the pole is cut at an angle of 45 degrees to prevent rain and snow water from damaging the pole. Standard tree pole lengths are 8- 8.5- 8.5- 9- 9.5- 9.5- 10- 10.5- 11- 11.5- 11.5- 12- 12.5- 13- 13.5 meters. For the transportation of conductors on wooden poles, insulators can be attached directly to the pole or carried with the help of insulators fixed to the brackets mounted on the poles. After erection, wooden poles should be supported with struts or steel ropes. Comparison of wooden poles with other poles is given in Table-1.

Table-1. Advantages and disadvantages of wooden poles

Advantages of wooden poles	**Disadvantages of wooden poles**
Cheap	Short lifespan, low peak force
Easy to transport and easy to plant	Because they are flexible, their secretions (feces) can change
Light and flexible	Can burn when struck by lightning
No painting costs	Not for use at high voltages
More reliable against stray currents	Wooden poles should be reinforced with steel wire or struts.

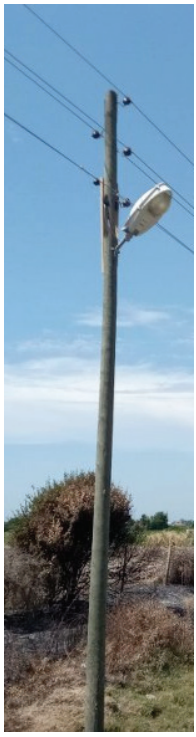

Picture 14. Tree pole

3.4.2. Iron Poles

They are poles made of iron and steel that can be used in all voltage levels. Iron poles can be manufactured as painted-welded and galvanized-bolted. A and cage type poles carrying low voltage (LV) and medium voltage conductors are usually painted-welded, while poles carrying high voltage (HV) conductors are galvanized-bolted. The iron structures in these poles are I, U, L shaped profiles. In transmission line poles carrying high voltage (HV) and very high voltage (MV) level conductors, one or two protection conductors are drawn from the top of the pole to protect the line depending on the type of pole. The protection conductor is connected to the earth.

Concrete should be used in the foundations of iron poles. Iron poles are longer lasting than wooden poles and lighter than concrete poles. Iron poles can be applied to any type of arrangement of conductors. It is also easy to repair pole failures that may occur for any reason. However, maintenance and operating costs are higher than concrete poles. Iron poles have guardrails to prevent living creatures from climbing.

2.4.2.1. Pipe Type Poles

Tubular poles are used in electrical energy transmission and distribution

in some countries, but in Turkey they are mostly used in special lighting, low voltage street, avenue, harbor, marina, site and garden lighting applications. It is also specially used as projector lighting poles. Their heights are between 4 and 8 meters. There are single, double, triple types.

Figure 15. Tubular iron (galvanized) poles [1]

2.4.2.2. A Type and Lattice Type Poles

Poles carrying conductors at low voltage and medium voltage level are standardized as A type and cage type iron poles. These standardized lengths are separate for short and long poles. Type A poles originate from the fact that the sheet metal structure connecting the uprights in the middle of the two main uprights resembles the letter A. The profile bars used in these poles are I and U shaped. Pole names according to profile width are 8I, 10I, 12I, 6,5U, 8U, 10U, 12U or 8Ik, 10Ik, 12Uk. Pole lengths are between 9m and 11m [1-12].

Picture 16. A type and lattice type iron pole pictures

2.4.2.3. Putrel (Pylon, Fork) Poles

The number of circuits of these poles, which are produced with galvanized bolts and painted-welded, can be 1, 2, 3 or 6. Their lengths can be enlarged and adjusted in desired dimensions and there is no standard length.

Figure 17. Pylon type and forked pylon type iron poles [11]

Table 2. Advantages and disadvantages of iron poles

Advantages of iron poles	Disadvantages of iron poles
• Peak forces are large	• High cost
• Easy to repair	• Not very safe against leakage currents
• Their lifespan is long	• Affected by weather conditions
• Easy to transport and assemble with the ability to be disassembled	• Maintenance is costly and requires care

3.4.3. Concrete Poles

Concrete poles are produced by using concrete and high-strength steel wire or steel rods. Vibration or centrifugation method is applied to ensure the compatibility of concrete and steel material in a non-porous manner. Poles produced by this method are called reinforced concrete poles. While centrifugal poles (SBA) are hollow, vibre poles (VBA) are filled. The cross-section of vibre concrete poles is rectangular, while the cross-section of centrifugal concrete poles is circular. The biggest advantage of reinforced concrete poles over iron poles is that they are less affected by harmful gases and vapors in weather conditions and especially in industrial areas. In addition, the amount of iron used is less (60%) compared to iron poles that do the same job, which saves iron material. The resistance of the pole to peak forces depends on the steel wires used inside. Concrete poles are made in circular cross-section and conical shape. The sleepers used in concrete poles, where the insulators are mounted, are also made of concrete or iron. Concrete poles can be made from 250 kg to 3500 kg according to the peak force. Their lengths range from 8 m to 26 m and their diameters are conical up to 50 cm and cylindrical after this diameter. They are generally used in medium and low voltages. They are also frequently used in road lighting. Centrifugal concrete poles used in medium and low voltage are manufactured in 39 different types in terms of peak forces. The pulling forces of the conductors and wind forces are assumed to be in the same direction, the force created by these two forces at the top of the pole is called the peak force.

Table-3. Properties of concrete poles

Advantages of concrete poles	Disadvantages of concrete poles
Concrete poles are cheaper than iron poles	Care should be taken when handling as they are fragile
Long life, maintenance free	They are heavy and difficult to transport
Peak forces are large	Difficult to assemble
Not much affected by atmospheric phenomena	
Safe against stray currents	

2.4.3.1. Centrifugal Poles

They are hollow concrete poles made of steel rods (as longitudinal reinforcement material) and pre-stressed steel wires as transverse reinforcement material using the centrifugal method. The centrifugal method is to expel the excess water in the concrete and to obtain a very tight impermeable concrete. The outer surface of the poles made with this method is smooth and smooth. Concrete with at least 300 doses is produced in lengths from 10 m to 26 m, increasing by one meter. SBA poles with 200 to 3500 kg peak force are made

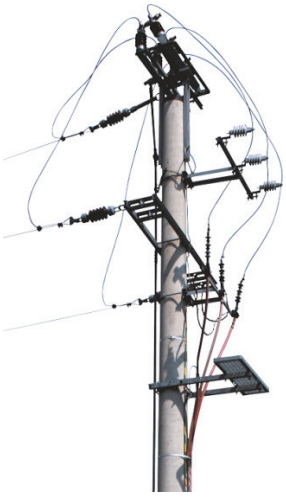

Figure 18. Centrifugal type round (SBA) concrete poles [12]

3.4.3.2. Vibre Poles

Vibrated concrete poles are obtained by placing the iron skeleton into the molds according to the results of static calculations and distributing the poured mortar homogeneously all over the mold by vibration.

Figure 19. Vibre-type concrete (VBA) pole picture [5]

4. Forces on Poles

We can divide the forces on the poles into two groups: horizontal and vertical forces.

4.1. Vertical forces

The vertical forces acting on a pole consist of the pole and sleeper weights and the insulator, conductor equipment and additional loads.

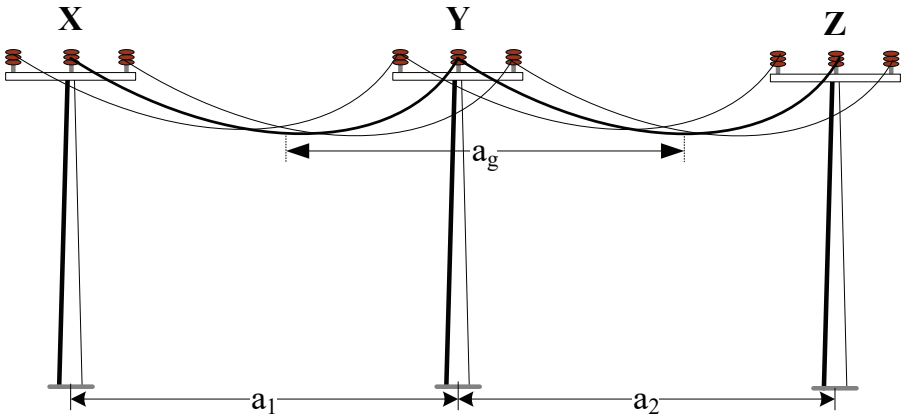

Figure 20. Illustration of the spacing of air line poles

If the vertical weight G_i acting on the pole Y due to the conductor it carries;

$$G_i = P_0 \cdot a_g \text{ (kg)} \qquad (1)$$

It's here, $P_0$is the bare weight of a 1 meter long piece of conductor (kg/m) and a_g is the weight range (m) of pole Y.

The pole's own weight (G_d) : Depending on the material the pole is made of, the weight of the pole can be calculated from catalog values or from the profile unit weight used for the designed iron pole.

Insulator weight (G_{iz}) : The weight of the insulator on the pole is obtained from the manufacturer's catalog information. The weight of the insulator bar, hanger or tensioner to be used for that insulator is added to this weight.

Assembler weight (G_m) : The weight of the worker who will work on the pole is also considered as 100 kg as vertical load in the design.

4.2. Horizontal forces

Wind force (W_d) The projection area (F) in the vertical plane (m^2) of the area exposed to the wind on the poles is calculated. In the calculation of the wind force acting on phase and earth conductors,

$$W_d = c \cdot q \cdot F \text{ (kg)} \quad (2)$$

Dynamic wind pressure coefficient c and its unit is kg/m. The coefficient of dynamic wind pressure depends on the type of mast, the shape, dimensions and structure of the wind-affected surface. Dynamic wind pressure q and its unit is kg/m^2. This value affects the length of the pole on the land, the pole, the traverse, the insulator and the conductor separately.

4.3. Additional Charges on the Conductor

Aerial line conductors are affected by climatic conditions. Changes in air temperature change the stresses in the conductor. Some ice may accumulate in the conductor with snow falling in winter. Additional ice and wind loads on the conductor should be taken into account in the line design. For this, long-term meteorological observations and records should be available in the region and evaluated accurately. For these reasons, countries establish ice and wind load research stations at various points and create maps of ice load zones.

4.3.1. Additional Ice Load on Conductor (P_b)

Experiments and observations have shown that ice forms between -8°C and 2°C. Since the moisture content of the air does not occur at temperatures lower than -10°C, ice will not form. As a result of the observations made in Turkey since 1960, five different regions were created according to the ice load zone map published in 1978 and the empirical equation (3) was created for the formation of ice load depending on these regions. In this equation P_b is the additional ice weight of the conductor in kg per meter, *k is a* zonal coefficient and *d is* the diameter of the conductor in mm.

$$P_b = k \cdot \sqrt{d} \text{ (kg/m)} \quad (3)$$

Table-4 Coefficient k values according to ice load zones

Ice Load Zone	k	Minimum Ambient Temperature	Maximum Ambient Temperature
1	0	-10	50
2	0,2	-15	45
3	0,3	-25	40
4	0,5	-30	40
5	1,2	-30	40

The additional ice load is a vertical force in the same direction as the weight of the conductor. Weight of the conductor with ice P_n is defined by equation (4).

$$P_n = P_0 + P_b \tag{4}$$

4.3.2. Additional Wind Load on Conductor (W_i)

In different geographies, the conditions for the maximum value of wind load may occur at different temperatures. In Turkey, this value is determined to occur at 5°C and is expressed in kg per meter of horizontal W_i load is calculated by Equation (5). In the formula d is the diameter of the conductor in mm [1].

$$W_i = c \cdot q \cdot d \cdot 10^{-3} \text{ (kg/m)} \tag{5}$$

The wind force per meter in kg on the conductor is calculated by Equation (6). *F* in the formula is the surface area of the conductor exposed to the wind in m^2 . The cross-section of the conductor with a vertical plane passing through the axis of the conductor is the length of the conductor in meters exposed to the wind shown in Equation (7), i.e. the wind range (a_w) multiplied by the conductor diameter (*d*).

$$P_w = c \cdot q \cdot F \text{ (kg/m)} \tag{6}$$

$$F = d \cdot a_w \cdot 10^{-3} \text{ } (m^2) \tag{7}$$

Hence, equation (8) will be used for wind force for wind range spans up to 200 m and equation (9) will be used for wind range spans greater than 200 m.

$$P_w = c \cdot q \cdot d \cdot a_w \cdot 10^{-3} \text{ (kg)} \tag{8}$$

$$W_d = c \cdot q \cdot d \cdot (80 + 60 \cdot a_w) \cdot 10^{-3} \text{ (kg)} \quad (9)$$

The wind load on the conductor is not in the direction of the conductor weight but perpendicular to this direction as can be seen in Figure 21. Equivalent conductor weight in windy state P_n is given by equation (10).

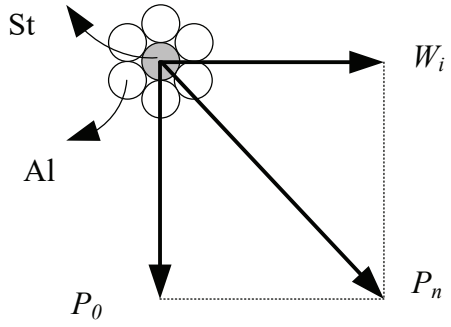

Figure 21. Forces on the air line conductor

$$P_n = \sqrt{P_n^2 + W_i^2} \text{ (kg/m)} \quad (10)$$

5. Conductors and Poles Used in Medium Voltage (MV)

Electricity distribution facilities consist of two main parts: city, town, village, industrial site LV-MV distribution network and distribution lines that enable the transportation of MV level energy with poles with large spans.

5.1. MV Conductors

In medium voltage power transmission lines, steel cored aluminum (St-Al) conductors are used to withstand mechanical stresses. Aluminum conductors are reinforced with a steel core to increase their mechanical strength. In other words, the strength of steel and the lightness and conductivity of aluminum are utilized. The conductors used for energy transmission at MV level in Turkey are 3 AWG, 1/0 AWG, 3/0 AWG, 266.8 MCM and 477 MCM steel cored aluminum (St-Al) conductors in order of diameter. As it is known, AWG stands for American Wire Gauge. In AWG, each number in the range 0000,000,000,00,0,1,2,3,...,40 represents a certain cross-sectional dimension. In the abbreviations, 000 can also be shown as 3/0, and there is also a coding that includes bird names to avoid confusion. MCM is a measurement deter-

mined by the Circular Mile expression used in the USA for larger cross-section steel cored aluminum (St-Al) conductors. Since 1 CM refers to the surface area of a circle with a diameter of 1/1000 inch, it is expressed as 1 CM=506,7x106 mm^2 or 1 CM=0,5067 mm^2 . In that case, the cross section of the Al part of the 266,8 MCM (Patridge) conductor is designed as 266,8x0,5067=135,18 mm^2.

Table-5. Technical Information of MV Conductor

St-Al Conductor Code	Name.	Cross Section (mm^2) Al	Cross Section (mm^2) St	Cross Section (mm^2) Total	Weight (Kg/Km)	Tensile Strength (Kg)
3 AWG	SWALLOW	26,69	4,45	31,14	108	1023
1/0 AWG	RAVEN	53,49	8,89	62,38	215,9	1940
3/0 AWG	PIGEON	85,01	14,22	99,23	342,9	3030
266.8 MCM	PATRIDGE	135,20	22,00	157,20	545,4	5100
477 MCM	HAWK	241,70	39,40	281,10	974,9	8820

5.2. Medium Voltage Poles

The poles used in Medium Voltage are named by specifying the name of the conductor they carry and the number of circuits.

5.2.1. 3 AWG, Single Circuit Iron Poles

Ilbank type painted welded iron poles were developed in lengths ranging from 10m to 20m with 2m intervals, in carrier, corner carrier, stopper, corner stopper, end and zaviye types. Figure 22. shows 3 AWG power transmission line carrier and stopper poles. Z and N poles are shown in Figure 23.

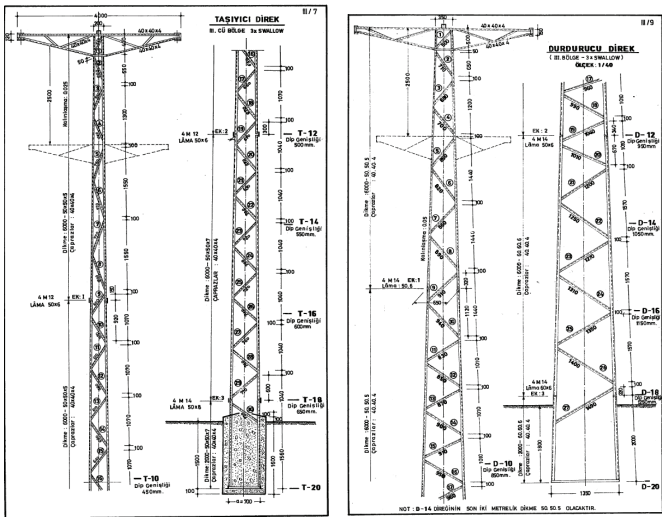

Figure 21. Technical Drawings of 3 AWG air line T and D Poles [8]

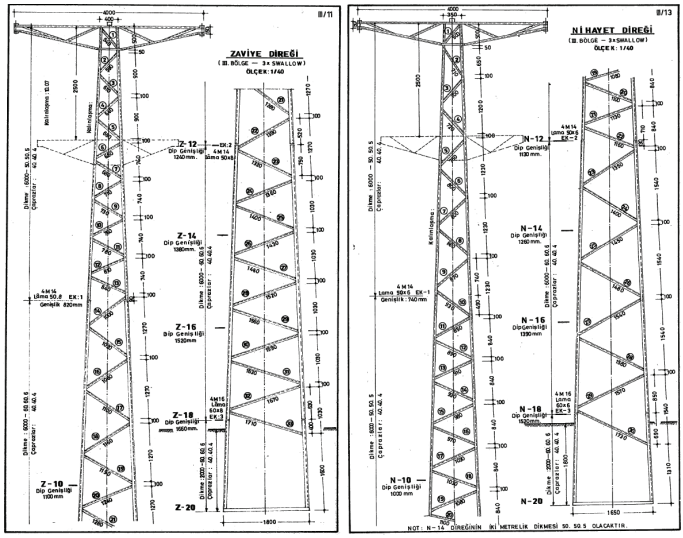

Figure 22. Technical Drawings of 3 AWG air line Z and N Poles [8]

5.2.2. 1/0 AWG (Raven), Single Circuit Painted-Welded Iron Poles

Some technical information about painted-welded poles with 1/0 AWG (Raven) conductors are given in Figure 23.

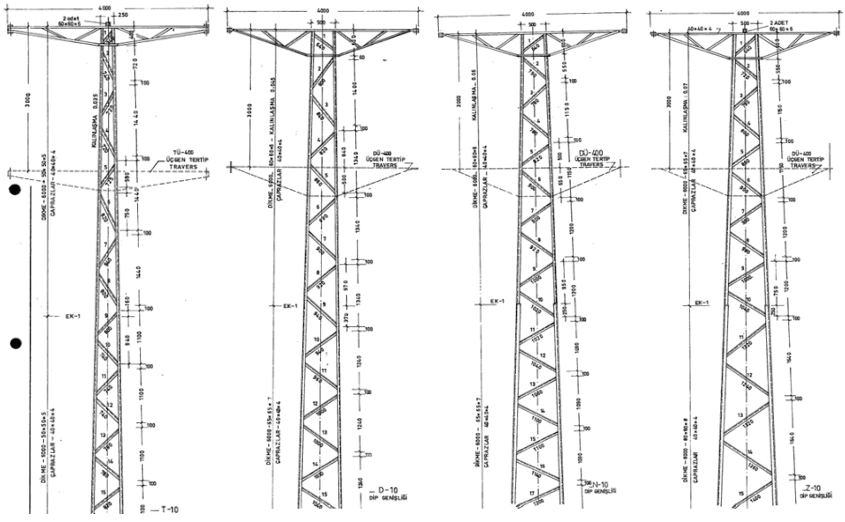

Figure 23. 1/0 AWG (Raven) air line Z and N Poles Technical Drawings [8]

5.2.3. Iron Poles with 3/0 AWG (Pigeon) Conductor

Iron poles with 3/0 AWG (Pigeon) conductors can be manufactured in

two types: painted welded and galvanized bolted.

5.2.3.1. Painted-Welded Iron Poles with 3/0 AWG Conductor

Some technical information of iron poles manufactured in painted welded type with 3/0 AWG (Pigeon) conductors are given in Figure 24.

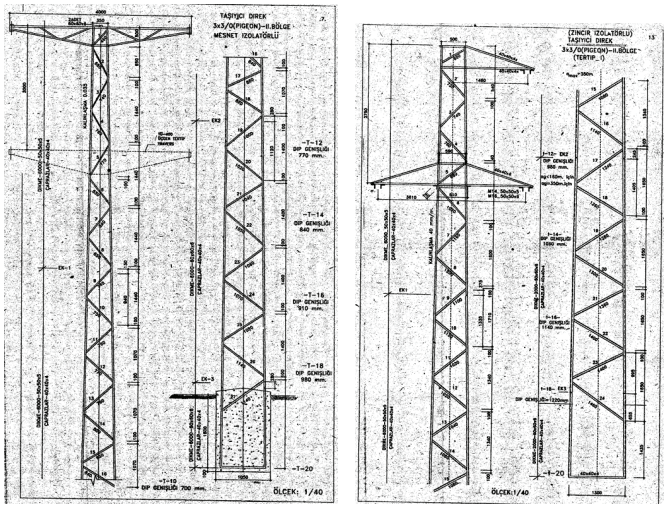

Figure 24. Technical Drawings of 3 AWG air line Z and N Poles

5.2.3.2. Galvanized-Bolted Iron Poles with 3/0 AWG Conductor

For galvanized-bolted iron poles with 3/0 AWG (Pigeon) conductors, single, two, four and six-circuit projects have been developed according to the number of circuits. The bolts of these poles are also galvanized and each type of pole has its own crossbar. Therefore, there is no need to select a separate traverse as in 3 AWG (Swallow) type and 1/0 AWG (Raven) type poles [1].

i. 3/0 AWG *Carrier Poles*

These single-circuit masts are manufactured in four types: BER, BES, BEY and BET. While the technical details are the same, the wind range of BEY and BET poles are different. Technical pictures of these poles are given in Figure 25.

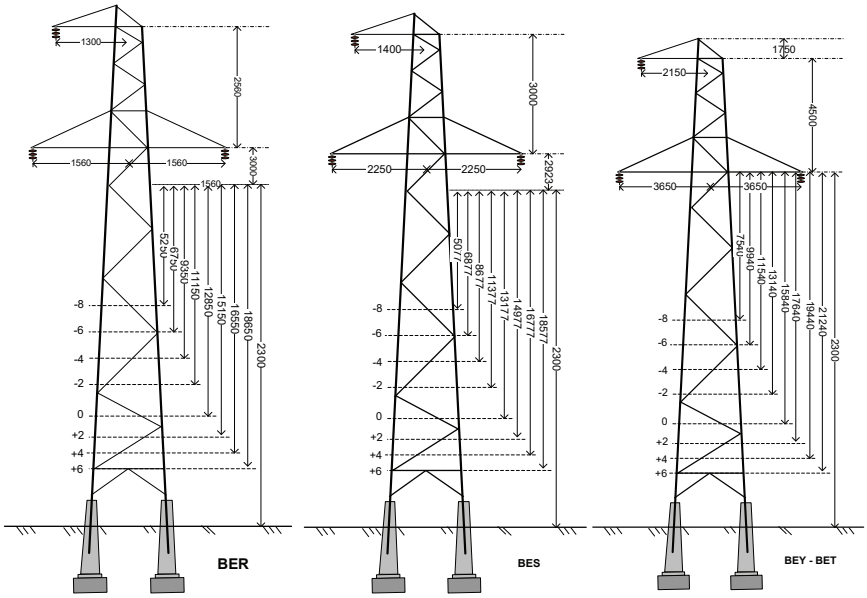

Figure 25. Technical Drawings of 3/0 AWG (Pigeon) air line BER, BES and BEY-BET Poles

ii. 3/0 AWG *Stopper Poles*

Among the galvanized-bolted iron poles with 3/0 AWG conductors, the pole that can only act as a stopper was manufactured as K type. The technical drawing of the K type pole is given in Fig. 26.

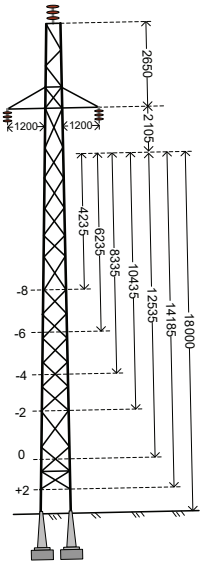

Figure 26. 3/0 AWG (Pigeon) air line Technical Information of K type Pole

iii. 3/0 AWG *Corner Stopper (KD) Poles*

Galvanized-bolted iron poles with 3/0 AWG (Pigeon) conductors were manufactured as L, LA, P, PA and R types. Technical pictures of these poles are given in Figure 27 and Figure 28 [1-12].

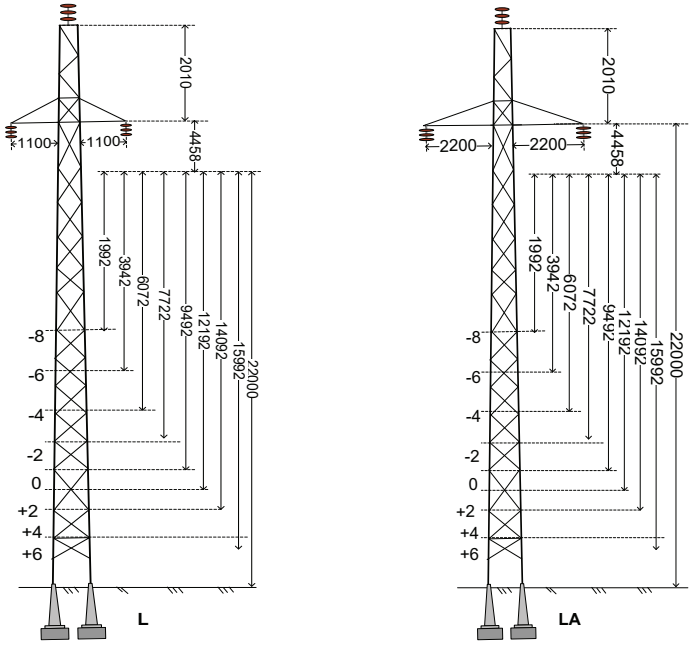

Figure 27. 3/0 AWG (Pigeon) air line Technical Information for L, LA, P, PA and R type Poles

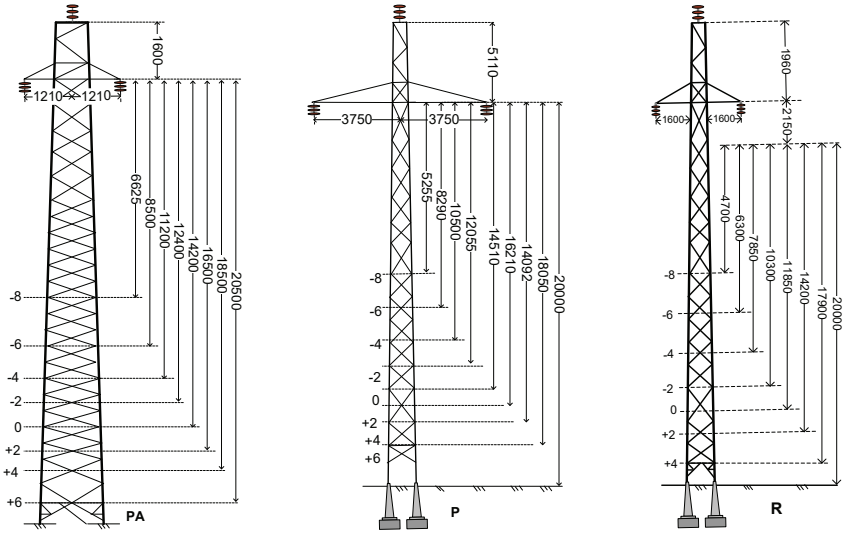

Figure 28. 3/0 AWG (Pigeon) air line Technical Information for L, LA, P, PA and R type Poles

iv. 3/0 AWG *End (N) Poles*

Galvanized-bolted iron poles with 3/0 AWG (Pigeon) conductors are L-type poles and these poles are manufactured in such a way that they can also serve as stopper poles at the corner.

6. Conclusion

In this study, basic information about the poles used in energy transmission and distribution is given. Specifications The classification of the poles carrying energy at MV level used in Turkey, information about their tasks and basic forms are given. Features Information on poles with 3 AWG (Swallow), 1/0 AWG (Raven) and 3/0 AWG (Pigeon) conductors are included.

7. References

[1] Yunusoğlu Atilla, High Voltage Power Transmission Lines Project and Special Dimensions of Power Transmission Lines.

[2] TEK, Distribution Networks, Project Department, Ankara, 1984.

[3] Low Voltage Iron Mast Resimleri, İller Bankası General Directorate Printing House, 1975.

[4] Altın Mahir, Mehmet Kızılgedik, Mustafa Üstünel, Electrification Basic Textbook, MEB, Ankara, 2001.

[5] Direkler, MEGEP, Ministry of National Education, Ankara, 2011.

[6] Transformer Pole Type Projects, Iller Bank General Directorate Printing House, 1985.

[7] 3 AWG (Swallow) Conductor 15 and 30 kV ENH Type Project, Iller Bank General Directorate Printing House, 1985.

[8] 1/0 AWG (RAVEN) 15-34,5 kV. Iron Direk Calculation and Drawings, Iller Bank General Directorate Printing House, 1981.

[9] Ortakek Demir Direk Resimleri, İller Bankası Genel Müdürlüğü Matbaası, 1981.

[10] Regulation on Electrical High Current Facilities, Ankara, 2000.

[11] Available at: https://cevikmuhendislik.com.tr/urun-kategori/boru-tipi-elektrik-diregi/.

[12] Available at: https://veravira.com/index.php/urun/enerji-nakil-hatti-direkleri-tip-2800-boy-20-mt/.

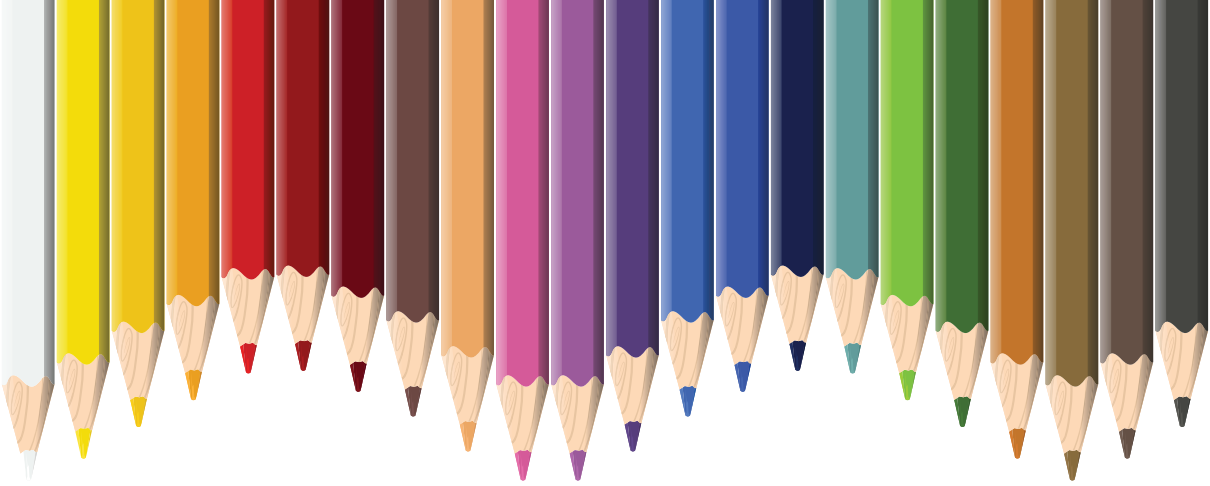

Chapter 7

ANALYSIS OF VIDEO-SHARING PLATFORM COMMENTS ABOUT FURNITURE PRODUCTS WITH WEB MINING APPROACHES

Selahattin BARDAK[1]

Timuçin BARDAK[2]

1 Associate Professor, Sinop University, Faculty of Engineering and Architecture, Department of Computer Engineering, Sinop, Turkey, ORCID ID: 0000-0001-9724-4762

2 Associate Professor, Bartın Vocational School, Department of Materials and Material Processing Technologies, Bartın, Turkey, ORCID ID: 0000-0002-1403-1049 E-mail: sbardak@sinop.edu.tr

INTRODUCTION

The furniture industry has an important position in all countries in terms of the employment and added value it provides. At the same time, furniture, an indispensable part of daily life, shapes living spaces with its aesthetic and functional features and increases users' comfort and quality of life. Innovation is considered an effective strategy for increasing organizational performance and strengthening competitiveness. In this context, it is stated that innovation includes critical elements for a more solid market positioning by ensuring the effective use of resources in organizations. (Guimarães et al., 2016). As in all industries, innovation is vital in the furniture industry.

Social media (SM) is a term that refers to innovative technological platforms that offer individuals the opportunity to produce and share their own original content. These platforms include popular social media tools such as Instagram, YouTube, and Facebook (Cox & Paoli, 2023; Mandiberg, 2012).

In recent years, with the influence of digitalization, the processes by which consumers determine their product preferences have changed greatly. In this change, video-sharing platforms play an important role. The furniture industry uses digital platforms effectively to understand consumers' aesthetic preferences and expectations, market their products and improve their designs. These platforms, especially video-sharing sites, offer companies in the sector the opportunity to introduce their products to large audiences, increase customer loyalty and interact with their target audience. By communicating directly with consumers through video-sharing platforms, furniture brands introduce their products more closely and have the opportunity to instantly evaluate consumer feedback. This trend is also taken into account in scientific research. Day by day, there is an increase in the number of studies on web mining in academic circles, and these studies generally focus on topics such as consumer behaviour, marketing strategies and design trends.

In the furniture industry, the use of new technologies, especially innovative approaches such as web mining, can bring about a significant transformation in design and production processes. In this context, the adoption of these advanced technologies allows actors in the sector to develop more innovative, effective, and high-value-added furniture designs and production processes.

WEB MINING

The advancement of artificial intelligence and big data technologies has led to a significant increase in the demand for big data experts in various industries. Governments, organizations, and businesses have adopted these technologies to discover the potential value contained in data, predict future trends, and contribute to smart decision-making processes (Ageed et al., 2021; Biao, 2023). Web mining is the process of obtaining important information by

analyzing the textual components of web content (Brauner et al., 2022; Xu et al., 2010). Nowadays, interest in web mining is constantly increasing. The main reason for this increase is that websites have the potential to provide access to a wide and diverse range of information sources. However, effectively extracting and using large amounts of information on the internet poses a significant challenge (Zhou et al., 2018). At this point, the need for innovative studies to transform large amounts of data into meaningful and usable information is increasing.

In the contemporary era, as e-commerce undergoes swift advancement, an increasing number of individuals are opting to make online purchases and share their reviews regarding the acquired products on the internet. Other methods based on survey data are also available for the evaluation of large-scale data; However, these methods are often costly and time consuming to implement in practice. Özellikle geniş örneklemlerle çalışmak, katılımcıları toplamak ve anket verilerini analiz etmek süreçlerinin karmaşıklığı nedeniyle araştırmacılara ciddi bir çaba gerektirebilir (Wu et al., 2014).

This study proposes a web mining-based method developed to help furniture manufacturers perform product evaluations more effectively. The proposed method aims to obtain more comprehensive information-based evaluations about furniture products by analyzing the data about furniture products on video-sharing sites and identifying keywords in the comments.

TEXT MINING

With recent developments in the field of text mining, web crawling, web extraction and text analysis software have become widely available, studies in various research areas have become easier (Schedlbauer et al., 2021). This allows various positive and negative comments about products around the world to be analyzed and important keywords to be extracted. In this way, companies can be directed to the areas they need to focus on primarily. Systematic text mining studies to be carried out to determine future design and production trends in the furniture industry are of critical importance in understanding, predicting, and influencing innovations and changing consumer demands in the sector.

MATERIAL AND METHOD

Data Collecting

This study is based on online search results conducted on public video sharing platforms between August 11, 2022 and August 11, 2023 in Turkey. Within the scope of the research, user comments in the 50 most watched furniture-themed videos were examined in detail and text data were collected systematically.

Data Analysis

RapidMiner software was used to analyze the obtained data. RapidMiner is a platform that is widely accepted in scientific research and contains important web mining tools. This software allows effective analysis of data and application of various statistical methods (Bardak et al., 2021; Ersen et al., 2023; Karayılmazlar et al., 2019; Ristoski et al., 2015; Sözen et al., 2018).

RapidMiner software enables data analysis by combining end-to-end operators to create complex processes. Within this software, each operator performs a specific task. For example, data reading operators are used to import the dataset and perform preprocessing steps, while model building operators create statistical or machine learning models suitable for analysis (Sözen et al., 2022).

Figure 1 shows the process diagram created with operators for the analysis of data obtained from video-sharing platforms.

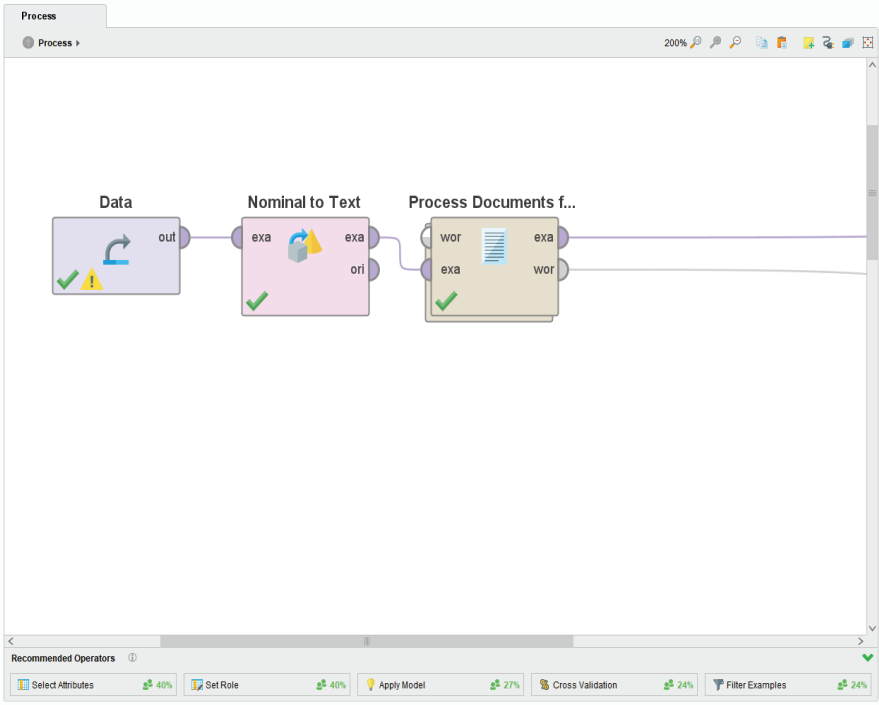

Figure 1. Process diagram created with operators for analysis of data obtained from video-sharing platforms.

Thanks to the analysis method, the most frequently mentioned keywords in the comments on video-sharing platforms were determined.

Figure 2 shows the process diagram created for detecting these keywords.

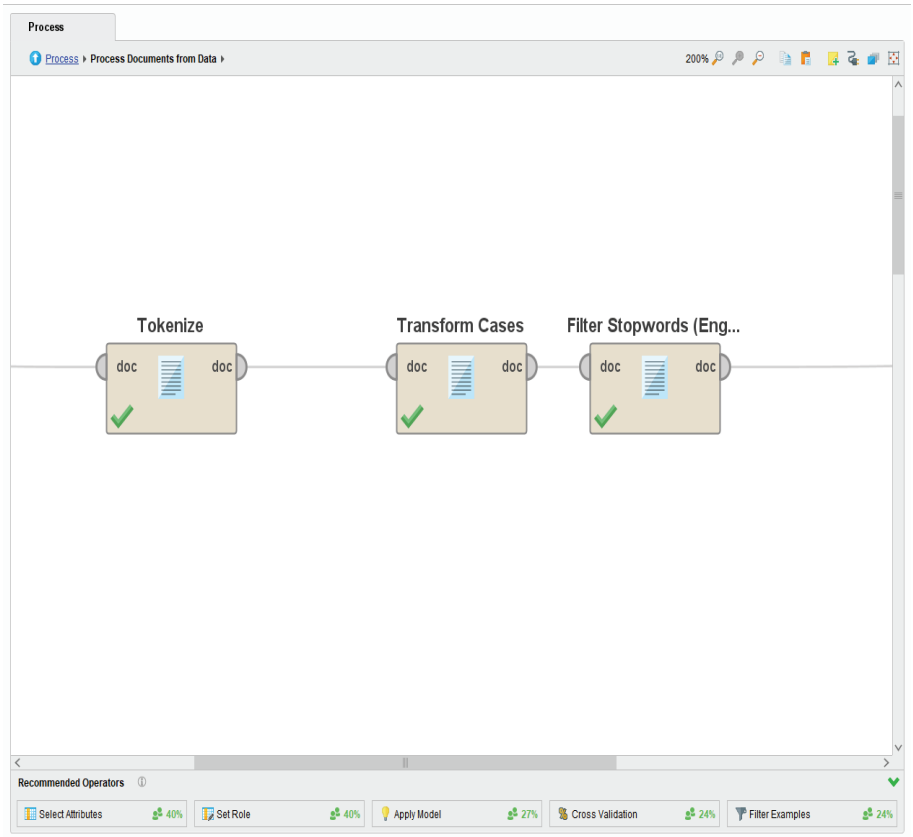

Figure 2. Process diagram created for the detection of keywords.

FINDINGS AND DISCUSSION

In this study, the 25 most frequently encountered words on video-sharing sites about furniture products were analyzed in line with the data obtained using web mining techniques. These words were determined as the key terms of the users regarding furniture products on online video platforms and were ranked by frequency analysis.

Table 1 shows the most common words obtained from comments on video-sharing platforms about furniture products.

Table 1. The most frequently used words obtained from the comments made on video sharing platforms about furniture products.

Word	**Frequency of occurrence of words in comments**	**Number of comments**
Many	125	96
Beautiful	81	75
Furniture	32	26
Good	28	21
Design	24	24
Great	23	23
Work	21	21
Video	17	15
Chic	17	17
Armchair	16	13
I want	14	13
Quality	11	11
New	11	9
Hello	10	10
Bed	10	8
Old	8	7
Easy	8	8
MDF	8	4
Modern	8	7
Perfect	8	8
Style	8	7
Changing	7	7
Brand	7	7
Table	7	6
Set	7	6

A word cloud is a tool that visually depicts word frequency in the text being analyzed. The more frequently the word is used in the text, the more prominently it appears in the created image. This tool is used to quickly understand the main themes and emphases of the text (R. Atenstaedt, 2012; R. L. Atenstaedt, 2021; McNaught & Lam, 2010).

Figure 3 shows the word cloud, which is a visualisation of the most frequently repeated words in viewer comments on furniture videos.

Figure 3. Word cloud, a visualization of the most frequently repeated words in viewer comments on furniture videos

According to the analysis results, it was determined that the most frequently used words were “very”, “beautiful”, “furniture”, “good” and “design”. These phrases show that furniture-related videos leave a positive impact on viewers. It also indicates that viewers are influenced by design, especially in videos. The obtained study results are consistent with the existing literature. In conducted research, it was determined which factors are prioritized in customers’ furniture purchasing decisions. More than half of the survey respondents stated that quality and design are determining factors in purchasing decisions (Pirc Barčić et al., 2021). Secondary important words include “great”, “effort”, “video”, “chic” and “seat”. These words show that labor-intensive content and sofa furniture attract special attention from the audience.

The study provides valuable insight into understanding the effects of digital platforms on the furniture industry. This analysis was conducted to de-

termine consumers' preferences and trends regarding furniture products, to optimize marketing strategies and to guide future research on the industry.

CONCLUSION

The furniture industry is a vital sector globally, and data analysis in this sector is fundamental to understanding consumer behaviour. This study was carried out through viewer comments obtained from furniture-focused videos on video-sharing sites. Using Rapidminer data platform software, keywords were successfully obtained from the comments. Keywords are critical to understanding the main themes and emphases of the comments. According to the analysis results, it was determined that the most frequently used keywords were "very", "beautiful", "furniture", "good" and "design". The context in which these words appear frequently shows that furniture videos have a positive impact on viewers, with particular emphasis on design. The findings underline the effectiveness of visual content and the importance of design in the field of furniture and show that content strategies to increase audience satisfaction and appreciation are valuable. These results provide important clues for digital marketing and content production strategies in the furniture industry. The study shows that comments on video-sharing sites can be considered an important source.

REFERENCES

Ageed, Z. S., Zeebaree, S. R. M., Sadeeq, M. M., Kak, S. F., Yahia, H. S., Mahmood, M. R., & Ibrahim, I. M. (2021). Comprehensive survey of big data mining approaches in cloud systems. Qubahan Academic Journal, 1(2), 29–38.

Atenstaedt, R. (2012). Word cloud analysis of the BJGP. British Journal of General Practice, 62(596), 148.

Atenstaedt, R. L. (2021). Word cloud analysis of historical changes in the subject matter of public health practice in the United Kingdom. Public Health, 197, 39–41. https://doi.org/https://doi.org/10.1016/j.puhe.2021.06.010

Bardak, S., Bardak, T., Peker, H., Sözen, E., & Çabuk, Y. (2021). Predicting Effects of Selected Impregnation Processes on the Observed Bending Strength of Wood, with Use of Data Mining Models. Bioresources, 16(3).

Biao, Z. Z. (2023). Design and realization of data mining simulation and methodological models. Journal of King Saud University - Science, 35(10), 102964. https://doi.org/https://doi.org/10.1016/j.jksus.2023.102964

Brauner, T., Heumann, M., Kraschewski, T., Prahlow, O., Rehse, J., Kiehne, C., & Breitner, M. H. (2022). Web content mining analysis of e-scooter crash causes and implications in Germany. Accident Analysis & Prevention, 178, 106833. https://doi.org/https://doi.org/10.1016/j.aap.2022.106833

Cox, L. T. J., & Paoli, L. (2023). Social media influencers, YouTube & performance and image enhancing drugs: A narrative-typology. Performance Enhancement & Health, 11(4), 100266. https://doi.org/https://doi.org/10.1016/j.peh.2023.100266

Ersen, N., Bardak, T., & Usta, U. C. (2023). Veri Madenciliğine Dayalı Olarak Çalışanların Örgütsel Bağlılık Düzeyinin Belirlenmesi: İstanbul ve Kocaeli Örneği. Bartın Orman Fakültesi Dergisi, 25(3), 398–410. https://doi.org/10.24011/barofd.1329758

Guimarães, J. C. F. de, Severo, E. A., Dorion, E. C. H., Coallier, F., & Olea, P. M. (2016). The use of organisational resources for product innovation and organisational performance: A survey of the Brazilian furniture industry. International Journal of Production Economics, 180, 135–147. https://doi.org/https://doi.org/10.1016/j.ijpe.2016.07.018

Karayılmazlar, S., Bardak, T., Avcı, Ö., Kayahan, K., Karayılmazlar, A. S., Çabuk, Y., Kurt, R., & İmren, E. (2019). Determining the orientation in choosing furniture based on social media based on data mining algorithms: Twitter example. Turkish Journal of Forestry | Türkiye Ormancılık Dergisi, 2019(4), 447–457. https://doi.org/10.18182/tjf.609967

Mandiberg, M. (2012). The social media reader. In The Social Media Reader. https://doi.org/10.18574/nyu/9780814763025.001.0001

McNaught, C., & Lam, P. (2010). Using Wordle as a supplementary research tool. Qualitative Report, 15(3), 630–643.

Pirc Barčić, A., Kitek Kuzman, M., Vergot, T., & Grošelj, P. (2021). Monitoring consumer purchasing behavior for wood furniture before and during the COVID-19 pandemic. Forests, 12(7), 873.

Ristoski, P., Bizer, C., & Paulheim, H. (2015). Mining the Web of Linked Data with RapidMiner. Journal of Web Semantics, 35, 142–151. https://doi.org/10.1016/J.WEBSEM.2015.06.004

Schedlbauer, J., Raptis, G., & Ludwig, B. (2021). Medical informatics labor market analysis using web crawling, web scraping, and text mining. International Journal of Medical Informatics, 150, 104453. https://doi.org/https://doi.org/10.1016/j.ijmedinf.2021.104453

Sözen, E., Bardak, T., Aydemİr, D., & Bardak, S. (2018). Estimation of deformation in nanocomposites using artificial neural networks and deep learning algorithms. Journal of Bartin Faculty of Forestry, 20(2), 223–231.

Sözen, E., Bardak, T., & Bardak, S. (2022). FP-Growth Algoritması Kullanılarak Tüketiciler ve Mobilya Kullanım Süresi Arasındaki İlişkilerin Belirlenmesi. Bartın Orman Fakültesi Dergisi, 24(2), 194–201. https://doi.org/10.24011/barofd.1033195

Wu, M., Wang, L., Li, M., & Long, H. (2014). An approach of product usability evaluation based on Web mining in feature fatigue analysis. Computers & Industrial Engineering, 75, 230–238. https://doi.org/https://doi.org/10.1016/j.cie.2014.07.001

Xu, G., Zhang, Y., & Li, L. (2010). Web mining and social networking: techniques and applications (Vol. 6). Springer Science & Business Media.

Zhou, J., Cheng, C., Kang, L., & Sun, R. (2018). Integration and Analysis of Agricultural Market Information Based on Web Mining. IFAC-PapersOnLine, 51(17), 778–783. https://doi.org/https://doi.org/10.1016/j.ifacol.2018.08.101

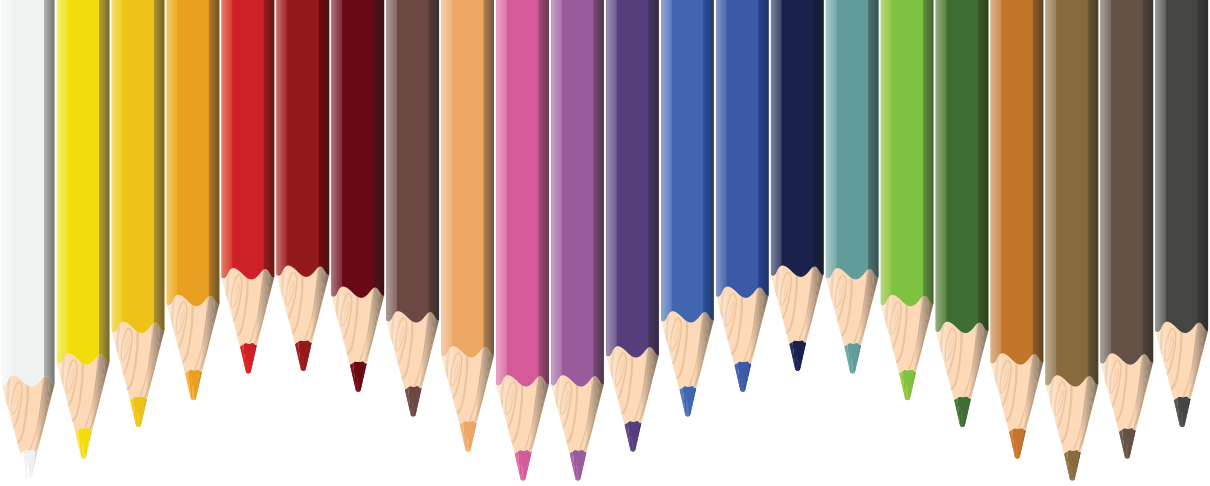

Chapter 8

EXPERIMENTAL INVESTIGATION OF DARRIEUS-SAVONIUS HYBRID VERTICAL AXIS WIND TURBINE PERFORMANCE FOR HOME APPLICATIONS[1]

Faruk KÖSE[2]

İsmail ARDIÇ[3]

1 This publication is derived from master's thesis entitled "Experimental Investigation of Vertical Axis Wind Turbine Performance for Domestic Applications", conducted by İsmail ARDIÇ under the supervision of Assoc. Prof. Dr. Faruk KÖSE, Konya Technical University, Institute of Graduate Studies, Department of Mechanical Engineering.

2 Assoc.Prof. Dr. Faruk KÖSE, Konya Technical University, Faculty of Engineering and Natural Sciences, Department of Mechanical Engineering. fkose@ktun.edu.tr ORCID NO: 0000-0003-2171-9148

3 Mechanical Engineer, Yıldız Technical University, Institute of Science and Technology, Department of Mechanical Engineering, PhD student. İsmail.ardic@std.yildiz.edu.tr ORCID NO: 0009-0005-2586-1004

1. INTRODUCTION

In our country, wind energy ranks first among the renewable energy sources used for electricity generation in recent years. However, wind turbines established to generate energy are built in places far from the areas where people live due to some technical and environmental reasons. Even small wind turbines have not yet adapted to social life. For our world in general and our country in particular to get rid of the increasingly harmful effects of the use of fossil fuels, it is necessary to increase the use of all renewable energy sources, especially wind energy.

In this publication, it is aimed to show that a certain part of the electrical energy consumed by people in the living areas where they continue their daily lives can be produced by small wind turbines that are compatible with the environment. In the study, a system combining a large number of Savonius and Darrieus turbines on a tree-type body was designed and manufactured. In this hybrid system, there is a Savonius turbine with two blades in the form of a truncated Φ (fi) with drag force effect and a H tpi Darrieus turbine with two blades. Since the non-helical Darrieus turbines need a starting motor to start the first movement, the Savonius turbine provides this first movement in this system. However, when these two turbines with different characteristics power a shaft coupled together, they have the effect of increasing and decreasing the efficiency of each other. In this study, the total system and the individual efficiencies of each turbine will be investigated and discussed. Thus, a contribution will be made to the dissemination of these turbines in domestic and small power usage areas.

1.1. Status of Wind Energy in the World and Türkiye

In recent years, the tendency towards renewable energy sources has been increasing day by day. Among renewable energy sources, wind energy has an important place in terms of efficiency. Wind energy has recently entered a rapid progress process in the world and in parallel with this in our country. Wind energy is one of the renewable energy sources whose use is increasing the most in the world. According to the 2023 report of the Global Wind Energy Association (GWEA), the historical development of the total installed capacity of wind energy in the world is shown in Figure 1.1 (Williams and Zhao, 2023).

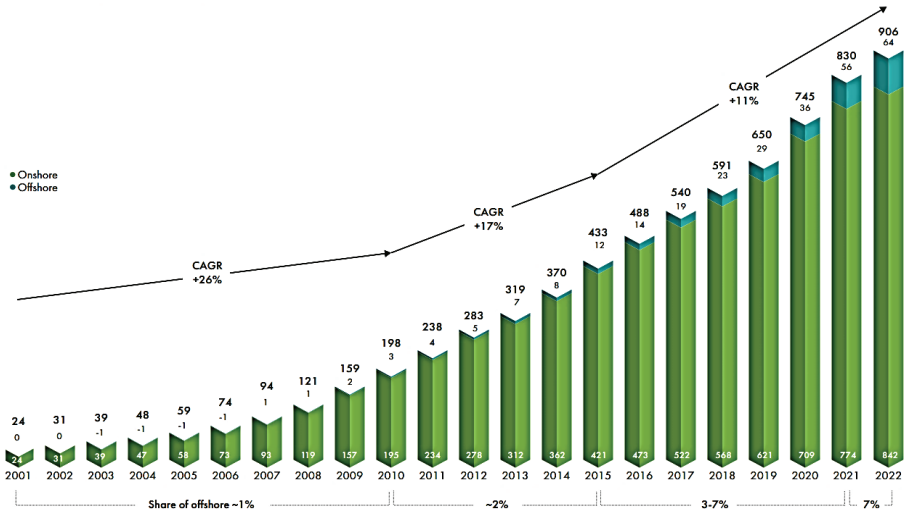

Figure 1.1. Development of the total installed wind power capacity in the world between 2001 and 2022, GW (Williams and Zhao, 2023).

As can be seen here, the installed capacity of wind energy in the world has continued to increase every year since 2001. Especially since 2007, the upward movement in the acceleration of increase is remarkable. This orientation towards wind energy has led to an increase in scientific studies to increase the efficiency of wind turbines. With 78 GW of new capacity added globally in 2022, the total global installed capacity increased to 906 GW. This represents an annual growth rate of 9 per cent.

According to the GWEA market analysis forecast, 2023 will be the first year to exceed 100 GW of new capacity added globally, with annual growth of 15%. The world's top five markets in terms of new installations in 2022 are China, the United States, Brazil, Germany, and Sweden. Together, these countries accounted for 71 per cent of global installations last year. With the return of strong growth in established European markets such as Germany, Spain, the UK, France, Italy, Italy and Türkiye, the European onshore market will re-energise from 2024 onwards. The GWEA market analysis forecasts 680 GW of new capacity over the next five years (2023-2027). This represents 136 GW per year until 2027. Whereas GWEA previously forecast that 1078 GW would be built between 2022 and 2030, it is now estimated that this will be supplemented by 1221 GW of new capacity between 2023 and 2030 (Williams and Zhao, 2023).

At the end of 2022, the total installed capacity of wind energy in the world is 906 GW, of which 842 GW is onshore and 64 GW is offshore wind power. Some of the leading regions in wind power plant installation are Oceania, North America, Asia, Eastern Europe, and Russia. According to the 2023 report of the GWEA, the top 11 countries are China, the United States,

Germany, India, Spain, Brazil, France, Canada, the United Kingdom, Sweden, and Türkiye (Figure 1.2) (Williams and Zhao, 2023).

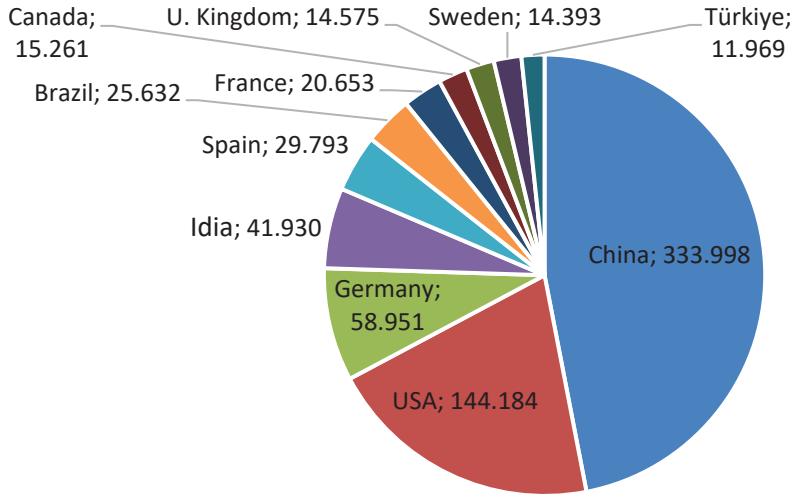

Figure 1.2. Eleven countries with the highest world wind installed capacity (MW) at the beginning of 2023

As of the beginning of 2023, Türkiye ranks 6th in Europe and 11th in the world in terms of total installed wind power capacity. Türkiye has a significant wind energy potential. As of the end of September 2023, Türkiye's installed capacity reached 105.667,8 MW (Table 1.1). As of the end of September 2023, the distribution of our installed capacity by resources is as follows: 29,9% hydraulic energy, 24,4% natural gas, 20,3% coal, 11% wind, 10,3% solar, 1,6% geothermal and 2,6% other resources. According to the results of Türkiye's National Energy Plan, electricity consumption is expected to reach 380,2 TWh in 2025, 455.3 TWh in 2030 and 510.5 TWh in 2035. In 2022, 34,6% of our electricity generation was from coal, 22,9% from natural gas, 20,3% from hydraulic energy, 10,6% from wind, 5,1% from solar, 3,4% from geothermal energy and 3% from other sources (EMRA, 2023).

Table 1.1. Türkiye 2022 September-2023 September electricity installed capacity and generation values (EMRA, 2023)

TYPE OF RESOURCE	TOTAL INSTALLED POWER* (MW)				TOTAL PRODUCTION* (MWh)			
	2022 SEPTEMBER	RATE (%)	2023 SEPTEMBER	RATE (%)	2022 JANUARY-SEPTEMBER	RATE (%)	2023 JANUARY-SEPTEMBER	RATE (%)
HYDRAULIC	31.567,74	30,86	31.594,72	29,90	57.066.065,86	22,94	48.997.843,44	19,94
WIND	**11.195,62**	**10,95**	**11.609,05**	**10,99**	**26.114.392,50**	**10,50**	**25.393.335,62**	**10,34**
SUN	8.961,71	8,76	10.899,25	10,31	12.339.932,62	4,96	15.031.175,63	6,12
BIOMASS	1.819,43	1,78	2.049,15	1,94	6.841.691,92	2,75	7.199.682,64	2,93
GEOTHERMAL	1.686,34	1,65	1.691,39	1,60	8.218.808,62	3,30	8.075.377,10	3,29
RENEWABLE	**55.230,83**	**54,00**	**57.843,56**	**54,74**	**110.580.891,5**	**44,45**	**104.697.414,4**	**42,62**
NATURAL GAS	25.681,83	25,11	25.742,93	24,36	57.439.356,83	23,09	53.831.845,35	21,91
IMPORTED COAL	9.713,80	9,50	10.373,80	9,82	42.950.341,46	17,26	52.537.031,10	21,39
LITH	10.138,96	9,91	10.193,96	9,65	33.643.700,97	13,52	30.277.927,41	12,32
HARD COAL	840,77	0,82	840,77	0,80	2.665.195,75	1,07	2.653.541,09	1,08
ASPHALT+ Fu.Oil	665,13	0,65	665,13	0,62	1.485.850,87	0,59	1.670.220,95	0,68
THERMAL	**47.048,21**	**46,00**	**47.824,31**	**45,26**	**138.194.830,6**	**55,55**	**140.970.565,9**	**57,38**
TOTAL	**102.279,04**	**100,00**	**105.667,86**	**100,00**	**248.775.722,2**	**100,0**	**245.667.980,3**	**100,00**

*Licenced and unlicensed power plants are included

In Türkiye, it is assumed that a wind power plant with a capacity of 5 MW per square kilometre can be established in areas 50 metres above ground level and with wind speeds above 7,5 m/s. In the light of these assumptions, a Wind Energy Potential Atlas (WEPA) was prepared in which wind resource information was provided using a medium-scale numerical weather forecast model and a micro-scale wind flow model. Türkiye's wind energy potential is determined as 48.000 MW. The total area corresponding to this potential corresponds to 1,30% of Türkiye's surface area. Considering the wind energy potential of 6 m/s and above, a total installed capacity of 78.000 MW can be reached. The energy obtained from wind energy has been increasing since the beginning of the 2000s. Figure 1.3 shows the development of wind power plants in Türkiye between 2011 and 2022 according to the data of Energy Market Regulatory Authority (EMRA) and Ministry of Energy and Natural Resources (MENR). According to this development, the installed capacity, which was 1729 MW in 2011, increased 6,6 times until 2022 and reached 11.367 MW.

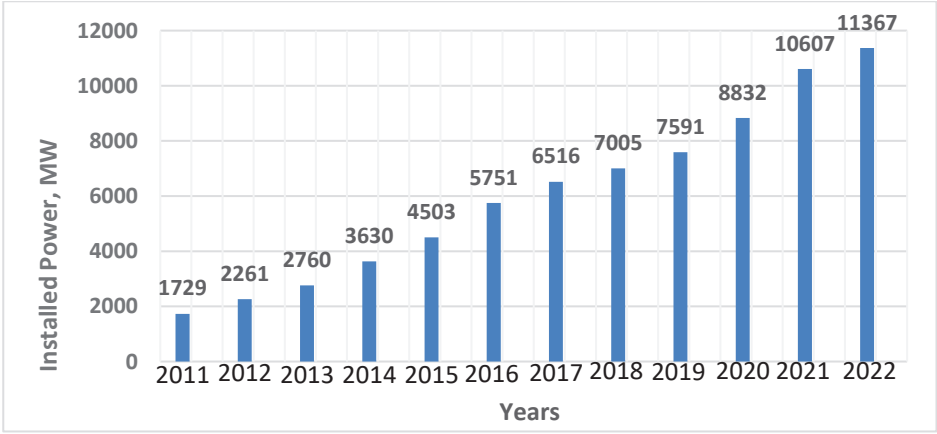

Figure 1.3. Development of wind power plants in Türkiye between 2011-2022

2. WIND TURBINE TYPES AND OPERATING PRINCIPLES

Wind turbines are a system that has a moving rotor and converts the kinetic energy of the air flow (wind) coming to its blades into mechanical energy and electrical energy in its generator. Although wind turbines are divided into certain types, their general principle is to generate electricity with the blade and rotor system that converts the kinetic energy in the wind into mechanical energy. Wind turbines are generally divided into 3 types according to the rotation axes of their rotors: horizontal axis, vertical axis and oblique axis.

2.1. Horizontal Axis Wind Turbines

The rotation axis of horizontal axis turbines is parallel to the direction of winds and the blades are perpendicular. As the number of rotor blades decreases, it rotates faster and generates more electricity. The efficiency of such turbines is approximately 45%. Horizontal axis turbines are usually placed at a height of 20 to 200 m from the ground, depending on the size of the turbine, with a tower height equal to the rotor diameter. The ratio of the wind speed to the peripheral speed of the turbine blade is called the tip speed ratio (λ).

Figure 2.1 shows the main parts of horizontal axis propeller type wind turbines and the principle of wind flow directions and forces on the turbine blade. Horizontal axis wind turbines consist of 4 main parts as tower, body, rotor, and blade.

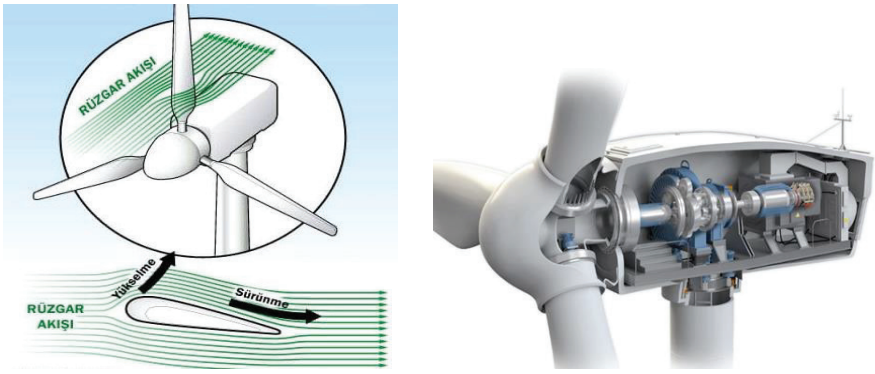

(a) (b)

Figure 2.1. Horizontal axis wind turbine (a) wind flow directions on the blade, (b) view of the turbine body and cabin parts (Ardıç, 2019)

2.2. Vertical Axis Wind Turbines

The axis of rotation of vertical axis wind turbines (VAWT) is perpendicular to the wind direction. VAWT can receive wind from all directions and generates electricity with rotation movement accordingly. With this feature, it has an advantage over other turbine systems. The efficiency of these turbines, which produce energy with the force of dragging the wind, is approximately 35%. The gearbox and generator of these turbines, which operate without the need for a tower as high as the horizontal axis ones, can be installed at ground level and therefore the lower parts of the turbine blades have to work at low wind speeds. Because of the roughness of the earth, the wind speed decreases as it approaches the ground level and its speed increases as it rises above the ground. Vertical axis turbines occupy less space than horizontal axis turbines but produce less power accordingly. The most common vertical axis wind turbines are.

1. Darrieus turbine,
2. They are divided into 2 as Savonius turbine.

Darrieus wind turbines were invented by George J.M. Darrieus, a French engineer. The tensile stress on the blades is very low as they have a slight inclination. It can operate at high wind speeds, but a drive motor is required for the first movement (rotation). Although there has been a significant increase in studies on Darrieus wind turbines in recent years, they have not yet become as widespread as horizontal axis wind turbines. Darrieus wind turbines are made in 5 different types: D type, H type, Fi type, Delta type and Helical type (Figure 2.2).

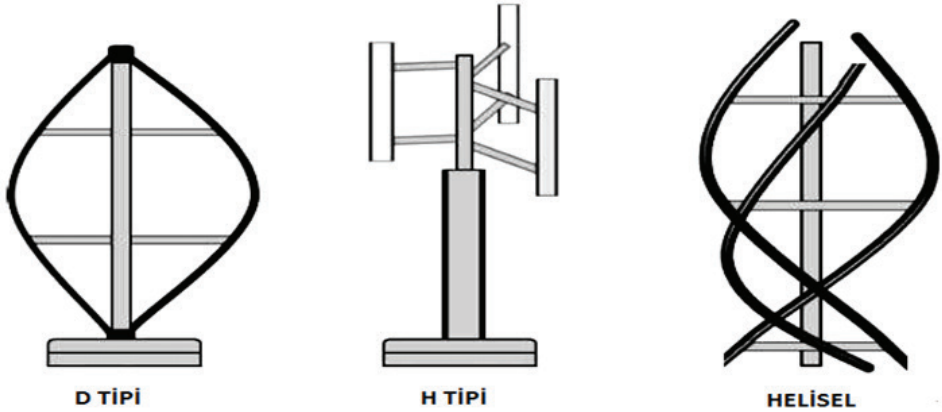

Figure 2.2. Three different variants of the Darrieus wind turbine (Deda et al., 2006)

Another vertical axis wind turbine that works with the effect of wind drag force is the Savonius wind turbine, named after the Finnish inventor Sigurd Savonius. The Savonius rotor is an "S" shaped rotor obtained by cutting the vertically standing cylinder in half and sliding it. The working principle of this rotor is that when the wind coming at a certain speed hits the rotor, a positive moment occurs in the inner part of the semicircular cylinder and a negative moment occurs in the outer part of the semicircular cylinder, and the Savonius rotor starts to rotate because the moment formed in the inner part is greater than the moment in the outer part. Figure 2.3 shows the rotation phase of the rotor. As can be seen from the figure, with the wind hitting the blades, the force generated due to the pressure on the wing facing inward to the wind (the advancing wing) is greater than the force on the returning wing. Thus, the Savonius wind turbine starts to rotate since the moment of the advancing blade relative to the centre point is greater than the returning blade. In vertical axis wind turbines, no matter which direction the wind blows, the turbine will start to rotate and generate power except for some critical points (Deda et al., 2006).

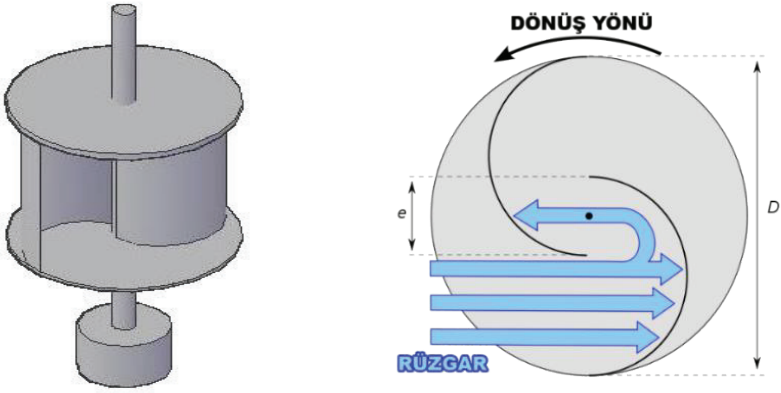

Figure 2.3. Savonius wind turbine rotor and drag force on the blade

Darrieus-Savonius Combined (Hybrid) Wind Turbines

In recent years, Darrieus and Savonius wind turbines have been designed together in order to utilise wind energy more. In this way, the first movement of the Darrieus wind turbine is given by the Savonius wind turbine. With the combined (hybrid) system, both the problem of the first movement for the Darrieus turbine is solved and the total power obtained increases. Figure 2.4. shows the front and top views of the Darrieus-Savonius hybrid wind turbine.

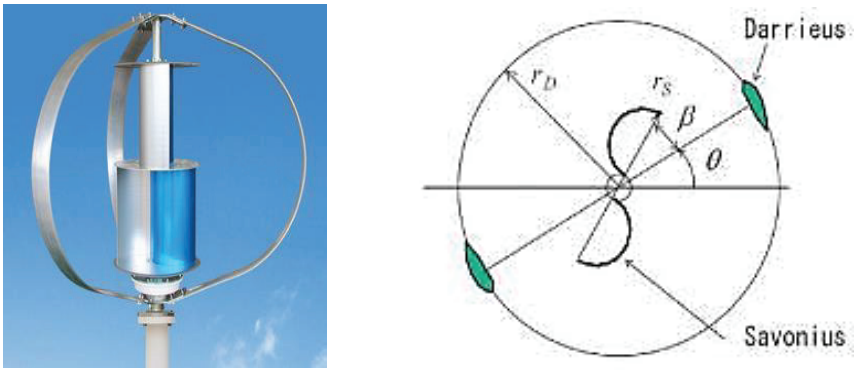

(a) (b)

Figure 2.4. Darrieus-Savonius hybrid wind turbine front (a) and (b) top views (Deda et al., 2006)

2.3. Source Research on Vertical Axis Turbines

Looking at the studies on vertical axis wind turbines in the literature, it is noteworthy that there has been a recent tendency towards hybrid turbines in order to increase performance.

In their study, Gavalda et al. (1990) proposed a new combined Darrieus-Savonius wind wheel design and conducted experiments. They analysed the starting moment and power coefficients of the Darrieus-Savonius wind wheel and found the maximum power coefficient to be 0,35. Köse (2003), in his study, showed that the electricity demand of wind measurement stations, which are generally established in places far from the grid, can be easily met with a mini Darrieus-Savonius wind turbine by calculating according to the wind measurement data of Selçuk University Campus. Deda et al. (2006) placed a screen in front of the Savonius wind turbine in order to increase the efficiency of the wind turbine and to prevent the negative moment acting on the convex surface of the turbine. The static and dynamic moments of the wind turbine were measured experimentally with and without a baffle. Using Computational Fluid Dynamics (CFD), the experimental data and CFD results were compared. It was observed that the power coefficient increased to 38% with the pitched model.

Aktemur (2010) performed computer-aided analyses of different Savonius wind turbines by keeping the wind speed and flow conditions constant. In the study, the ratio of wing sliding distance to wing diameter was selected as 0, 0,4 and 0,8. As a result of the computer-aided analyses, the best performance was observed in the design with a 3-blade slip distance/blade diameter ratio of 0,4. Lee et al. (2016), in their study, investigated the effect of twist angle on Savonius wind turbine performance. The power coefficient (Cp) at different tip speed ratios (TSR) and torque coefficient (CT) at different azimuths for helical blade angles of 0, 45, 90 and 135 were observed under a fixed projection field condition. Our results showed that the maximum power coefficient (Cp, max) values in both cases have similar trends for the TSR range considered in this study, i.e. between 0.4 and 0.8, except for the 45^{o} bend angle.

Ramesh et al. (2017), in their study, investigated the power coefficient of a hybrid turbine including the combination of Savonius and Darrieus. For this purpose, the Savonius turbine was first tested experimentally with two, three and four blades. The tests showed that the 3-blade rotor has a higher power coefficient than the two and four blades at low wind speeds. In Balduzzi (2017), the effect of using Kline-Fogleman blades in a Darrieus turbine on power generation was investigated by means of pre-validated computational fluid mechanics (CFD) analyses. As a result, he found that, contrary to expectations, stepping the blade reduces the power generated by 28% (externally stepped) to 44% (internally stepped) at high tip speeds (rotational

speeds). However, at low tip speeds (rotational speeds), the external stepping increased the power and torque by 33%.

Hashem et al. (2018), in their study, investigated the aerodynamic performance improvements of the H-rotor Darrieus wind turbine. In the aerodynamic performance evaluation, the cross-sectional profiles of the Darrieus turbine blade were performed for 24 new airfoils (symmetric and non-symmetric) to increase the generated power. As a result, it is shown that the symmetrical S1046-type is the blade type with the best performance for a typical tip speed ratio ranging from 2 to 7 and that the maximum power coefficient of a three-blade Darrieus turbine (consisting of S1046 blades) equipped with a cycloidal surface diffuser is equal to 0,3463.

Douak et al. (2018), in their study, aimed to design an optimised Darrieus type wind turbine capable of starting at low wind speeds. The study consists of three parts: firstly, the angle of attack monitoring and control system allowing self-starting at low wind speeds is presented, the second part presents a general method to obtain a profile with a good starting torque and the third part. As a result, it is shown that $\alpha=15°$ is the optimal angle of attack that provides maximum torque. It is also shown that a three-bladed rotor will self-start regardless of the starting position and verified by tests on a turbine model in a wind tunnel.

3. EXPERIMENTAL STUDY OF DARRİEUS-SAVANİUS HYBRID TURBINE

The experiments to be carried out in the study were carried out by placing an appropriate size turbine in a ready-made wind tunnel. The turbine design to be tested was manufactured according to the formulae and assumptions given in the existing literature. For this, in the first stage, the most appropriate dimensions and technical parameters of the vertical axis wind turbine with Savonius airfoil were determined and the airfoil drawings of the turbine to be designed were made. The number of blades was taken as 2 and DC generator was used as generator. "National Advisory Committee for Aeronautics (NACA)" and other suitable profiles were taken into consideration in the blade profile selection. A mould was prepared from Styrofoam material and the turbine blade was manufactured from polyester impregnated glass fibre. During the experiments, a recorder feature thermometer, and an anemometer to measure the air velocity were installed in the necessary sections on the experimental set. As a result, the efficiency of the designed hybrid system was compared and interpreted with the Savonius wind turbine operating alone. Figure 3.1 shows the shapes of Savonius and Darrieus-Savonius hybrid wind turbine.

The Darrieus turbine, which will work in conjunction with the Savonius turbine, was designed and tested alone. After the manufacturing according to the formulae and assumptions in the existing literature, the designed Savonius

and Darrieus turbines were mounted on the same chassis and a hybrid system was formed. This system was subjected to a number of tests in the wind tunnel test setup and the turbine power and power coefficient were calculated. As a result, the most suitable parameters for the vertical axis Savonius wind turbine with Darrieus turbine are determined and interpreted.

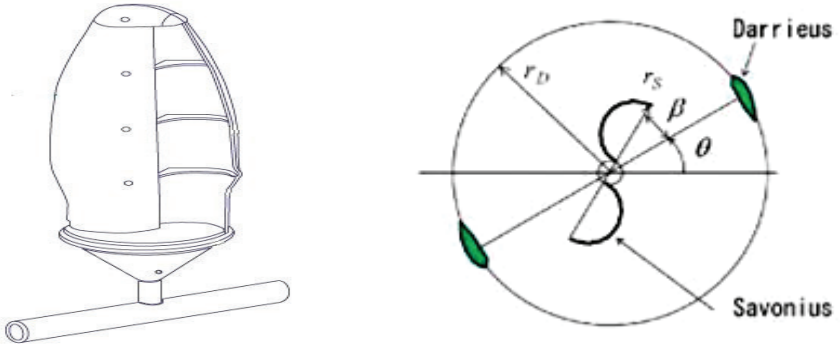

(a) (b)

Figure 3.1. Savonius (a) and Darrieus-Savonius wind turbine (b) (Ardıç, 2019)

The turbine output power is given by (3.1), the turbine current duty is given by (3.2) and the turbine efficiency is given by (3.3).

$$P_t = \frac{2\pi\eta_t M}{60} \tag{3.1}$$

$$P_{tot} = \Delta P_t \dot{Q}v \tag{3.2}$$

$$\eta_t = \frac{P_t}{P_{tot}} \tag{3.3}$$

In these expressions, M is the rotational torque, $\dot{Q}v$; is the volumetric air flow rate and ΔP_t; is the pressure change across the turbine region. In addition, the power coefficient (C_p) of the turbine will be calculated by equations (3.4) and the potential power of the wind by equations (3.5).

$$C_p = \frac{P}{P_o} \tag{3.4}$$

$$P_o = \frac{1}{2} * \rho * S * v^3 \tag{3.5}$$

In these equations, P is the electrical power (W) obtained from the turbine, P_o; is the potential power of the wind, ρ is the density of the air (kg/m³), A is the area affected by the wind (m²) and v is the wind speed (m/s).

3.1. Manufacturing of Savonius Wind Turbine

The designed Savonius wind turbine will continue with an increasing diameter dimension from the top to the middle part and then it will be narrowed again and completed at the value of the diameter dimension at the top. In this context, from the top to the bottom of one bucket of the turbine is divided into 6 circular regions. Their radii were chosen as 1st 10 cm, 2nd 12,5 cm, 3rd 15 cm, 4th 316 cm, 5th 15 cm and 6th 10 cm. The height was determined as 75 cm. Figure 3.2. shows the drawing of the designed Savonius wind turbine.

The rotor radius d of the Savonius turbine is calculated according to equation (3.6);

$$S=2.d.h \tag{3.6}$$

Where; S=Swept area of the impeller (m^2), d=Radius (m), h=half the height (m)

$S=2x0,32x0,75 =0,48\ m^2$

Calculated as.

For the density of the air, the density at sea level (1,25 kg/m3) and the average wind speed is taken as 10 m/s. In this case, the power of the air passing over the turbine is obtained by equation (3.7).

$$P_{max} = \frac{1}{2}\rho S V^3 \tag{3.7}$$

$$P_{max} = \frac{1}{2}1,25x0,48x10^3 = 300\ \text{W}$$

is found as. If we use the power coefficient c_p=0.15, the power of the Darrieus wind turbine is found using equation (3.8.).

$$P = C_p . P_{max} \tag{3.8}$$

$$P = 0,15x300 = 45\ W$$

is found as. Various materials are used for wind turbine blades. Some of these materials are metal, wood and epoxy. In this project, glass fibre reinforced polyester was used to make the blade of the Savonius wind turbine strong and light enough to withstand high speed winds. In order to manufacture the blade, firstly a mould was created from styrofoam material.

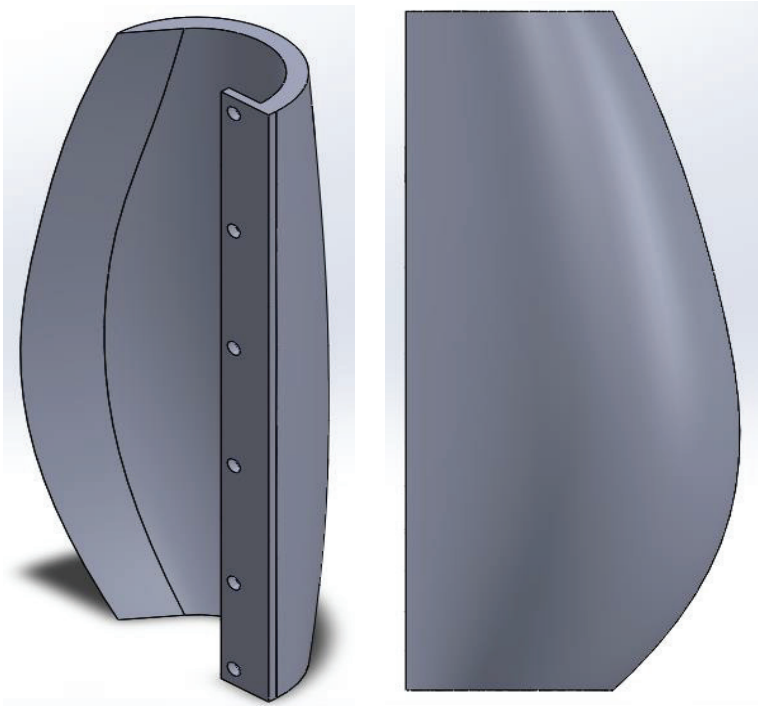

Figure 3.2. Designed Savonius wind turbine blades to be manufactured (Ardıç, 2019)

Firstly, mould release liquid was applied on the mould. The mould was covered with glass fibre in 3 layers. Figure 3.3. shows the mould wrapped with glass fibre.

Figure 3.3. Mould wrapped with glass fibre and glass fibre ready for polyester impregnation (Ardıç, 2019)

After each layer was wrapped in the mould, polyester was impregnated. While preparing the polyester mixture, 0,5% accelerator and 2% hardener were added. After the 3rd layer was completed, it was left on the mould for 1 day and left to harden.

After drying and hardening on the mould, the mould was removed from the glass fibre reinforced polyester and the final shape of the wing was given. In order to remove the roughnesses on the wing, the roughnesses were covered with putty and sanding and smoothness was provided. Rubber material was wrapped around the wing for smoothness and painted.

3.2. Manufacturing of Darrieus Wind Turbine

H type Darrieus wind turbine was selected for the Darrieus wind turbine to be designed. The dimensions of the turbine are height h=75 cm, radius r=32 cm and the number of blades is selected as 2 blades. Figure 3.4 shows the drawing of the designed Darrieus wind turbine blade.

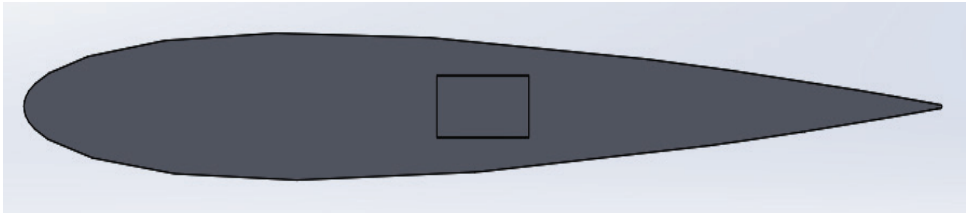

Figure 3.4. Cross section of the Darrieus wind turbine blade to be manufactured (Ardıç, 2019)

Air density was taken as ρ = 0,225 kg/m3 which is the standard seaside value. Wind speed V=10 m/s and rotational speed n=596,83 rpm. The tip speed ratio of the Darrieus wind turbine was calculated according to equation (3.9).

$$\lambda = \frac{2.\pi.n.r}{60.V} \quad (3.9)$$

$$\lambda = \frac{2.\pi.596,83.0,32}{60.10} = 2$$

Finding. The relation between the tip velocity ratio λ and the wing chord length is given in equation (3.10).

$$\lambda^2 = \frac{5.r}{b.c} \quad (3.10)$$

is found as. Taking these values into account, the power of the wind turbine is calculated using equation (3.11);

$$P = \rho . S . v^3 \quad (3.11)$$

Where; P: Power (W), S: Sweeping area of the impeller (m^2) and v: Wind speed (m/s).

To calculate the sweeping area, equation (3.12) is used.

$$S = \frac{2}{3} . 2r . 2h \quad (3.12)$$

$$S = \frac{2}{3} \times 2 \times 0{,}32 \times 2 \times 0{,}75 = 0{,}32\ m^2$$

Finding. If the power of the wind turbine;

$$P = 0{,}25x0{,}64x10^3 = 80\ W$$

is found as. After the calculations of the Darrieus wind turbine were made in this way, the manufacturing stage was started. NACA 0012 airfoil profile was used as the blade profile. Wood material was preferred as the manufacturing material. Figure 3.5. shows the drawing of the Darrieus wind turbine blade.

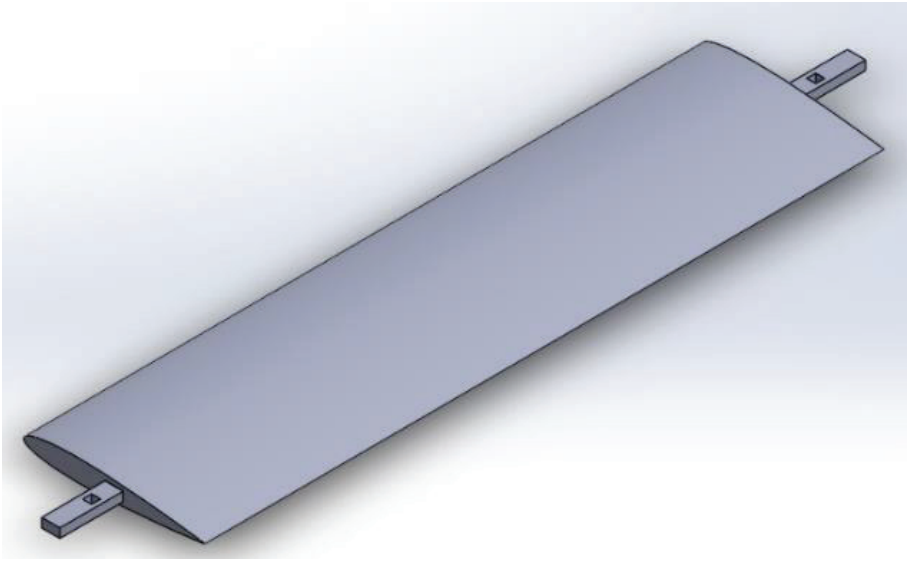

Figure 3.5. Darrieus wind turbine blade (Ardıç, 2019)

In order to adjust the angles of the blades of the Darrieus wind turbine to the turbine to be 90o and 45o degrees, a special fastener was manufactured. Figure 3.6. shows the mounting elements that will enable the Darrieus and Savonius wind turbines to be mounted together.

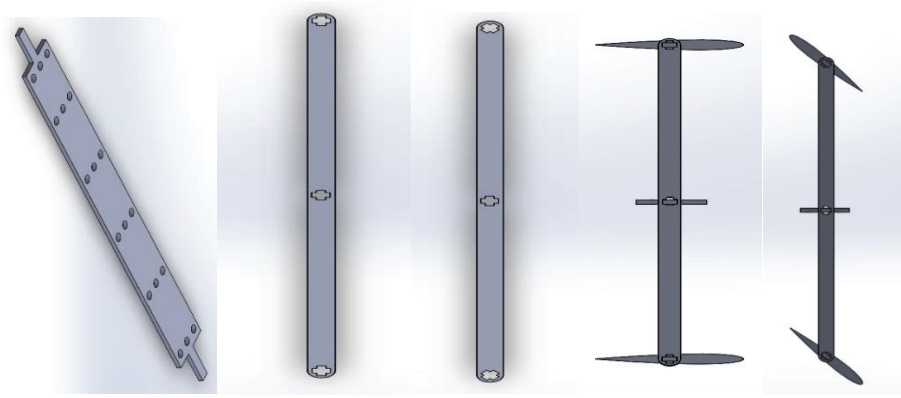

(a) (b)

Figure 3.6. (a) Mounting elements of the turbines and (b) assembled Darrieus turbine blades (Ardıç, 2019)

Finally, the blades were connected to the shaft with fasteners and experiments were carried out. Figure 3.7. shows the assembly drawing of the assembled Darrieus-Savonius hybrid turbine blades.

3.3. Darrieus-Savonius Hybrid Wind Turbine Assembly

Holes were drilled in the centre of the shaft designed for air circulation in the manufactured Savonius wind turbine (Figure 3.6-a).

After the Savonius turbine blades were mounted on the shaft, the Darrieus turbine blades were connected to the Savonius wind turbine with the fasteners manufactured. Experiments were carried out by changing the angles of the Darrieus turbine blades to 90^{o} and 180 degrees and the position of the Darrieus turbine with respect to the Savonius blades. The assembly drawing of the Darrieus-Savonius hybrid wind turbine is shown in Figure 3.7.

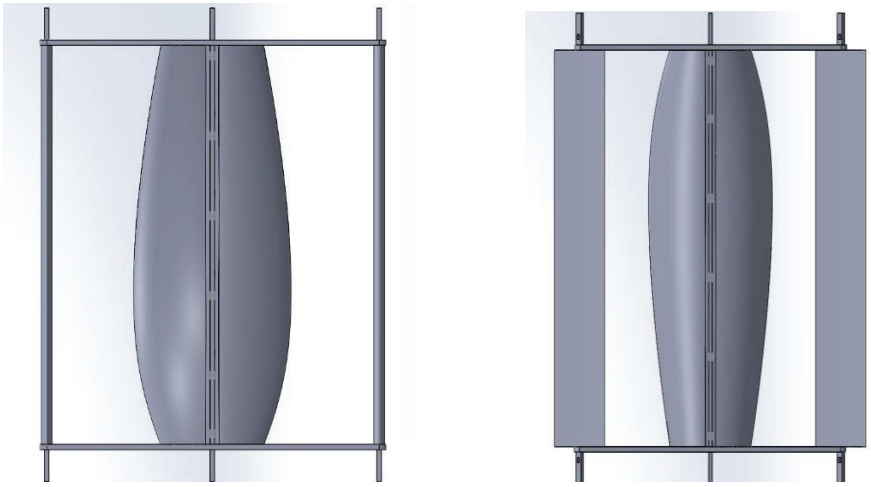

Figure 3.7. Views of the Darrieus-Savonius hybrid wind turbine from different angles (Ardıç, 2019)

Installation pictures of the fabricated Savonius (Figure 3.8-a) and Darrieus-Savonius (Figure 3.8-b) turbines placed in front of the wind tunnel are given.

(a) (b)

Figure 3.8. Savonius (a) and Darrieus-Savonius hybrid (b) wind turbines in front of the wind tunnel (Ardıç, 2019)

4. CONCLUSION AND EVALUATION

Of the Savonius and Darrieus turbines, firstly only the Savonius wind turbine was tested in a wind tunnel with a maximum wind speed of 9 m/s. Then the Darrieus wind turbine was installed to the Savonius wind turbine. This hybrid Darrieus-Savonius wind turbine was again tested in a wind tunnel

with a maximum wind speed of 9 m/s. In the experiments, measurements were made by changing the blade angles of the Darrieus wind turbine. In the measurement results, the highest power values were reached in the 90° degree blade of the Darrieus-Savonius hybrid wind turbine.

Multimeter was used to calculate the turbine power. Electrical power was calculated by measuring volt and ampere values. Equation 4.1. was used in electrical power calculation.

$$P = V.I \tag{4.1.}$$

The manufactured Savonius and Darrieus-Savonius hybrid wind turbines were tested in the wind tunnel between 3-9 m/s wind speed values. As a result, the number of revolutions, power coefficient, tip speed ratio and electrical power values were obtained. Turbine speed values obtained at different wind speeds in the wind tunnel are given comparatively in Figure 4.1.

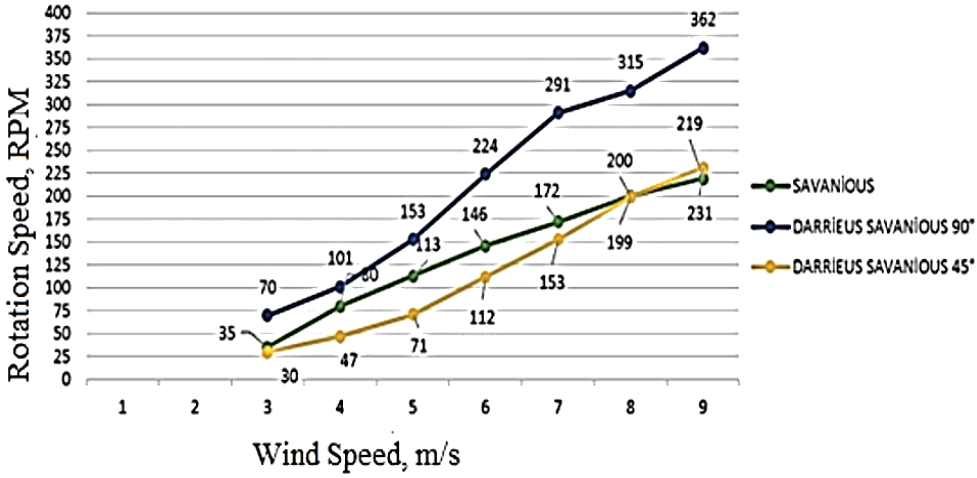

Figure 4.1. Wind speed-rotation speed change values of Savonius and Darrieus-Savonius hybrid wind turbines (Ardıç, 2019)

The variation of the obtained power values with wind speed is shown comparatively in Figure 4.2.

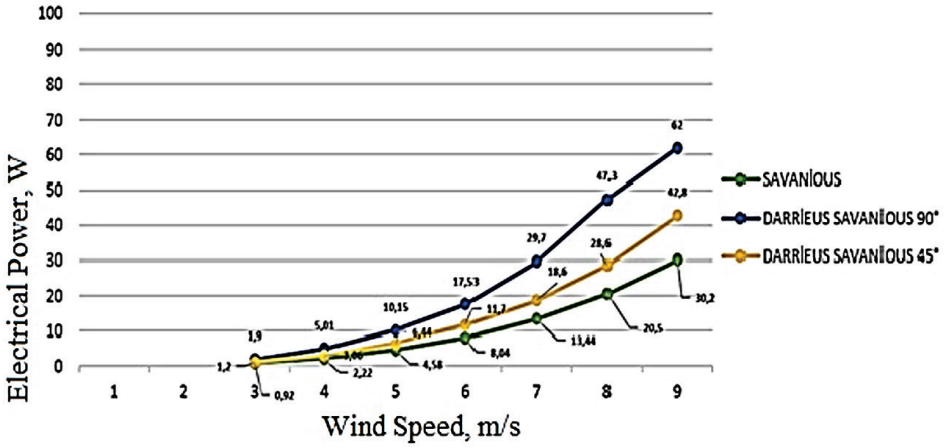

Figure 4.2. Changes of measured turbine power values with wind speed (Ardıç, 2019)

Using the obtained speed and power values, the tip speed ratio λ was calculated according to equation (4.2).

$$\lambda = \frac{2.\pi.n.R}{60.V} \qquad (4.2.)$$

Here, n: Number of revolutions, R: Radius, P: Wind power.

As a result of these calculations, the tip speed ratio values obtained at wind speeds between 3-9 m/s are given in Figure 4.3.

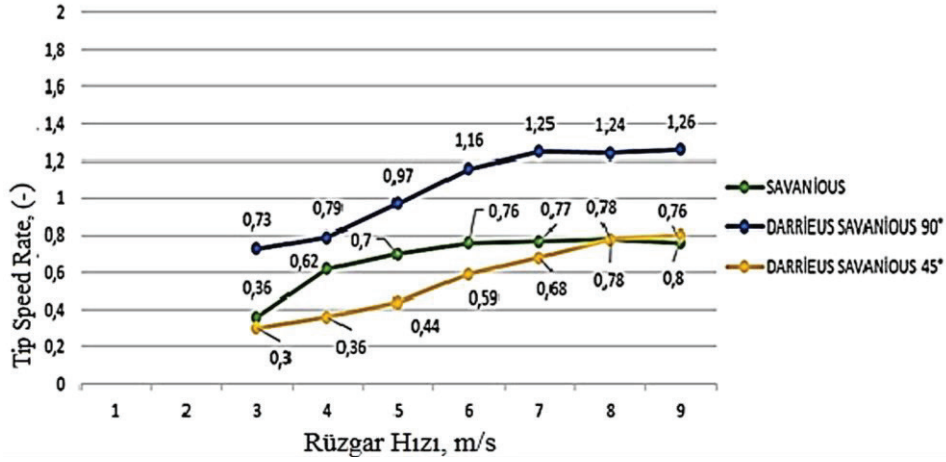

Figure 4.3. Changes of tip speed ratio values calculated according to measured values with wind speed (Ardıç, 2019)

Based on the power values obtained because of the experiments, Cp power factor calculation is given in equation (4.3) made using.

$$C_p = \frac{P_f}{P} \tag{4.3.}$$

Here, Cp: Power coefficient, P_f: Useful power (W), P: Calculated wind power (W).

A comparison of the Cp power coefficient values obtained because of the calculations is given in Figure 4.4.

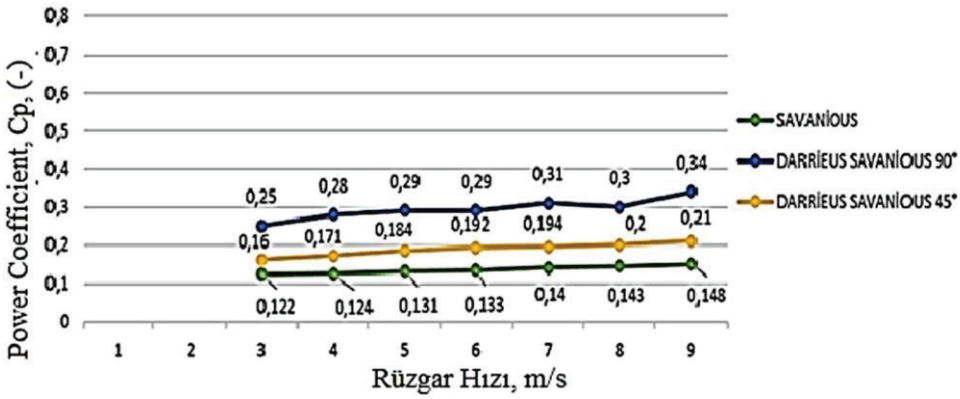

Figure 4.4. Variations of Cp values obtained according to the measurement results with wind speed (Ardıç, 2019)

As a result, the Darrieus-Savonius wind turbine was designed for home applications with a power of 50-100 watts. First, the Savonius wind turbine was designed and produced. Later, the Darrieus wind turbine, suitable for the Savonius turbine, was designed and produced. Darrieus and Savonius turbine blades were mounted together, and experiments were carried out in the wind speed range of 3-9 m/s. The experiments carried out are as follows; It was built in the form of a Savonius turbine (1), a Darrieus-Savonius hybrid wind turbine (2), where the Darrieus blades are 90° away from the Savonius blades, and a Darrieus-Savonius hybrid wind turbine (3), where the Darrieus blades are 45° away from the Savonius blades, in the speed range of 3-9 m/s.

The results of the speed measurement values were obtained as 219 rpm in experiment (1), 362 rpm in experiment (2), and 231 rpm in experiment (3). Results of power measurement values; 30,2 W was obtained in experiment (1), 62 W in experiment (2), and 42,8 W in experiment (3). The Cp power coefficient values calculated according to these measurement results were 0,148 (14,8%) in experiment-(1), 0,34 (34,0%) in experiment-(2), and 0,21 (21%) in experiment-(3). The tip speed ratio values calculated from the

measurement results were obtained as 0,76 in experiment-(1), 1,26 in experiment-(2), and 0,8 in experiment-(3) (Ardıç, 2019).

According to these results, the Savonius turbine efficiency, which is around 15% in the literature, has been achieved. Among the hybrid systems, it is seen that the 90^{o} angle turbine layout reaches the highest power coefficient value with 34,0%. The results obtained were compatible with the literature.

Uncertainty analysis of the multimeter and anemometer, which are the measuring instruments used in the experiments, was performed. The uncertainty of the Cp power coefficient was calculated as 0,46% and the result was appropriate. According to these results, it can be seen that a Darrieus-Savonius hybrid turbine of a certain size can be used to meet domestic electrical energy.

REFERENCES

Aktemur, K., 2010, Computer Aided Analysis of a Wind Turbine, Istanbul University, Institute of Science and Technology, Department of Mechanical Engineering, master's Thesis, Istanbul.

Ardıç, İ. 2019, Experimental investigation of vertical axis wind turbine performance for household applications, Konya Technical University, Institute of Graduate Studies, Department of Mechanical Engineering, Master Thesis, Turkish, Konya.

Balduzzi F., Drofelnik J., Bianchini A., Ferrara G., Ferrari L., Campobasso M. S., 2017, Darrieus wind turbine blade unsteady aerodynamics: a three-dimensional Navier-Stokes CFD assessment, Energy, 128 (2017), 550-563

Deda, B., Atılgan, M., and Öztürk, H.K., 2006, Examination of the performances of Savonius wind wheels, III. National Clean Energy Symposium, Istanbul, 423-430.

EMRA, 2023, Energy Market Regulatory Authority Electricity Market Sector Report, September 2023 Ankara, Access address: https://epdk.gov.tr/Detay/Icerik/3-0-23-3/elektrikaylik-sektor-raporlar

Douak M., Aouachria Z., Rabehi R., Allam N., 2018, Wind energy systems: Analysis of the self-starting physics of vertical axis wind türbine, Renewable and Sustainable Energy Reviews, 81 (2018), 1602–1610.

ETKB, 2023, Ministry of Energy and Natural Resources (ETKB) website, Access date: 15.12.2023, Website address: https://enerji.gov.tr/bilgi-merkezi-enerji-elektrik

Gavalda, J., Massons, J., and Diaz, F., 1990, Experimental Study on a Self-Adapting Darrieus- Savonius Wind Machine, Solar&Wind Technology, 7(4), 457-461.

Hashem I., Mohamed M.H., 2018, Aerodynamic performance enhancements of H-rotor Darrieus wind türbine, Energy, 142 (2018), 531-545.

Hutchinson M., Zhao F. (Lead Authors), "Global Wind Report 2023 (GWEC)", Published: 27 March 2023, Global Wind Energy Council Rue de Commerce 31 1000 Brussels, Belgium. info@gwec.net www.gwec.net

Karaoglan, I. and Altıparmak, F., 2015, A memetic algorithm for the capacitated location-routing problem with mixed backhauls, *Computers & Operations Research,* 55 (1), 200-216.

Kirke B.K., 2011, Tests on ducted and bare helical and straight blade Darrieus hydrokinetic turbines, Renewable Energy, 36 (2011), 3013-3022

Köse, F., 2003, Meeting the electricity needs of the wind measurement station with a mini Darrieus-Savonius wind turbine, Renewable Energy Resources Symposium and Exhibition, Kayseri, Türkiye, 217-223.

Lee J.-H., Lee Y.-T., and Lim H.-C., 2016, Effect of twist angle on the performance of Savonius wind türbine, Renewable Energy, 89 (2016), 231-244.

Patel V., Eldho T.I., Prabhu S.V., 2017, Experimental investigations on Darrieus straight blade türbine for tidal current application and parametric optimization for hydro farm arrangement, International Journal of Marine Energy, 17 (2017), 110–135.

Ramesh K., Kavade and Pravin M. Ghanegaonkar 2017, Design and Analysis of Vertical Axis Wind Turbine for Household Application, Journal of Clean Energy Technologies, Vol. 5, No. 5, September 2017.

Saif ed-Dın, Fertahi, T. Bouhal, Omar Rajad, T. Kousksou, A. Arid, T. El Rhafiki, A. Jamil, A. Benbassou, 2018, CFD performance enhancement of a low cut-in speed current Vertical Tidal Turbine through the nested hybridization of Savonius and Darrieus, Energy Conversion and Management, 169 (2018), 266–278

Williams R., Zhao F. (Lead Authors), "Global Offshore Wind Report 2023" Published: 28 August 2023, Global Wind Energy Council Rue de Commerce 31 1000 Brussels, Belgium, info@gwec.net www.gwec.net

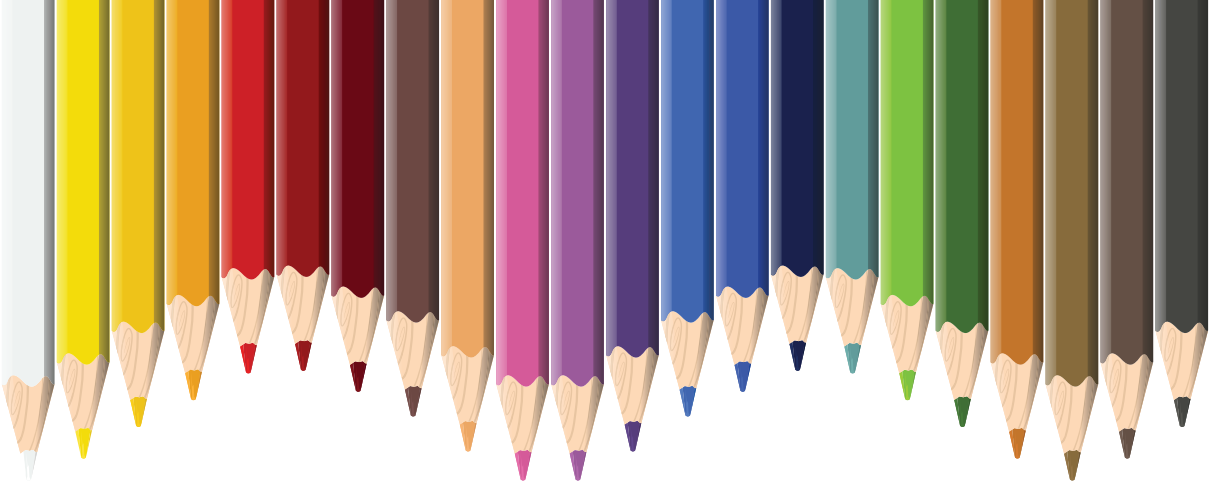

Chapter 9

THE NECESSITY AND ADMISSIBILITY OF GAINING ANDROID SMARTPHONES' ROOT PRIVILEGES[1]

Tayfun YILDIRIM[2]
Nursel YALÇIN[3]

1 This work was composed from MSc Thesis named "Analysis of android smartphones in the context of digital forensics: Processes, methods and the legal dimension". Author: Tayfun Yıldırım. Supervisor: Assoc. Prof. Nursel Yalçın. 2023. Gazi University, Institute of Informatics, Department of Computer Forensics.

2 Gazi University, Institute of Informatics, Department of Computer Forensics, 0000-0001-8942-6953

3 Assoc. Prof., Gazi University, Faculty of Education, Department of Computer and Educational Technologies Education, 0000-0002-0393-6408

I. INTRODUCTION

Digital forensics is a branch of science that provides evidence to be presented to the court as a documentation by collecting digital devices and analyzing them. By reaching the material truth through this branch of science, it is possible to catch the perpetrators, punish them or acquit the innocent or prevent the crimes planned to be committed (Kılıç, 2012).

Digital forensics: It is the whole of the stages of examining digital evidence on digital media of various qualities by applying scientific methods to reach the material truth, preserving the integrity of the digital evidence related to the crime, making it ready to be presented to the judicial authorities in an understandable way without being corrupted, and applying certain scientific techniques (Ekizer, 2014).

According to the theory known as "Locard's Principle of Change" by Criminologist Prof. Edmond Locard, before a perpetrator leaves the crime scene, he will either leave a trace of himself there or carry a trace of there on himself. Since this evidence are concrete evidence, they are very important as they cannot be refuted by abstract witness statements. The principle of change is valid in the field of digital forensics as well as in the physical environment of a crime scene. In this respect, it is very difficult to act on information technology systems without leaving any indications, just as every behavior in the physical environment leaves indications (Başlar, 2019).

The Android operating system is the most widely used operating system in all devices with a 38.33% market share among all operating systems in November 2023 (StatCounter, 2023).

Since smartphones are relatively more affordable than personal computers, it can be much easier to reach these devices. And it is possible for people in the low-income group without using any digital device other than smartphone, and basically continue their lives with the operations they do on their smart phones. If these people commit a crime, there is the potential to have large amounts of digital evidence on their smartphones relates to the crime (Petraityte, Dehghantanha, and Epiphaniou, 2017).

Smartphones are constantly carried with their owners, often physically held closer to them than other potential digital devices, such as computers. The size of these devices to be carried in the pocket makes it easier for people to carry these devices with them, causing them to be in constant interaction throughout the day. For these reasons, the evidence potential of these devices is greatly increased following factors like: the possibility of the devices were taken to the area where the crime was committed; the possibility of the formation of location information as a result of communicating with people by using a smart phone at the scene; the possibility of audio, video recording or

photographing at the scene with a smartphone; the possibility of criminal messaging recordings on the smartphone. Moreover, it is likely to commit crimes by using these devices directly as a tool. Because smart phones have very powerful hardware and functions today, and they can contain rich data types that equivalent to personal computers (Walnycky et al., 2015). Smartphones have become the most critical and important piece of evidence in many investigations (Kim and Lee, 2020).

Although the methods used in digital forensics have developed, the previously developed forensic methods may become dysfunctional with the continuous technological developments and the updating of the versions of operating systems and applications. For this reason, digital forensics is a science that still needs development and needs to be studied continuously.

For example, it is very important to gain root privileges during the examination of Android smartphones, and it is getting harder and harder to gain root privileges on newly released Android smartphones and operating system versions.

Because it is often necessary to gain root privileges to effectively perform forensic investigations of Android smartphones and reach the material truth. However, gaining root privileges can be seen as unlawful method. In this study, acceptability of gaining root privileges also discussed.

II. IMPORTANCE, ADMISSIBILITY AND CHALLENGES OF GAINING ROOT PRIVILEGES

A. Root Privileges

Rooting Android smartphones is like having administrator privileges using the "sudo" command in the Linux operating system. As a matter of fact, since Android is based on Linux, just as it is necessary to have administrative authority with the use of the "sudo" command line to perform many development or modification operations in the Linux operating system, root privileges are required to have broad authorities on Android smartphones (Hoog, 2011).

With root privileges, it is possible to make changes to system files, access system files and important files where application's data are stored. Although it is possible to access user data without root privileges, this data will often be too limited.

ADB (Android Debug Bridge) commands will need to be used when it is desired to take a logical or physical image from an Android smartphone with a computer on the workstation. It is possible to take both logical and physical images with ADB commands. However, additional components and applications must be installed like BusyBox application on the device to obtain a physical image.

Android Debug Bridge (ADB) system consists of three elements: client, daemon, and server. The client runs on the computer in the workstation and sends commands to the device. The daemon runs in the background of the Android smartphone, executing the commands that the client sends to it. The server handles the communication between the daemon and the client. It is possible to backup non-rooted device data via an application on Android smartphone or ADB commands, or to obtain data from the device through the information provided by the content providers (Lin, 2018).

For ADB commands to be executed, USB debugging mode must be turned on from the target device (Figure 1) and this permission must be given to the computer on the workstation (Figure 2).

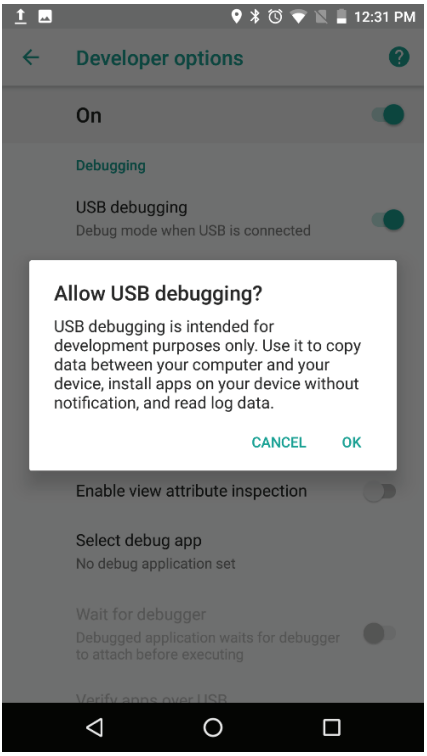

Figure 1. *Enabling USB debug mode on target device.*

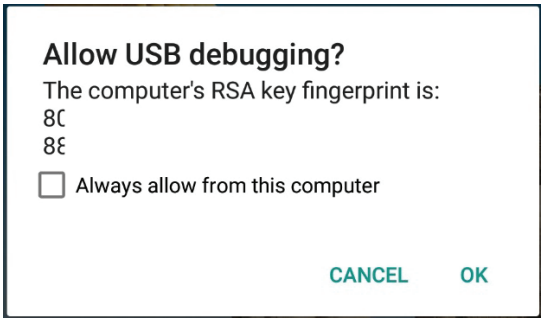

Figure 2. *Screenshot of the smartphone that shows giving permission to use ADB commands on target device from workstation specific computer.*

After connecting an Android smartphone to the workstation, then binding to the terminal of the target device with root privileges with the command "adb shell su", the screen that appears in the superuser application is shown whether to allow root privileges on the device (Figure 3).

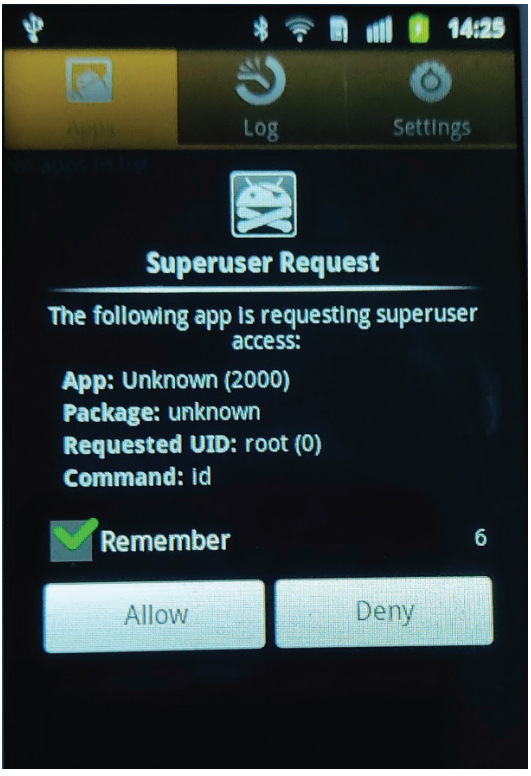

Figure 3. *Permitting to using root privileges of the Android Smartphone.*

The command prompt screen showing that the device can be accessed to the /data directory without encountering any problems on the rooted device by typing the “ls /data” command on the computer at the workstation (Figure 4).

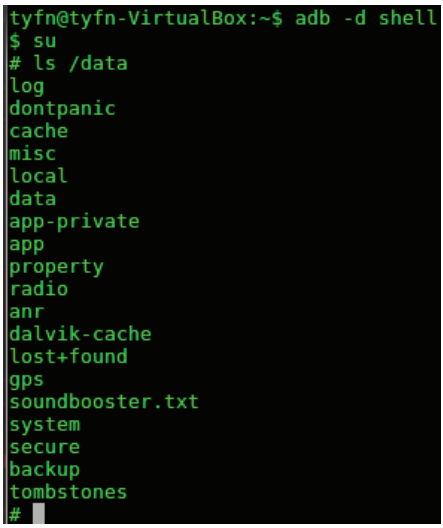

Figure 4. *Checking if root privileges has been acquired by digital forensic examiner or has not from workstation computer command prompt.*

The command prompt screen showing that many permissions, and the permission to view the subfolders and subfiles information in the /data directory are denied, even when the workstation is requested to examine the base directories of the target device (Figure 5).

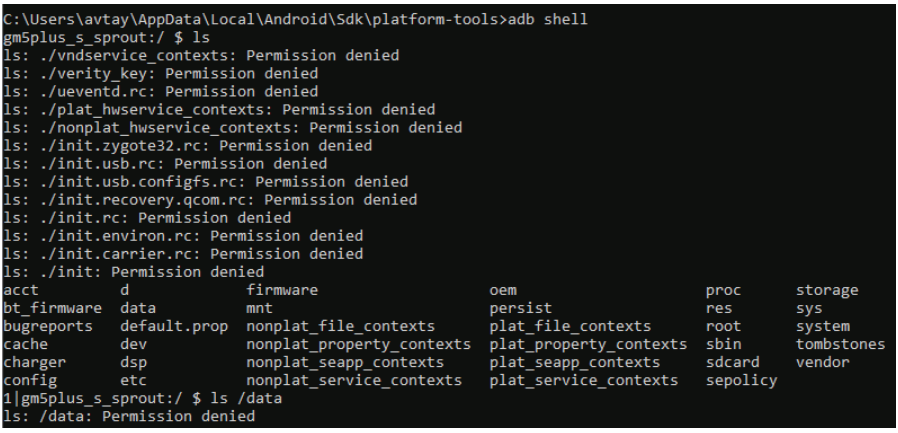

Figure 5. *ADB commands that shows without root privileges it is not possible to access /data directory that contains user data, and even to view some directories on the smartphone flash memory.*

As seen above, it is not possible to access the /data directory where user data is stored without having root privileges. Therefore, even when a logical image of the device is desired, the data in this directory will not be available.

B. Importance of Root Privileges

There are basically two different ways to obtain data on Android smartphones. One of them is taking the logical image, while the other is taking the physical image. The importance of rooting Android smartphones in terms of digital forensics is gathered at the point of obtaining data with these two different ways.

If it is preferred to logically obtain data from Android smartphones, it will not be possible to access the /data directory where the user data is stored or the /system directory where the system files are stored (Skulkin, Tindall, and Tamma, 2018c) . If these directories cannot be reached, although it is possible to obtain various data via Android backup files or content providers, the data obtained will be very poor compared to the data that can be acquired with gaining root privileges. In fact, Android applications can prevent the data that can be obtained with the Android backup feature with a Boolean type code called as a flag that they add to the manifest.xml file (Breitinger and Baggili, 2019). Again, content providers are the data that an Android application shares with other applications and it is obvious that these applications will keep this data within a certain limit.

To take the physical image of the target device with software tools, it is a requirement to have root privileges. It is not possible to take the physical image of the device in any way with software tools without having root privileges. With the physical image, it is possible to create a byte-to-byte copy of the flash memory of the target device. In this way, not only the file system, but also the unallocated space of the device's flash memory can be obtained. Therefore, data deleted by the user can also be recovered by obtained physical image.

With hardware level methods like JTAG or Chip-off, the physical image of the target device can be taken without gaining root privileges. However, the implementation of both methods has great difficulties. The implementation of the JTAG method may not always result in success or it may not be possible because the smartphone manufacturer has closed the JTAG inputs on the circuit board (Skulkin, Tindall, and Tamma, 2018b). Besides that, Chip-off method is much more time consuming and costly than JTAG, and it may harm hardware of device (Skulkin, Tindall, and Tamma, 2018a).

At the same time, software tools such as LiMe or AMExtractor must be used to obtain the volatile memory of the Android smartphone. However, to use these software tools on the target device, it is mandatory to have root priv-

ileges of the target device. The Linux kernel source code of the target device is needed for LiMe (504ENSICS Labs, 2014). It can be found on the manufacturer's website or other resources. Along with the Linux kernel source code, the file named "config.gz" must be obtained from the /proc directory of the device's file system and this file which is related to target device kernel must be cross compiled with the Linux kernel source code. Later, by transferring the module created by LiMe to the target device, volatile memory can be obtained. However, this Linux kernel source code may not be available for every target device because the manufacturer does not share the kernel source code, or the kernel source code has not been published by a third source. This reduces the effectiveness of the tool called LiMe.

Although the Linux kernel source code is not required to use the AMExtracotor tool, it is necessary to learn the various features of the RAM (Random Access Memory), to create the kernel module based on these features, and to obtain the data of the volatile memory by transferring the created kernel module file to the device (Haiyu Yang, 2022).

However, root privileges are needed both to obtain the "config.gz" file of the target device for the LiMe tool, and to obtain various features of the RAM for the AMExtractor tool. Again, it is obligatory to have root privileges during the transfer of the created module to the device for acquiring volatile memory.

Therefore, obtaining useful data for forensic analysis on the target device without having root privileges will be very limited.

C. Legal Acceptability of Gaining Root Privileges

When it comes to ensuring data security, the confidentiality, integrity, and availability of evidence, known as the CIA trio, will be evaluated. These basic principles, which have their roots in providing data privacy on a military basis, are also used in ensuring data security for organizations (Samonas and Coss, 2014). Confidentiality of evidence means taking precautions and measures so that only authorized persons can access the data. Integrity, on the other hand, is that the wholeness of the data is maintained continuously, and its accuracy is not lost. Availability means that it is possible to access the data by authorized persons when necessary.

These features can also be applied to the admissibility of digital evidence by courts. Ensuring the confidentiality of the evidence is important in terms of the privacy of personal data through the investigation, and the fundamental rights and freedoms of the suspect. Preserving the integrity of the evidence is a necessity to be able to prove that the alleged crime was committed by the defendant. Availability, on the other hand, is an essential for the competent authorities like judge, lawyer, or prosecutor to examine the digital evidence during the trial and form the judgment.

Having the integrity feature of digital evidence will also mean that evidence has the accuracy and reliability. It demonstrates that the data on the device preserved without any changes since the first acquisition of the digital evidence (University Of East London and Ay, 2020). By ensuring this feature, the existing digital evidence does not undergo any changes during all processes from obtaining it to its presentation to the court and afterwards during its storage. Thus, that the originality of the data created by the user can be preserved at all stages (Alfred and Scott, 1997).

Since appellate proceedings can take a long time, an environment that will constantly protect the integrity and especially the authenticity of the digital evidence should be provided even after the convict (Granja and Rafael, 2017).

Rooting Android smartphones will inevitably cause a change in the target device. Therefore, since the integrity of digital evidence cannot be protected by rooting, it can be claimed that it is unlawful evidence.

However, as explained above, it is very important to gain root privileges for Android smartphones to obtain many user data. Otherwise, the material truth may not be reached, and the perpetrators may not be punished.

Gaining root privileges of Android smartphones does not corrupt or change user data. It causes a change only at the system level (Almehmadi and Batarfi, 2019) (Hassan and Pantaleon, 2017). In addition, after the physical or logical image of the target device is taken, it is possible to undo the rooting process and restore the device's system to its original state.

Processes made in digital forensics operations should be reasonable and reliable (McKemmish, 2008). Therefore, the analyzes made within the scope of digital forensics should also have the quality of justifiability, it should be explained why the root privileges were gained and the user data was not changed in any way (Montasari, 2016).

In this context, another situation that should be considered is that if it is possible to reach the material truth with evidence other than digital evidence, it is necessary to be just content with this evidence. Otherwise, the balance between fundamental rights and freedoms against public interest may be disrupted. Considering the best evidence rule, the use of digital evidence obtained because of gaining root privileges can be used as a last resort (Mason and Seng, 2017). The Turkish Law of Criminal Procedure states that if other non-digital evidence is sufficient to reach the truth, should be contented with these non-digital evidence (CMK, 2004).

However, in an investigation, the Android smartphone's evidential value is important, and if it is necessary to refer to this evidence in reaching the material truth, this situation can be overcome with documentation, which is

the cornerstone of digital forensics. With documentation, it is necessary to present the digital evidence as a whole by considering all aspects of how it was obtained and what it relates to (Tenhunen, 1997).Using the "Five Ws" (and one H) questions, by explanations of where, when, why, who, what, and how questions, the processes of gaining root privileges can be presented in the documentation (Cosic and Baca, 2010).

The judge, lawyer or prosecutor may not have sufficient technical knowledge about the authenticity of digital evidence (Montasari, 2016). Although gaining root privileges does not affect user data, the running principles of the Android operating system should be effectively disclosed to the court subjects with the documentation. Thus, it will be efficient to discuss digital evidence. It is great importance for defense lawyers to have knowledge of the authenticity of digital evidence. Otherwise, the digital evidence presented to the courts can be accepted as accurate digital evidence (Roscini, 2016). In this respect, it is very important for the trial subjects to have basic knowledge of the Android operating system architecture in terms of reaching the material truth. During the acquisition of root privileges, discussing whether the limit is exceeded, and the user data has been modified will help to give an accurate convict.

It has great importance that the user data remains unmodified to ensure authenticity. In this way, it will be possible to prove that the user data on the target device was created by the suspect (Antwi-Boasiako and Venter, 2017). In terms of reaching the material truth, the protection of the authenticity of the digital evidence is more important than the integrity feature. As a matter of fact, the integrity is not an absolute condition, but is important in relation with the authenticity. Therefore, with the authenticity preservation of the digital evidence, mandatory changes to be made on the digital evidence can be accepted (Mason and Seng, 2017). Otherwise, if data is obtained from the target devices by logical acquisition, the rejection of these digital evidence may occur due to the lack of complete physical image and so integrity feature. Today, in many digital devices, it may not be possible to take the physical image of the target device for various reasons such as password protection and lack of access authorization. Rejecting the obtained logical image, on the ground that it does not have integrity feature, will cause most of the digital evidence to be unavailable in trials and so reaching to truth for punishing perpetrators or acquitting innocents.

In this context, digital forensics experts can reveal that they did not change any user data by documenting the processes they made while gaining root privileges, with the timestamps, video recording of the smartphone and workstation screen, and reporting the processes to the finest detail. Performing this process with technically competent digital forensics experts, it should be ensured that the user data part of the target device is not changed, and that the system part is changed only to gain root privileges so that no damage is caused

to the operability of the device. In the created documentation, it should also be explained why gaining root privileges is necessary to access user data. Thus, the admissibility of digital evidence by the courts will be protected.

The integrity of the evidence must also be protected after gaining the root privileges, during the chain of custody (Antwi-Boasiako and Venter, 2017). Since the device will be rooted, different forensic experts should take this situation into account when analyzing the device. Since experts who do not know about this situation or do not take it into account may think that their actions will not be allowed by the target device anyway, and they may cause loss or change of user data.

One of the principles used for the acceptance of digital evidence in the United States is the Dauber test method. In this method, the admissibility of digital evidence is not tied to strict principles, but it is evaluated whether the accepted scientific methods are applied according to the type of digital evidence (Montasari 2016). Rooting of Android smartphones has also been widely used in many academic studies like analysis of TikTok application (Khoa et al., 2020), analysis of instant messenger applications (Mahajan, Dahiya, and Sanghvi, 2013), analysis of Wickr application (Mehrotra and Mehtre, 2013), acquisition of Android smartphone volatile memory (Yang et al., 2016). Therefore, it is obvious that rooting is a scientific method in digital forensics investigation of Android smartphones. So, gaining root privilege is forensically sound if user data is not modified or lost (Kong, 2015).

Otherwise, if the data obtained by not making any changes in the target device with traditional approaches, it may cause that many perpetrators cannot be punished, and justice cannot be established. As explained in the "Introduction" section, Android smartphones are the most widely used smartphones in the World, and because these devices are in constant interaction with the perpetrators, their potential evidence value in a crime committed is quite high.

D. Challenges

Rooting Android smartphones is not a simple process and requires competence. It is obligation to apply different methods according to each Android operating system version or phone brand and model.

In operating system versions prior to Android 5.0.0, it is possible to gain root privileges by installing a file that will change the system data over the bootloader, which will be accessed by using various key combinations during startup of the device, without the need to unlock the bootloader. However, unlocking the bootloader is a must for Android 5.0.0 and higher versions. Once the bootloader is unlocked, it is possible to gain root privileges with a special recovery system file (like TWRP) to be installed (Skulkin, Tindall, and Tamma, 2018d).

Many Android smartphones only permit unlocking the bootloader on the condition of deleting the data on the device. In these cases, instead of gaining root privileges by unlocking the bootloader, it is necessary to gain root privileges by finding a different vulnerability. If a different vulnerability cannot be found, a forensic investigation will have to be made on the data that can be accessed in a limited way. Unlocking the bootloader may cause the Android smartphone to crash and not start (soft brick/hard brick), loss of the manufacturer's warranty, and security vulnerability (Skulkin et al., 2018c).

III. RESULT AND DISCUSSION

The process of gaining root privileges causes changes only at the system files level on the target device. It does not change any user data of the device. However, this process is not a simple process and requires competence. In case of an unsuccessful attempt, irrecoverable data loss may occur. By demonstrating the necessity of gaining root privileges and no user data has been changed, the admissibility of the digital evidence obtained by gaining root privileges can be ensured. Thus, this digital evidence will be accepted as lawful evidence by the courts.

If there is no previous experience in successfully rooting the relevant device or operating system version, practices should not be carried out directly on the target device, and root privileges should be successfully acquired on an exact sample device. The process steps applied in successful acquisition should be detailed, and the same steps should be applied to the target device to prevent the user data of the target device from being modified or lost.

For all these reasons, the digital forensics expert to gain root privileges must be quite competent. Whether it is necessary to gain root privileges should be evaluated by considering the balance between the benefit that is thought to be gained in terms of each concrete case and fundamental rights and freedoms. It should be evaluated whether it is possible to reach the material truth with any other evidence other than the data to be obtained from the Android smartphone, and the process of gaining root privileges should be used as a last resort. Because after gaining root privileges on the device, system data will change. If it is necessary to gain root privileges, it should be tried to gain authority with minimal changes in system files and user data should not be damaged by any means. While gaining root privileges, it is necessary to act in such a way that it is possible to undo rooting. (Akarawita, Perera, and Atukorale, 2015).

If it is possible to reach the material truth with the limited data that can be obtained on the Android smartphone without gaining root privileges, should be contented with this limited data. The aim of the Criminal Law is to reach the material truth, and fundamental rights and freedoms of individuals should

not be harmed by going beyond this purpose.

IV. CONCLUSION

Smartphones are pocket-sized and the users is constantly interacting with their smartphones. Android smartphones are dominantly used in the smartphone market. For this reason, the potential of the Android smartphones containing evidence in relation to a committed crime is quite high. It is not possible to access the directories where Android smartphones store user data without root privileges. For this reason, even if a logical image is taken without root privilege, many user data will not be obtained. Besides that, the physical image of the device will not be obtained with software tools. Obtaining the physical image is very important in terms of digital forensics, since the physical image also contains data that has been deleted by the user. In traditional digital forensics approaches, it is foreseen that no changes should be made to the device. For this reason, gaining root privilege should be used as a last resort. If it is possible to reach the material truth with other evidence, should be contented with just other evidence without making any changes in the Android smartphone. Although gaining root privileges causes changes in the data on the target device, this change only occurs in system files level. Therefore, gaining root privileges by competent forensic experts will be effective in reaching the material truth. At the same time, it can be proven that no modification has been made in the user data, by documenting every step of the process of gaining root privileges, supported with video recordings. Thus, the claim that the digital evidence has been altered can be refuted and its legality can be preserved.

V. REFERENCES

504ENSICS Labs. 2014. “LiME (Linux Memory Extractor).”

Akarawita, Indeewari, Amila Perera, and Ajantha Atukorale. 2015. “ANDROPHSY - Forensic Framework for Android.”

Alfred, Menezes, and Vanstone Scott. 1997. *Handbook of Applied Cryptography*. CRC press.

Almehmadi, Tahani, and Omar Batarfi. 2019. “Impact of Android Phone Rooting on User Data Integrity in Mobile Forensics.” Pp. 1–6 in *2019 2nd International Conference on Computer Applications & Information Security (ICCAIS)*. IEEE.

CMK. 2004. *Ceza Muhakamesi Kanunu*.N. 5271.

Antwi-Boasiako, Albert, and Hein Venter. 2017. “A Model for Digital Evidence Admissibility Assessment.” Pp. 23–38 in *IFIP International Conference on Digital Forensics*. Springer.

Başlar, Yusuf. 2019. “Adli Bilişim Sürecinde Karşılaşılan Sorunlar ve Çözüm Önerileri.” *TBB Dergisi* (2020 (148)).

Breitinger, Frank, and Ibrahim Baggili, eds. 2019. “If I Had a Million Cryptos: Cryptowallet Application Analysis and a Trojan Proof-of-Concept.” in *Digital Forensics and Cyber Crime*. Vol. 259, *Lecture Notes of the Institute for Computer Sciences, Social Informatics and Telecommunications Engineering*. Cham: Springer International Publishing.

Cosic, Jasmin, and Miroslav Baca. 2010. “Do We Have Full Control over Integrity in Digital Evidence Life Cycle?” Pp. 429–34 in *Proceedings of the ITI 2010, 32nd International Conference on Information Technology Interfaces*. IEEE.

Ekizer, A. Hakan. 2014. “Adli Bilişim (Computer Forensics).” Retrieved December 22, 2022 (URL: https://www.ekizer.net/adli-bilisim-computer-forensics/, Last Access Date: 22.12.2022.).

Granja, Fernando Molina, and Glen D. Rodríguez Rafael. 2017. “The Preservation of Digital Evidence and Its Admissibility in the Court.” *International Journal of Electronic Security and Digital Forensics* 9(1):1–18.

Haiyu Yang. 2022. “AMExtractor.”

Hassan, Mohamed, and Lutta Pantaleon. 2017. “An Investigation into the Impact of Rooting Android Device on User Data Integrity.” Pp. 32–37 in *2017 Seventh International Conference on Emerging Security Technologies (EST)*. Canterbury: IEEE.

Hoog, Andrew. 2011. “Android and Mobile Forensics.” in *Android forensics*. Waltham, MA: Syngress.

Khoa, Nghi Hoang, Phan The Duy, Hien Do Hoang, and Van-Hau Pham. 2020. “Forensic Analysis of TikTok Application to Seek Digital Artifacts on Android

Smartphone." Pp. 1–5 in *2020 RIVF International Conference on Computing and Communication Technologies (RIVF)*. IEEE.

Kim, Dohyun, and Sangjin Lee. 2020. "Study of Identifying and Managing the Potential Evidence for Effective Android Forensics." *Forensic Science International: Digital Investigation* 33:200897.

Kılıç, Mehmet Serkan. 2012. "İşletim Sistemlerinin Adli Bilişim Açısından Incelenmesi." Yüksek Lisans Tezi, Polis Akademisi Güvenlik Bilimleri Enstitüsü, Ankara.

Kong, Joe. 2015. "Data Extraction on Mtk-Based Android Mobile Phone Forensics." *Journal of Digital Forensics, Security and Law* 10(4):3.

Lin, Xiaodong. 2018. "Android Forensics." Pp. 335–71 in *Introductory Computer Forensics*. Springer.

Mahajan, Aditya, M. S. Dahiya, and Hitesh P. Sanghvi. 2013. "Forensic Analysis of Instant Messenger Applications on Android Devices." *ArXiv Preprint ArXiv:1304.4915*.

Mason, Stephen, and Daniel Seng. 2017. *Electronic Evidence*. University of London Press.

McKemmish, Rodney. 2008. *When Is Digital Evidence Forensically Sound?* Springer.

Mehrotra, Tarun, and B. M. Mehtre. 2013. "Forensic Analysis of Wickr Application on Android Devices." Pp. 1–6 in *2013 IEEE International Conference on Computational Intelligence and Computing Research*. IEEE.

Montasari, Reza. 2016. "Digital Evidence: Disclosure and Admissibility in the United Kingdom Jurisdiction." Pp. 42–52 in *Global Security, Safety and Sustainability-The Security Challenges of the Connected World: 11th International Conference, ICGS3 2017, London, UK, January 18-20, 2017, Proceedings 11*. Springer.

Petraityte, Milda, Ali Dehghantanha, and Gregory Epiphaniou. 2017. "Mobile Phone Forensics: An Investigative Framework Based on User Impulsivity and Secure Collaboration Errors." Pp. 79–89 in *Contemporary Digital Forensic Investigations of Cloud and Mobile Applications*. Elsevier.

Roscini, Marco. 2016. "Digital Evidence as a Means of Proof before the International Court of Justice." *Journal of Conflict and Security Law* 21(3):541–54.

Samonas, Spyridon, and David Coss. 2014. "The CIA Strikes Back: Redefining Confidentiality, Integrity and Availability in Security." *Journal of Information System Security* 10(3).

Skulkin, Oleg, Donnie Tindall, and Rohit Tamma. 2018a. "Chip-Off." in *Learning android forensics: analyze android devices with the latest forensic tools and techniques*. Packt Publishing Ltd.

Skulkin, Oleg, Donnie Tindall, and Rohit Tamma. 2018b. "JTAG." in *Learning android forensics: analyze android devices with the latest forensic tools and techniques*. Packt Publishing Ltd.

Skulkin, Oleg, Donnie Tindall, and Rohit Tamma. 2018c. *Learning Android Forensics: Analyze Android Devices with the Latest Forensic Tools and Techniques*. Packt Publishing Ltd.

Skulkin, Oleg, Donnie Tindall, and Rohit Tamma. 2018d. "Recovery and Fastboot." in *Learning android forensics: analyze android devices with the latest forensic tools and techniques*. Packt Publishing Ltd.

StatCounter. 2023. "Operating System Market Share Worldwide." *StatCounter Global Stats*. Retrieved December 9, 2022 (URL: https://gs.statcounter.com/os-market-share, Last Access Date: 15.12.2023.).

Tenhunen, Matti. 1997. "The Integrity of Electronic Evidence." *Integrity and Internal Control in Information Systems: Volume 1: Increasing the Confidence in Information Systems* 153–86.

University Of East London, and Ofori Ay. 2020. "Digital Forensics Investigation Jurisprudence: Issues Of Admissibility Of Digital Evidence." *Journal of Forensic, Legal & Investigative Sciences* 6(1):1–8. doi: 10.24966/FLIS-733X/100045.

Walnycky, Daniel, Ibrahim Baggili, Andrew Marrington, Jason Moore, and Frank Breitinger. 2015. "Network and Device Forensic Analysis of Android Social-Messaging Applications." *Digital Investigation* 14:S77–84.

Yang, Haiyu, Jianwei Zhuge, Huiming Liu, and Wei Liu. 2016. "A Tool for Volatile Memory Acquisition from Android Devices." Pp. 365–78 in *IFIP International Conference on Digital Forensics*. Springer.

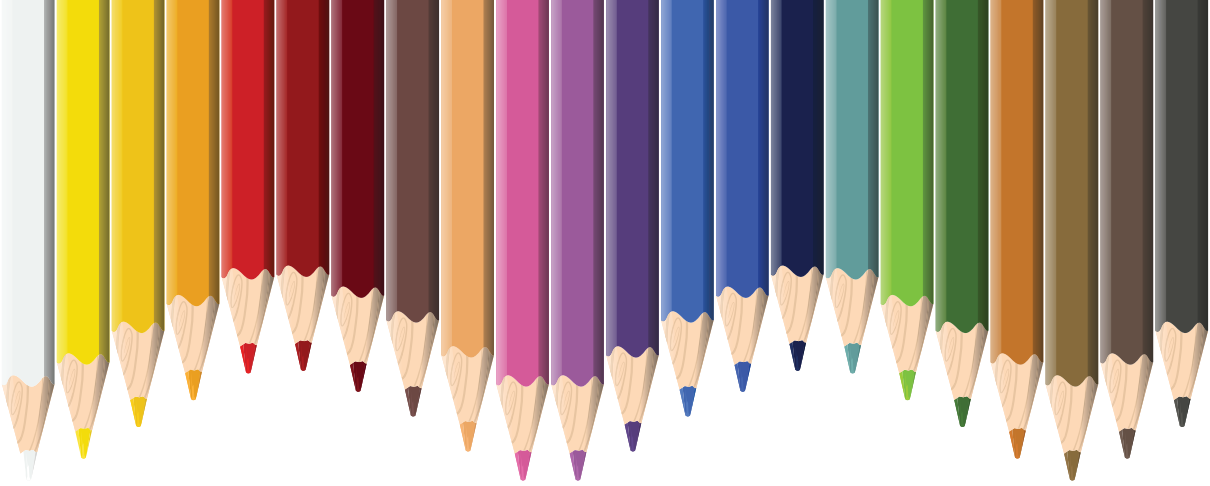

Chapter 10

ANALYSIS OF ENERGY INTENSITY INDICATORS OF TÜRKİYE AND THE NECESSITY OF NUCLEAR ENERGY FOR SECURITY OF SUPPLY

Oğuzhan ERBAŞ[1]
Halit ARAT[2]

1 Assoc. Prof. Dr., Kütahya Dumlupınar University, Engineering Faculty, Mechanical Engineering Dpt, Kütahya, Türkiye, oguzhan.erbas@dpu.edu.tr, Orcid: 0000-0001-9424-4273,
2 Asst. Prof. Dr., Kütahya Dumlupınar University, Engineering Faculty, Mechanical Engineering Dpt., Kütahya, Türkiye, halit.arat@dpu.edu.tr, Orcid: 0000-0002-6634-2535,

INTRODUCTION

Since the energy needs arising from the increase in human population and the rapid development of technology cannot be met at the same pace by today's resources, the efficient use of energy has become the most important agenda of societies in recent years. In addition, the greenhouse effect caused by hot gases released due to increasing energy consumption day by day, and the resulting climate change due to global warming, reveals the importance of energy use for the future of humankind (Iris and Lam, 2019). Our world's dependence on fossil fuels is expected to continue to increase until the middle of the century. Due to their heterogeneous distribution on earth, more than a quarter of energy resources and more than half of oil are subject to international trade. Although the concern that they will go extinct has diminished, the competition, especially over oil, will become increasingly harsh. All countries consider the uninterrupted supply of the energy resources they need at reasonable prices to be a security problem. As such, the world energy supply system presents national and international security risks. The fact that more than half of the surplus oil is in the hands of the Middle Eastern members of OPEC makes the geography in which Türkiye is located strategically important (Yemelyanov et al., 2021).

The main way to minimize the production cost in energy-intensive industrial production systems is by minimizing the total energy consumption in the production systems. The energies used can be in the form of fuels and fuel-derived secondary energies. Energy efficiency should be ensured in converting fuels, which are energy raw materials, into secondary energy and in the transmission, distribution, and usage stages of secondary energies. The chemical energy stored in fuels is converted into heat energy through the combustion process. Thermal energy consists of the sum of work potential (exergy) and anergy (dead energy). The basic definition of energy efficiency is to benefit from fuel exergy as much as possible (Utlu and Hepbasli., 2005). In industrial energy-saving studies, all inputs of the relevant production system, input preparation systems, production processes, outputs, and output conditioning systems are examined in terms of energy and operating economy, and energy, mass, and mass balances are calculated. Data are determined individually for all energy usage areas, types of energy used, usage load conditions, the specific energy consumption of energy-using units, etc. Combustion, thermal performance, functional tests based on input features and energy efficiency tests are performed on energy-consuming systems and compared with the current best technological system and energy performance of this system and unit. As a result of the economic analysis, the annual depreciation expense that will occur if the existing unit is replaced with new units and the annual monetary return of less annual energy use that will be provided by the change (Utlu and Hepbasli., 2007). In this case, nuclear energy, limited fossil fuel resources,

and the environment, etc., in a situation where energy costs are increasing, are options that have a significant share in meeting the world's energy needs. This type of energy, in addition to meeting energy needs, also promises important technological development and use opportunities in other areas (Lenzen, 2008).

As of November 2023; approximately 60 reactors are under construction worldwide and 110 more are planned. Most of the reactors under construction or planned are in Asia. The decommissioning of older facilities has largely offset new active facilities in recent years. In the past 20 years, 108 reactors have been retired and 97 have become operational. Today, approximately 440 nuclear power reactors operate in 32 countries besides Taiwan, with a total capacity of approximately 390 GWe. These provided 2545 TWh in 2022, approximately 10% of the world's electricity. Many countries with existing nuclear energy programs either plan to build or build new energy reactors. Approximately 30 countries are considering, planning or initiating nuclear energy programs. Figure 1 shows the distribution rate and capacity of nuclear power plants worldwide (Operable NPR, 2023).

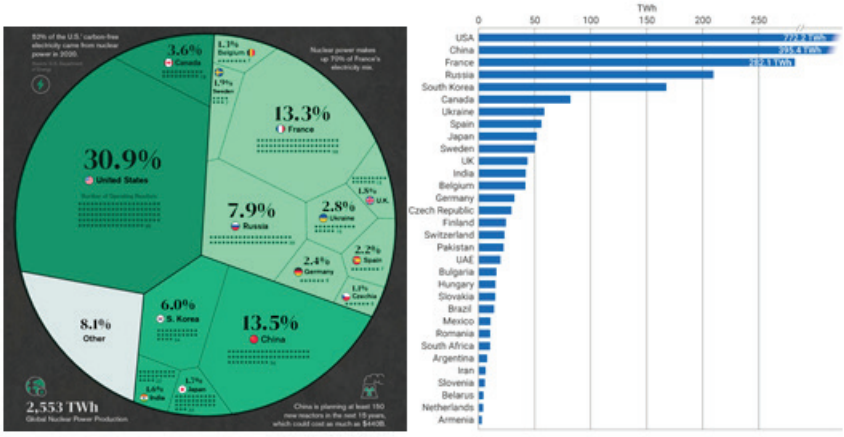

Figure 1. Distribution Rate and Capacity of Nuclear Power Plants Worldwide (Operable NPR, 2023)

Nuclear power plants depend on external conditions (climate conditions) like renewable energy power plants, the quality of the fuel like coal power plants, and the amount of reserves like oil and natural gas power plants. Since it is not connected, it provides continuity in electricity production. Renewable energy is safe but unreliable (constant); it is an alternative energy source as nuclear power plants can be operated continuously, regardless of season and climate conditions. The wind does not always blow, the sun does not always

shine, and the rainfall is not always abundant, but the nuclear power plant always works. Suppose maintenance periods are excluded from 8760 hours a year. In that case, the nuclear power plant can operate for approximately 8000 hours, but in hydraulics, this is an average of 4000 hours, an average of 3000 in the wind, also the average time in the sun is 2500 hours (Davydov et al., 2019; TR Energy Ministry, 2023).

When considered as a whole, the nuclear energy production chain is the cleanest option regarding greenhouse gas emissions. Harmful gases that cause the formation of greenhouse gases such as carbon monoxide, carbon dioxide, sulfur dioxide and nitrogen dioxide, released by the burning of fossil fuels, are not released into the atmosphere while nuclear power plants are operating. Therefore, nuclear energy can not cause climate change and also plays a major role in reducing the concentration of greenhouse gases in the atmosphere. Today, nuclear power plants cause an annual reduction of approximately 17% in greenhouse gas emissions from the electricity sector. If electricity was obtained from fossil fuel power plants instead of these power plants, 1.2 billion tons of carbon would be released into the atmosphere every year (Dinçer, 2019).

There are six nuclear power plants in France (Nogent, Dampierre, Saint-Laurent, Penly, Paluel, Belleville) less than 200 km from Paris. The distance of the Nogent power plant to Paris is only 90 km. Additionally, there are fourteen nuclear power plants on the Loire River in France. Despite the nuclear power plants, an idyllic boat trip along the river with historical castles is a popular tourist activity. Regarding the impact of nuclear power plants on agriculture, it is known that the USA, which has the most nuclear power plants, is the country that exports the most agricultural products in the world, with 42.8 billion dollars. France is also the second country that exports the most agricultural products. On the other hand, for Türkiye, which is mainly dependent on foreign sources to meet its increasing energy needs, nuclear energy is still an option that is not adequately utilized, despite the existence of some investments started a long time ago. For this reason, nuclear energy is of great importance for Türkiye in terms of ensuring energy supply security and reducing energy import dependency and current account deficit [8].

OVERVIEW OF TÜRKİYE'S ENERGY INTENSITY INDEX

Energy intensity is an energy efficiency indicator that measures how much energy is required to produce one unit of gross domestic product on a country or region basis. The required amount of energy is calculated from the primary energy density in terms of total unconverted energy supplied in the country. Final energy intensity is defined as the energy consumed by sectors such as industry, housing, and transportation. Trends in energy density are affected by structural changes in the economy and industry, changes in the

energy consumption structure, efficiency development of sectors, and devices and equipment preferred by end users. The density calculated by dividing primary energy consumption by gross domestic product is called primary energy density, and the density calculated by dividing final energy consumption by gross domestic product is called final energy density.

Additionally, primary energy intensity is an energy efficiency indicator that measures how much energy is required to create one unit of gross domestic product on a regional and country basis (GD-RE, 2023). Türkiye's primary energy density in 2022 is calculated as 0.132 toe/thousand 2015$, and the final energy density is calculated as 0.101 toe/thousand 2015$. 6.2% increase in primary energy intensity in 2022 compared to the previous year; there was a 7.9% reduction in final energy density. Compared to 2000, primary energy density was 31.2% and there is a 32.3% improvement in final energy density. Figure 2 shows primary and final energy intensity data by year (Indicators toe/thousand 2015$) (GD-RE, 2023).

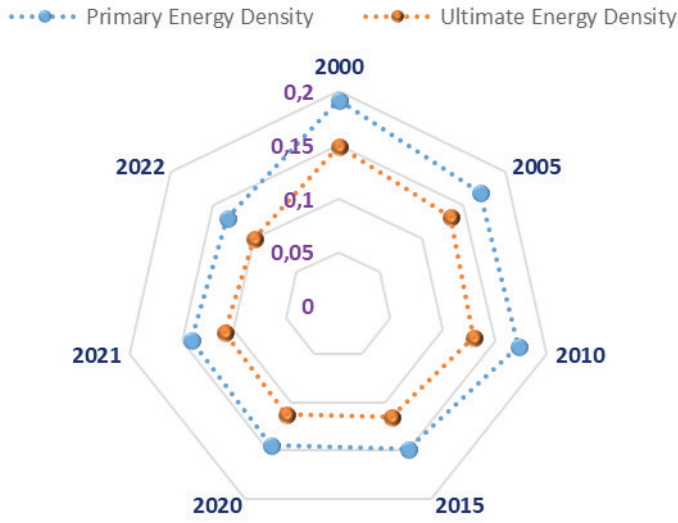

Figure 2. Primary and Final Energy Intensity Data by Years (GD-RE, 2023)

Suppose an international comparison is to be made. In that case, Türkiye's primary energy density, which is 0.132 toe/thousand $2015 for 2022, is lower than the world average (0.169 toe/thousand $2015), but remains above the OECD average (0.097 toe/thousand $2015). The average primary energy intensity of the European Union countries is better than the OECD and Türkiye, with 0.086 toe/thousand in 2015$. As of the end of 2022, 46% of Türkiye's

total electricity capacity and approximately 58% of gross electricity production were provided by fossil fuels. As a country that imports almost all of the fossil fuel oil and natural gas, Türkiye's dependence on these resources causes it to be directly affected by price increases in global markets. Therefore, Türkiye's need for low-carbon energy transformation is critical to reduce its dependence on foreign energy and prevent its fragility in the current account deficit. Table 1 shows the monthly distribution of Türkiye's gross electricity production according to primary energy sources until September 2023.

Table1.Monthly Distribution Of Türkiye's Gross Electricity Generation By Primary Energy Resources (2023)

Unit: GWh	JANUARY	FEBRUARY	MARCH	APRIL	MAY	JUNE	JULY	AUGUST	SEPTEMBER	OCTOBER	TOTAL
Hard Coal + Imported Coal	7.429,0	5.990,6	6.171,7	4.118,7	4.691,0	5.652,7	7.494,5	7.612,6	7.186,8	7.049,1	63.396,8
Lignite	3.958,1	3.274,3	3.303,0	2.774,2	3.073,6	3.349,9	3.647,6	3.497,0	3.400,3	3.589,4	33.867,3
Liquid Fuels	51,6	25,3	42,2	62,9	66,3	65,5	68,9	64,9	65,4	58,2	571,3
Naturl Gas + LNG	7.251,8	7.375,1	5.520,6	3.797,1	4.919,3	2.643,2	6.817,2	9.588,0	6.905,2	5.733,4	60.550,9
Renew and Wastes	851,9	709,7	847,0	842,8	845,465	827,114	818,498	834,2	814,6	817,3	8.208,7
Thermal	19.542,4	17.375,0	15.884,4	11.595,8	13.595,7	12.538,5	18.846,7	21.596,7	18.372,3	17.247,4	166.595,0
Hydro	2.949,5	2.408,6	5.343,2	7.415,4	7.501,5	7.533,6	6.510,2	5.433,0	3.893,4	3.853,7	52.842,1
Geothermal + Wind + Solar	4.630,1	4.892,8	5.294,5	4.937,2	5.135,9	5.146,9	6.235,9	6.160,5	6.130,5	4.811,1	53.375,6
Gross Generation	27.122,0	24.676,5	26.522,1	23.948,4	26.233,1	25.219,0	31.592,9	33.190,2	28.396,3	25.912,3	272.812,7
IMPORTS	903,2	569,1	559,9	374,9	365,1	332,4	461,3	495,0	462,1	553,8	5.076,8
EXPORTS	240,2	222,1	164,0	172,5	120,4	149,2	188,9	166,7	164,5	157,3	1.745,7
GROSS DEMAND	27.785,0	25.023,5	26.918,0	24.150,8	26.477,7	25.402,2	31.865,3	33.518,5	28.693,9	26.308,8	276.143,7

Models applied especially to solar and wind energy sources in the last 20 years have enabled Türkiye to progress faster than expected in the low-carbon energy transformation, with the influence of the steps taken by policymakers to combat climate change. Carrying this point to even better levels has become a goal compatible with the 2053 net zero emission target. Türkiye's total electricity demand did not show a decrease between 2000 and 2022, except for the years 2001, 2009, 2019, and 2022, and it continued its increasing trend. While the total electricity demand was 306.1 TWh (terawatt hours) in 2020, it reached 329.6 TWh by the end of 2021, with the recovery year after the Covid-19 pandemic. With the impact of geopolitical developments and macroeconomic factors, electricity demand decreased by 0.3% in 2022 and reached 328.7 TWh (TSKB, 2023). Table 2 shows the monthly distribution of gross electrical energy production in Türkiye according to producer organizations (2023). Türkiye's total installed power, which was around 27.3 gigawatts (GW) as of 2000, reached 105.7 GW by the end of September 2023.

Incentives given to power plants that produce electricity from renewable energy sources and domestic resources until 2022 played an essential role in this increase, and the increasing trend in Türkiye's total installed power continues.

Table 2. Monthly Distribution Of Türkiye's Gross Electricity Generation By The Electricity Utilities

Unit : GWh		JANUARY	FEBRUARY	MARCH	APRIL	MAY	JUNE	JULY	AUGUST	SEPTEMBE	OCTOBER	TOTAL
EUAS	THERMAL	1.422,6	1.880,7	1.310,5	932,3	1.007,2	758,3	1.573,7	2.269,6	1.866,8	1.538,7	14.560,5
	HYDRO. GEOTHERM. WIND	1.588,2	1.035,7	1.488,4	1.789,3	2.001,2	2.484,6	3.112,9	2.990,9	2.264,5	2.123,3	20.879,0
	TOTAL	3.010,8	2.916,4	2.799,0	2.721,7	3.008,4	3.242,9	4.686,5	5.260,5	4.131,3	3.662,1	35.439,6
UNLICENSED STATIONS	THERMAL	154,2	133,8	194,4	149,1	125,7	159,1	117,7	127,6	95,8	95,6	1.353,0
	HYDRO. WIND SOLAR	728,1	856,4	974,2	1.246,6	1.450,8	1.598,4	1.852,4	1.702,4	1.540,8	1.258,8	13.209,0
	TOTAL	882,3	990,2	1.168,6	1.395,7	1.576,4	1.757,5	1.970,2	1.830,0	1.636,7	1.354,4	14.562,0
PRODUCTION COMP.	THERMAL	17.824,9	15.306,0	14.379,5	10.514,3	12.462,8	11.621,1	17.155,3	19.199,4	16.409,7	15.613,1	150.486,2
	HYDRO. GEOTHERM. WIND SOLAR	5.117,0	5.266,8	7.898,9	8.935,1	8.685,5	8.082,0	7.281,5	6.460,2	5.909,0	5.036,7	68.672,6
	TOTAL	22.941,9	20.572,8	22.278,3	19.449,5	21.148,3	19.703,2	24.436,8	25.659,6	22.318,7	20.649,8	219.158,8
TOOR	THERMAL	140,6	54,6	0,0	0,0	0,0	0,0	0,0	0,0	0,0	0,0	195,2
	HYDRO. GEOTHERM. WIND	146,3	142,5	276,2	381,5	500,0	515,5	499,4	440,0	309,7	246,0	3.457,0
	TOTAL	286,9	197,0	276,2	381,5	500,0	515,5	499,4	440,0	309,7	246,0	3.652,2
TURKEY'S TOTAL GENERATION	THERMAL	19.542,4	17.375,0	15.884,4	11.595,8	13.595,7	12.538,5	18.846,7	21.596,7	18.372,3	17.247,4	166.595,0
	HYDRO. GEOTHERM. WIND SOLAR	7.579,6	7.301,4	10.637,7	12.352,6	12.637,4	12.680,5	12.746,2	11.593,5	10.023,9	8.664,8	106.217,7
	TOTAL	27.122,0	24.676,5	26.522,1	23.948,4	26.233,1	25.219,0	31.592,9	33.190,2	28.396,3	25.912,3	272.812,7

Between 2012 and 2022, the average annual net increase in installed power was 4.6 GW. The increase in installed capacity in this period was higher than the increase in total electricity demand, and one of the biggest reasons for this is the incentives given to renewable energy plants. The average annual installed power of renewable energy power plants commissioned between 2012 and 2022 was around 3.3 GW. 80% of the net installed power increase, around 1,891 megawatts (MW) in the first nine months of 2023, occurred from power plants producing electricity from renewable resources. An increase in installed capacity of 1,473 MW was provided by solar power plants (SPP), 213 MW of the total increase came from wind power plants (RES), and 23 MW came from hydroelectric power plants (HEPP) (TSKB, 2023). Figure 3 shows the distribution of licensed electricity generation facility investments according to installed capacity (MWe) for 2023.

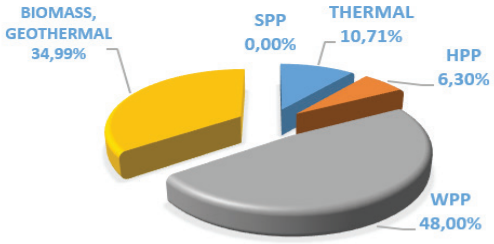

FACILITY TYPE	INSTALLED CAPACITY
THERMAL	35,550
HPP	20,916
WPP	159,375
BIOMASS GEOTHERMAL	116,171
SPP	0,000
TOTAL:	***332***

Figure 3. Distribution of licensed electricity generation facility investments by installed capacity for 2023 (MWe).

According to Türkiye National Energy Plan, considering our country's renewable energy potential, renewable energy capacity aims to reach 122.7 GW and its share in the installed electricity capacity to 64.7% in 2035. According to the plan, it is envisaged to reach a capacity of 29.6 GW in wind (24.6 GW onshore, 5 GW offshore), 52.9 GW in solar, 35.1 GW in hydroelectricity, and a total of 5.1 GW in geothermal and biomass. It is also stated that battery capacity is expected to reach 7.5 GW in 2035 (TSKB, 2023). In Table 3, the targeted installed power values for 2035 within the Turkish National Energy Plan framework are given.

Table 3. Installed Capacity Targeted within the Framework of Türkiye National Energy Plan

Installed Power (GW)	2035 (GW)	Share in Renewable Energy Resources (%)	Share in Grand Total (%)
Solar	52,9	43,1	27,9
Hydro	35,1	28,6	18,5
Wind	29,6	24,1	15,6
Geothermal Biomass	5,1	4,2	2,7
Renewable Total	122,7	100	64,7
Source	**2035 (GW)**	**Share in Total Gas, Coal and Nuclear (%)**	**Share in Grand Total (%)**
Gas	35,5	53,0	18,7
Coal	24,3	36,3	12,8
Nuclear	7,2	10,7	3,8
Grand Total	189,7	100	100

NECESSITY OF NUCLEAR ENERGY FOR TÜRKİYE

The energy sector is also one of the sectors with the most damaging environmental impact. Emissions caused by fossil fuel addiction raise local, regional, and global environmental questions, and these problems are gradually increasing to the extent of climate change. Therefore, it is necessary to introduce technologies that use these resources more cleanly, to develop and implement technologies that reduce negative environmental impacts, and, in part, to gradually move away from these resources and turn to more expensive, renewable energy sources. This is mostly performed by developed countries with sufficient economic power (Kalair et al., 2021).

On the other hand, we encounter nuclear energy as a type of energy that does not pollute the atmosphere. However, after the Chernobyl accident, doubts about the safety of this technology and the resulting intense reactions are one of the most important problems of this technology. On the other hand, efforts to inform the public are continuing in countries that have or plan to have this technology. In order to satisfy the public, it is necessary to convince the public of the existing solution proposals regarding radioactive wastes resulting from spent fuels and to finalize the efforts to produce solution methods. Nuclear energy is one of the most important options to be considered if OECD countries decide to fulfill their Kyoto Protocol obligations.

On the other hand, with the “INPRO Project” being carried out at the International Atomic Energy Agency (IAEA), studies on the design of an ‘intrinsically safe reactor’ continue. In parallel, IV is being carried out by ten countries (Argentina, Brazil, Canada, France, Switzerland, Japan, Korea, South Africa, England) under the leadership of the USA. The first phase of

the studies on generation nuclear energy systems (A Technology Roadmap for Generation IV Nuclear Energy Systems) has been completed; 6 nuclear reactor designs suitable for use in 2030 and beyond have been determined.

Overcoming the inadequacies that the world energy supply is expected to encounter towards the middle of the century, limiting the negative environmental impacts, and repairing them effectively depend on the solutions that research in the energy field can bring. However, it takes time for technological research to introduce new products and for these products to become commercialized and infiltrate the markets. The fact that the sector is already a slowly changing sector indicates the need to accelerate this research by allocating greater resources. Türkiye also has to do its share. On the other hand, Türkiye is dependent on foreign sources due to insufficient own resources, and this dependency rate is gradually increasing. Therefore, in order to keep under control the risks arising from dependence on energy imports. It has to carefully prioritize the energy technology fields in which it can have a chance to compete, focus on research, and gain an influential place in the international energy market with contemporary product contributions in the directions indicated by the driving forces in the energy world. For this reason, there is necessary and obligation for Türkiye to turn to safe, reliable, environmentally and economically proven technologies in nuclear energy (Türbitak, 2003).

Akkuyu Nuclear Power Plant Technical Parameters and Settlement Area Features

Türkiye's investment targets in nuclear energy started in the 1950s, and various initiatives have been made since then, but these initiatives have not turned into investments. In 2010, an intergovernmental agreement was signed between Türkiye and Russia on 12.05.2010 regarding the construction and operation of a nuclear power plant by Rosatom, a public institution affiliated with the Russian Federation. Rosatom will install and operate the facility in the project based on the build-own-operate model. Akkuyu Nuclear Power Plant (Akkuyu NPP), which is under construction in Gülnar district of Mersin province, will consist of four VVER-1200 reactors, each with an installed power of 1,200 MW, and the total installed power of the facility will be 4,800 MW. The first reactor is expected to be put into operation in 2024 (TSKB, 2023).

The total area of the Akkuyu nuclear power plant site is 1023 hectares, consisting of the project land allocated for the Akkuyu nuclear power plant construction area, protection dam, western and eastern piers, civil assembly base, and access roads. Akkuyu nuclear power plant construction site is 125 hectares. The complex power output structures are envisaged to the north of the Akkuyu nuclear power plant construction site on a terrace within a fenced area of 14 hectares. Akkuyu Nuclear Power Plant site is located in the southern

part of Türkiye, on the Mediterranean coast (Mersin Province), with a radius of approximately 3 km. Hills surround the site up to 200 m high. These hills form the natural border of the nuclear power plant location area in the north and east directions. The site overlooks Aksaz and Akkuyu-Çamalanı bays in the south-west direction (Akkuyu Nuclear Joınt Stock Company, 2017).

The main requirements for the selection of the Akkuyu site, which was allocated for the construction of the first nuclear power plant in Türkiye as of 1976, can be summarized as follows:

• Due to the large amount of cooling water and land transportation problems of heavy components required in Türkiye, the facility must be located on the seashore;

• Site selection studies conducted since 1968 have shown that earthquake risk is the most critical site selection factor in Türkiye. Regarding earthquake risk, the Mediterranean coastal area is considered one of the safest regions in Türkiye

.

• The Akkuyu area and its surroundings are one of the most sparsely populated areas in Türkiye, and in addition, the area is not deemed suitable for developing tourist, agricultural, or industrial activities.

• Due to the favorable meteorological conditions in this coastal region, the site was expected to have suitable atmospheric dispersion characteristics.

• Since the maximum flood level is not expected to be more than six meters, tsunamis or other floods are not considered to pose a significant danger to the facility, and the site's topography has been deemed suitable for construction at various altitudes.

• The natural drainage direction of surface water and groundwater in the Akkuyu site is towards the sea and will not likely affect off-site wells. The location of Akkuyu nuclear power plant reactors is shown in Figure 4.

Figure 4. Location of Akkuyu Nuclear Power Plant Reactors

A Nuclear Power Plant's rated electrical power (base load) is defined as the active electrical power produced at the generator terminals at nominal conditions. The expected value of the nominal electrical power (gross) for each Akkuyu Nuclear Power Plant unit under nominal conditions (at 3300 MW reactor thermal power and 22 ºC cooling water temperature) is not less than 1200 MW. Taking into account site requirements and service (cooling) water resource consumption, the electrical energy consumed for the auxiliary equipment of each unit of the Akkuyu Nuclear Power Plant is up to 7% of the generated energy.

Akkuyu Nuclear Power Plant units use a direct service (cooling) water source flow system with a single circulation of Mediterranean water as the final heat sink. At a cooling water temperature of 25 ºC, the cooling water flow to the turbine condensers of each nuclear power plant unit is around 254000 m^3/hour. The total flow of cooling seawater to the turbine condensers, consid-

ering backup equipment operation, is 272273 m3/h per unit, correspondingly 1089092 m^3/h for four nuclear power plant units. The total flow of distilled water consumption for the technical needs of the facility is 554 m^3/hour. Under accident conditions, the total flow of main service cooling seawater to the safety systems is 8754 m^3/hour for each nuclear power plant unit. By operating the four nuclear power plant units in baseload mode, the expected electricity output will be up to 35 billion kWh per year. Table 4 gives the essential technical characteristics of the reference site and the Akkuyu nuclear power plant unit (Akkuyu Nuclear Joınt Stock Company, 2017).

Table 4. Basic Technical Specifications of the Reference Site and Akkuyu Nuclear Power Plant Unit Parameter Value (Akkuyu Nuclear Joınt Stock Company, 2017)

	Reference Facility	Akkuyu Nuclear Power Plant
Reactor thermal energy (at nominal conditions), MW	3200	3300
Active electrical energy, MW greater than this value	1200	1200
Number of reactor coolant circulation circuits	4	4
Parameters of primary and secondary circuits		
Cooling water pressure at core outlet, MPa (abs.)	16,2	16,2
Cooling water temperature at the reactor inlet / outlet, °C	298,2 / 328,9	297,2 / 328,8
Reactor coolant flow, m^3/s	86000	87460
Steam pressure in steam generators, MPa (abs.)	7,0	7,0
Steam flow from each steam generator, t/s	1602	1652
Feed water temperature, °C	225	225
Maximum new fuel enrichment for U-235, %	4,95	4,95
Nuclear combustion of spent fuel (average/maximum in uncharged fuel assemblies), MW×d/kgU	55,8 / 59,7	49,4 / 54,3
Refueling interval, months	12	18
Operating time of fuel in the reactor core (in steady-state fuel cycle), years	4	3-4,5
Number of fuel assemblies in the reactor core	163	163

The Importance of Nuclear Energy for Türkiye

With the construction of the Akkuyu Nuclear Power Plant, it is aimed to meet the increasing electricity demand in the country by providing a reliable

energy source at reasonable prices. The nuclear power plant will contribute to the diversity of energy resources in the national energy mix. It will help reduce dependence on imported natural gas and the volatile prices of fossil fuels. Thus, nuclear energy production is expected to increase the country's energy security. Additionally, the facility will provide electricity without carbon emissions. The construction of the Akkuyu Nuclear Power Plant will greatly positively impact the macroeconomic and social environment at both regional and national levels (Akkuyu Nuclear Joınt Stock Company, 2017).

Across the European Union, a significant amount of resources is allocated to developing nuclear power plants, and nuclear capacity is expected to be increased by 2030, most of which will be the renewal of existing capacity. There are no restrictions on using nuclear power plants within the European Union. The increase in oil and natural gas prices and limitations in carbon dioxide emissions are increasing the tendency towards nuclear energy again (Yolcan, 2023). It is inevitable for Türkiye to invest in nuclear energy in order to protect itself from the extreme risks brought by dependence on imported resources. Considering the limited domestic resource potential and environmental impacts, it is seen that activities are continuing to complete the necessary technical and legal infrastructure studies to ensure that nuclear power plants take their place in the supply portfolio.

According to the Mining Technical Exploration Agency, the proven thorium reserve in Türkiye is 380,000 tons. According to OECD and IAEA, the thorium reserve in Türkiye is at least 744,000 tons, and Türkiye has the second largest thorium reserve after India. Compared to uranium, thorium-uranium mixed fuels appear to produce less plutonium. In addition, these fuels can operate at a high burn rate, extending the fuel's residence time in the reactor and the fuel reload period, increasing the facility capacity factor. Considering the high thorium reserves in Türkiye, turning to technologies in this field will significantly reduce our foreign dependency on energy (Dinçer, 2019). The share of initial investment expenses in the total cost of nuclear power plants is high. However, the share of operating and fuel expenses is higher than that of a natural gas power plant. In this case, sudden changes in fuel costs have little impact on the unit cost of electricity produced from the nuclear power plant. In a natural gas power plant, even the slightest change in fuel costs can significantly increase the cost of electricity (Jurakulov, 2023).

CONCLUSION AND RECOMMENDATIONS

The three main pillars of the energy sector are fossil fuels, nuclear energy, and renewable energy. Making the energy system more flexible, diversifying resources locally, increasing renewable energy production capacities, and providing cheap, sustainable energy are among Türkiye's priority issues. Nuclear energy is seen as an essential alternative on a global scale, together with

new and renewable energy sources, for controlling greenhouse gas emissions and emissions arising from energy production within the scope of the Framework Convention on Climate Change, to which Türkiye has been a party since 2004. It is observed that many European countries prefer nuclear technology. Nuclear energy is of great importance for Türkiye in terms of ensuring energy supply security and reducing energy import dependency and current account deficit.

To this end,

- Introducing R&D and domestic manufacturing obligations in international agreements regarding Renewable Energy Resource Areas Model Applications and nuclear power plants

- To develop evaluation criteria for new-generation nuclear reactor technologies and to apply

- Acquiring materials, control systems, and manufacturing technologies for nuclear technology.

- In addition to electricity production, hydrogen production, industrial heat production, and seawater purification, the development of nuclear reactor technologies for applications

- Regarding the conversion of long half-life nuclear fuel wastes into short half-life wastes, the development of technologies

- The work on the renewal of the legislation regarding improving infrastructure in the nuclear field, and in this context, institutional and legal regulations, must be completed to establish independent organizations in nuclear safety and radiation safety. In conclusion, it should accelerate investments that will ensure energy supply security, such as establishing an advanced natural gas storage infrastructure, increasing electricity production from domestic and renewable resources, including nuclear energy in the energy production portfolio, commissioning new global oil and natural gas pipelines, and projecting alternative energy sources.

REFERENCES

Akkuyu Nuclear Joınt Stock Company. (2017). Akkuyu Nuclear Power Plant Field Parameters Report, Ankara.

Davydov, R., Antonov, V., Makeev, S., Batov, Y., Dudkin, V., & Myazin, N. (2019). New high-speed system for controlling the parameters of a nuclear reactor in a nuclear power plant. In *E3S Web of Conferences* (Vol. 140, p. 02001). EDP Sciences.

Dinçer, İ. (Ed.). (2019). *TÜBA-Nuclear energy report. Turkish Academy of Sciences*.

GD-RE (General Directorate of Renewable Energy). (2023) https://enerji.gov.tr/ Energy Intensity Report.

Iris, Ç., & Lam, J. S. L. (2019). A review of energy efficiency in ports: Operational strategies, technologies and energy management systems. *Renewable and Sustainable Energy Reviews*, *112*, 170-182.

Jurakulov, S. Z. (2023). Nuclear energy. *Educational Research in Universal Sciences*, *2*(11), 514-518.

Kalair, A., Abas, N., Saleem, M. S., Kalair, A. R., & Khan, N. (2021). Role of energy storage systems in energy transition from fossil fuels to renewables. *Energy Storage*, *3*(1), e135.

Lenzen, M. (2008). Life cycle energy and greenhouse gas emissions of nuclear energy: A review. *Energy conversion and management*, *49*(8), 2178-2199.

Operable NPR (nuclear power reactors) (2023), https://elements.visualcapitalist.com. Operable nuclear power reactors worldwide 2023, by country.

TR Energy Ministry. (2023) https://enerji.gov.tr/neupgm-nukleer-enerji. Nuclear Information Booklet.

TSKB. (2023). 2023 Energy Outlook Report. Turkish Industrial Development Bank, Istanbul.

Tübitak. (2003). Vizyon 2023 Teknoloji Öngörü Projesi.

Utlu, Z., & Hepbasli, A. (2005). Analysis of energy and exergy use of the Turkish residential–commercial sector. *Building and Environment*, *40*(5), 641-655.

Utlu, Z., & Hepbasli, A. (2007). A review and assessment of the energy utilization efficiency in the Turkish industrial sector using energy and exergy analysis method. *Renewable and sustainable energy reviews*, *11*(7), 1438-1459.

Yemelyanov, O., Symak, A., Petrushka, T., Vovk, O., Ivanytska, O., Symak, D., ... & Lesyk, L. (2021). Criteria, indicators, and factors of the sustainable energy-saving economic development: the case of natural gas consumption. *Energies*, *14*(18), 5999.

Yolcan, O. O. (2023). World energy outlook and state of renewable energy: 10-Year evaluation. *Innovation and Green Development*, *2*(4), 100070.

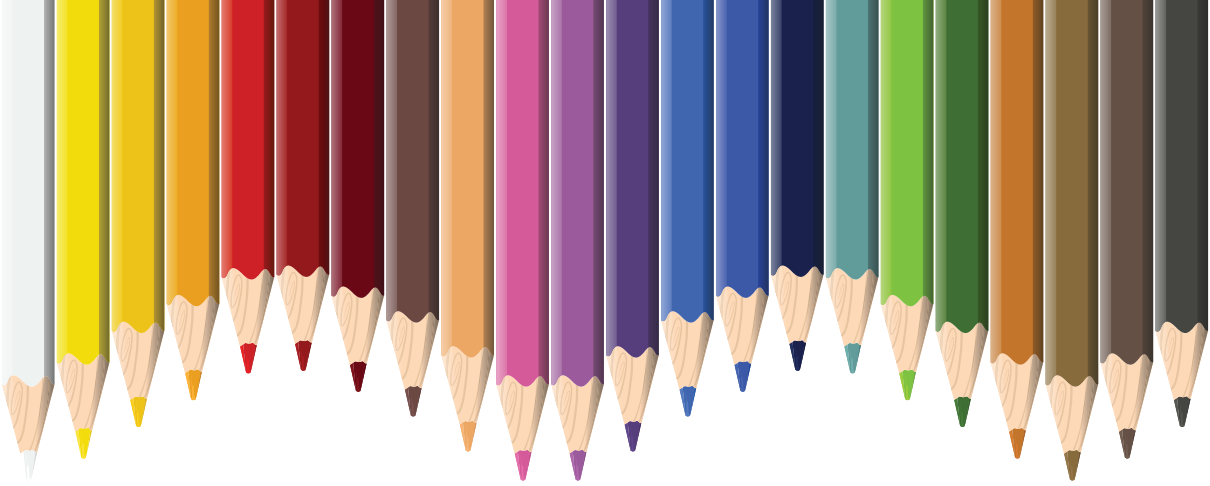

Chapter 11

A REVIEW OF TITANIUM METAL POWDER PRODUCTION THROUGH PLASMA ATOMIZATION

Ahmet DAYANÇ[1]
Mustafa GÜLEŞEN[2]

1 Res. Asst., Kutahya Dumlupinar University, ahmet.dayanc@dpu.edu.tr – ORCID: 0000-0002-5214-9021
2 Asst. Prof., Kutahya Dumlupinar University, mustafa.gulesen@dpu.edu.tr, ORCID:0000-0001-8781-2746

INTRODUCTION

Engineering is a multidisciplinary approach that uses principles of science and mathematics to solve technical problems, designing and improving systems, and applying these solutions as a service. At its core, it aims to improve life, simplify tasks, enhance efficiency, and develop sustainable solutions. Theoretical knowledge merges with practical applications to drive innovations and technological advancements across various fields. In the process of creating solutions to complex problems and fostering innovation, numerous parameters play a significant role, among which the choice and features of materials are paramount. When considering the entirety of a good engineering process, including the importance of materials, we observe that:

- Design and Functionality: Engineering projects serve specific purposes, and the properties of the materials used directly affect the outcome of the work. For instance, in the construction of a structure, the materials used directly impact its structural integrity, durability, and safety. Therefore, the behavior of the structure in adverse scenarios, as well as the engineering objectives and their impact on human life, are dependent on this. Similarly, the correct choice of materials for more complex applications, such as the fatigue resistance of airplane parts or the biocompatibility of biomedical implants, directly affects the functionality of the product and the value it offers to the user.

- Durability and Safety: Materials play a critical role not only in structural strength but also in ensuring longevity. The right choice of materials can provide resistance to environmental factors, wear, and fatigue, thus making structures and devices safer and more durable over time.

- Sustainability and Environmental Impact: The choice of materials also affects the environmental footprint of a project. Factors like energy efficiency, reusability, and ease of recycling are crucial in minimizing environmental impact. Moreover, the use of materials obtained from sustainable sources or those consuming less energy enhances environmental sustainability. Therefore, in an engineering scenario, using materials with characteristics beyond the expected requirements is unnecessary and leads to wastage.

- Aesthetics and Design Flexibility: In architectural and industrial design processes, the right choice of materials is crucial for aesthetic appeal and user experience, hence playing a significant role in aesthetics and design flexibility.

- Cost-Effectiveness: Considering today's limited resources, the cost of materials holds a significant share in the total budget of a project. Selecting cost-effective materials generally reduces overall costs, but it is essential to make a balanced choice that does not compromise performance and quality, which is a major skill in engineering.

- Machinability and Applicability: The manufacturing of certain designs may require special processing or production techniques. In such cases, the machinability and applicability of the chosen material can affect the practical implementation of the design.

- Innovation and Technological Development: The discovery of new materials, their forms, or the improvement of existing ones, can enable innovation in engineering. This may facilitate engineering applications that were previously impossible to realize.

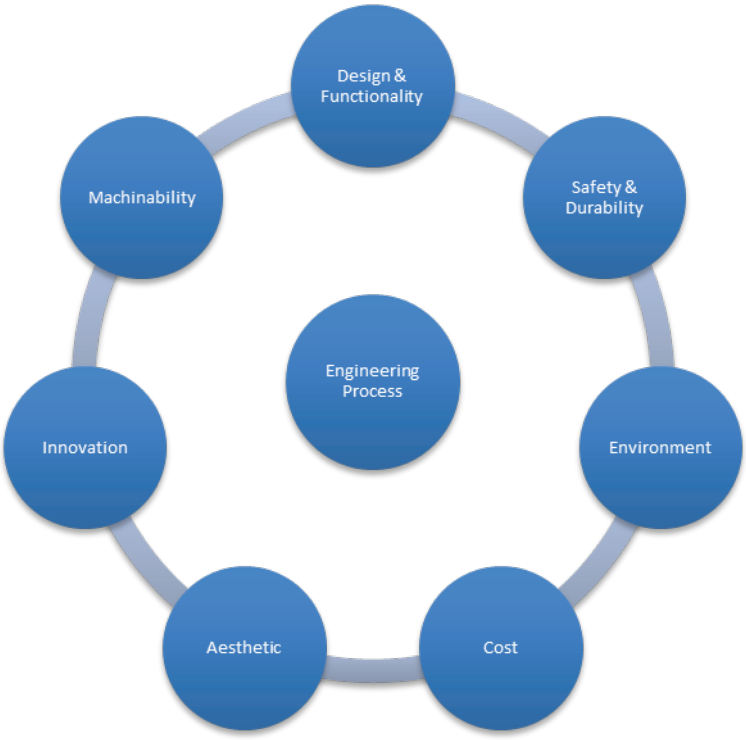

Figure 1. *Graphic Abstract of Basic Engineering Process.*

To meet the expectations summarized in the above Figure 1, and considering only material selection in the engineering process, material classifications can be considered. Metals for high strength and conductivity, ceramics for high temperature and corrosion resistance despite their brittleness, polymers for their lightness and easy molding, elastomers for high flexibility, composites formed from different materials, or advanced materials can be selected depending on the situation. After classification, the correct selection of materials based on technical properties like strength, hardness, flexibility, fatigue

resistance, corrosion resistance, thermal conductivity, electrical conductivity, density, low temperature tolerance, and thermal expansion becomes crucial.

In the fascinating world of engineering, especially in sectors like biomedical, automotive, aerospace, and defense industries, which require high-performance products and advanced engineering applications with strict criteria, the use of titanium material has been notably increasing in recent years [1]. The recent popularity of titanium metal in these sectors is due to its physical and chemical properties, making it an ideal material for various industrial applications, with some of its notable properties being as follows [2]:

- Lightness and High Strength: Titanium is known for being lightweight yet extremely durable, offering a significant advantage in areas such as aerospace, high-speed automobiles, and other fields where structures need to be strong yet light.

- Resistance to Corrosion: Titanium is renowned for its high resistance to corrosion. When it comes into contact with oxygen, it forms a dense, non-porous passivation layer that protects titanium from further oxidation, making it highly resistant to corrosive environments such as water, salt solutions, and some acids. This property makes titanium an ideal material for use in special conditions and harsh environments.

- High Fatigue Resistance: Titanium maintains its strength even under long-term use and dynamic loads, possessing high fatigue resistance. This makes it an excellent choice for long-lasting structural components.

- Biocompatibility: Titanium is biocompatible with the human body, making it a common choice for biomedical applications such as medical devices and implants.

- Thermal Treatment and Surface Properties Enhancements: The properties of titanium can be enhanced with thermal treatments to reduce internal stresses and increase ductility, as well as various surface properties, thus expanding its range of applications.

- Chemical Composition and Standards Compliance: The physical structures and chemical compositions of various titanium alloys can be produced in accordance with international standards, making them more competitive in the global market. Examples of these standards include ASTM F3001, ASTM B348, ASTM F3302, and ASTM F136 [3].

With the above properties, titanium holds a significant place in engineering for solving important problems. However, it also has some disadvantages:

- High Cost: Titanium is a relatively expensive material.

- Machining Difficulty: It is difficult to machining, requiring special tools and techniques for manufacturing. Additionally, titanium is prone to

overheating during machining.

However, the high cost and machining difficulties of titanium are major factors that significantly limit its use. Considering these disadvantages, it is necessary to use titanium in as small a quantity as possible. Additionally, minimizing the machining of titanium can help reduce the impact of these disadvantages. Taking these two factors into account, additive manufacturing technology becomes prominent. Figure 2 below shows a 3D metal additive manufacturing printer capable of producing parts using titanium metal powder [4].

Figure 2. *Metal 3D Printer*
(EOS M 400-4 Series The Ultra Fast Four-Laser System)

The method of metal additive manufacturing aims to produce a part that is as close to its final shape as possible, excluding the application of final tolerances. Being close to the final shape reduces the need for machining and indirectly prevents material wastage. However, a significant capability of additive manufacturing, which can potentially save a large amount of material, is the production of designs with complex internal structures and voids [5].

To create these designs, the implicit modeling technology adopted by nTopology software can be used [6], [7]. When advanced design tools for sophisticated engineering, like the nTopology software, are used, topology optimization of an engineering part can be done, or complex lattice structures

can be created for desired porosity [8]–[10]. Based on the "SIMP" algorithm, topology optimization ensures that material is only present where needed within the design space [11]. With "Field optimization" technique, weak areas in lattice structures are automatically enhanced by the software in accordance with specific constraints and objectives [12], [13]. When the structural integrity of the designed parts is confirmed through analyses, the desired strength can be achieved with the least amount of material [14]. In this way, optimizing the amount of titanium metal powder used can potentially lead to significant reductions in material costs.

A specific challenge that can arise with Additive Manufacturing is due to the working principle of this technology. Since it fabricates in a layered manner, if the design of the manufactured part or its orientation during manufacturing is inappropriate, the amount of required support structures increases. This situation contradicts the principle of material saving, so the orientation during manufacturing must be carefully considered. Additionally, it is necessary to design according to the rules of DfAM (Design for Additive Manufacturing) [15], [16]. Apart from the removal of support structures and the necessary final surface treatments on required parts, the post-processing needs of titanium materials can be reduced. From these perspectives, titanium metal powders have ideal characteristics for additive manufacturing applications. Below, Figure 3 provides a Scanning Electron Microscope (SEM) image of titanium metal powder [17].

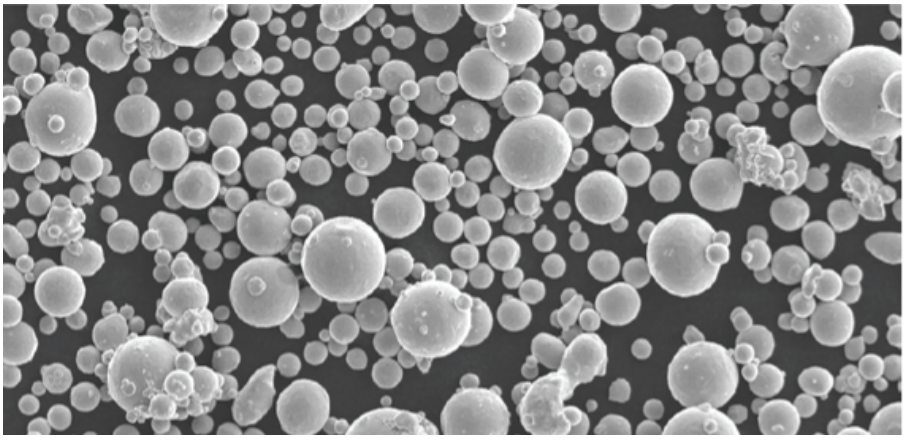

Figure 3. *SEM picture of EOS Titanium Ti64 Grade 23 powder.*

Titanium metal powders can be produced in specific morphologies and particle sizes suitable for modern manufacturing techniques like 3D printing and powder metallurgy. This allows for their broader application in engineer-

ing. Consequently, titanium and the additive manufacturing process represent a continuously evolving technology in the fields of engineering and manufacturing, standing at the forefront of a revolution and opening new horizons.

Below, Figure 4 displays some innovative designs created using optimization techniques that can be produce with additive manufacturing [18], [19]. In this context, the use of titanium metal powders in additive manufacturing for producing innovative designs holds the potential to create a revolution across various sectors.

Figure 4. *Innovative Designs*

At this point, where the production of high-quality titanium metal powders is necessary and extremely important, plasma atomization, an effective and advanced method, is used to obtain titanium powders that meet specific standards and desired properties. The key features of different stages in the Plasma Atomization process are as follows:

- Wire Usage: The use of titanium in wire form allows for excellent control over the process for consistent particle size distribution and standardization between productions at different times.

- Prevention of Contamination and High Purity: The metal wire does not contact any solid surface, ensuring the production of a high-purity product and preventing contamination.

- Reactor Preparation: Before each production process, the reactor is vacuumed, and then it is conditioned with high-purity argon to minimize the oxygen content that could react with the titanium powder being produced.

- High-Energy Plasma Source: The titanium metal wire used in plasma atomization is made from pure molten material and is initially melted using a high-energy plasma torch. The liquid state of the metal at this stage is a pre-process for the subsequent atomization.

- Atomization and Cooling Phase: The melted titanium metal is pulverized by a high-velocity gas flow ejecting from the nozzle. At the end of this process, the melt rapidly solidifies and forms the desired spherical metal powders.

- Low Concentration of Suspended Particles: The concentration of suspended particles in the reactor chamber is kept low. This prevents the formation of satellites and resulting in spherical powders with excellent flow characteristics.

- Powder Size and Sieving: The size distribution of the produced powder ranges from 0 to 150 μm, with most of the powder typically in the range of 0 to 100 μm or 0 to 75 μm. The produced powder can be sieved according to the needs of the users.

Below, Figure 5 shows a schematic of the method [3].

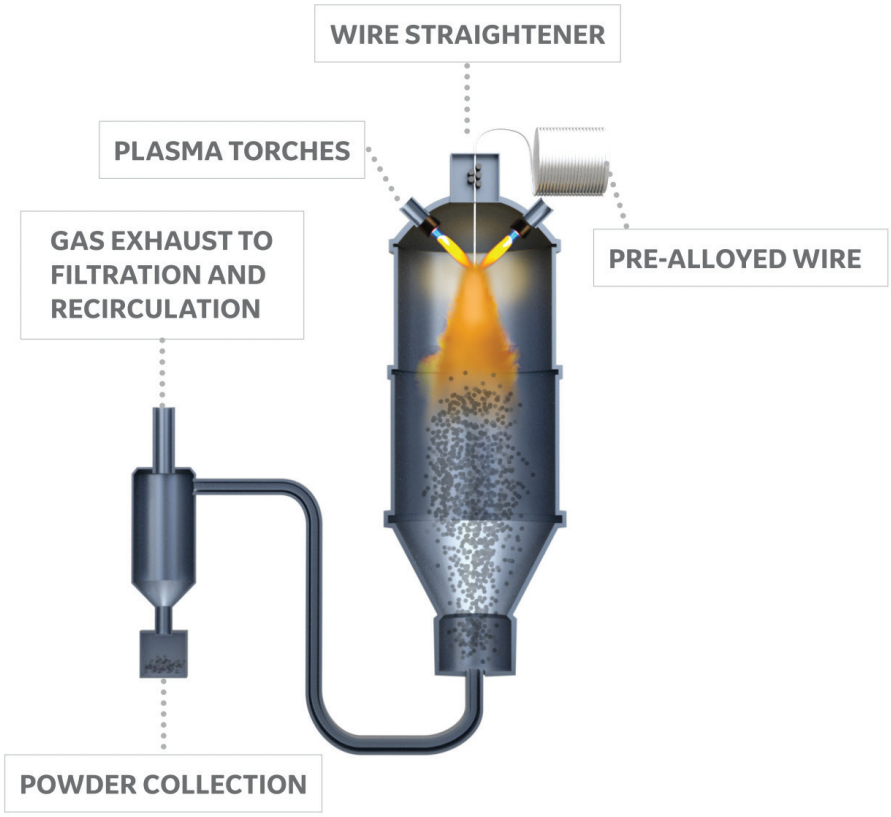

Figure 5. *Schematic View of Plasma Atomization*

Plasma atomization provides desired results in terms of particle size and morphology of the powder, making it an ideal manufacturing method for the production of powders to be used in applications like additive manufacturing and powder metallurgy. Additionally, since the liquid metal does not come into contact with refractory metals or other solid materials during the process, contamination of the powder is reduced, thereby achieving high purity. However, when dealing with reactive metals like titanium, the use of inert gases such as argon and reducing the oxygen level in the production environment, i.e., atmospheric conditioning, is crucial. This helps prevent oxidation and maintain the chemical composition [20]. Critical parameters affecting the plasma atomization process include the plasma torch, pulverization process, reactor chamber, atmospheric conditioning, wire feed mechanism, and powder collector. Below, Figure 6 provides a view of the observation window [21]. Below, Figure 7 presents a visual related to the wire feeding mechanism [22].

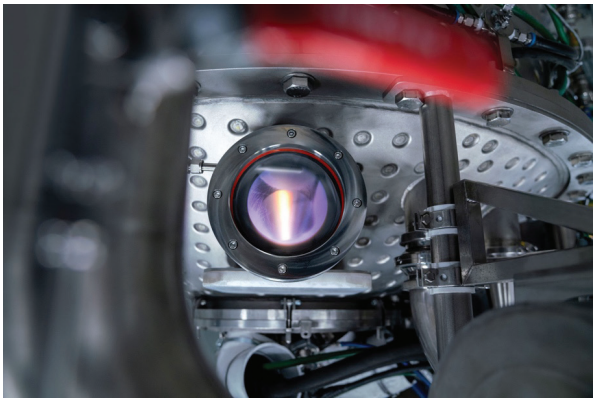

Figure 6. *Observation Window*

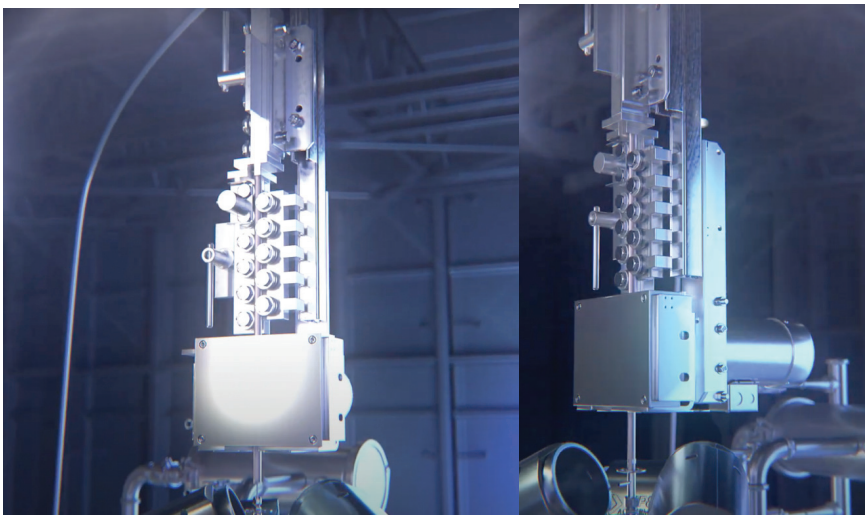

Figure 7. *Wire Feed System*

Below, Figure 8 shows a powder produced by plasma atomization [3].

Figure 6. *Metal Powder*

RESULTS AND CONCLUSION

This study focuses on the production of titanium metal powders using the plasma atomization method and their importance in sectors like aerospace, automotive, biomedical, and defense industries. Titanium is frequently preferred in various fields due to its lightness, high strength, superior corrosion resistance, durability, and biocompatibility. However, its high cost and machining difficulties are factors that limit its use. This study indicates that additive manufacturing technology has the potential to mitigate these disadvantages. This technology enables the production of designs with complex internal structures and voids, leading to less material usage and reduced post-processing requirements. Furthermore, the critical role of plasma atomization in producing titanium powders necessary for the additive manufacturing process is highlighted. This method precisely controls the particle size and morphology of powders, producing high-purity powders ideal for additive manufacturing. The control of atmospheric conditions using inert gases and the prevention of oxidation are critical steps in this process. In conclusion, this study thoroughly examines the value of titanium in engineering and the effectiveness of plasma atomization in powder production, highlighting the potential of additive manufacturing to reduce the disadvantages of titanium.

REFERENCES

[1] GE Additive, “Powders Overview.” Accessed: Dec. 24, 2023. [Online]. Available: https://www.ge.com/additive/powders-overview

[2] EOS, “Titanium for Industrial 3D Printing.” Accessed: Dec. 25, 2023. [Online]. Available: https://www.eos.info/en/3d-printing-materials/metals/titanium-ti64-ticp

[3] Advanced Powders, “Specialist in powder solutions for additive manufacturing,” 2018.

[4] EOS, “EOS M 400-4 - Ultra Fast 3D Printing.” Accessed: Dec. 25, 2023. [Online]. Available: https://www.eos.info/en/industrial-3d-printer/metal/eos-m-400-4

[5] GE Additive, “What is Additive Manufacturing.” Accessed: Dec. 25, 2023. [Online]. Available: https://www.ge.com/additive/additive-manufacturing

[6] nTop, “Implicit modeling for engineering design.” Accessed: Aug. 20, 2023. [Online]. Available: https://www.ntop.com/resources/blog/implicit-modeling-for-mechanical-design/

[7] nTopology, “How implicits succeed where B-reps fail.” Accessed: Jan. 30, 2023. [Online]. Available: https://ntopology.com/blog/how-implicits-succeed-where-b-reps-fail/

[8] B. Becergen, M. Çakmak, M. F. Maral, A. Dayanç, and F. Karakoç, “Design Approaches on Inner Bodies of Gears with Methods Topology Optimization and Lattice Structures,” *Temmuz 2022 European Journal of Science and Technology Special Issue*, vol. 39, no. 39, pp. 85–90, 2022, doi: 10.31590/ejosat.1144818.

[9] nTopology, “Next-gen topology optimization software.” Accessed: Dec. 24, 2023. [Online]. Available: https://www.ntop.com/software/capabilities/topology-optimization/

[10] nTop, “The most advanced lattice generation software.” Accessed: Dec. 17, 2023. [Online]. Available: https://www.ntop.com/software/capabilities/lattice-structures/

[11] Dassault Systemes, “SIMP Method for Topology Optimization.” Accessed: Dec. 24, 2023. [Online]. Available: https://help.solidworks.com/2021/english/SolidWorks/cworks/c_simp_method_topology.htm

[12] nTop, “Field Optimization.” Accessed: Dec. 24, 2023. [Online]. Available: https://www.ntop.com/software/capabilities/field-optimization/

[13] nTopology, “Field-driven design.” Accessed: Aug. 20, 2023. [Online]. Available: https://www.ntop.com/field-driven-design/

[14] nTopology, “How to run a static analysis – nTop.” Accessed: Aug. 20, 2023. [Online]. Available: https://support.ntop.com/hc/en-us/articles/360038372754

[15] Jabil, “What is Design for Additive Manufacturing?” Accessed: Dec. 25, 2023.

[Online]. Available: https://www.jabil.com/blog/design-for-additive-manufacturing.html

[16] nTopology, “Design for additive manufacturing: 3 levels of DfAM.” Accessed: Dec. 25, 2023. [Online]. Available: https://www.ntop.com/resources/blog/what-is-design-for-additive-manufacturing/

[17] EOS, “EOS Titanium Ti64 Grade 23 Material Data Sheet Metal Solutions,” 2023.

[18] A. DAYANÇ and F. KARAKOÇ, “Innovative Designs and Design Rules for Additive Manufacturing,” *NEW FRONTIERS IN ENGINEERING*, pp. 5–20, Nov. 2023, doi: 10.59287/nfe.884.

[19] A. DAYANÇ, M. CANLIDİNÇ, and F. KARAKOÇ, “3D-Printed Bio Applications Using Additive Manufacturing,” *INNOVATIVE RESEARCH IN ENGINEERING*, pp. 23–38, Sep. 2023, doi: 10.59287/ire.504.

[20] C. J. Tsai and L. M. Wang, “The plasma atomization process for the Ti-Al-V powder production Influence of Alloying Elements Content on High Temperature Properties of Ti-V-Cr and Ti-Al-V Series Titanium Alloys: A JMatPro Program Calculation Study Ruochen Sun and Guangbao Mi-The Effect of Thermal Hydrogenation Processing on the Oxide Layer Formation of Ti-6Al-4 V Alloy,” 2021, doi: 10.1088/1742-6596/1942/1/012046.

[21] GE Additive, “Get the facts on plasma and metal additive powders.” Accessed: Dec. 24, 2023. [Online]. Available: https://www.ge.com/additive/blog/get-facts-plasma-and-metal-additive-powders

[22] GE Additive, “Advanced plasma atomization process: How powder is made for additive manufacturing - YouTube.” Accessed: Dec. 25, 2023. [Online]. Available: https://www.youtube.com/watch?v=vouCR6bhCt0

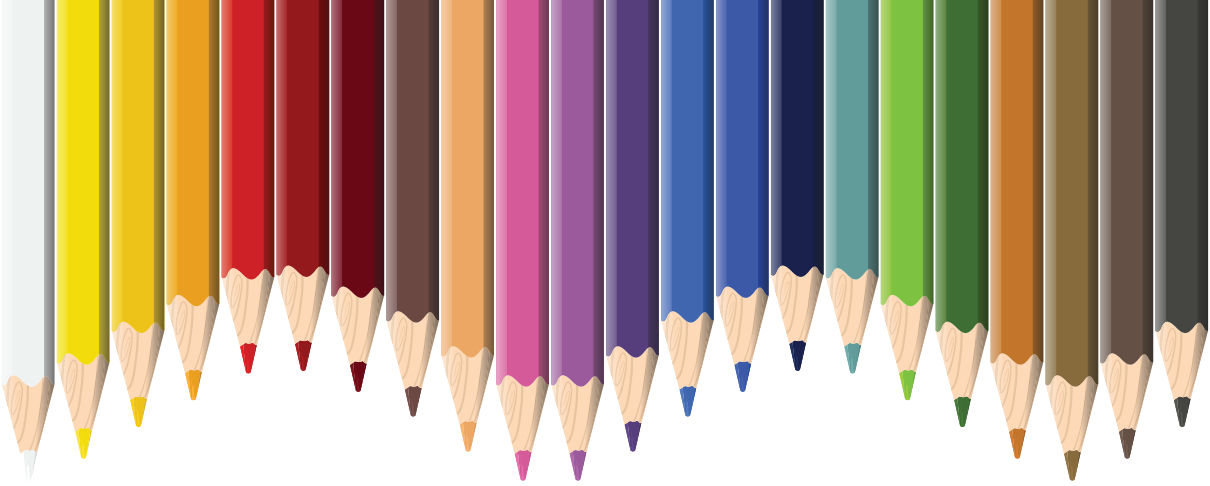

Chapter 12

TESTING METHODS OF MAGNETIC MATERIALS

Dursun EKMEKCİ[1]
Emrah KAPLAN[2]

1 Res. Assist. Dr., Gümüşhane University, Faculty of Engineering and Natural Sciences, Department of Mechanical Engineering, Gümüşhane, TURKEY, ORCID: 0000-0001-9045-7909
2 Assist. Prof. Dr., Gümüşhane University, Faculty of Engineering and Natural Sciences, Department of Electrical and Electronics Engineering, Gümüşhane, TURKEY, ORCID: 0000-0002-2350-7424

1. Introduction

This study focuses on the characterization of various materials using magnetic testing methods. The fundamental understanding of magnetic properties such as magnetic field characteristics, permeability, and reactivity of these materials is crucial in advancing technological innovations and ensuring the reliability and efficiency of devices employing these materials [1]. Non-contact magnetic testing methods serve as effective techniques for evaluating the internal structure and quality of materials. These methods are employed to identify surface defects and cracks in response to magnetic fields, determine intrinsic properties through magnetic permeability measurements, and detect different types of flaws using magnetic reactivity measurements [2]. In this study, we delve into these testing methods, which find critical applications in areas such as material quality control, reliability analysis, and durability tests in industrial settings. Non-contact magnetic material testing methods are precise techniques that can be rapidly and effectively integrated into production processes. The characteristics of these methods play a significant role in enhancing the reliability and performance of materials in the fields of material engineering and industry.

2. Magnetic Permeability Measurement

Magnetic permeability refers to how well a material transmits a magnetic field and plays a critical role in electromagnetic applications. Magnetic permeability properties of materials may vary depending on different factors. In the literature, 3Cr-1Mo-0.25 V steel has been studied with various heat treatment procedures and grain size changes, and magnetic permeability has been found to be inversely proportional to mechanical properties. Additionally, other properties such as electrical resistance and ultrasonic speed also reflected the effects of heat treatment procedures [3]. In another study, magnetic characterization of high-quality commercial steels was investigated using cut drilling and water jet technologies. This study analyzed magnetic properties such as magnetic permeability, total energy losses, coercive field and residual magnetic polarization and investigated the effect of cutting technology on these properties [4]. Moreover, techniques like decarburization annealing and cold rolling have been employed to enhance the magnetic characteristics of electrical sheet steels, with optimized grain size being linked to magnetic permeability. The impact of various processes on magnetic properties was assessed by evaluating the percentage of cold rolling in different scenarios [5]. Finally, magneto-mechanical characterization examined the magnetic behavior of the material under the plastic deformation level and applied stress. It has been observed that the magnetic behavior of the material deteriorates under plastic deformation, and this behavior is associated with internal stress and dislocation density [6]. These investigations play a crucial role in compre-

hending and enhancing the magnetic properties of materials, offering valuable insights applicable across various areas of application.

2.1. Magnetic Permeability Measurement with Magnetic Current Probe

Developments of soft magnetic materials fabricated using laser powder bed fusion (L-PBF) have been reported. Fe-49Co-2V powder was produced by gas atomization and printed in the L-PBF device. Very low porosity was achieved using optimized parameters during the process [7]. The magnetic properties of the materials were assessed through quasi-static direct current and alternating current measurements conducted at various frequencies and magnetic flux densities. Additionally, the mechanical properties were evaluated through tensile tests. The effect of heat treatment cycles on magnetic properties was investigated. Additionally, the effect of the stress state created by the cutting process of ferromagnetic cores during production on their magnetic properties was examined. Plastic deformation of the steel during the cutting process caused deterioration in magnetic properties, and releasing this deformation led to further deterioration [8]. In another study, the surface microstructure of Fe-3 wt%Si alloy was modified by surface mechanical etching and the efficiency of Si penetration was increased. This change affected the magnetic and mechanical properties, reduced core losses, especially at high frequency, and increased ductility. Additionally, magnetic field structure and magnetostriction were measured [9]. These studies provide important information regarding the production and characterization of magnetic materials, and this information can be used in applications such as energy efficiency.

2.2. Magnetic Permeability Spectroscopy

In the literature, comprising Fe powder insulated by Ni-Zn/Cu-Zn ferrite nanoparticles, soft magnetic composites were joined with boron-modified phenolic resin at varying resin-ferrite ratios and iron volume contents. The magnetic, electrical, and mechanical characteristics of these composites were examined and contrasted with samples containing iron and resin. With the effect of ferrite nanoparticles, an interaction was observed that maintains the continuity of the magnetic flow and improves the magnetic properties. Magnetic properties include differential and irreversible permeability, coercivity, power losses, and high DC bias stability. Additionally, high electrical resistivity and complex permittivity spectra are also notable features. These spectra provided stability at high frequency. In conclusion, this study shows that magnetic composites modified with ferrite nanoparticles have several important properties [10].

3. Magnetic Field Distribution Measurement

By measuring the distribution of the magnetic field on the material, it is possible to evaluate the magnetic properties of the material. Such measurements can provide information about microstructures, stresses and deformations within the material. In the literature, alternating magnetic field aging testing examined its effect on the mechanical properties of AA2219 aluminum alloy. The investigation, employing TEM analysis, Vickers hardness measurement, and mechanical tensile testing, demonstrated a notable enhancement in the microstructure and mechanical properties of the alloy through the magnetic field aging process. A conventional aging test was used as a benchmark to illustrate the impact of magnetic field aging on the material's microstructure and properties. The solid solution process was first carried out at 535°C for 35 minutes. Subsequently, the oscillating magnetic field was sustained at a temperature of 175°C, operating at a frequency of 50 Hz and an intensity of 0.5 T. The schematic diagram is shown in Figure 1 [11]. Moreover, an exploration was conducted to examine the influence of filler content and concentration on the structural, electrical, mechanical, and electromagnetic shielding effectiveness (SE) in hybrid composites consisting of epoxy, graphene, and nickel ferrite. In this study, dielectric and magnetic loss enhancement was attempted by adding magnetic nanoparticles of nickel-ferrite. Within this investigation, the influence of filler content and magnetic alignment on SE was scrutinized and deliberated upon across the frequency range of 8.2–12.4 GHz [12].

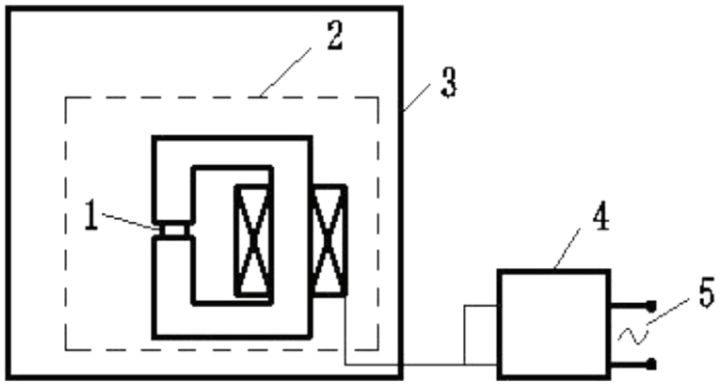

Figure 1. *Schematic diagram illustrating the stages of the magnetic field aging process used in the study of AA2219 aluminum alloy, highlighting the combination of temperature and magnetic field applications (1. test sample, 2. magnetic field generator, 3. aging oven, 4. voltage regulator, 5. AC power) [11].*

The effect of high magnetic field (HMF) on the solidified microstructure of Cu28 wt%Ag alloys was also studied. Application of HMF increased the local microhardness in pre-eutectic Cu regions as it increased the growth rate

of Ag precipitates and caused changes in Ag morphology and concentration. Additionally, HMF increased electrical resistance but decreased hardness and tensile strength [13]. As a result, there are a number of studies in the literature in which the magnetic field plays an effective role on the properties of materials and this effect is investigated using various analysis methods. The magnetic properties of the electrical steel sheet used in motor cores were affected by mechanical stress due to the adverse effect of magnetostriction [14]. Additionally, in this study, the detrimental effect of material processing steps on the magnetic, mechanical and microstructural properties of silicon alloy steel was investigated. Forming processes and mechanical tensile loads occurring during machine production with both water jet and guillotine cutting were examined. Mechanical processes such as guillotine cutting have induced internal stresses that change external magnetic material properties such as coercivity and residual induction. In comparison, waterjet cutting causes smaller residual stresses. Attention has been paid to the effect of magneto-crystalline anisotropy, that is, the effect of the cutting direction relative to the rolling direction [15]. Additionally, in this study, the synthesis of aluminum-based magnetic hybrid composites using volumetric iron nanoparticles, nickel nanoparticles and carbon nanotubes was examined. The results obtained evaluated the magnetic and mechanical properties of different compositions [16]. Ongoing progress in additive manufacturing and magnetoelectric composites has resulted in the production of materials that exhibit flexibility and are suitable for wearable electronic applications. Surprisingly, the inclusion of magnetic particles had a negligible impact on the mechanical performance of the composites, contrary to expectations based on mixing rules. Notably, the introduction of a mere 2 wt% of polyvinylidene difluoride (PVDF) significantly enhanced both the mechanical and magnetic properties of the composite samples, leading to a 25% increase in ductility and over a 160% improvement in magnetization compared to their PVDF-free counterparts [17]. Furthermore, high entropy alloys of Al_xCoFeNi and CoFeNiSi_x were synthesized, varying the mole ratios of Al and Si (x = 0, 0.25, 0.5, 0.75, and 1). Figure 2 illustrates that a high molar ratio of Al induces a transition from the FCC structure to the BCC structure, while increased Si content results in the formation of new compounds. The incorporation of both Al and Si contributes to heightened yield strength and hardness. Analysis of magnetic properties and hysteresis loops confirms the ferromagnetic behavior of these alloys. The saturation magnetization experiences a decline from 151.3 emu/g (x=0) to 101.8 emu/g (x=1) with variations in Al content and decreases from 151.3 emu/g (x=0) to 80.5 emu/g (x=0.75) with Si addition. Notably, Si addition has a more pronounced effect on reducing saturation magnetization compared to Al addition [18]. It is aimed to compress pure aluminum (Al) powder in the radial direction using the electromagnetic forming method. First, pure Al powder was placed inside the Al tube and then tightly sealed with end plugs. He created magnetic fields using

a copper solenoid coil to create Lorentz forces. These forces are achieved by high current passage through the solenoid coil and induced impulse current in the adjacent tube. The magnetic field pressure acting in the radial direction changed the shape of the Al tube, thus forming a dense Al compact. Additionally, the Archimedes principle was used to determine the density of samples sintered at various energies, and Brinell and Vickers hardness testers were used to perform hardness tests on normal sections [19]

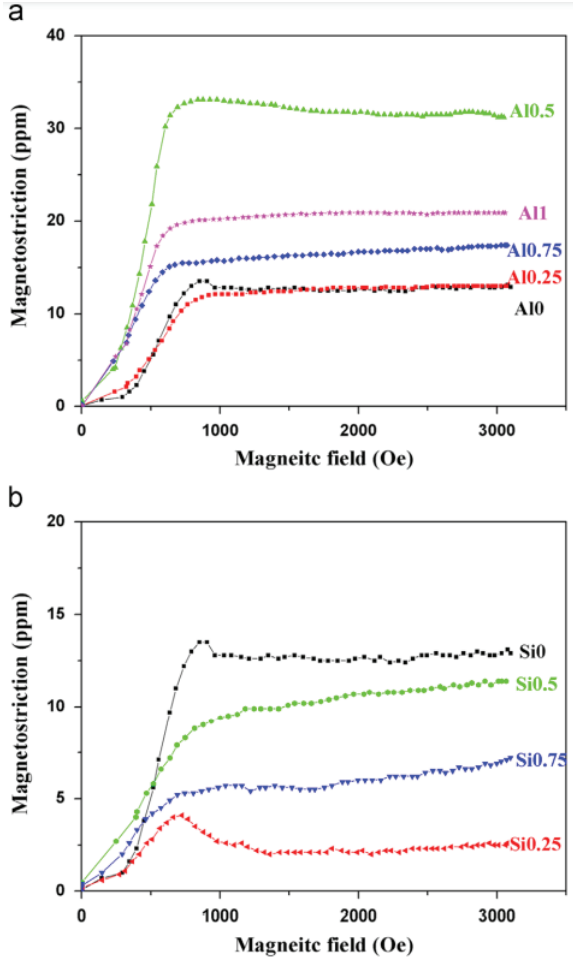

Figure 2. *Magnetostrictive curves of (a) $Al_xCoFeNi$ and (b) $CoFeNiSi_x$ alloys [18].*

The properties of nanotwinned materials have garnered significant interest across various research fields due to their numerous advantages. In this research, the origin and effects of twin defects in the nanoregime are elucidated through modeling, experiments, or both. Recent research focusing on coupling has helped better understand changes in material properties (such as

electrical, mechanical, optical and magnetic properties) and has led to metallic semiconductor materials. Hysteresis loops showing the magnetic moment of carbon-coated platinum nanoparticles in a given magnetic field at different temperatures are presented in the research [20]. As shown in Figure 3, the effects on the magnetization behavior and electrical conductivity of hybrid Ni-graphene polyimide nanocomposites in the direction of the magnetic field were examined. The in-plane tensile modulus of polyimide increased with the addition of 0.16 vol% Ni-graphene to polyimide, and the tensile strength of Ni-graphene nanocomposites was doubled compared to pure polyimide [21].

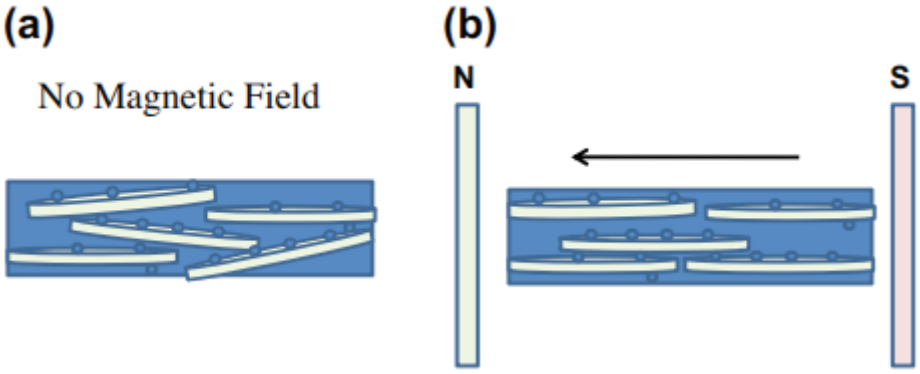

Figure 3. *Schematics of Ni-graphene orientation in polyimide film; (a) without magnetic field, (b) with magnetic field [21].*

3.1. Hall Effect Measurement

In the literature, there are experimental tests and numerical results examining reverse magnetostrictive effects on electrical steel samples. The presence of a magnetic field induces elastic deformation, and alterations in mechanical stresses result in changes to magnetic properties. Increasing mechanical stresses cause the material to contain more flux density. Additionally, numerical results helped us identify field variables at any point within and outside the sample. Hall probe was used to measure the magnetic field strength outside the sample, and the field strength was measured at several points at a distance of 2 mm, 5 mm and 20 mm from the sample, according to ASTM standard V3.04 A341. Figure 4 shows the path passing through the sample with the Hall probe. The curve was extracted to estimate the field strength in the sample [22].

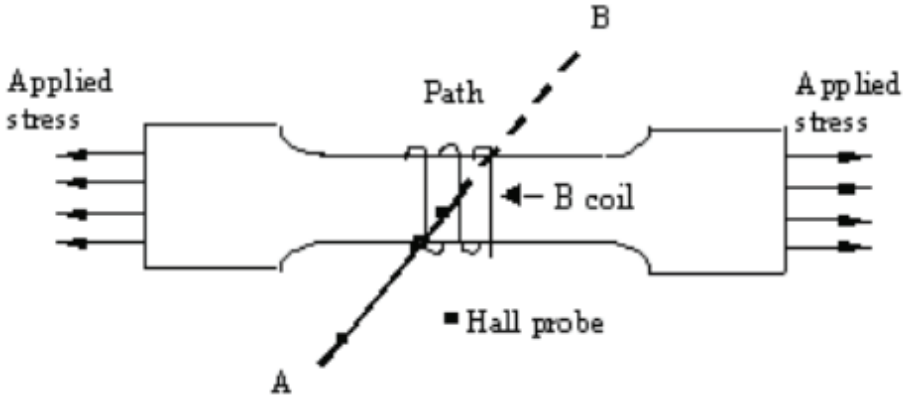

Figure 4. *The path through the sample with the Hall probe [22].*

3.2. Magnetic Field Mapping using Magnetic Field Sensors

In ferromagnetic materials, the interaction of magnetic domain walls with the microstructure occurs through dislocation mechanisms. The magnetic properties of these materials often correlate with mechanical attributes like hardness and strength, forming the foundation for micromagnetic material characterization. Given that interactions at the electron spin level are contingent upon molecular structure and dictate magnetic behavior, a similar relationship is postulated for para- and diamagnetic materials in terms of their magnetic and mechanical properties. Limited information is available regarding the mechanical properties and magnetic susceptibility of non-ferromagnetic materials like graphite, aluminum, and plastic. A magnetic sensor principle, relying on force, has been suggested for imaging susceptibility in materials of this nature. The susceptibility imaging sensor designed for paramagnetic and diamagnetic materials has been developed and validated through testing on numerous practical examples [23]. Figure 5 displays a prototype of a magnetic force sensor, which is a capacitive sensor used to measure the deflection of a cantilever bearing a sensing magnet. The cylindrical detection magnet, with dimensions of 10 mm in height and diameter, is positioned perpendicular to the magnetic field surface.

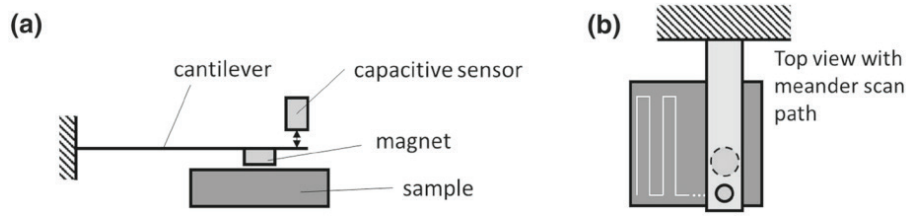

Figure 5. *Magnetic force sensor installation [23].*

In another study, an autonomous two-state MEMS sensor was proposed. This sensor achieves bistable behavior using a piezoelectric cantilever beam equipped with two oppositely magnetized permanent magnets. This beam switched between two stable equilibrium states through magnetic force due to the interaction of magnetic fields and electric current. Measurement of AC electric currents was carried out by the number of commutations of the two-state structure based on the current magnitude. This sensor is capable of harvesting its own energy and offers internal digital output [24]. In this study, the properties of biomimetic ferrogels were examined through synthesis and their mechanical, electrical and magnetic properties were comparatively analyzed. Additionally, a magnetoimpedance sensor prototype with multilayer Fe-Ni-based sensitive elements was developed [25]. The developed piezoelectric magnetostrictive smart composite consists of a distribution of single-walled carbon nanotubes and magnetostrictive Terfenol-D nanoparticles. Numerical studies examined the piezoelectric and magnetostrictive self-sensing responses of this composite, and its physical characterization was also carried out by tensile tests. In particular, it was found that increasing the volume fraction of Terfenol-D nanoparticles affected the magnetization and the optimum change was at 0.35% volume fraction [26]. Induction heating method has been developed by adding various ferromagnetic and electrically conductive particles into polymeric matrices for heating purposes. Different particle materials and frequency levels were used in the experiments, and mechanical characterization of these materials was carried out. It has been observed that the heating effect depends on the material type and frequency, and it has been determined that ferromagnetic particles such as iron and magnetite give the best results [27]. Hydrogels with reversible cross-links containing magnetite nanoparticles were developed and these hydrogels were cross-reassembled using magnetic fields. These hydrogels have been used for multifunctional biosensor applications [28]. The mechanisms and applications of shape memory polymers activated by temperature, magnetic fields and other stimuli have been examined [29].

4. Magnetic Reactivity Measurement

Magnetic reactivity measurements can be used to evaluate how the material responds when a magnetic field is applied. The magnetic properties of the material can be related to mechanical properties and deformations.

4.1. Hysteresis Curve Measurement of Ferromagnetic Materials

$Bi_2Sr_2CaCu_2Ag_xO_y$ samples with small amounts of Ag were studied and the effect of Ag was examined. The impact of Ag doping was explored through examinations involving electrical resistivity, scanning electron microscopy, X-ray diffraction (XRD), mechanical testing, and dc-magnetization

techniques. The results revealed that even a minor amount of Ag doping markedly enhanced both the physical and magnetic properties of the samples. The samples with 0.05 Ag doping exhibited the highest critical current density (Jc) values. Additionally, magnetic hysteresis loops were performed in applied external fields on all samples at 15 and 25 K [30]. Finally, the magnetoelastic effect in truss structures made of 13CrMo4-5 steel was examined. Magnetoelastic windings integrated into the beams using magnetic circuit lattice construction were used to study the internal stresses of the beams. During these magnetoelastic measurements, three element samples were placed on the beams and placed under the truss mechanical load. While the shape of the magnetic hysteresis B(H) loops was related to the strain, the force was calculated based on the magnetic induction measurement. These calculations are combined with mechanical properties to determine whether internal stresses in the beam pose a threat to the structure [31]. Also, b.c.c. Fe-Ga alloys have offered a great development in the field of magnetostriction, and magnetostriction studies have expanded further thanks to Fe alloys that do not have a certain stress limit. Ferromagnetic shape memory alloys have high energy conversion capacity as magnetomechanical sensing materials. Therefore, magnetostriction and magnetomechanical sensing research has been emphasized as being of great importance for advanced technology applications [32]. Nanocomposites offer the perfect combination of magnetic and conductive properties and can be used in a variety of applications. Additionally, modeling and examining experimental data on magnetostriction has helped to better understand the magnetomechanical properties. As shown in Figure 6, the effect of applied mechanical stresses and frequency on the magnetic hysteresis of ferromagnetic sheets has been studied with magneto-mechanical models. The results were obtained in accordance with the experimental data in the literature [33].

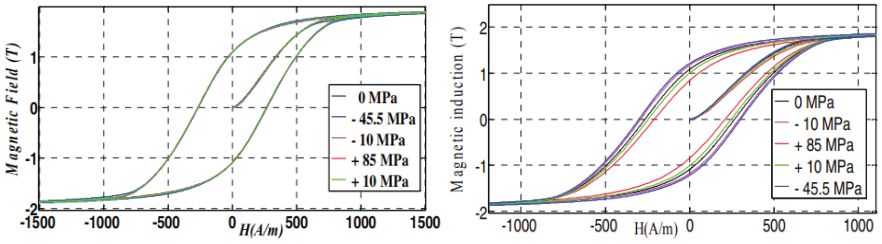

(a) *(b)*

Figure 6. *(a) Effect of mechanical stress on hysteresis loop, (b) Variation of magnetic hysteresis with mechanical stress [33].*

In another study, the synthesis of double perovskites with the general formula $A_2BB'O_6$ was studied. The magnetic, electronic, elastic and thermo-

electric properties of Ba_2NiMoO_6 were studied using density functional theory and Monte Carlo simulations. In this material, which exhibits antiferromagnetic insulator behavior, it has been found that the antiferromagnetic order is explained by superexchange processes between Ni^{2+} orbitals. While the elastic properties of the material show high mechanical stability and ductility, magnetic and magnetocaloric properties have also been investigated [34]. Furthermore, a research investigation was carried out to characterize how magnetic losses are influenced by mechanical stress. The relationship of two different magnetic loss components with mechanical stress is explained and, in particular, it is stated that two loss coefficients are defined [35]. A different scientific research contributes to the synthesis of different materials and understanding their properties. The sensitivity of ferromagnetic materials to mechanical stress is critical to the performance of electrical machines. In this study, the magnetic properties of a conventional electrical steel containing 2.4% Si were examined in terms of the effect of tensile and compressive stress. The relationship between anisotropy and mechanical stress was determined, and hysteresis loops were shown comparatively at 0°, 45° and 90° angles, 50 Hz and 1.0 T, with 50 MPa and 100 MPa tensile loading [36]. In another study, nanocomposites were produced using magnetic hexaferrite nanoparticles and epoxy resins, and the morphological, thermomechanical and dielectric properties of these nanocomposites were examined in detail. The data showed that the electrical and mechanical properties of the nanocomposites improved with the distribution of nanoinclusions and increasing filler concentration, proving that these materials have ferromagnetic properties at room temperature. Additionally, the magnetic hysteresis loops of $BaFe_{12}O_{19}$ and $SrFe_{12}O_{19}$ nanoparticles were also examined [37]. In conclusion, this research is also focused on the development of gel-based magnetic materials for biomedical applications. Ferrogels were produced in a suspension in which γ-$Fe_{2.04}O_{2.96}$ nanoparticles were synthesized by radical polymerization of acrylamide. The gel network density and NP concentration were adjusted, and mechanical and electrical properties were observed to improve with the addition of a small amount of NPs. Additionally, it has been stated that it has positive effects on the biocompatibility of the NP polymer network [38]. Another study focusing on the development of mother-of-pearl-like composites is discussed. The use of iron as the "mortar" phase has enabled the production of composites with high fracture toughness and hardness combined with magnetic, electrical and thermal properties. These metal-ceramic composites were prepared by applying iron coatings to alumina wafers and then assembling them by magnetic excitation. Since magnetic hysteresis losses are low and saturation magnetization is high, it was evaluated as a function of the applied field [39]. Finally, another study was mentioned in which the preparation of BSCCO ceramic superconductors and their structural, magnetic, electrical and mechanical properties were examined. This study focused on the preparation methods and measurement

results of the samples and examined their effects on many properties. For example, Vickers microhardness measurements were correlated with the indentation dimensions of the samples and mechanical properties were calculated [40].

4.2. Magnetic Reactivity Measurement using Magnetic Flow Probe

In a study characterizing the electrical and mechanical properties of a silicone membrane electromagnetic microactuator, the effect of the geometry and structure of the actuator system on the actuator performance of a liquid-injected silicone-based membrane was examined. It has been found that the height of the magnetic force produced increases significantly with the applied power [41]. Another study, which examined the magnetic behavior of electrical steel in detail in terms of mechanical stress, direction of the magnetic field, excitation frequency and cutting edge effects, focused on the comparison of magnetic properties with mechanical properties. In this study, material properties of a soft magnetic nature that depend on external factors were extracted from magnetic measurement data. These properties were then employed in the simulation of a synchronous machine designed for the traction drive of an electric vehicle, utilizing finite element simulations. The height of the magnetic flux density increased with the amount of applied current, and the maximum of the flux indicated anisotropy in the 60°–70° direction [42]. Finally, a study using a magnetic fork probe non-destructively measured the magnetic properties of ferromagnetic materials, as shown in Figure 7. The magnetic properties measured by this probe were compared with the mechanical properties and a good correlation was found [43].

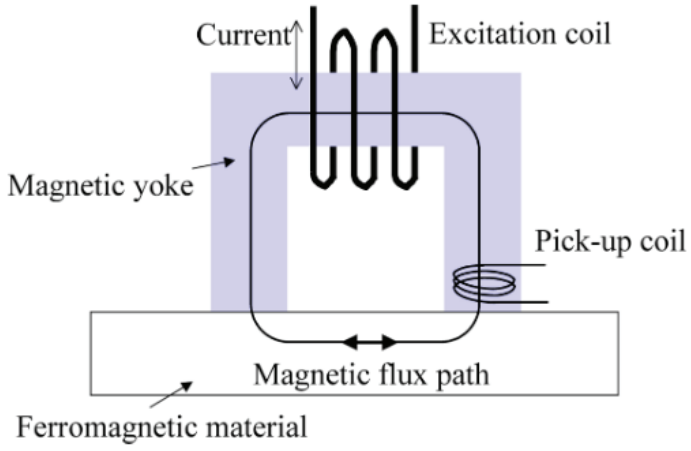

Figure 7. *Illustration of the magnetic fork probe setup used for non-destructive measurement of ferromagnetic materials' magnetic properties, demonstrating the correlation with their mechanical properties [43].*

Electromagnetic stresses occur in motor cores due to the magnetostrictive effect of silicon steel and the electromagnetic force between the stator and rotor. In this context, an electromagneto-mechanical coupled numerical model is proposed and the stress distribution of the motor cores is calculated [44]. The effect of plastic mechanical stresses that may occur on the magnetic core during the production of electrical machines on their magnetic properties may deteriorate the performance of magnetic materials. Therefore, an approach to reduce plastic mechanical stresses by generating highly localized heterogeneous deformations is proposed to maintain magnetic core performance. Non-directional FeSi (1.3%) electrical steel was characterized and the relationship between magnetic properties and mechanical deformations was examined [45]. Moreover, in the study of modeling the multi-axial mechanical stress effect of M400-50A quality unoriented silicone sheet, the stress dependence of magnetic losses was examined and a model was developed using statistical loss theory. This study has helped us understand the change of magnetic properties under mechanical stress [46].

5. Conclusion

Magnetic field, permeability, and reactivity measurements are foundational in non-contact magnetic material testing. They offer a thorough method to study materials' internal structures and detect flaws. Magnetic field tests pinpoint surface defects by applying a magnetic field to the material, allowing early identification of surface issues like cracks and holes in metal manufacturing. This enhances quality control and mitigates expensive mistakes. Magnetic permeability measurements assess a material's magnetic characteristics by its response to a magnetic field. This approach reliably reveals the material's internal structure and magnetic properties, crucial for quality evaluation. It's key in characterizing magnetically responsive materials, used in devices like electric machines and transformers. Magnetic reactivity measurements detect various defect types by observing material behavior in a magnetic field. This method aids in understanding materials' magnetic responses, vital in product design and industrial applications. Non-contact magnetic testing methods, due to their non-invasive nature, quick application, and precise defect detection, are essential in modern manufacturing and materials engineering. These methods offer detailed insights into the mechanical property evaluation process.

REFERENCES

[1] Xu, Y., Xu, K., Wang, H., Zhao, L., Tian, J., Xie, Y., & Liu, J. (2023). Research progress on magnetic memory nondestructive testing. Journal of Magnetism and Magnetic Materials, 565, 170245.

[2] Wang, Z., Fei, Y., Ye, P., Qiu, F., Tian, G., & Woo, W.L. (2020). Crack characterization in ferromagnetic steels by pulsed eddy current technique based on GA-BP neural network model. Journal of Magnetism and Magnetic Materials, 500, 166412.

[3] Nam, Y.H., & Nahm, S.H. (2013). Evaluation of material properties of 3Cr-1Mo-0.25V steel by magnetic, electrical and elastic properties. Metals and Materials International, 19, 1215-1220.

[4] Paltanea, G., Paltanea, V.M., Gavrila, H., Nicolaide, A., & Dumitrescu, B. (2016). Comparison between magnetic industrial frequency properties of non-oriented FeSi alloys, cut by mechanical and water jet technologies. Revue Roumaine Des Sciences Techniques, 61, 26–31.

[5] Ramadan, R., Ibrahim, S.A., Farag, M., Elzatahry, A.A. & Es-Saheb, M.H. (2012). Processing optimization and characterization of magnetic non-oriented electrical silicon steel. International Journal of Electrochemical Science, 7, 3242-3251.

[6] Domenjoud, M., & Daniel, L. (2023). Effects of plastic strain and reloading stress on the magneto-mechanical behavior of electrical steels: Experiments and modelling. Mechanics of Materials, 176, 104510

[7] Riipinen, T., Metsä-Kortelainen, S., Lindroos, T., Keränen, J.S., Manninen, A., & Pippuri-Mäkeläinen, J. (2019). Properties of soft magnetic Fe-Co-V alloy produced by laser powder bed fusion. Rapid Prototyping Journal, 25, 699-707.

[8] Daem, A., Sergeant, P., Dupré, L., Chaudhuri, S., Bliznuk, V., & Kestens, L. (2020). Magnetic properties of silicon steel after plastic deformation. Materials, 13, 4361.

[9] Yu, H., & Bi, X. (2018). Surface modification and its role in the preparation of FeSi gradient alloys with good magnetic property and ductility. Journal of Magnetism and Magnetic Materials, 451, 373-378.

[10] Bircakova, Z., Füzer, J., Kollar, P., Szabo, J., Jakubcin, M., Streckova, M., Bures, R., & Faberova, M. (2020). Preparation and characterization of iron-based soft magnetic composites with resin bonded nano-ferrite insulation. Journal of Alloys and Compounds, 828, 154416.

[11] Liu, Y.Z., Zhan, L.H., Ma, Q.Q., Ma, Z.Y., & Huang, M.H. (2015). Effects of alternating magnetic field aged on microstructure and mechanical properties of AA2219 aluminum alloy. Journal of Alloys and Compounds, 647, 644-647.

[12] Manobalan, S., Mahender, C., Rajan Babu, D., Rahaman, A., Sreekanth, M.S., Sharma, D., Bose, S., & Sumangala, T.P. (2022). The mechanical, dielectric, and EMI shielding properties of nickel Ferrite (NiF) / Graphene (Gr) - doped epoxy

composites. Journal of Inorganic and Organometallic Polymers and Materials, 32, 4077-4091.

[13] Zuo, X., Han, K., Zhao, C., Niu, R., & Wang, E. (2014). Microstructure and properties of nanostructured Cu28 wt%Ag microcomposite deformed after solidifying under a high magnetic field. Materials Science and Engineering: A, 619, 319-327.

[14] Elgamli, E., & Anayi, F. (2023). Advancements in electrical steels: A comprehensive review of microstructure, loss analysis, magnetic properties, alloying elements, and the influence of coatings. Applied Sciences, 13, 10283.

[15] Leuning, N., Steentjes, S., Hameyer, K., Schulte, M., & Bleck, W. (2016). Effect of material processing and imposed mechanical stress on the magnetic, mechanical, and microstructural properties of high-silicon electrical steel. Steel Research International, 87, 1638-1647.

[16] Tugirumubano, A., Go, S.H., Shin, H.J., Joseph, V.S., Kwac, L.K., Kim, H.G. (2021). Magnetic and mechanical characterization of Al-MWCNT-Fe-Ni hybrid metal matrix composites. Materials Science and Engineering: B, 266, 115045.

[17] Malley, S., Newacheck, S., & Youssef, G. (2021). Additively manufactured multifunctional materials with magnetoelectric properties. Additive Manufacturing, 47, 102239.

[18] Zuo, T.T., Li, R.B., Ren, X.J., & Zhang, Y. (2014). Effects of Al and Si addition on the structure and properties of CoFeNi equal atomic ratio alloy. Journal of Magnetism and Magnetic Materials, 371, 60-68.

[19] Thirupathi, N., Kumar, R., & Kore, S.D. (2022). Effect of electromagnetic force on the strength of electromagnetic impulse powder compaction. Journal of Materials Engineering and Performance, 31, 10021-10034.

[20] Uttam, P., Kumar, V., Kim, K.H., & Deep, A. (2020). Nanotwinning: Generation, properties, and application. Materials & Design, 192, 108752.

[21] Yoonessi, M., Gaier, J.R., Peck, J.A., & Meador, M.A. (2015). Controlled direction of electrical and mechanical properties in nickel tethered graphene polyimide nanocomposites using magnetic field. Carbon, 84, 375-382.

[22] Mohammed, O.A., Ganu, S.C., & Liu, S. (2004). Numerical analysis of magnetostrictive effects in an electrical steel sample including experimental testing. IEEE SoutheastCon Proc, 428-432.

[23] Gupta, B., & Szielasko, K. (2016). Magnetic sensor principle for susceptibility imaging of para- and diamagnetic materials. Journal of Nondestructive Evaluation, 35, 41.

[24] Andò, B., Baglio, S., L'Episcopo, G., Maiorca, F., & Trigona, C. (2013). Autonomous bistable microsensors for noninvasive AC electrical current measurements. IEEE Instrum Meas Technol Conf, 13662561.

[25] Blyakhman, F.A., Buznikov, N.A., Sklyar, T.F., Safronov, A.P., Golubeva, E.V.,

Svalov, A.V., Sokolov, S.Y., Melnikov, G.Y., Orue, I., & Kurlyandskaya, G.V. (2018). Mechanical, electrical and magnetic properties of ferrogels with embedded iron oxide nanoparticles obtained by laser target evaporation: Focus on multifunctional biosensor applications. Sensors, 18, 872.

[26] Qhobosheane, R.G., Elenchezhian, M.R.P., Das, P.P., Rahman, M., Rabby, M.M., Vadlamudi, V., Reifsnider, K., & Raihan, R. (2020). Smart self-sensing composite: Piezoelectric and magnetostrictive FEA modeling and experimental characterization using wireless detection systems. Sensors, 20, 6906.

[27] Bayerl, T., Schledjewski, R., & Mitschang, P. (2012). Induction heating of thermoplastic materials by particulate heating promoters. Polymers and Polymer Composites, 20, 333-342.

[28] Puiggalí-Jou, A., Babeli, I., Roa, J.J., Zoppe, J.O., Garcia-Amorós, J., Ginebra, M.P., Alemán, C., & García-Torres, J. (2021). Remote spatiotemporal control of a magnetic and electroconductive hydrogel network via magnetic fields for soft electronic applications. ACS Applied Materials & Interfaces, 13, 42486-42501.

[29] Li, J., Duan, Q., Zhang, E., & Wang, J. (2018). Applications of shape memory polymers in kinetic buildings. Advances in Materials Science and Engineering, 2018, 7453698.

[30] Özkurt, B., Madre, M.A., Sotelo, A., & Diez, J.C. (2013). Effect of metallic Ag on the properties of Bi-2212 ceramic superconductors. Journal of Materials Science: Materials in Electronics, 24, 3344-3351.

[31] Jackiewicz, D., Szewczyk, R., & Bieńkowski, A. (2015). Utilizing magnetoelastic effect to monitor the stress in the steel truss structures. Journal of Electrical Engineering, 66, 178-181.

[32] Nisar, M., Bernd, M.G.S., Filho, L.C.P.S., Geshev, J., Basso, N.R.S., & Galland, G.B. (2018). Polypropylene nanocomposites with electrical and magnetic properties. Journal of Applied Polymer Science, 135, 46820.

[33] Malika, Y., Sebti, B., & Adel, B. (2018). A theoretical characterization of the coupling effects of frequency and mechanical stresses on the magnetic properties of the ferromagnetic material. International Conference on Communications and Electrical Engineering, 18434931.

[34] Harbi, A., Azouaoui, A., Toual, Y., Hourmatallah, A., & Moutaabbid, M. (2023). Synthesis, characterization, and magnetocaloric properties of double perovskite $BaSrNiMoO_6$ for magnetic refrigeration applications. Journal of Superconductivity and Novel Magnetism, 36, 1171-1179.

[35] Baghel, A.P.S., Blumenfeld, J.B., Santandrea, L., Krebs, G., & Daniel, L. (2019). Effect of mechanical stress on different core loss components along orthogonal directions in electrical steels. Electrical Engineering, 101, 845-853.

[36] Leuning, N., Steentjes, S., & Hameyer, K. (2017). Effect of magnetic anisotropy on Villari effect in non-oriented FeSi electrical steel. International Journal of Applied Electromagnetics and Mechanics, 55, S23-S31.

[37] Sanida, A., Stavropoulos, S.G., Speliotis, T., & Psarras, G.C. (2018). Magnetic nanoparticles – polymer matrix nanodielectrics: Manufacturing, characterization and functionality. Materials Today: Proceedings, 5, 27491-27499.

[38] Blyakhman, F.A., Safronov, A.P., Zubarev, A.Y., Shklyar, T.F., Makeyev, O.G., Makarova, E.B., Melekhin, V.V., Larrañaga, A., & Kurlyandskaya, GV. (2017). Polyacrylamide ferrogels with embedded maghemite nanoparticles for biomedical engineering. Results in Physics, 7, 3624-3633.

[39] Poloni, E., Bouville, F., Dreimol, C.H., Niebel, T.P., Weber, T., Biedermann, A.R., Hirt, A.M., & Studart, A.R. (2021). Tough metal-ceramic composites with multifunctional nacre-like architecture. Scientific Reports, 11, 1621.

[40] Safran, S., Ozturk, H., Bulut, F., & Ozturk, O. (2018). Experimental and theoretical approaches for electrical, magnetic, micromechanical, and structural characterization of BSCCO ceramic superconductors. Ceramics International, 44, 11674-11681.

[41] Yunas, J., Pawinanto, R.E., Indah, N., Alva, S., & Sebayang D. (2018). The electrical and mechanical characterization of silicon based electromagnetic micro-actuator for fluid injection system. Journal of Engineering Science and Technology, 13, 2606-2615.

[42] Xiao, X., Müller, F., Bavendiek, G., Leuning, N., Zhang, P., Zou, J., & Hameyer, K. (2020). Modeling of scalar dependencies of soft magnetic material magnetization for electrical machine finite-element simulation. IEEE Trans Magn, 56, 7505704.

[43] Kikuchi, H., Liu, T., Ara, K., Kamada, Y., Kobayashi, S., & Takahashi, S. (2008). A magnetic yoke probe for in situ magnetic measurements. Electrical Engineering in Japan, 165, 1-7.

[44] Tong, B., Qingxin, Y., Rongge, Y., & Lihua, Z. (2017). Stress analysis of motor cores based on the measurement of magnetostriction of nonoriented silicon steel sheet. IEEE 20th Int Conf Electr Mach Syst, 17225420.

[45] Youssef, M.E., Clenet, S., Gorp, A.V., Benabou, A., Faverolle, P., Mipo, J.C. (2021). Improving global ferromagnetic characteristics of laminations by heterogeneous deformation. IEEE Trans Energy Convers, 36, 1953-1961.

[46] Aydin, U., Rasilo, P., Martin, F., Belahcen, A., Daniel, L., & Arkkio, A. (2020). Modeling of multi-axial stress dependent iron losses in electrical steel sheets. Journal of Magnetism and Magnetic Materials, 504, 166612.

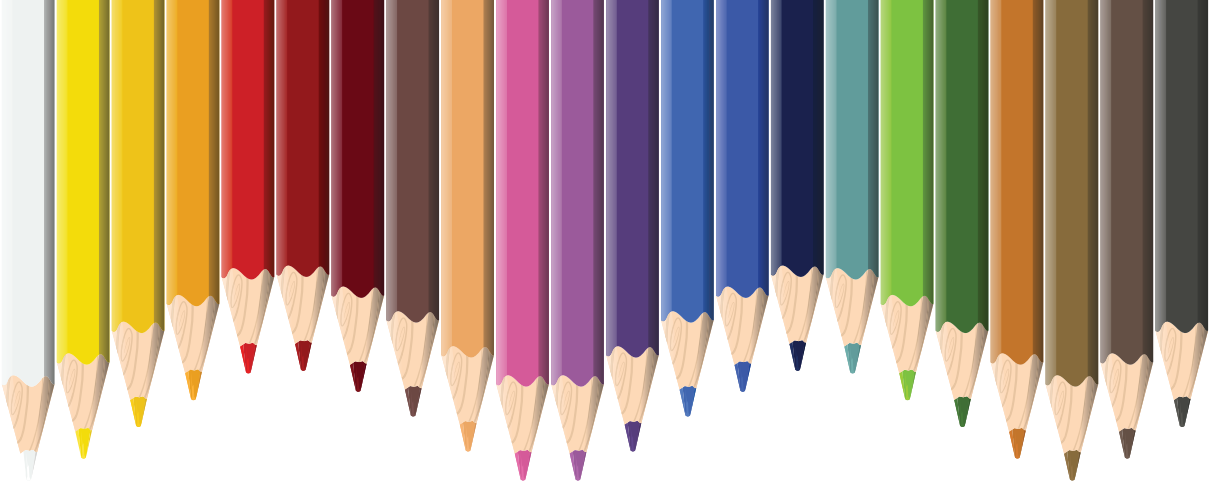

Chapter 13

ZINC-ALUMINUM BASED METAL MATRIX COMPOSITES

Mustafa GÜLEŞEN[1]
Osman Selim KİBAR[2]

1 Assit. Prof. Dr.,Kütahya Dumlupınar University, Mechanical Engineering Departmant mustafa.gulesen@dpu.edu.tr - 0000-0001-8781-2746
2 Senior Mechanical Engineer, Kütahya Health Sciences University, Constraction and Technical Works Departmant, osmanselim.kibar@ksbu.edu.tr 0000-0002-8452-1406

1. INTRODUCTION

In recent years, the usage areas of zinc aluminum alloys have been increasing for many reasons such as mechanical, physical properties and low production costs. With the increasing demand and developing technologies, it is desired to be able to respond to the needs, improve the existing features and reduce the production cost. Zinc aluminum alloys are used in many areas such as automotive and decoration. It is seen that zinc aluminum alloys are generally produced by methods such as casting, extrusion and forging. However, the increased use of composite materials in recent years has brought the powder metallurgy method to the fore. With the powder metallurgy method, it is possible to obtain composite materials with various compositions by mixing powders in different combinations homogeneously.

In this study, a compilation of studies on how the mechanical properties, microstructures, corrosion resistance, wear behavior of the products obtained by mechanical alloying and various reinforcements, which are among the powder metallurgy methods of zinc-aluminum-based metal matrix composites in recent years, are affected and the optimum parameters are determined, has been prepared. The fact that metal matrix composites have mechanical properties such as high wear resistance, tensile strength, corrosion resistance and high strength attracts the attention of many researchers. In the casting method, the powder metallurgy method comes to the fore due to its disadvantages such as insufficient particle distribution during melting, sedimentation rate and gas compression. The simplicity of adjusting the ratios of the elements used by mechanical alloying, which is one of the powder metallurgy methods, makes it stand out as an alternative to the casting method in terms of production costs.

Zamak, which is a zinc aluminum alloy; It is an alloy containing zinc, aluminum, magnesium and copper. Zamak alloy highlights many mechanical and physical properties such as corrosion resistance, wear resistance, low melting point, high strength and conductivity. At the same time, features such as low cutting force and good surface quality, which are the features needed in machining, are also important features of zinc aluminum alloys.

Zamak alloys can be produced by various production methods such as casting, extrusion and forging. Products made from this alloy are used in many areas. The main ones are in many areas such as printing machines, household appliances, automotive industry, door handles, ornaments, door locks, pipes and clamps where corrosion resistance is required. The fact that the alloy is used in so many areas causes many ways to be sought to reduce costs in production. One of the most sought-after features is that products made of alloy are suitable for mass production. For this reason, many studies focus on the suitability of this alloy for mass production.

Powder metallurgy is the technology of turning metals or alloys into

powder using physical or chemical methods and shaping them using various methods. It is preferred in many areas because the structures of the parts produced in powder metallurgy are under control, highly homogeneous structure formation and suitability for mass production. Complex shaped parts can be produced in powder metallurgy, and the need for machining after shaping is minimal. Powder production can be done by choosing one of the mechanical, electrolysis, chemical and atomization methods.

Mechanical alloying is a method that enables the production of powdered elements or alloys by mixing them using various methods. The process is based on the mixing of various amounts of powders and their deformation by colliding with each other during this mixing. This method is suitable for obtaining particle reinforced metal matrix composite products. Composite material contains two or more components. Metal matrix composite material is obtained by mixing the reinforcement material into the metal matrix (Cambronero et al, 2003, Suryanarayana, 2001.,Thummler, Oberacker, 1994., Tarralba et al, 2002., Sankar, Singh, 1998., Sudha et al, 2020).

This review study includes studies on how the reinforcement materials used in metal matrix composites of zinc aluminum based alloys affect their microstructure, mechanical and corrosion behavior.

2. EXPERIMENTAL STUDIES

In the study conducted by Ataç and Güral, research was conducted on ZA-8, ZA-12 and ZA-27, which are zinc aluminum alloys. Within the scope of this study, the producibility of alloys was investigated using the mechanical alloying method, which is one of the powder metallurgy methods. Mechanical alloying was carried out for 1, 3, 5 and 8 hours. Since the powders tend to stick together and grow after the 4th hour, the optimum alloying time was determined as 4 hours. It has been determined that in the absence of lubricant during mechanical alloying, powder grains show brittleness without flaking. It has been observed that these crushed powders later combine to form structures of various shapes and sizes. The images of the elements before mechanical alloying are given in Figure 1, and the images after alloying are given in Figure 2. Changes in grain sizes were observed as the mechanical alloying time changed. After the powders were examined under an electron scanning microscope, they were subjected to hot pressing at 625 MPa pressure and 320 ºC. The sintering process was carried out at 320 ºC and Sem and EDS analyzes were performed. In the alloy analysis, it was seen that the Al ratio was higher than the Cu percentage. It is thought that this situation is caused by some powders adhering to the grinding device chamber walls. Oxidations were detected on Al and Zn. The density value of all alloys after pressing was higher than after sintering. The reason for this is thought to be the volume increase in the size of the alloys with temperature (Ataç and Güral, 2013) .

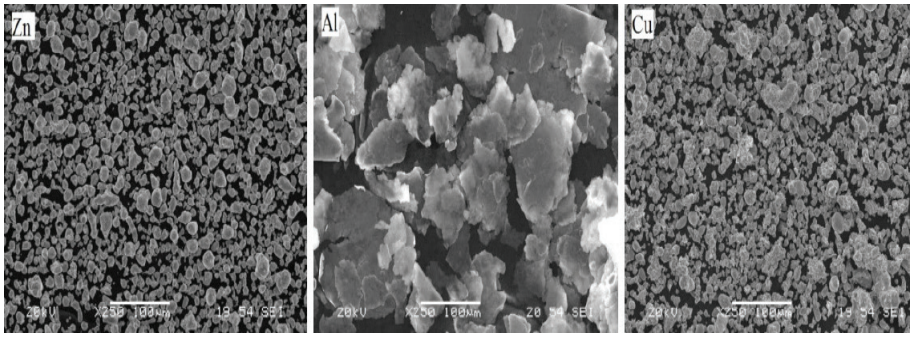

Figure 1. Zn, Al and Cu powder images before alloying (Ataç and Güral, 2013)

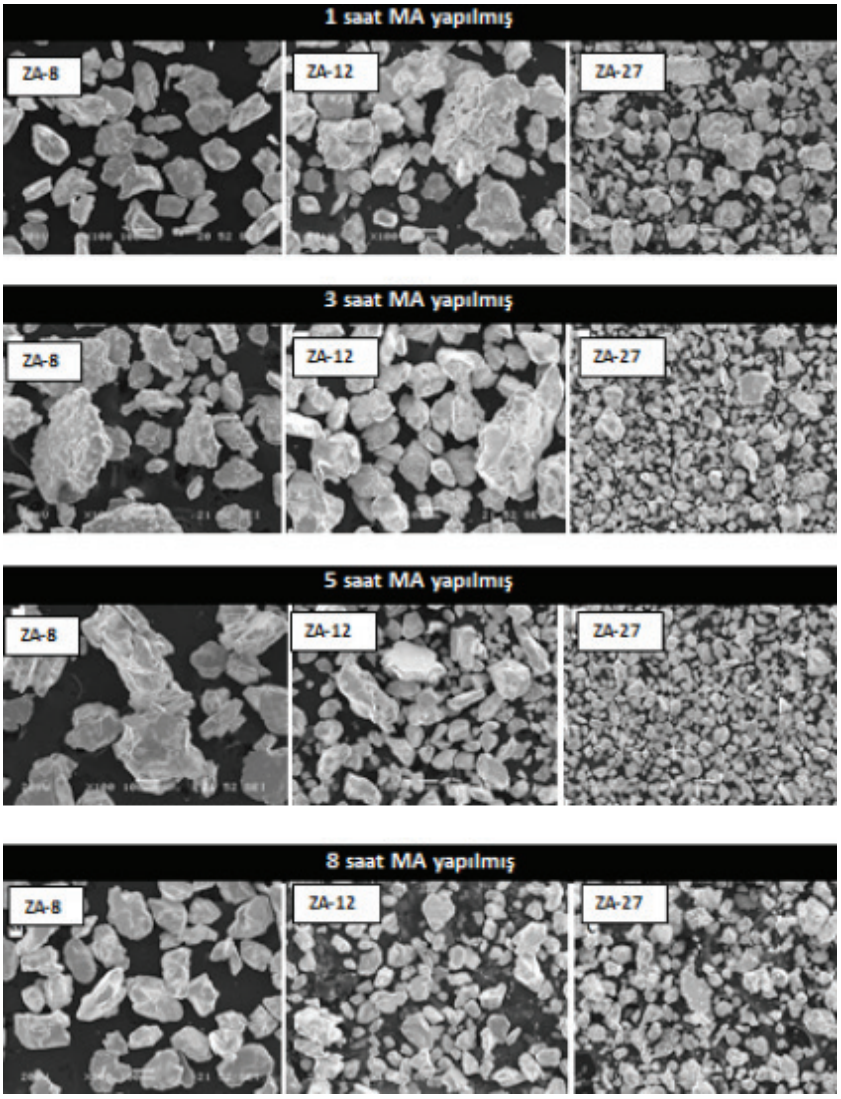

Figure 2. Images of ZA powders after alloying (Ataç and Güral, 2013)

In the study carried out by Yalçın and Çanakçı, a nanocomposite material was produced by combining ZA-27 matrix alloy and graphene nanosheet using the powder metallurgy method. Graphene is a product that attracts attention due to its mechanical, thermal and electrical properties. The powder mixture was made with nanoplate reinforcement as 0%, 1%, 2% and 3%. The mixtures were subjected to mechanical alloying process with the help of a ball mill. Then they were compressed with 500MPa at 435 ºC. Compression was done by hot pressing method for 3 hours. In the study, the internal structure and corrosion behavior of the produced products were investigated. As seen in Figure 3, ZA-27 powder before mechanical alloying is irregular and ligament-shaped. Graphene powders appear in the form of sheets (Yalçın and Çanakçı, 2018).

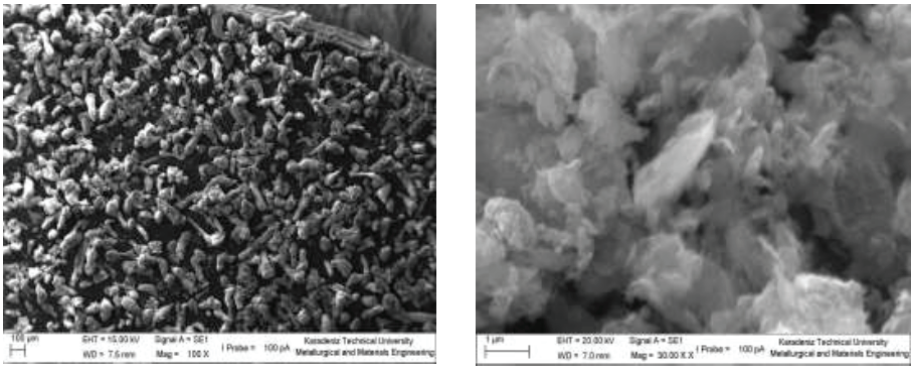

Figure 3. Images of ZA-27 and graphene powder before mechanical alloying (Yalçın and Çanakçı, 2018)

The mechanical alloying process was carried out at 400 rpm for 15 minutes. Homogeneous distribution of components is of great importance in composite materials. As seen in Figure 4, although there is accumulation in some areas, there appears to be a homogeneous distribution in general.

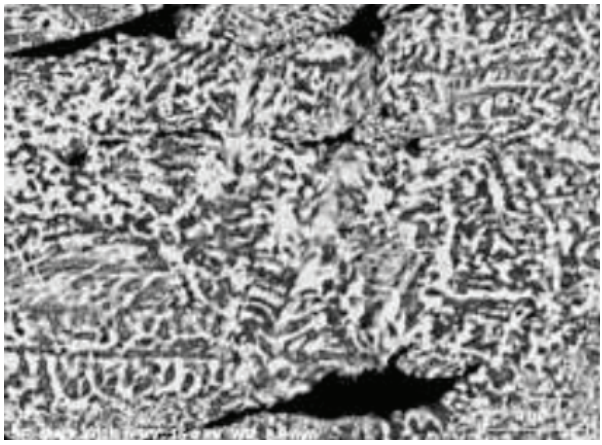

Figure 4. SEM image of ZA-27 3% graphene nanosheet composite (Yalçın and Çanakçı, 2018)

Considering the general results of the study, it was seen that the ZA-27 nanocomposite was produced successfully, the graphene distribution in the composite was homogeneous, and the amount of corrosion decreased with the increase in the amount of graphene nanosheets (Yalçın and Çanakçı, 2018).

In another study by Yalçın and Çanakçı, research was conducted on the alloying of ZA-40 alloy, which is a zinc aluminum alloy, with silicon carbide. Within the scope of this research, ZA-40 and SiC composites were produced using the powder metallurgy method. SiC additives were added to ZA-40 at various rates (0-0.5-1-1.5-2%). Mechanical alloying time was chosen as 2 hours. Hot pressing method was chosen for compression. Pressing was done at 600 MPa and 500 ºC. The obtained samples were taken to the wear test device and traveled 100 meters. In the study where 2 different loads (10N and 20N) were used, the wear resistance, weight loss and friction coefficient of the samples were calculated. In addition, SEM images of the samples were evaluated. In the samples obtained, an increase in the amount of porosity and a decrease in hardness were observed as the amount of SiC additive increased. The wear behavior of the samples was less than that of the pure state in both loads. Here, it is thought that the lubrication feature of SiC is the reason for this. As for the wear behavior of the products, with the increase in the amount of SiC, the wear mechanism changed from abrasive to adhesive, as shown in Figure 5 and Figure 6 (Yalçın and Çanakçı, 2022).

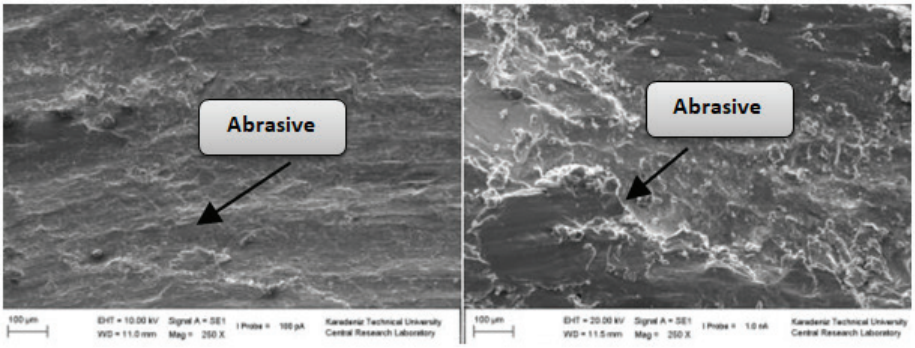

Figure 5. SEM image of wear surfaces (SiC 0%) (Yalçın and Çanakçı, 2022)

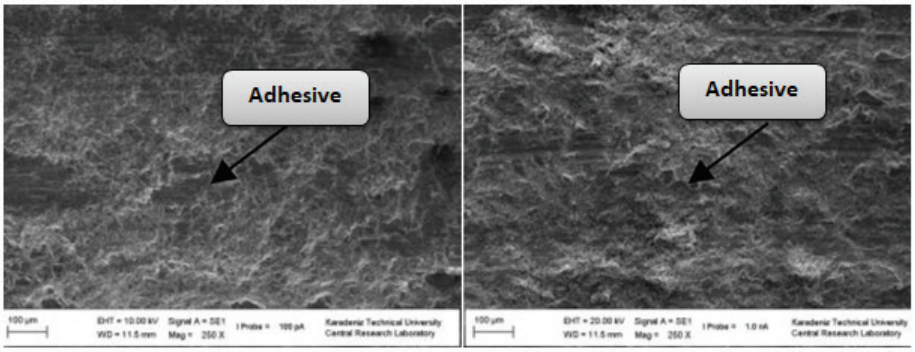

Figure 6. SEM image of wear surfaces (SiC 2%) (Yalçın and Çanakçı, 2022)

As a result of the study, it was seen that the ideal time for the mechanical alloying time of ZA-40 with SiC additive was 2 hours. With the increase in the amount of SiC, porosity increased and hardness decreased. As the load increases, the weight loss increases due to wear (Yalçın and Çanakçı, 2022).

In Azizi and Haghigi's research, zamak-2 alloy, which is a zinc-aluminum alloy and stands out with its properties such as self-lubrication and sound dampening, was examined. In this study, the mechanical properties of zamak-2 produced by powder metallurgy were examined. The produced powders were pressed with 500, 400 and 350 MPa pressure. Then, it was subjected to sintering process at 375, 260 and 160 ºC. Properties such as hardness, stress and density of the obtained samples were evaluated (Azizi and Haghigi, 2015).

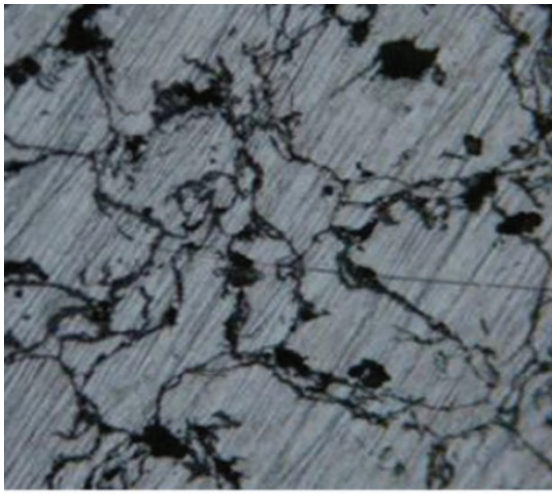

Figure 7. SEM image of the sample pressed with 500 MPa pressure x50 magnification (Azizi and Haghigi, 2015)

The SEM image of the sample obtained by 500 MPa pressing is shared in Figure 7. The sample with the highest density belongs to the sample sintered at 500 MPa pressure and 375 ºC temperature. Likewise, the highest hardness was observed in this sample with 101 Brinell. Considering that the hardness of zamak-2 as cast is 85 HB, this value is 19% higher. The increase in sintering temperature did not have a strong effect on the increase in hardness (Azizi and Haghigi, 2015).

The research conducted by Ataç, Özyürek and Güral was conducted with ZA powders with different contents, which are zinc aluminum alloys. In this study, mechanical alloying process was applied to ZA-8, ZA-12 and ZA-27 alloys. Alloying was carried out for 5, 6, 7 and 8 hours. The samples, whose alloying process was completed, were subjected to hot pressing at 320 ºC under 625 MPa pressure. The same samples were sintered in the oven at 320 ºC for 2 hours. Wear tests were carried out on a disk to test the behavior of the alloys in a dry friction environment. The wear load was selected as 10N, the sliding speed was 1m/s and the sliding distance was 600 meters. Studies have shown that as the Al content in the alloys increases, the hardness of the materials increases, however, mechanical alloying time does not have a significant effect on the hardness. In the study, they found that the most wear was in ZA-8 and the least in ZA-27 alloy, which has the highest hardness. Due to this situation, it has been determined that the volumetric loss is the highest in ZA-8. It has been said that this situation is more likely to be damaged in materials with a face-centered cubic structure due to the high Zn ratio and the anisotropic feature due to the hexagonal tightly packed crystal structure. Researchers have

found in wear tests that volumetric loss decreases as alloying time increases. It has been stated that the increase in the hardness of mechanically alloyed powder particles due to deformation hardening of aluminum also causes volumetric losses. SEM images of the wear surfaces of ZA-8, ZA-12 and ZA-27 are given in Figure 8, Figure 9, Figure 10 and Figure 11 (Ataç et al, 2014).

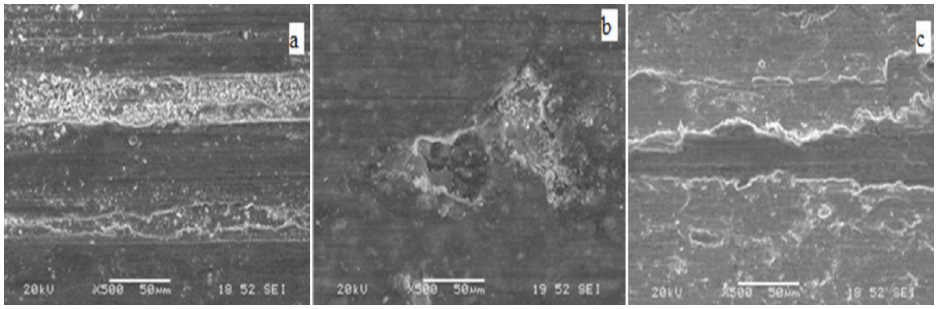

Figure 8. Surfaces as a result of mechanical alloying for 5 hours a)ZA-8, b)ZA-12, c) ZA-27 (Ataç et al, 2014)

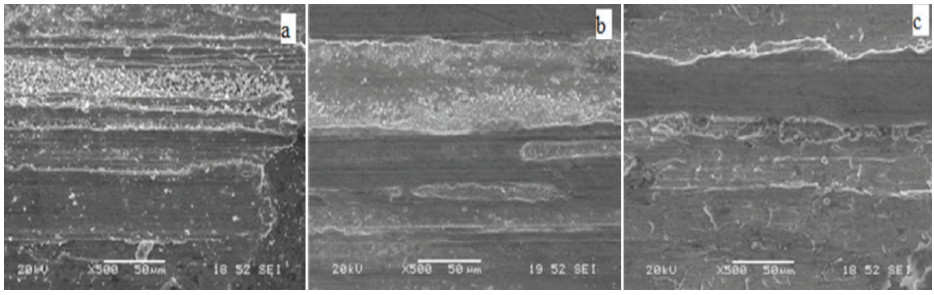

Figure 9. Surfaces after 6 hours of mechanical alloying a)ZA-8, b)ZA-12, c)ZA-27 (Ataç et al, 2014)

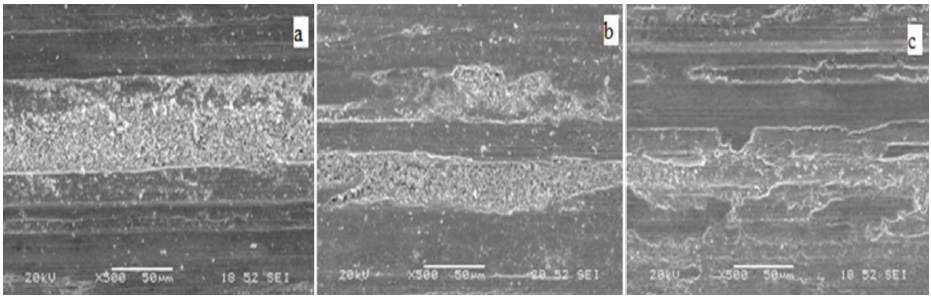

Figure 10. Surfaces as a result of 7-hour mechanical alloying a)ZA-8, b)ZA-12, c)ZA-27 (Ataç et al, 2014)

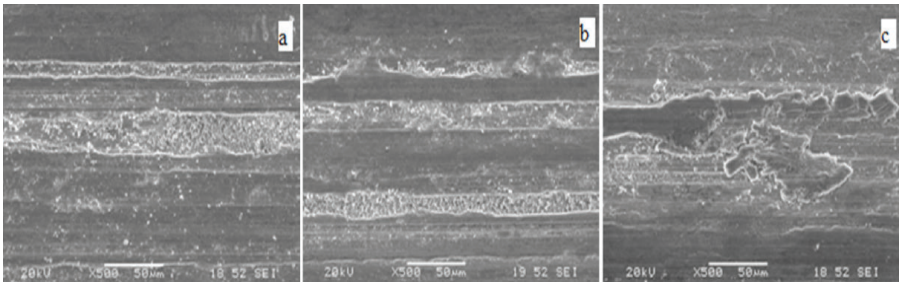

Figure 11. Surfaces as a result of 8-hour mechanical alloying a)ZA-8, b)ZA-12, c)ZA-27 (Ataç et al, 2014)

The highest degree of volumetric loss occurred in ZA-8 and abrasive wear is observed on the surfaces. When the images of ZA-27 are examined, the wear surfaces are mostly in the form of plastering. In this case, it is said that the volume loss is lowest due to fewer tears on the surface of ZA-27 (Ataç et al, 2014).

In the study conducted by Silva et al., zinc, aluminum and copper elemental powders were combined and alloyed in a ball mill for 0, 10, 20 and 30 hours. The time specified as zero hour in the study means manual mixing for 15 minutes before putting it in the mill. To reduce contact with oxygen during mechanical alloying, the processes were carried out in an argon atmosphere. During alloying, an anti-adhesion agent was added to make the dust particles ductile and prevent them from sticking to the container walls. The produced powders were subjected to compression at 500 MPa pressure. The sintering process was carried out at 400 ºC for 2 hours. Other samples were hot pressed at 500 MPa and 350 ºC. It was observed that the particles underwent deformation after the 10th hour of mechanical alloying. It has been stated that it turns into spherical structures after the 20th hour. It was stated that at the 30th hour, an evenly distributed equiaxed structure was observed. Figure 12 shows the visual of these changes (Silva et al, 2017).

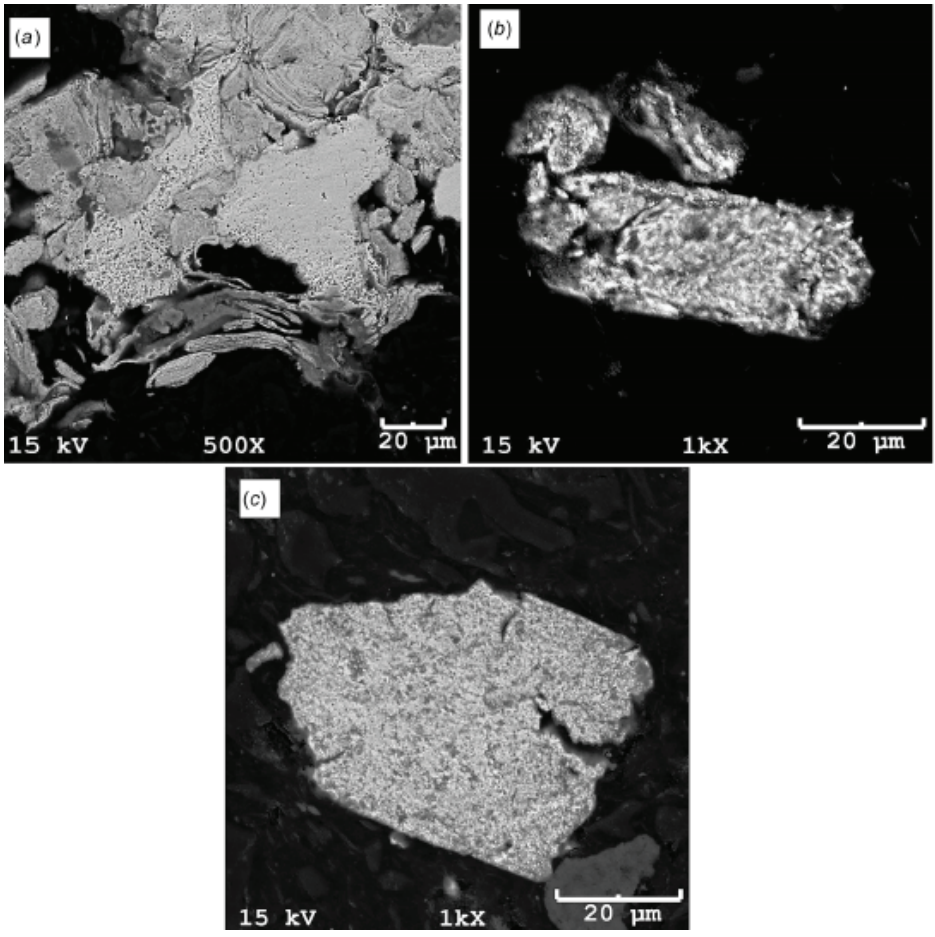

Figure 12. Powder structures at various alloying times a)10h, b)20h, c)30h (Silva et al, 2017)

While the average powder size after mechanical alloying was 100 micron meters, it decreased to 30 micron meters after 30 hours of alloying. This represents a decrease of approximately 70%. The pores in the structure of the sample produced by sintering are seen in Figure 13. It is stated here that the sintering process is not sufficient and therefore the adhesion is weak. The reason for this is thought to be oxidation or insufficient sintering time. Figure 13(b) shows the visual of the sample produced by hot pressing. Here the amount of porosity is low and at the same time the particles adhere well to each other. The hardness of zamak-2, produced by hot pressing, was determined as 97HV. This is 53% more than zamak-2 produced by casting (Silva et al, 2017).

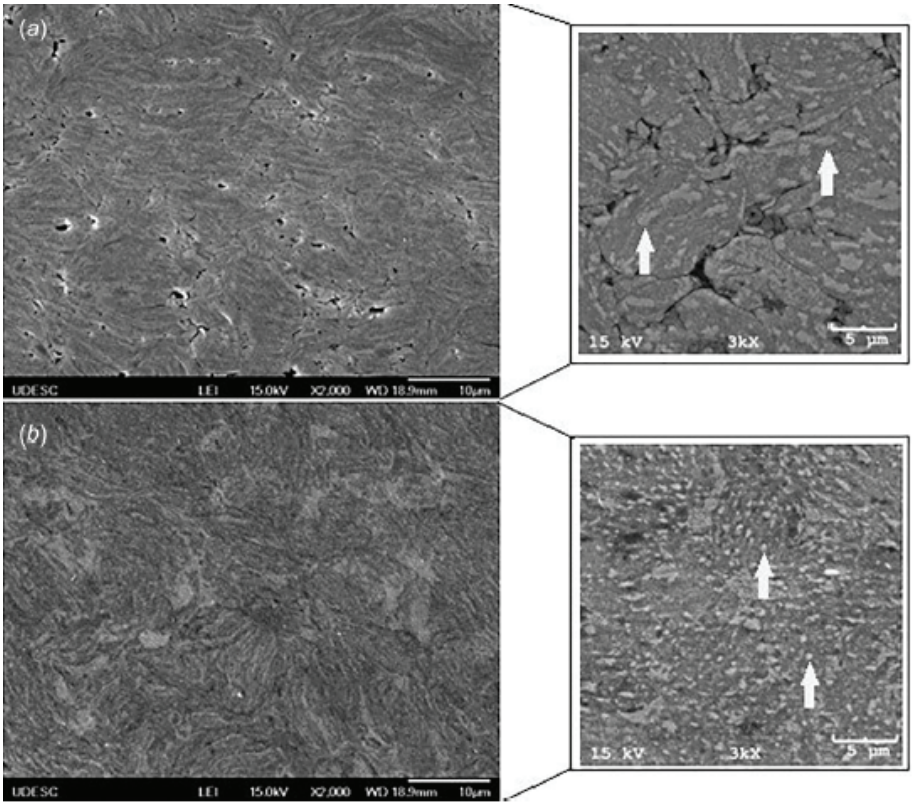

Figure 13. Zamak-2 microstructure a) sintered sample b) Hot pressed sample (Silva et al, 2017).

3. RESULT

As a result of the studies, it has been observed that the optimum time in the mechanical alloying method varies depending on the alloying elements in the metal matrix composite material. In the study conducted by Aytaç and Güral, it was stated that the optimum time for the mechanical alloying of ZA-8, ZA-12 and ZA-27 powders was 4 hours. In the study conducted by Yalçın and Çanakçı, it was concluded that the mechanical alloying time of graphene with ZA-27 was 15 minutes. In another study by the same authors, ZA-40 was mixed with SiC powders, and they determined the ideal alloying time to be 2 hours. It has been understood that the alloying time has an upper limit because the particles tend to grow by sticking to each other after a certain period of time. As can be understood from the studies conducted on different zamak alloys, differences have been detected in the alloying time.

Nanographene sheets incorporated into zinc aluminum alloys showed a

homogeneous distribution. It has been stated that as the amount of nanographene sheet added as 0%, 1%, 2% and 3% nanosheet reinforcement, respectively, increases, corrosion resistance increases.

It was observed that the wear resistance and porosity amount increased with the addition of SiC (0-0.5-1-1.5-2%) into the ZA-40 alloy. It was stated that the lowest hardness value was 87 HB in 2% SiC reinforcement. The highest hardness was measured as 127 HB at 0%. It is thought that as the SiC reinforcement ratio increases, the hardness value decreases due to the increase in the amount of porosity.

In Azizi and Haghigi's research, the hardness of zinc aluminum powders increased with the increase in compression pressure. By measuring 101HB at 500 MPa pressure and 375 ºC, it is seen that the hardness increased by 19%. This study also stated that while the increase in sintering temperature did not cause a significant increase in hardness, the hardness values increased with the increase in compression pressure.

Researchers have observed that as the Al content increases in Zn-Al alloys, the hardness increases. At the same time, volume losses decreased due to the increase in hardness. In wear tests, abrasive wear was observed on the surfaces. It has been determined that the wear rate decreases as the mechanical alloying time increases.

It has been determined that as the mechanical alloying time increases in Zamak-2 alloy, the powder structure tends towards spherical. Zamak-2 hardness was measured as 97 HV by hot pressing at 500 MPa pressure and 350 ºC. It is stated that this is 53% higher than the hardness of zamak-2 produced by casting.

REFERENCES

Ataç, A. M., and Güral, A. (2013). Çinko-Alüminyum (ZA) Alaşımlarının Mekanik Alaşımlama Yöntemiyle Üretilebilirliği Üzerine Bir Çalışma. *Politeknik Dergisi, 16,4,* 147-154.

Ataç, A., Özyürek, D., Güral, A. (2014). Mekanik Alaşımlama ile Üretilmiş Çinko-Alüminyum (ZnA) Alaşımlarının Kuru Sürtünmeli Aşınma Davranışlarının İncelenmesi. *Gazi Üniversitesi Fen Bilimleri Dergisi, Part C, Tasarım ve Teknoloji, 2(4),* 309-313.

Azizi, A., and Haghighi, G.G. (2015). Fabrication of Zamak-2 Alloys by Powder Metallurgy Process. *The International Journal of Advanced Manufacturing Technology, 77,* 2059-2065.

Cambronero, L.E.G, Sanchez, E., Roman, J.M.R. and Prieto, J.M.R. (2003). Mechanical Characterisation of AA7015 Aluminium Alloy with Ceramics. *J. Mater. Proces Techno, 143*, 378-383.

Costa da Silva, F.i Kazmierczak, K., Edil da Costa, C., Milan, J. C.G., Torralba, J. M. (2017). Zamak-2 Alloy Produced by Mechanical Alloying and Consolidated by Sintering and Hot Pressing. *Journal of Manufacturing science and Enigneering, 139,9*, 091011.

Sankar, R. And Singh, P. (1998). Synthesis of 7075 Al/SiC Particulate Composite Powders by Mechanical Alloying. *Metarials Letters, 36*, 201-205.

Sudha, G.T., Stalin, M., Ravichandran, M., Balasubramaian, M. (2020). Mechanical Properties, Chracterization and Wear Behavior of Powder Metallurgy. *Composites-a rewiew, Materials TodayProceedings, Vol., 22,* 2582-1596.

Suryanarayana, C. (2001). Mechanical Alloying and Milling, *Progressing. in Mater Sci., 46,* 1-184.

Tarralba, M., Velasco, F., Costa, C.E., Vergara, I. And Caceresa, D. (2002). Mechanical Behaviour of the Interphase Between Matrix and Rainforcement of Al2014 Matrix Composites with (Ni3Al). *Composites:Part A-33*, 427-434.

Thummler, F. And Oberacker, R. (1994). *Introduction to Powder metallurgy*, The Institue of Materials, London, UK, 1-10.

Yalçın, E.D., and Çanakçı, A. (2018). Toz Metalurjisi Yöntemiyle Üretilen ZA27/Grafen Nanokompozitlerin Korozyon Davranışı. *Technological Applied Sciences, 13,2,* 157-164.

Yalçın, E.D. and Çanakçı, A. (2022). Silisyum Karbür (SiC) ile Güçlendirilmiş Çinko-Alüminyum (ZA40) Alaşımının Aşınma Parametrelerinin İncelenmesi. *Afyon Kocatepe Üniversitesi Fen ve Mühendislik Bilimleri Dergisi, 22,1*, 207-213.

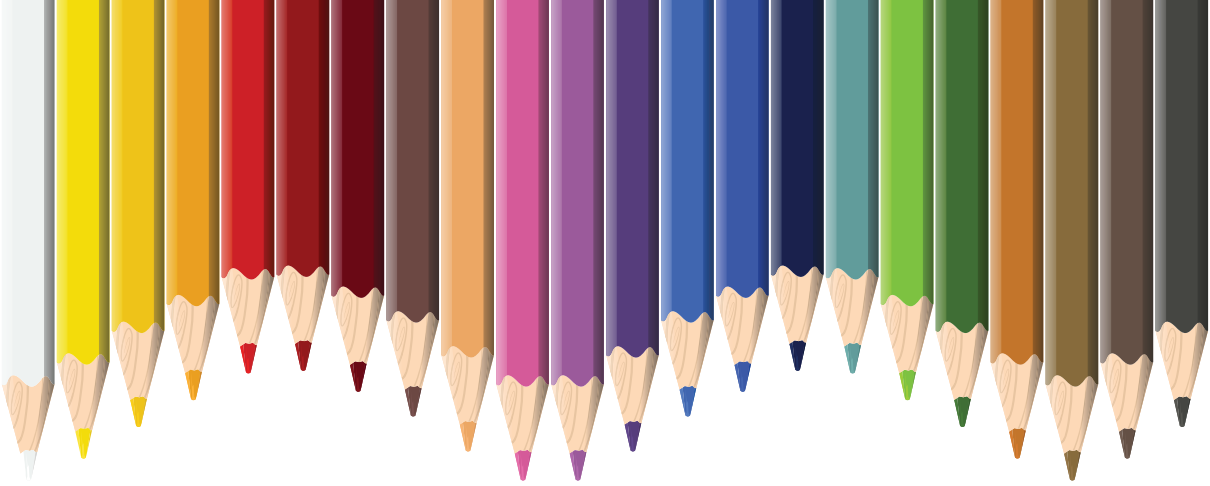

Chapter 14

GRAPE DRYING USING WITH RENEWABLE ENERGY SYSTEM CONTROLLED BY ARDUINO IOT CLOUD

Gökhan UÇKAN[1]

Nilay AKKAYA[2]

Fatma Bildirici AKDENİZ[3]

1 Dr.Öğr.Üye.Gökhan UÇKAN, Pamukkale Üniversitesi, Bilgisayar Mühendisliği Bölümü, guckan@pau.edu.tr, ORCID:0009-0004-7938-0401

2 Nilay Akkaya, Pamukkale Üniversitesi, Bilgisayar Mühendisliği Bölümü, nilay.akkaya91@ gmail.com, ORCID: 0009-0000-0708-3986

3 Fatma B.Akdeniz, Pamukkale Üniversitesi, Bilgisayar Mühendisliği Bölümü, fatmabildirici@hotmail.com, ORCID: 0009-0001-6782-4261

1. INTRODUCTION

Drying has been used as a preservation method for centuries and continues to play a significant role in the food industry today. While grains are the most commonly dried food, fruits and vegetables also make up a portion. Microbial growth inside the product can be redused by decreasing the value of water and humidity. The transportation of the products will be more economical when the value of humidity inside the product is decreased. This is because the volume of products will decrease as well.

The main purpose of drying is to remove water and prevent spoilage caused by microorganisms. Different terms such as drying, dehydration, and dewatering are often used to describe the process. When drying small fruits and vegetables, it is important to consider factors such as light exposure, oxidation, and heat, in order to preserve bioactive compounds (Naseer,A,2013). Traditional and new drying methods and pre-treatment techniques, such as considering factors efficiency, quality preservation, and cost-effectiveness are used (Naseer,A,2013). Previous studies show that drying cabinet supported by air collectors are much more efficient than the others (Öztürk, H.K,2022). A significant quantity of fruits and vegetables is cultivated by numerous developing countries, both for local consumption and export. According to the Food and Agricultural Organization's data from 1991, the estimated production for the year 1990 reached an impressive 341.9 million metric tons globally. Specifically, within Asia, India contributed 27.8 million metric tons, accounting for 8.1% of the total, while China had a production capacity of 21.5 million metric tons, representing 6.3% of the world's total production. The increasing agricultural products resulting from developments in the agricultural sector bring along various challenges in terms of storage and marketing. The foremost challenge is to create suitable storage conditions for the products and preserve the profits. Therefore, there has been a need to dry food products using clean energy sources instead of traditional drying methods, in a more efficient and healthy way. The energy sources used in traditional drying methods are either fossil fuels or direct exposure to the However, these methods have environmental impacts and sustainability issues. In this regard, the use of solar panels in regions where the sun's impact is strongly felt has enabled the involvement of technology in this drying process. In this study, a grape drying system in a closed cabinet supported by a renewable energy source controlled via arduino IoT cloud is described. In order to reduce the moisture content of grapes grown in Aydın province, drying process is required. In this regard, a computer system established in Denizli province, using Arduino Create Agency, The humidity level and the air temperature inside the grape drying

cabinet is controlled through the developed program. Values are obtained using sensors which are integrated to Arduino and sent to the Arduino Agency through IoT Cloud. Then, the taken values are analyzed within the developed program. Depending on the situation, the rotation speed of the fan supplying air to the cabinet is controlled during the drying process. As rapid drying may lead to undesired results, the drying process is conducted based on the most suitable humidity and temperature values. As a result, the fan operation is optimized and managed by the developed program.

2. DIFFERENT FRUIT DRYING METHODS

Sun drying is a safe method for preserving fruits due to their high sugar and acid content, which helps prevent food spoilage. However, it is not recommended for vegetables and meats. Vegetables have lower sugar and acid levels, increasing the risk of spoilage. Meats, on the other hand, are rich in protein, creating an ideal environment for microbial growth when heat and humidity cannot be controlled. Sun drying, is best to choosen when hot, dry, breezy days with temperatures are no lower than 86 Fahrenheit. Higher temperatures are even more beneficial. It should be kept in mind, that outdoor sun drying can take several days to fully dry the food (Öztürk,H.K,2013).

2.1 Low Cost Dryning Methods

Affordable drying technologies that are appropriate for rural farming regions. Several crucial factors affecting their suitability are taken into account, these are;

low cost, easy to build, easy to operate, better results, the ability to easily intervene in the case of breakdowns. Fluidized bed, spouted bed, infrared, solar, simple convective and desiccant drying are the methods which the selected drying technologies are including. The chosen drying technologies encompass fluidized bed, spouted bed, infrared, solar, simple convective, and desiccant drying (Chua, J.K, 2003).

2.1.1 Fluidized Bed Dryers

While industrial fluidized bed dryers have proven effective in drying wet solid particles over the years, the process of developing these dryers for specific applications are riddled with challenges. Issues like scaling-up, suboptimal fluidization, and inconsistent product quality pose significant obstacles. Among these challenges, scaling-up stands out as the primary concern, and the scarcity of robust theoretical models compounds the

difficulty, making it challenging to substitute costly laboratory experiments and pilot-plant trials (Wan,R, 2008).

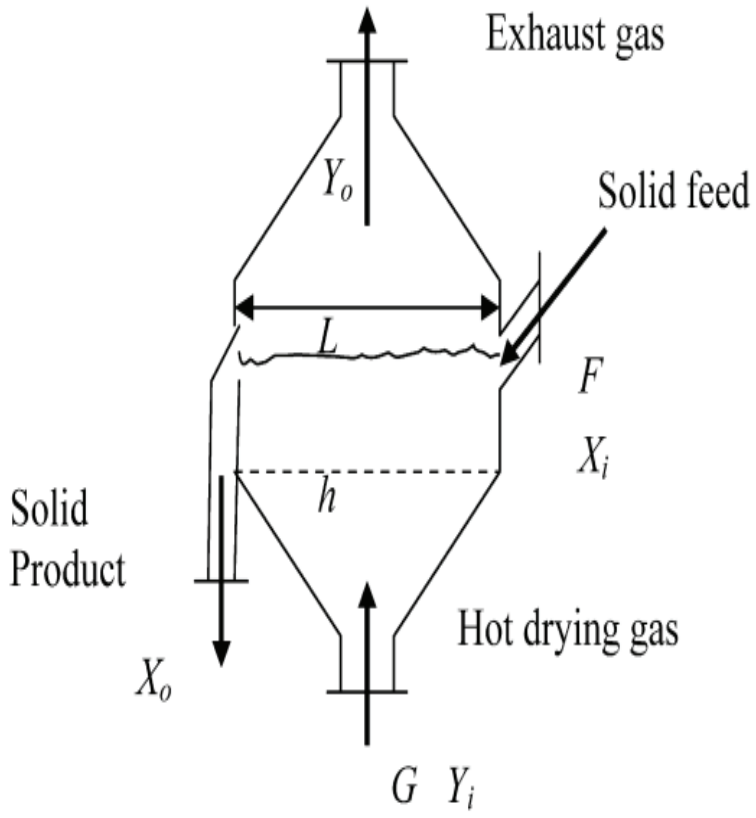

Figure 1. Fluidized Bed Dryer blok diagram.

Above at Figure1, a Fluidized Bed Dryer is shown. Here are the explanations for the used parameters. Above the given parameters stands for; inlet of solid dry basis moisture content where it is given as “Xi”, outlet solids dry basis moisture content given as “Xo”, output gas dry basis humidity given as “Yo” and inlet gas dry basis humidity given as “Yi”. All units of the given parameters are in (kg/kg).

2.1.2 Spouted Bed Drying

Spouted-Bed drying is generally considered for a suitable solution of drying coarse grained products which are difficult to fluidize efficiently. A typical design for Spouted-Bed dryer is a draft tubular Spouted-Bed Dryer (SBD), which consists of a cylindrical container with a conical bottom. The

inlet nozzle is used to introduce the spraying air, which acts as a drying medium. A draw pipe has been installed in the center to increase the height at which granular particles can be sprayed. The wet material enters through a side inlet port and undergoes gushing with the help of a draw pipe. Drying air is passed through an opening conical base ensuring effective interaction with particles (Wan,R,2008).

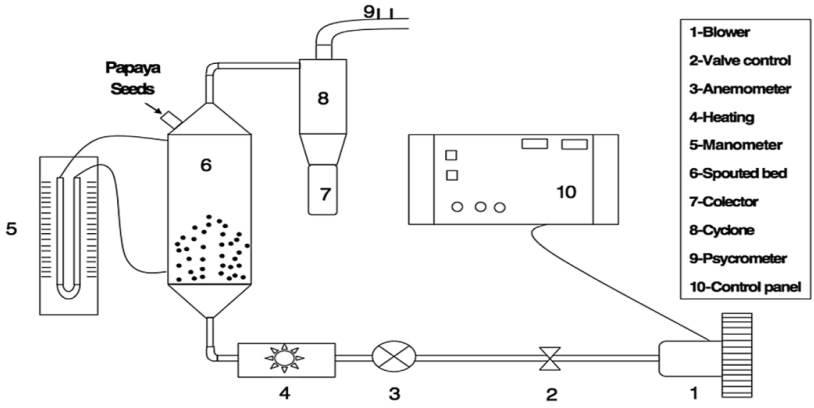

Figure 2. A Spouted-Bed drying blok diagram for papaya seeds (Daniel, P. C, 2016).

2.2 Sun Drying Method

The primary goal of drying agricultural products is to decrease their moisture content to a level that ensures they can be safely stored for a prolonged period. Additionally, this drying process results in a significant reduction in weight and volume, which helps to minimize packaging, storage, and transportation expenses (Okos,N,1992). A sun drying application is shown in Figure 3.

Figure 3. Sun drying application (Mavis, O.A,2018).

The direct type of solar dryer operates by allowing solar radiation to pass through a transparent cover, which is typically made of glass. This radiation is then directed onto the grapes that are placed inside the dryer for the drying process. One of the advantages of using a glass cover is the effectively reduced direct convective losses, preventing the escape of heat to the surrounding environment. Additionally, the presence of the glass cover which helps to enhance the temperature within the dryer, creating optimal conditions for the drying process.

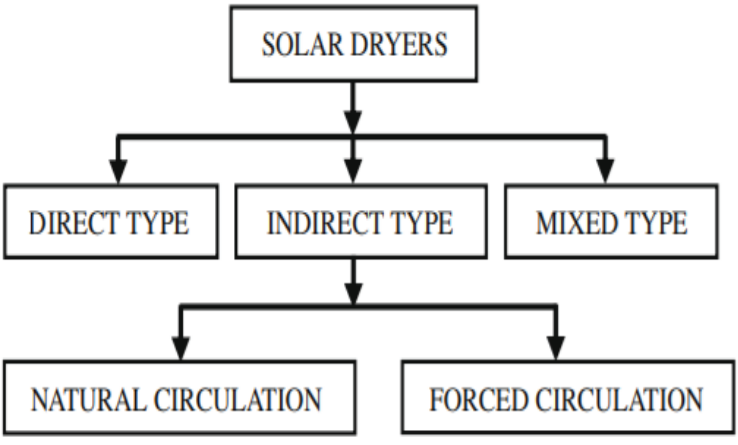

Figure 4. Classification of solar dryers (Daniel, P. C,2016).

Above the classification of solar dryers is seen. Below in Figure 5. a Solar cabinet dryer is shown.

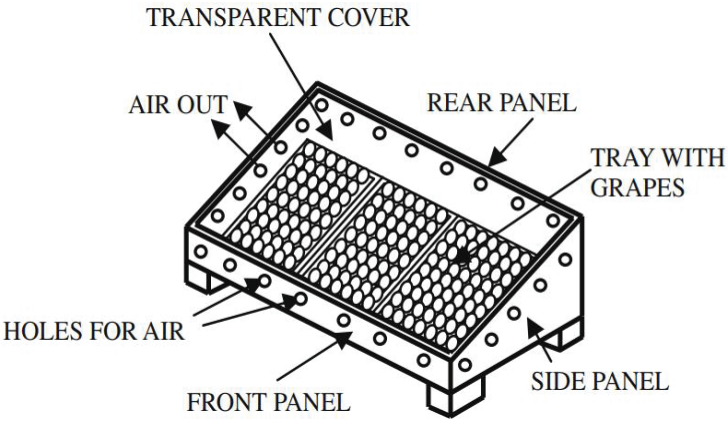

Figure 5. Solar cabinet dryer (Daniel, P. C,2016).

3. FRUIT DRYING WITH REMOTE CONTROL USING ARDUINO IOT CLOUD

The most popular application of today that aims to make human life easier is Internet of Things (IoT) applications. It aims to minimize human intervention to enable with devices communicating each other and large systems. This allows for easy monitoring and control of devices from different locations. Smartphones and tablets, smart home automation, unmanned aerial vehicles (UAVs), drones, and smart factory automation are the most well-known examples. Remote control systems have become preferred in factories due to their time-saving and cost-effective work environment. This approach has enabled the production of smart factory automation. Various hardware and user-friendly interfaces for using this hardware have made IoT user-friendly (Taştan, 2019).

3.1 Arduino IoT Cloud and Create Agent Technology

Arduino IoT Cloud is a cloud-based service that is widely preferred for its ability to facilitate the design and management processes of remote control projects. It enables the remote control of devices by managing them over the internet. The system gathers and evaluates data from sensors used in the developed systems. As it does not require extensive academic knowledge, projects can be easily prepared and developed. Agent Technology enables data exchange between devices while using Arduino IoT Cloud, establishes secure connections, and provides ease of sharing.

3.1.1 Application Areas and Implemented Projects of IOT CLoud Technology

It is known that remote control is used in many fields due to the convenience it provides. Some of these areas are as follows;

Education: Remote control of lighting and heating-cooling systems in schools for energy saving purposes.

City Systems: Control of traffic lights, parking lot control, collection of environmental data such as air quality.

Health and Medicine: Wearable devices tracking health data, medication reminders, monitoring health status related to diseases such as blood pressure and diabetes.

Art and entertainment: Developing art projects, creating Arduino-based projects and games.

Home Automation: Remote control of lighting systems, home ventilation control with temperature and humidity data, use of cameras and sensors for security.

Agriculture and Garden Automation: Control of automatic irrigation systems, monitoring and control of agricultural conditions, collecting plant growth data. Industrial automation: Remote monitoring and control of factories, evaluation of data obtained during production, control of energy usage.

4. THE PROPOSED SOLAR DRYING SYSTEM

The aim of the proposed system is to dry food using a fan system that can be remotely controlled with the energy obtained from the sun. Solar panels, which are directed towards the side where the sun rays are the most intense, are used to charge the battery in order to make the most of the sun throughout the day. The charged battery operates the fan that blows air into the cabinet where the food is being dried. The most important factors during the operation of the fan are the values received from the humidity and temperature sensors inside the cabinet. In order to dry the food at an optimum level, the temperature should be sufficiently high and the humidity should not be too high. With the fan operated under these conditions, the food is dried effectively. As the internal temperature of the cabinet decreases, the fan will rotate faster, providing more hot air intake. On the other hand, as the internal temperature of the cabinet increases, the fan will rotate slower, allowing the hot air to move towards the food at a slower pace. The operation of the fan will be controlled remotely, allowing drying systems located in different locations to be controlled from a single center.

4.1 Fan Speed Control Using Arduino IoT Cloud

The operation of the developed system, which is controlled via Arduino IoT Cloud, is demonstrated in Figure. 6. As seen, air enters the system naturally from bottom to top. However, in cases where the air pressure is low, this effect will decrease, so it needs to be supported by a fan. The humidity inside the cabin is measured with an integrated Arduino system. The measured humidity value is evaluated by a program running on Create Agency on the Arduino IoT cloud. Depending on the result obtained, the Arduino is accessed via the IoT cloud to adjust the fan speed.

4.2 Arduino IoT Cloud and Create Agent Technology

They are the most preferred interface and software for those who want to develop a remote control project, due to the ease of project design and management operations. Arduino IoT Cloud is a cloud-based service and manages devices over the internet. Thus, the equipment can be controlled remotely. Data can be collected and evaluated from the sensors used in the developed systems. Since it does not require much academic knowledge, projects can be easily prepared and developed. Create Agent Technology enables data exchange between devices when using Arduino IoT Cloud, establishes secure connections, provides convenience in sharing. For this reason, it is necessary to use Arduino IoT Cloud.

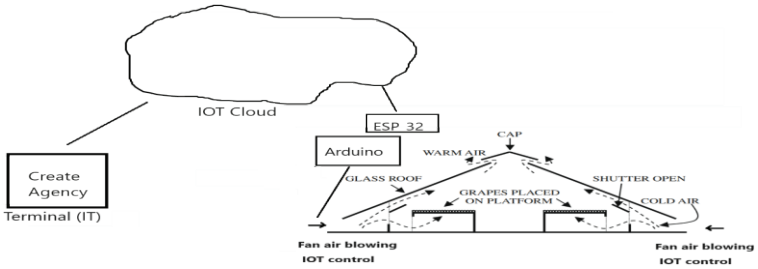

Figure 6. Demonstration of the proposed IoT system.

4.3 The Solar Tracking System

Using the Arduino IDE program, commands that control the movement of the solar panels are loaded onto the Arduino Uno. The hardware sensors responsible for this movement are LDRs (Light Dependent Resistors).

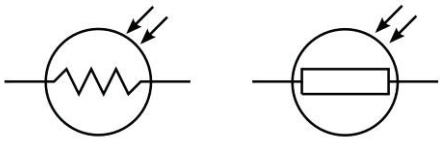

Figure 8. LDR symbol.

LDRs are circuit components that exhibit less resistance as the intensity of light falling on them increases, and more resistance as it decreases. LDRs are placed in positions where they can receive the maximum amount of sunlight in the established setup. Based on the detected light intensity, the solar panel is directed towards the angle indicated by the LDR that receives the most light. Tower Pro SG90 Servo Motor is used as the circuit component to facilitate this movement.

Figure 9. Tower Pro SG90 servo drive.

The Tower Pro SG90 Servo Motor has a rotation angle between “0” and “180” degrees and is connected to the circuit using three wires (5V power, GND ground, PWM signal). It is referred because of its low power consumption and ability to easily move the solar panel. The power cable of the Tower Pro SG90 Servo Motor is connected to the “5V” pin of the Arduino Uno, the ground cable is connected to the GND pin, and the signal cable is connected to the PWM pin number “11”.

4.4 Flowchart of the System Control using Arduino IoT Cloud

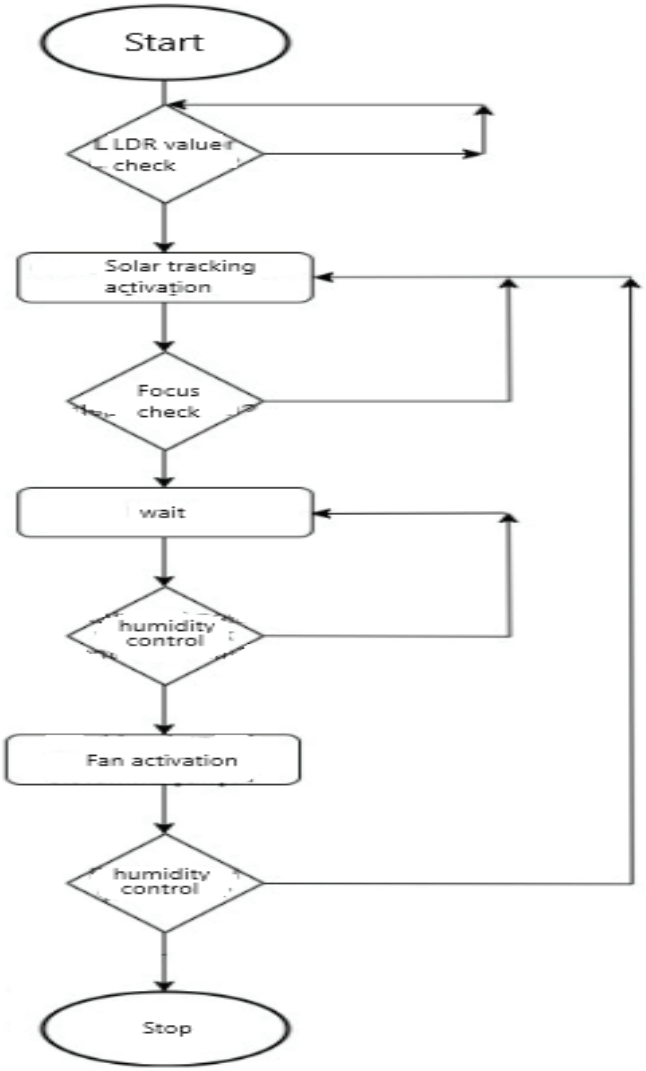

Figure 7. Flowchart of the Arduino IoT control program.

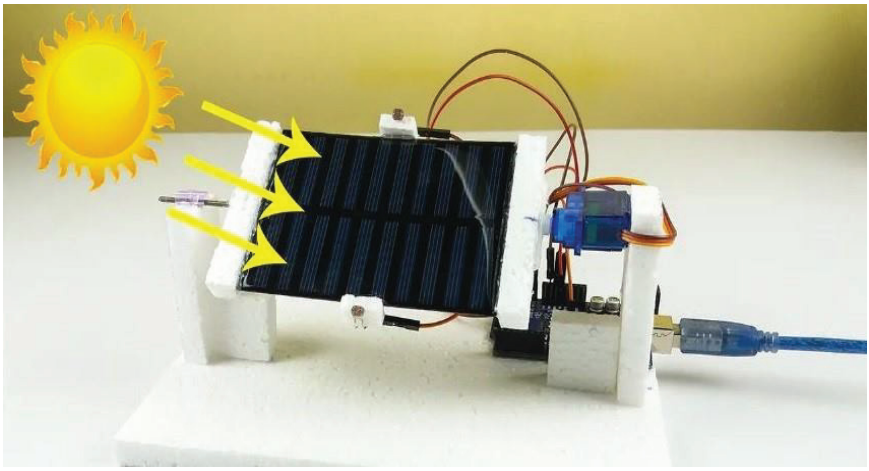

Figure 10. Solar tracking system.

The energy generated by the sun-tracking panel, through LDRs, will be stored in the energy battery, which will be used to power the fan.

4.5 Converting the Fan System Arduino Using Create Agency for Remote Control

After signing up for the Arduino IoT Cloud online development environment, the Arduino Create Agent program is downloaded. The Arduino Create Agent is a platform that provides project development and management services, allowing local operation on the computer. Once the Arduino Create Agent program is launched, the "Go to Arduino Create" option is selected from the system tray, and login to the Arduino Cloud is performed. The login steps are shown in Figure 11, Figure 12, and Figure 13.

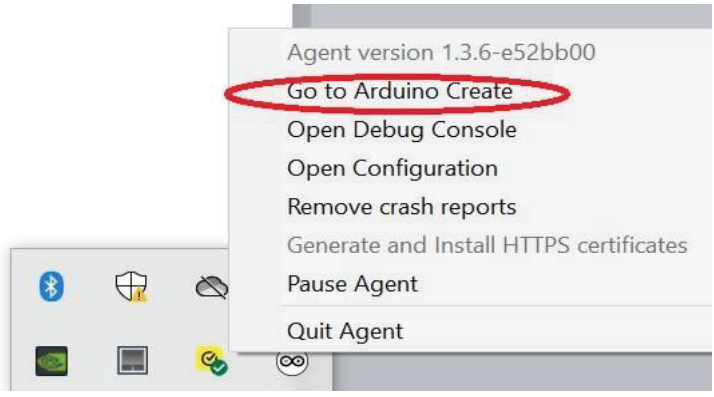

Figure 11. Arduino Create Agent user input.

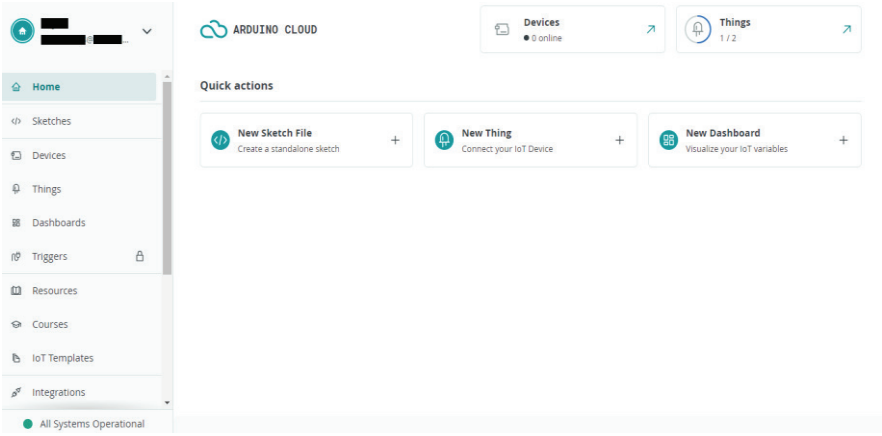

Figure 12. Arduino Create Agent user interface.

A new project is created by selecting the "Create Thing" option from the Things menu and determining the objects to be used and the variable names to be used in programming with the "Add Variable" option. In this project, button, humidity, and temperature variables are used.

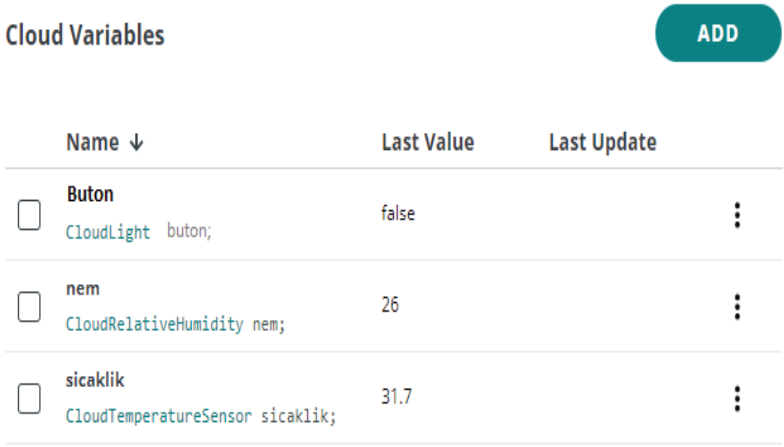

Figure 13. Cloud variable interface.

By selecting the “Add Device” option from the Device menu, the remote control circuit board to be used in the system is selected. In this work, ESP32, one of the third party devices, is selected with the Third Party

Device option and DOIT ESP32 DEVKIT V1 is used from the “Select mode” menu.

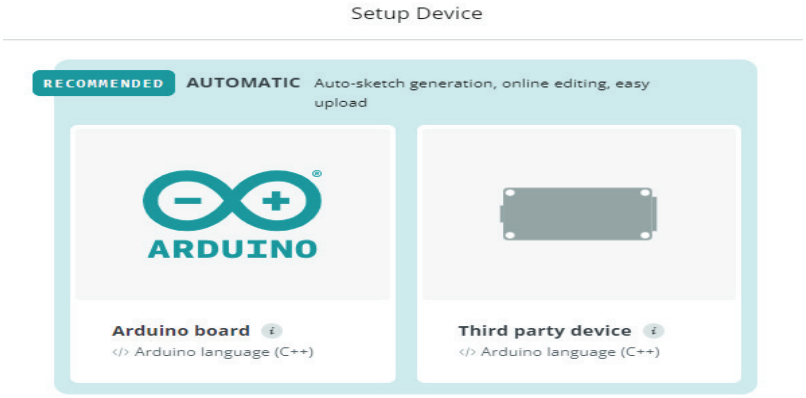

Figure 14. Device setup screen output.

The design screen for mobile devices allows for customizing the layout and appearance of the dashboard on smaller screens. This can include rearranging widgets, adjusting font sizes, and adding additional elements like images or logos. Once the design screen is created, it can be previewed and tested on mobile devices to ensure optimal user experience. Any changes made to the design screen will automatically be reflected on the mobile devices as well. In addition to the design screen, the project settings also allow for configuring user access and permissions. This includes setting up user accounts and defining the level of control each user has over the dashboard and its associated objects. Overall, the project section in the device settings provides a comprehensive platform for creating and managing dashboards, widgets, and user access for IoT devices.

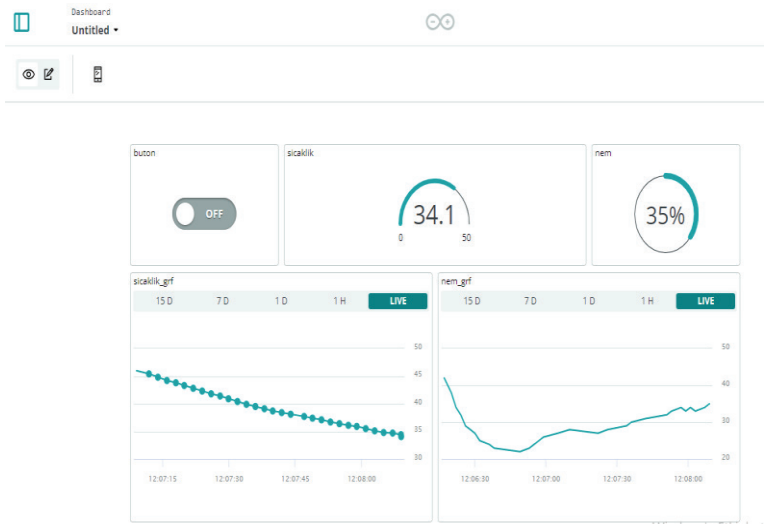

Figure 15. Dashboard screen output.

From the Sketch menu, an interface can be accessed where the code is written without the need for the Arduino IDE program. Since the libraries to be used during coding are already available, there is no need to reinstall them. This provides convenience to software developers. To be able to send code and perform control via the web, the Arduino Create Agent program needs to be installed. In the hardware structure of the system, ESP32, L298N motor driver board, DC motor, and DHT11 (humidity and temperature sensor) are used. The ESP32 is a microcontroller chip with Bluetooth and 2.4 GHz WiFi connectivity features, interaction with sensors and other devices, and a dual-core CPU. Its ability to be used in remotely controlled applications and its low power consumption are the main reasons for its preference.

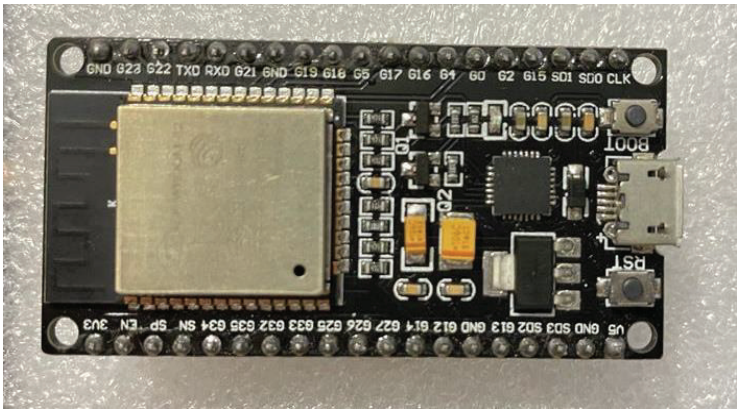

Figure16. ESP32 ESP-32S WiFi + Bluetooth Dual-Mode Development Card (30 Pin).

L298N motor driver board is a motor driver board that can drive DC motor with voltage regulator up to 24V. With the Motor-A and Motor-B sections, two different motors can be controlled simultaneously and independently. The Motor-A section of the L298N motor drive board circuit and the connected IN1, IN2 and ENA pins are used. For DC motor control with the ESP32 card, a signal was applied to the motor driver card from the PWM pins of the ESP32 card. One-way rotation of the motor was achieved by applying pin number 26 to IN1 as HIGH and pin number 27 to IN2 as LOW from PWM pins. The ENA pin adjusts the motor speed.

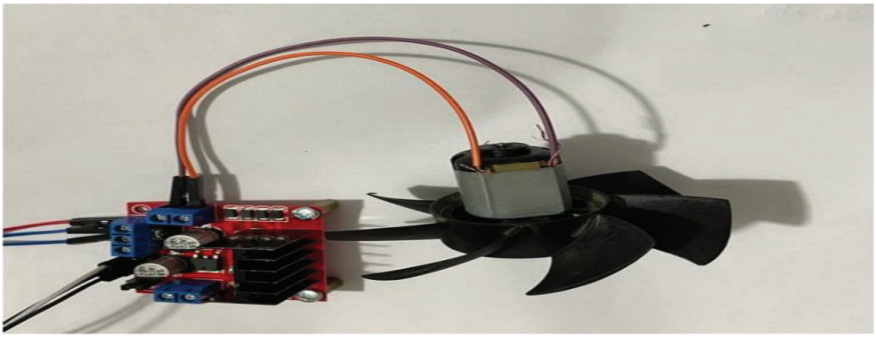

Figure 17. DC Driver Card and Fan Circuit.

4.6 Realizing the Cabin Dryer

They can be in the form of a cabinet or room where hot air circulates. The cabinets can have shelves or the items can be laid out on a wheeled cart and

inserted into the cabin. To ensure equal drying on all shelves, the order of the shelves should be changed at regular intervals. A cabinet with shelves is used. The DHT11 sensor inside the cabinet collects the humidity and temperature data, which is then sent to the relevant port of the ESP32, and from there, it is transmitted to the Arduino Cloud platform through the network connected to the ESP32. The humidity and temperature information is displayed on the dashboard screen both numerically and graphically. The fan motor that provides air to the cabinet can be turned on and off using the button on the dashboard. The ESP32 receives the temperature information from the relevant pin and uses it to adjust the fan speed. As the temperature inside the cabinet decreases, the fan will spin faster. The system can be controlled from any environment that can access the Arduino IoT Cloud interface via the web.

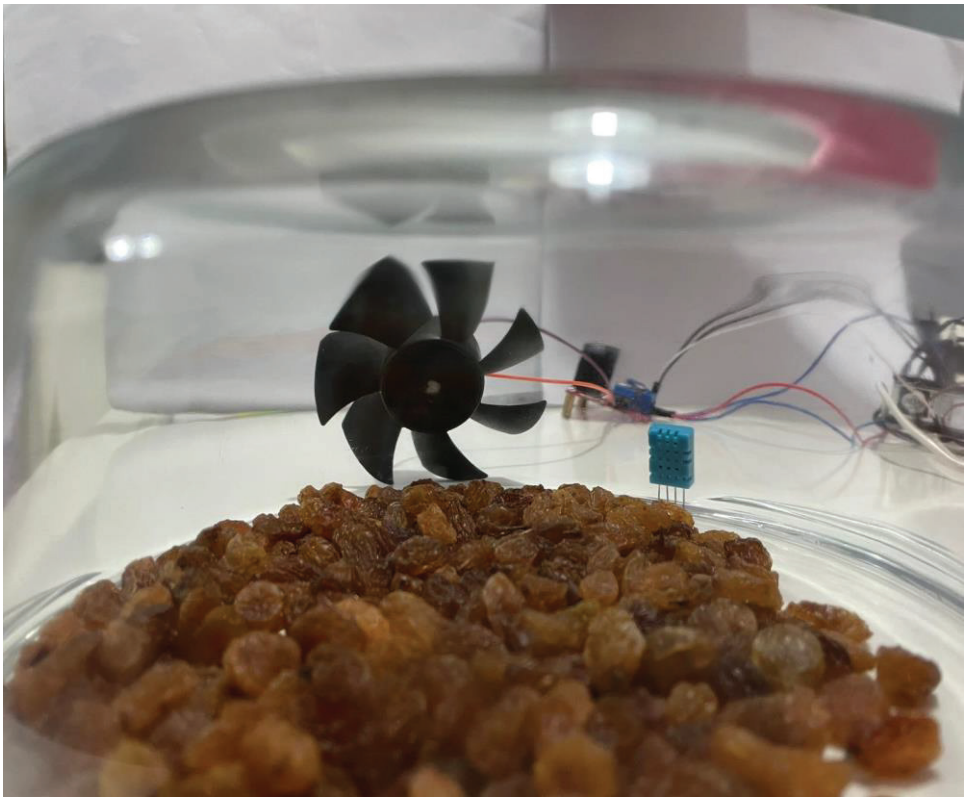

Figure 18. Grape Drying Cabine.

When the low temperature of the high humidity values in the cabinet is measured as seen on Figure 19 at graph1, the remotely controlled fan by Arduino IoT Cloud, rotates fast while the fan rotates slowly when high

temperature has been achieved with low humidity values measured as seen on Figure 20 at graph 2.

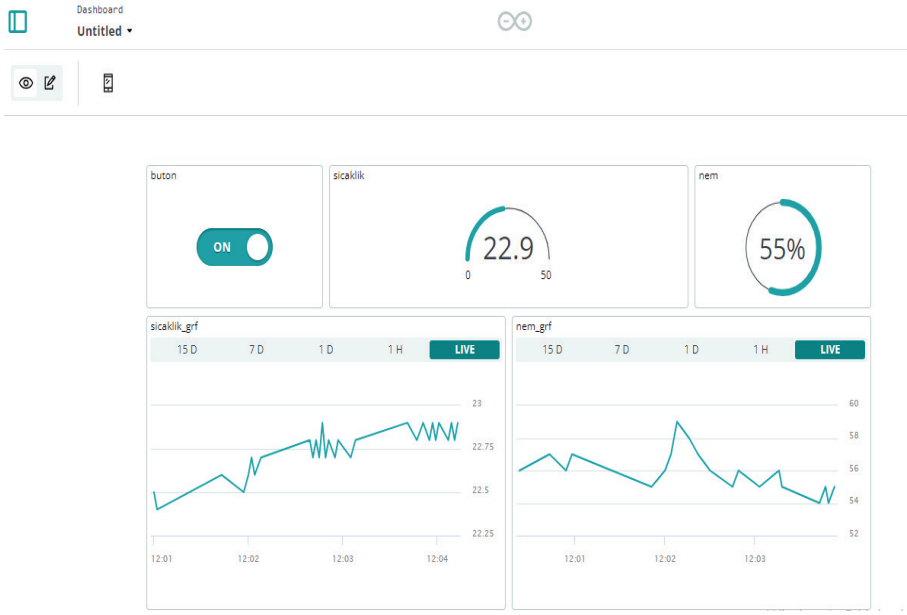

Figure 19. Low temperature-high humidity grah-1.

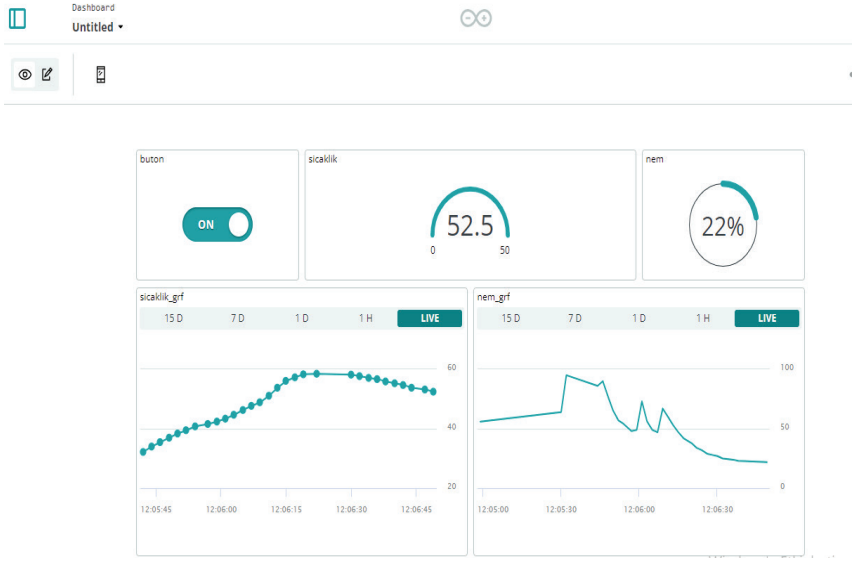

Figure 20. High temperature-low humidity grah-2

4.7 The Developed Program Codes

The given codes below are processed on the Arduino for realizing the solar tracking process of the system.

4.7.1 Programming Codes of the Tracking System

The necessary parametric values are taken at certain periods through sensors.

```
/*Solar tracking system
  https://srituhobby.com
*/
//Include the servo motor library

#include <Servo.h>
//Define the LDR sensor pins
#define LDR1 A0
#define LDR2 A1
//Define the error value. You can change it as you like
#define error 10
//Starting point of the servo motor
int Spoint =  90;
//Create an object for the servo motor
Servo servo;

void setup() {
//Include servo motor PWM pin
  servo.attach(11);
//Set the starting point of the servo
  servo.write(Spoint);
  delay(1000);}

void loop() {
//Get the LDR sensor value
  int ldr1 = analogRead(LDR1);
//Get the LDR sensor value
  int ldr2 = analogRead(LDR2);

//Get the difference of these values
  int value1 = abs(ldr1 - ldr2);
  int value2 = abs(ldr2 - ldr1);
```

```
//Check these values using a IF condition
  if ((value1 <= error) || (value2 <= error)) {

  } else {
    if (ldr1 > ldr2) {
      Spoint = --Spoint;
    }
    if (ldr1 < ldr2) {
      Spoint = ++Spoint; } }
//Write values on the servo motor
  servo.write(Spoint);
  delay(80);

}
```

4.7.2 Programming Codes Required to Drive the Driver

The code required to drive the ESP32 driver, which prepares Arduino to connect to the IoT Cloud application, is given below.

```
#include "thingProperties.h"
#include "DHT.h"
#define DHTPIN 4
#define DHTTYPE DHT11
int motorPin1 = 26;
int motorPin2 = 27;
int motorPin = 17;
float hiz = 0;
DHT dht(DHTPIN, DHTTYPE);
void setup() {
  Serial.begin(9800);
  delay(1700);
  pinMode(motorPin1,OUTPUT);
  pinMode(motorPin2,OUTPUT);
  digitalWrite(motorPin1,LOW);
  digitalWrite(motorPin2,LOW);
  dht.begin();
  initProperties();
  ArduinoCloud.begin(ArduinoIoTPreferredConnection);
  setDebugMessageLevel(2);
```

```
  ArduinoCloud.printDebugInfo();}
void loop() {
  ArduinoCloud.update();
  sensorOku(); }
void onLambaChange()
void sensorOku(){
  float h = dht.readHumidity();
  float t = dht.readTemperature();
  hiz = map(t,70,10,0,255);
  sicaklik = t;
  nem = h;
  if(led == 1){
    analogWrite(motorPin, speed);
    digitalWrite(motorPin1,HIGH);
    digitalWrite(motorPin2,LOW);}
  else{
    digitalWrite(motorPin1,LOW);
    digitalWrite(motorPin2,LOW);}
    Serial.print(speed);
  //Serial.print("heat:");
  //Serial.print(t);
  //Serial.print("Nem: ");
  //Serial.print(h);
  //delay(1000);  }
```

5. CONCLUSION

There are many methods developed for drying processes. In this work, traditional and new technological methods are compared. In the traditional method, solar energy was used in the fan system operated by remote control while the food was placed in the exhibition using solar energy, but the food was left to dry in the food drying cabinet. Grapes, which are widely produced in the Aegean Region, were preferred as food. Since its production is in excess, raisin trade is carried out as well as fresh grape trade. In both methods, the weights of fresh grapes and raisins were measured and moisture and weight information were used as drying criteria. The drying process is completed when the final moisture content of the grape reaches about 20%. When the laying method was used in the exhibition, 1 kg of fresh grapes dried completely in about 260 hours and 250 g of raisins were

obtained. 1 Kg of fresh grapes with the method developed for this work using renewable energy system controlled by Arduino IoT Cloud is dryed up in totally of 151 hours. Different types of panels can be preferred in order to be able to provide more energy than solar panels. When the stored electrical energy increases, more motor-fan assemblies can be included in the system. In order to shorten the time elapsed during the transportation and drying of the product collected in food drying factory automations, increasing the fan system may be preferred in order not to lose the quality of the product and to dry it in a shorter time. An integrated weight sensor in the cabinet can be used instead of a weight system outside the cabinet to detect that the grape is dryed out. Instead of a cabinet system with shelves, a wheeled shelving system can be used, which will be placed later in the cabinet.

REFERANCES

Naseer,A, Jagmohan,S, Harmeet,C, Prerna,G.A, Harleen,K. (2013), Different drying methods: Their applications and recent advances, *International Journal of Food Nutrition and Safety, 4(1):* 34-42.

Öztürk, H.K.(2022), Öztürk, H.M, Drying of apricot using ambient air, solar water collector assisted drying system and oslar air collector assisted drying system, *Çukurova. J. Agric. Food Sci. 37(2):*198 - 210, doi:10.36846/CJAFS.2022.87

Ibrahim,D *,(2004,November) Sun drying of figs: an experimental study department of chemical engineering, *Yildiz Technical University, 34210 Esenler, Istanbul, Turkey.*

Chua, J.K, Chou,S.K, (2003), Low-cost drying methods for developing countries, *Food Sience& Technology, 14,* 519-528. https://doi.org/10.1016/j.tifs.2003.07.003.

Mavis, O.A, Ibok, N., Firibu, K.S, Kingsly, A. (2018, September), Physicochemical and nutritional characteristics of solar and sun-dried tomato powder, *Journal of Food Research*, DOI: 10.5539/jfr.v7n6p1.

Wan,R, Wan D, (2008), Fluidized Bed Dryers — Recent Advances, *Advanced Powder Technology, Volume 19, Issue 5*, 403-418.https://doi.org/10.1016/S0921-8831(08)60909-7

Daniel, P. C, Daniel, A.B, Lucas,M, Eduardo,H.T, Guilherme,L.D, (2016), Spouted bed drying of papaya seeds for oil production , *LTW Food Sience and Technology,* 852-860.

Okos, M.R., Narsimhan, G., Singh, R.K., Witnauer, A.C., (1992), Food dehydration: In Heldman, *D.R., Lund, D.B., edn. Handbook of food engineering Marcel Dekker,* New York.

Jairaj, K.S, Singh, S.P, Srikant, K. A, (2009, June), Review of solar dryers developed for grape drying, *Solar Energy,* 1698-1712, DOI: 10.1016/j.solener.2009.06.008.

Taştan, M., (2019). A Real-Time Remote Monitoring and Control Application with a New Generation IoT Controller for Smart Home Applications. *Journal of Suleyman Demirel University Institute of Science .23(2), 481-487.*

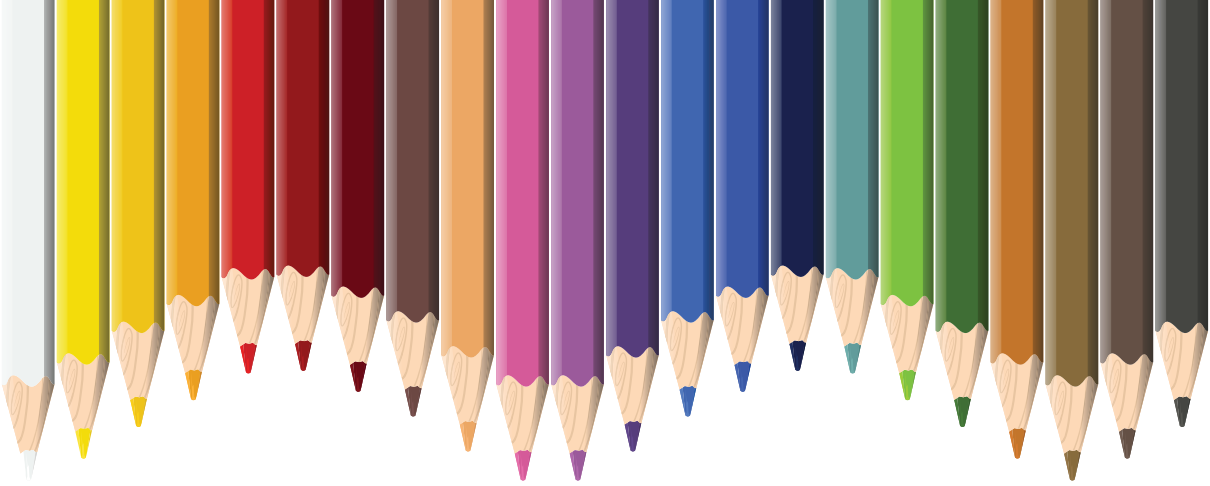

Chapter 15

LOCAL OPTIMIZATION OF INLET AIR COOLING COGENERATION CYCLES

Rabi KARAALI[1]

1 Assoc.Prof.Dr.:Department of Mechanical Engineering, Bayburt University, 69000 Bayburt, Turkey. rabikar@gmail.com ORCID No: 0000-0002-2193-3411

INTRODUCTION

The transmission, production, use and storage efficiencies of energy are very important in today's competitive world as they directly affect the cost. Losses in the production, use, storage and transmission of energy are the most important factors that increase inefficiency. The most important ways to reduce losses are cogeneration (producing two types of energy, more electricity and heat, in the same system and at the same time), trigeneration (producing three types of energy, more electricity, cooling and heat, in the same system and at the same time), using efficient devices in cycles and using non-conforming equipment. are working conditions [1, 2, 3]. Today, the most common and most consumed energy types in industry and daily life are electricity and heat. It is necessary for high efficiency to produce these with cogeneration, not in conventional systems. Conventional systems produce heat and electrical energy separately, so their efficiency is lower. Energy and exergy efficiency in cogeneration plants is around 30% higher than conventional plants [4, 5, 6].

The most critical step in the design of the thermal systems is to determine the design characteristics. What is required of the system and to provide them numerically. The design that meets all the required specifications is workable design. The best of the workable designs is called optimal design. This means applying the best of various alternative considerations such as reliability, optimal cost, weight. Generally, the system that minimizes the cost is considered optimal. It is sometimes impossible to determine the right optimum. However, the design closest to the optimum can be determined. The design that provides the greatest return from the fuel supplied for the thermal system is called better design. The thermal systems are complex, since each device is complexly affected by the other, and the maximum efficiency of a device can minimize the efficiency of another device. Which can reduce the efficiency of the entire system. Therefore, the optimization of the entire system should be performed instead of each devices optimization [7, 8, 9].

Mathematical optimization of a design reveals the conditions under which that design works best. But mathematical optimization must be made and compared in other designs, as it does not demonstrate the superiority of the solution that other designs bring to the problem. Avoiding unnecessary processes, using heat and power in the form of cogeneration, avoiding throttle valves as much as possible, using turbines with more than 100 kW power generation, avoiding mixing of different pressure, temperature and chemical compositions in combustion are crucial. It is recommended to reduce the use of or avoid unnecessary combustion, preheating before combustion, the use of the most efficient devices, reducing the heat transfer to the cold environment or environment. The second law of thermodynamics is applied to process-specific design paths, but this is not sufficient because

it does not indicate unnecessary investments, so thermoeconomic analysis must be performed [10, 11].

The relationship between emissions and performance has been demonstrated by various studies in the literature, so many different and separate objective functions have been set up for energy system design and optimization has been made. With the optimization of multi-purpose functions, more advantageous results have been obtained in the literature than the optimization of single-purpose or dual-purpose (such as energy and economical) functions [12, 13]. When the amounts of carbon dioxide and nitrogen oxide emissions are associated with the cost, a function for environmental impact can be established and its optimization can be studied. Thus, the effect of environmental and economic conditions on performance was also examined. In the literature, there are studies that define the ecological function as the ratio of the power obtained to the entropy produced and the economic function as the ratio of the obtained power to the total costs. According to Rosen (2008), some researchers have used the concept of sustainability instead of the environmental factor in extended exergy-based economic methods. For example, they suggested using the disciplines of thermodynamics and economics together to obtain exergy-based indicators of sustainable development (development). Since these methods take into account the decreasing resources and increasing pollution situations, they can offer different alternatives for industrial companies to achieve their environmental goals [12, 13]. There are many studies in the literature that make exergy-based economic evaluations on thermal systems [12, 13]. Öztürk et al., (2006) explained how to optimize the hot water pipe radius and insulation thickness with minimum exergy loss and minimum cost optimization with thermoeconomic methods [14].

There are studies on thermoeconomic optimization of power plants based on nuclear oil and coal, and some of them will be mentioned in this thesis when appropriate. M.A. Rosen and I. Dincer (2003) proposed a new method based on exergy, cost, energy and mass quantities, which they briefly called EXCEM analysis in their article [15]. With the help of the Aspen Plus computer program, this new method has been applied on the computer for various processes (electricity, hydrogen fuel cells). In their article, they described the EXCEM analysis they developed after discussing the prices of materials and flows containing energy and exergy. Accordingly, while different amounts of exergy, energy, cost and mass ratios enter the system, they leave the system at different rates. The balance equations of these quantities are obtained by subtracting the sum of the inputs and the produced and the consumed, and the accumulated amount is obtained. For continuously open systems with continuous flow, the amount accumulated is zero. For an open or closed system, the accumulated mass is obtained when the mass leaving the incoming mass is subtracted, and the entropy

accumulated is obtained if the entropy produced is subtracted from the sum of the entropy produced by the input entropy [15].

Likewise, if the energy or exergy is subtracted from the input energy or exergy, the accumulated energy or exergy is obtained, and if the costs are subtracted from the sum of the input and produced costs, the accumulated costs are obtained. The costs produced here are the costs spent for the formation of the process in the system and the repair and maintenance operation [15]. Although values other than costs are defined by scientific functions and scientific relations, costs are subjective and depend on the type and purpose of the system and other economic factors. They also gave examples of various devices in their articles. For example, the incoming costs for a pump are fluid cost and electricity cost (assuming adiabatic), and the outgoing cost is the sum of the flow and electricity costs with the produced cost [15].

Ballı (2008) evaluated the performance of cogeneration plants by using energy, availability (exergy) and exergeoeconomic analysis methods in his doctoral thesis. In this study, in which a cogeneration plant (combined heat power system (high and low pressure turbines are added to the sample cycle) (CHP)) and a dual fuel (gas-diesel) diesel engine trigeneration plant established in Eskişehir, the exergy and thermoeconomic analysis of both plants is analyzed. made in detail for a certain working situation. In addition, the energy performance evaluation parameters for both systems are energy efficiency, relative energy loss rate (the rate of energy loss in the device to the energy loss in the whole system), fuel energy consumption rate (the ratio of energy loss in the device), energy loss rate, energy improvement potential, the economic value of energy loss, power-to-heat ratio and fuel energy saving ratio were calculated [16]. Exergy efficiency, relative exergy loss rate (the ratio of exergy destruction and loss in the device to exergy destruction and loss in the whole system), fuel exergy consumption rate, incoming exergy loss rate, exergy improvement potential, economic value of exergy loss, power heat exergy rate and exergy performance evaluation parameters are among the exergy performance evaluation parameters [16].

From the exergetic performance evaluation parameters, the average unit costs of fuel and product, exergy loss costs, exergy destruction costs, relative cost difference (the difference between the cost of entering and leaving the device) and exergetic factor were calculated (Ballı, 2008). Absorption refrigeration unit is not explained in detail and system analysis is made by considering it as a single device (as in this thesis). According to the establishment design of the cogeneration plant, while the energy efficiency is 50.04%, the energy efficiency of the trigeneration plant is calculated as 40.78% under current operating conditions and 58.89%. While the exergy efficiency was 42.21% according to the design of the establishment, it was calculated as 39.22% under the current operating conditions, and the exergy efficiency of the trigeneration plant was calculated as 36.13% [16].

MATERIAL AND METHOD

As shown in Figure 1, high pressure compressed air from the compressor are combusted with methane in a combustion chamber. At the outlet of the combustion chamber high temperature exhaust gases are given to the gas turbine to convert some of its energy into electrical energy. After gas turbine some of the exhaust gases energies are used to produce cooling in an absorption cooling device to cool the inlet air of the system. After that, most of the remaining energy of the exhaust gases are used in the waste heat recovery device to produce steam. The combustion equation is taken as follows [17, 18, 19].

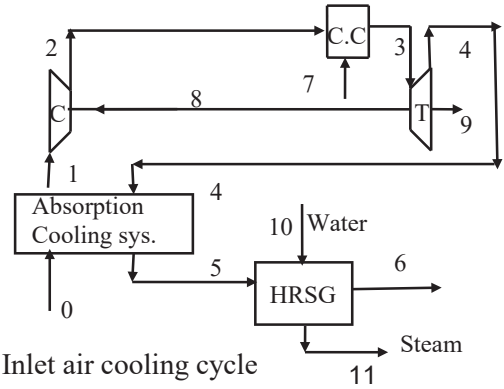

Figure 1. Inlet air cooling cycle

$$\overline{\lambda}\, CH_4 + (0.7748\, N_2 + 0.2059\, O_2 + 0.0003\, CO_2 + 0.019\, H_2O \rightarrow (1 + \overline{\lambda})(X_{N2}N_2 + X_{O2}O_2 + X_{CO2}CO_2 + X_{H2O}H_2O)$$

In this study, T_0 = 298.15 K and P_0 = 101.3 kPa, pressure loss in the combustion chamber 5% the saturated steam pressure for heat exchanger at 2000 kPa, gas turbine net electrical power 30000 kW, combustion chamber fuel mass flow m_f = 1.64 kg/s methane was taken. The thermodynamic equations are given in Table 1 and Table 2 of the system [10, 11, 13].

Since there is no specific general method for finding the optimum value, there are certain methods available for each type of problem and can be classified as follows. One dimensional (univariate) unconstrained, multidimensional (multivariable) unconstrained and multidimensional (multivariable) constrained optimization problems. One-dimensional (univariate) unconstrained optimization problems are solved with methods that are analytical method, region elimination (equal spacing region elimination, half, gold region, fibonacci) methods, polynomial approximation (quadratic, cubic) methods, derivative evaluation (derivative

half, steeping descent), Newton Ralphson, finite differences Newton, secant) [10, 11, 13].

Table 1. Masses, energies and entropies equations for the devices of the inlet air cooling cycle [10, 11, 13].

Devices	Mass	Energy	Entropy
Compressor	$\dot{m}_1 = \dot{m}_2$	$\dot{m}_1 h_1 + \dot{W}_C = \dot{m}_2 h_2$	$\dot{m}_1 s_1 - \dot{m}_1 s_2 + \dot{S}_{gen,C} = 0$
HRSG	$\dot{m}_5 = \dot{m}_6$ $\dot{m}_{10}$ $= \dot{m}_{11}$	$\dot{m}_5 h_5 + \dot{m}_{10} h_{10}$ $= \dot{m}_6 h_6 + \dot{m}_{11} h_{11}$	$\dot{m}_5 s_5 + \dot{m}_{10} s_{10} - \dot{m}_6 s_6$ $- \dot{m}_{11} s_{11} + \dot{S}_{gen,HRSG} = 0$
Combustion Chamber	$\dot{m}_2$ $+ \dot{m}_{10}$ $= \dot{m}_3$	$\dot{m}_2 h_2 + \dot{m}_7 h_7$ $= \dot{m}_3 h_3$ $+ 0.02 \dot{m}_7 LHV$	$\dot{m}_2 s_2 + \dot{m}_7 s_7 - \dot{m}_3 s_3$ $+ \dot{S}_{gen,CC}$ $= 0$
Turbine	$\dot{m}_3 = \dot{m}_4$	$\dot{m}_3 h_3$ $= \dot{W}_T + \dot{W}_C + \dot{m}_4 h_4$	$\dot{m}_3 s_3 - \dot{m}_4 s_4 + \dot{S}_{gen,T} = 0$
Overall Cycle	$\bar{h}_i = f(T_i)$ $\bar{s}_i = f(T_i, P_i)$ $\dot{m}_{air} h_{air} + \dot{m}_{fuel} LHV_{CH4} - \dot{Q}_{Loss,CC} - \dot{m}_{eg.,out} h_{eg.,out} - \dot{W}_T$ $- \dot{m}_{steam}(h_{water,in} - h_{steam,out}) = 0$ $\dot{Q}_{Loss,CC} = 0.02 \dot{m}_{fuel} LHV_{CH4}$		

Table 2. Exergies and exergy efficiencies equations of the devices of the inlet air cooling cycle [10, 11, 13].

Component	Exergy Equation	Exergy Efficiency
Compressor	$\dot{E}_{D,C} = \dot{E}_1 + \dot{W}_C - \dot{E}_2$	$\eta_{ex,C} = \dfrac{\dot{E}_{out,C} - \dot{E}_{in,C}}{\dot{W}_C}$
HRSG	$\dot{E}_{D,HRSG} = \dot{E}_5 - \dot{E}_6$ $+ \dot{E}_{10}$ $- \dot{E}_{11}$	$\eta_{ex,HRSG}$ $= \dfrac{\dot{E}_{steam,HRSG} - \dot{E}_{water,HRSG}}{\dot{E}_{in,exhaust,HRSG} - \dot{E}_{out,exhaust,H}$
Combustion Chamber	$\dot{E}_{D,CC} = \dot{E}_2 + \dot{E}_7 - \dot{E}_3$	$\eta_{ex,CC} = \dfrac{\dot{E}_{out,CC}}{\dot{E}_{in,CC} + \dot{E}_{fuel}}$
Turbine	$\dot{E}_{D,T} = \dot{E}_3 - \dot{E}_4 - \dot{W}_C$ $- \dot{W}_T$	$\eta_{ex,T} = \dfrac{\dot{W}_{net,T} + \dot{W}_C}{\dot{E}_{in,T} - \dot{E}_{out,T}}$
Overall Cycle	$\dot{E} = \dot{E}_{ph} + \dot{E}_{ch}$ $\dot{E}_{ph} = \dot{m}(h - h_0 - T_0(s - s_0))$ $\dot{E}_{ch} = \dfrac{\dot{m}}{M}\left\{\sum x_k \bar{e}_k^{ch} + \bar{R} T_0 \sum x_k \, ln x_k\right\}$ $\eta_{ex} = \dfrac{\dot{W}_{net,T} + (\dot{E}_{steam,HRSG} - \dot{E}_{water,HRSG})}{\dot{E}_{fuel}}$	

Multidimensional (multivariate) unconstrained optimization problems are solved by random search, green search, simplex (flexiblepolyhedral), univariate search, steeping descent, Newton, conjugate directions (conjugate directions) methods. Multidimensional constraint optimization problems are solved by linear programming, simplex, NLP programming, penalty, Lagrange multipliers, integer programming (enumeration), branch and bound. Apart from all these methods, many other methods are available in the literature [10, 11, 13]. Design optimization of thermal systems is the most frequently occurring and examined case of multivariate constrained nonlinear programming. There are n independent variables and m constraints, and the objective function consists of these variables. If the equality of constraints m can be eliminated or expressed in the objective function, then the derivative of the objective function can be optimized by equalizing to zero. Since only a few simple problems can be solved with this simple method, other methods are used in complex systems [10, 11, 13].

Lagrange, iterative quadratic, iterative linearization, penalty function, and direct search methods are used in constrained nonlinear programming problems. In general problems, iterative quadratic, iterative linearization and penalty function are better than the other methods. In the Lagrange method, the constrained optimization problem is transformed to the unconstrained problem by obtaining the extended objective function by multiplying it with the Lagrange multiplier and adding it to the objective function. The resulting extended objective function is derived from the variables, Lagrange multiplier and redundancy variable, and then equalized to zero and solved. Most of the time, nonlinear equations of thermal systems are complex and numerous, and cost equations make them even more complex, so there are no values that equalize derivatives to zero [8, 10, 11, 13].

The iterative quadratic programming method is the minimization of the constrained second order function, linear equality or inequality. Iterative linearization method is the method of solving nonlinear equations by converting to linear equations by one of the linear programming methods. The penal function method is a method of minimizing the constrained equation. Among the direct search methods (random search, sequential simplex and cyclic coordinate methods are the most important), the Box's complex method, which is a kind of simplex direct search method, is one of the most effective methods and in reference [6] was used accordingly [8, 10, 11, 13].

The first stage, the system and the sub-systems that affect the performance of the system, needs to be clearly defined. Accurate determination of the boundaries of subsystems by dividing complex systems into subsystems is important for subsystem optimization. The optimization criterion is characterized by minimum or maximum as it can be economic (such as minimum cost), technological (such as maximum efficiency) or

environmental (such as minimum pollution). In practice, multiple optimization criteria are identified and the best design and operating conditions are sought. When more than one criteria are identified, these criteria may contradict or match each other. In case of contradictory criteria (such as minimum pollution, maximum power or efficiency), one and the most important one is selected and the others are considered as parameters or constraints of the problem and optimization is performed [8, 10, 11, 13].

In the optimization problem, the variables are four types: dependent, independent, decision variables and parameters. The independent variables should include all variables that affect performance and cost, should not include insignificant and detailed variables, and should be chosen to ensure that the independent variables subject to change are separate from each other. In the optimization study, only the decision variables can be changed, and the parameters and independent variables cannot be changed for the model being compared or for a particular model. Dependent variables are the variables obtained as a result of the mathematical model calculation. The mathematical model is the definition of the system as functions and equations, and includes and identifies all independent variables and relationships that affect performance criteria. It also includes objective function, equality and inequality constraints to be maximized or minimized. The objective function can be linear or nonlinear, with one or more decision variables, continuous or with discontinuity in some parts [8, 10, 11, 13]. The constraints may be linear or nonlinear, but have nonlinear properties in the cogeneration systems.

The objective in optimization is to get ideas for improving the cycle rather than finding the mathematical global maximum or minimum. As the demand for steam and electricity changes, it is not practical to use the global maximum or minimum to be found in a constant production quantity, since there are varying quantities of production rather than production, and also because the temperature, pressure and humidity of the air constantly change. However, finding the optimum points in thermoeconomic optimization is important in terms of giving an idea for improvement as it will indicate the optimum working area [8, 10, 11, 13].

There are many advanced computer programs in the market for the analysis and optimizations. In sequential module approach programs, the devices are combined by selecting from the menu, the program is run by giving input values and the results are obtained. The user cannot see the mathematical and thermodynamic models, equations, and relationships between the devices. Programs such as ASPEN PLUS, PROCESS, CHEMCAD are such programs. The mathematical model of each device is established in hundreds of equations by solving each system in equations approaching programs and these are solved for common variables. SPEED UP is an example of such programs. Here, mathematical and economic models of the systems have been developed and solved in VISUAL

FORTRAN programming language by using hundreds of linear and nonlinear equations as separate sequential modules and synthesis of these two types. Conventional optimization methods can be used to optimize very simple cycles (for example according to the first law), but complex systems cannot be optimized with these methods. If the cost and performance calculations will be involved in optimization, even the simplest cycle is impossible to do with traditional optimization methods [8, 10, 11, 13].

RESULTS

Figure 2 shows the effects of compression rates on electric and heat power with various combustion temperature for inlet air cooling cogeneration cycle. Increasing compressor ratio decreases the heat power, however increases the electric power. The reason of it is that, as the compressor rate increases, since the combustion chamber outlet temperature is not taken constant, the turbine outlet temperature decreases at high pressure, which reduces the amount of heat obtained in the waste heat recovery device (HRSG). It can be understood from the slope of the obtained curves that the network to be obtained will decrease as the higher values are reached. This is more clearly seen in Figure 3 that the effects of excess air coefficient on exergetic efficiency for various compression rates are given. In Figure 3, this can be seen that the exergy efficiency of the system increases as the compression rates increases. The inlet air cooling cycle reaches maximum efficiency at excess air rate coefficient of 2–2.5 and then decreases with the increasing of the excess air rate. As the compressor compression ratios of the inlet air cooling cycle increase, the exergy efficiency going to be maximum at lower excess air ratios.

In Figure 4, the effects of excess air coefficient on fuel energy saving ratio for various compression ratios are given. Fuel energy saving ratio is a comparison of the fuel required for the given loads of heat and electricity in the cycle with conventional system. Fuel energy saving ratio measures the extent of fuel savings in a cogeneration plant. Increase in the rate of the FESR gives information about the electrical increases of the cycle according to the law of the 1. For the classical cycles boiler efficiency are $\eta_B = 0.9$ and electrical efficiency are $\eta_{el} = 0.4$ accepted [2, 3].

$$FESR = \left(\frac{Q}{\eta_B} + \frac{W}{\eta_{el}} - Q_{fuel}\right) / \left(\frac{Q}{\eta_B} + \frac{W}{\eta_{el}}\right)$$

As can be seen in Figure 4, increasing compressor ratio increases the FESR. The inlet air cooling cycle reaches a maximum of fuel energy saving ratio at excess air rate coefficient of 2–2.5 and then decreases with increasing excess air rate.

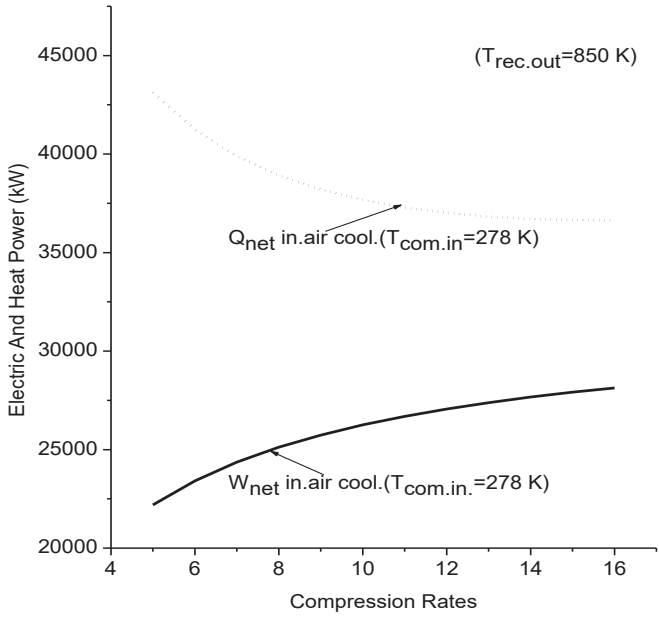

Figure 2. Effects of compression rates on electric and heat power with various combustion temperature for inlet air cooling cogeneration cycle. m_{fuel}=1,64 kg/s, m_{air}=91,3 kg/s, ex.air rate=2,5, $\eta_{isC}=\eta_{isT}$=0,86, $T_{rec.out}$=850 K, T_{steam}=485,57 K, $T_{eg.}$=426 K.

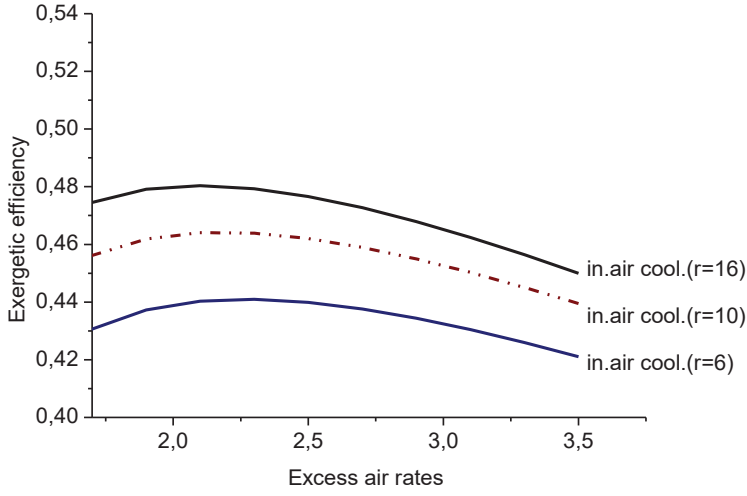

Figure 3. Effects of excess air coefficient on exergetic efficiency for various compression rates.

Since the efficiency increases rapidly as the compression ratio for the compressor is increased, but because it can be maximum 16, the

compression ratio is maximum 16 because of this limitation. Since the increase in the isentropic efficiency of the compressor and turbine increases the efficiency, they should be close to the maximum values of ηsc <0,90 and ηst <0,92. For this, these values will be taken as ηsc = 0.88 and ηst = 0.90. As the combustion chamber outlet temperature increases, the efficiency of the system will increase and at the same time this temperature is the gas turbine inlet temperature and the temperature that the gas turbine blades can withstand is 1550 K, the combustion chamber outlet temperature will be maximum around 1550 K. Parameters for local optimization can be listed as follows [6, 7, 8]. (These values are also taken in this study.)
1-Obtained net power (turbine power and thermal power),
2- Temperature, pressure and flow rate of the obtained saturated steam.
3-Air compressor inlet temperature T_1 = 298,15 K (25 ^{0}C) and pressure P_1 = 1,013 bar (1atm) and air molar components 77.48% N_2, 20.59% O_2, 0.03% CO_2, 1%, 9 H_2O (g).

As dependent variables, exhaust products are the energy used by the compressor, the power and pressure from the turbine and the pressure and temperature in the flow lines. These are air compressor outlet pressure and temperature, combustion chamber outlet pressure and temperature, gas turbine outlet pressure and temperature and waste heat recovery device exhaust outlet temperature [7, 8].

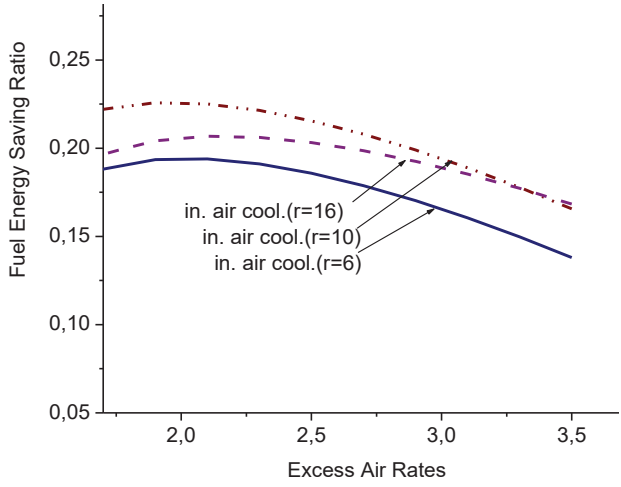

Figure 4. Effects of excess air coefficient on FESR for various compression ratios.

The maximum yield values obtained are local values when the modified nonlinear simplex direct search method is applied to achieve this power by taking the net power constant (30 MW and 14 kg / s steam). If this search is performed in all operating conditions where the power is constant and the cycles can operate, the values obtained are global maximums and the

maximum efficiency value that the cycle can output. These maximum efficiency values should be sought for all compressor compression rates in which the systems can operate. The iteration steps of the thermodynamic local optimizations of the inlet air cooling cycle are given in Table1.

Table 3. Iteration for local maximum efficiency values for constant power (30 MW and 14 kg/s steam)

Air Mass Rate (kg/s)	T_4 (K)	Energy Efficiency	Exergy Efficiency	Steam Mass Capacity (Kg/s)	Electric Power (kW)	Fuel Mass Rate (kg/s)
91.3[1]	1272	0.7074	0.4609	14.17	26212	1.64[1]
91.3[2]	1334	0.7074	0.5032	12.16	31628	1.64
91.3[3]	1334	0.7365	0.5137	13.15	31628	1.64
86	1373	0.7446	0.5143	13.53	31322	1.64
82	1405	0.7507	0.5142	13.85	31025	1.64
78	1440	0.7568	0.5135	14.19	30657	1.64
78	1422	0.7538	0.5139	13.68	30094	1.6
78	1426	0.7545	0.5138	13.81	30236	1.61
76	1445	0.7577	0.5134	13.98	30037	1.61
75.7	**1447**	**0.758**	**0.5133**	**14[4]**	**30000**	**1.609**

[1] η_{sc}=0.86 and η_{st}=0.86 and r=10
[2] η_{sc}=0.88 and η_{st}=0.90 and r=16 is taken
[3] For exhaust outlet temperature 400 K
[4] Steam mass rate 14 kg/s

The global maximum yields are the values found when the power is not taken constant and all the operating conditions in which the cycles can work are taken into consideration. The efficiency decreases when the combustion chamber outlet temperature is increased. This is due to the fact that the maximum efficiency is achieved at a certain air fuel ratio, which decreases when the air fuel ratio value is reduced to increase the combustion chamber outlet temperature.

CONCLUSION

As the compressor compression ratio increases in the specified conditions and range, the work obtained increases, but the heat energy obtained decreases. As the excess air coefficient of the inlet air cooling cogeneration cycle is higher than 3.5, the network starts to decrease. As the compression rate increases, the heat power of the system decreases (as more electrical power is obtained). Since the increase in the air excess rate decreases the combustion chamber outlet temperature, the temperature of the exhaust at the turbine outlet decreases and the amount of heat to be transferred in the waste heat recovery device decreases. The system's exergy

efficiency increases as the compression rate increases. The inlet air cooling cycle reaches maximum efficiency at a rate of the excess air rate of 2–2.5 and then decreases with increasing the excess air rate. As the compressor compression ratios of the inlet air cooling cycle increase, the exergy efficiency is going to be on maximum at lower excess air rates. When the change in the electric power of the cycle with the excess air coefficient is examined in the changing compressor inlet air temperatures, the power obtained from the turbine increases as the work spent in the compressor decreases as the inlet air temperatures decrease.

In the literature, cycles are optimized for a given power, which gives local optimizations. However, the global optimum is obtained when the optimum search is made considering all operating conditions in which the cycle can operate.

REFERENCES

[1]Keven, A. (2023). Performance analyses of detonation engine cogeneration cycles. Open Chemistry, 21;1 – 9. DOI: 10.1515/chem-2022-0313.

[2]Karaali R., Keven, A. (2022). Evaluation of four different cogeneration cycles by using some criteria. Applied Rheology, 32;122 – 137. DOI: 10.1515/arh-2022-0128

[3]Keven, A., Karaali, R. (2022). Analysis of Some Tribological Properties of Hazelnut Oil in Gasoline engines. *Erzincan University Journal of Science and Technology*.15;75–83.

[4]Keven, A. (2023). Exergy Analyses of Vehicles Air Conditioning Systems for Different Refrigerants. International Journal of Computational and Experimental Science and Engineering, 9; 20 – 28. DOI: 10.22399/ijcesen.1258770

[5]Keven, A. (2023). Exergetic performance analyses of three different cogeneration plants. Open Chemistry, 21;1 – 13. DOI: 10.1515/chem-2022-0295.

[6]Keven, A., Karaali, R. (2015). Investigation of an Alternative Fuel for Diesel Engines. *Acta Physica Polonica A*, 128(2B);282 – 286. DOI:10.12693/APhysPolA.128.B-282

[7]Peters MS, Timmerhaus KD, West RE. (2003). *Plant design and economics for chemical engineers.* Mc Graw Hill chemical engineering series. 5th ed.

[8]Horlock, J.H. (1997). *Cogeneration-Combined Heat and Power (CHP). CRİEGER Pub.,Florida*

[9]Jaluria, Y. (2008). *Design and Optimization of Thermal Systems*.2. ed. *CRC Press*, New York.

[10]Karaali, R. (2010).Thermoeconomic Optimization of Cogeneration Power Plants, PhD Thesis, Kocaeli Univ.

[11]Bejan, A., Tsatsaronis, G., Moran, M. (1996).*Thermal Design and Optimization*, *Wiley Pub,* New York.

[12]Rosen, M.A. (2008). A Concise Review Of Exergy-Based Economic Methods. *3rd IASME/WSEAS Int. Conf. On Energy & Environment,* University Of Cambridge, UK,

[13]Rosen, M.A. Dincer, I. (2003). Exergy-Cost-Energy-Mass Analysis of Thermal Systems and Processes. *Energy Convers. Mgmt.* 44, 1633-1651.

[14]Öztürk, İ.T., Karabay, H., Bilgen, E.(2006). Thermo-economic Optimization Of Hot Water Piping Systems: A Comparison Study. *Energy* 31, 1758-1771, Elsevier Science Ltd.

[15]Rosen, M.A., Dincer, I. (2003). Exergy-Cost-Energy-Mass Analysis Of Thermal Systems And Processes. *Energy Convers. Mgmt.,* 44, 1633-1651, Elsevier Science Ltd.

[16]Ballı, Ö. (2008). Kojenerasyon Sistemlerinin Enerji, Kullanılabilirlik (Ekserji), ve Ekserjoekonomik Analiz Yöntemleri Kullanılarak Performansının Değerlendirilmesi. Doktora Tezi, *Eskişehir Osmangazi Üniversitesi, Fen Bilimleri Enstitüsü*, Eskişehir.

[17]Karaali, R., and Ozturk, I.T. (2017). Efficiency improvement of gas turbine cogeneration systems. *Tehnicki vjesnik - Technical Gazette*, 24, Suppl.1 p:21-27. DOI: 10.17559/TV-20140509154652

[18]Karaali, R., and Ozturk, I.T. (2017). Effects of Ambient Conditions on Performance of Gas Turbine Cogeneration Cycles. *J. of Thermal Science and Technology*, Volume 37 No. 1, pages 93-102.

[19]Karaali, R., and Ozturk, I.T. (2017). Performance Analyses of Gas Turbine Cogeneration Plants. *J. of Thermal Science and Technology*, Volume 37, No. 1, pages 25-33.

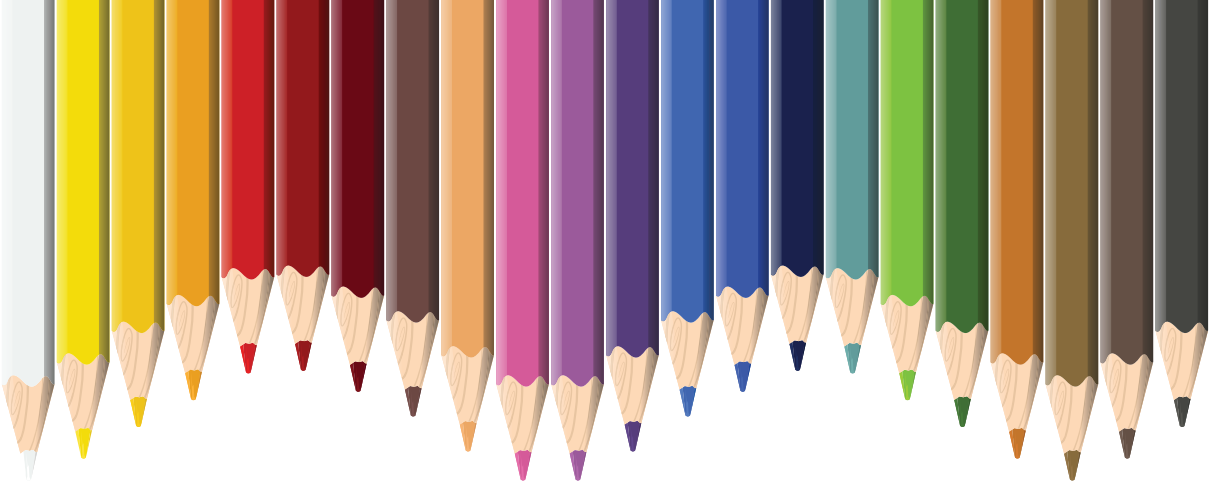

Chapter 16

DIGITAL AGRICULTURE APPLICATIONS OF SUGAR BEET PRODUCTION

Ayten YILMAZ YALÇINER[1]
Tijen ÖVER ÖZÇELİK[2]
Zeynep Banu YAMAN[3]

1 Doç. Dr. -0000-0001-8160-812X Sakarya Üniversitesi, Mühendislik Fakültesi, Endüstri Mühendisliği Bölümü
2 Doç. Dr 0000-0002-9614-8119 Sakarya Üniversitesi, Mühendislik Fakültesi, Endüstri Mühendisliği Bölümü
3 End. Müh. - 0000-0002-5860-0530, Sakarya Üniversitesi, Mühendislik Fakültesi, Endüstri Mühendisliği Bölümü

1. INTRODUCTION

Regardless of the level of development of the food and agriculture sector, it affects an area ranging from the social and economic systems of countries and societies to nutrition and health systems. This sector is not only limited to meeting the food demand but also has a position that meets the input needs in many fields. It is an economically critical sector, such as providing labor to the industry and service sector and contributing to rural development and growth.

With the rapidly increasing population, a long-term sustainable solution is needed for nutrition, which is a basic need. Future population growth projections made by the United Nations every two years are estimated to be 9.7 billion in 2050 and 10.9 billion in 2100 at the 95% confidence interval. To meet the nutritional needs of this population, it is foreseen that today's production capacity will increase by 70%. The projected population growth graph is given in Figure 1 (PM, 2020). The rapid increase in the world population, the global epidemic, the employment of agricultural workers causes problems in the farming sector and food. Naturally, with the rise in population, there is a need for more food globally. The agricultural sector, which has an increasingly strategic place, is experiencing severe difficulties meeting this demand.

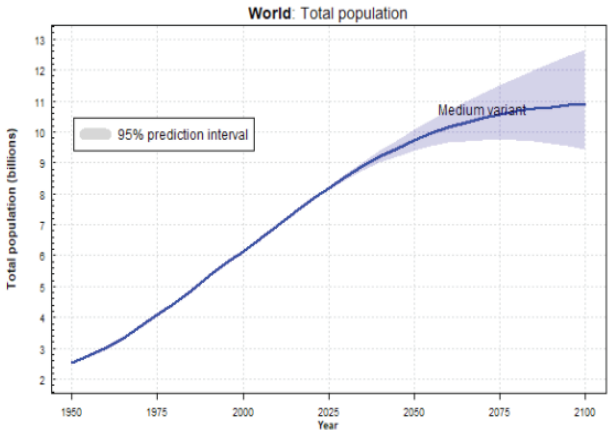

Figure 1. Population growth graph predicted with 95% confidence over the years

On the one hand, the world population, on the other hand, the increase in urbanization increases the demand for food. Agricultural areas gradually decrease due to soil erosion, deforestation, misuse, overgrazing, improper crop rotation, and unbalanced fertilizer use. In addition, climate changes cause a decrease in yield and production in agriculture. Deterioration of arable land in the world over time and reducing usable water resources have caused the eyes

to turn to agriculture and climate changes. Even the scenarios where there may be wars over food and water in the future reveal the issue's importance. In addition to these adverse effects, it is expected that the rate of agricultural land that can be cultivated will decrease with the climate changes. In the study carried out, it was emphasized that 44% to 57% of all greenhouse gas emissions originate from the global food system, while 11%-15% of them are caused by agriculture. Most of these emissions come from industrial inputs such as chemical fertilizers and gasoline to power tractors and irrigation machines.

The continuation of this increase in harmful gas emissions accelerates climate change, and the future is being taken away from us gradually. In Figure 2, the contribution of Grain's industrial food system to the climate crisis is modeled (Grain, 2020).

The difficulties/problems in meeting the global food need with the current agricultural production model have accelerated the establishment and spread of the technology-intensive production model in agriculture.

Kaya, 2019 also stated that agricultural production and food supply are decreasing in an environment where the world population is increasing. There is a concern that a global food crisis may occur. Each country should take measures to meet its domestic consumption and increase production permanently.

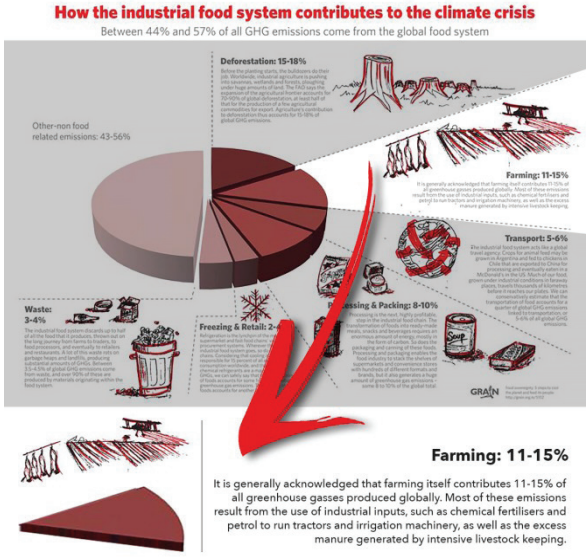

Figure 2. Contribution of the industrial food system to the climate crisis.

The need for sustainable agriculture and food systems in the agricultural sector, which has more strategic importance with each passing day, has made

integration with technology a necessity. Artificial intelligence and digital technologies in many different production processes such as irrigation, spraying, fertilization, and harvesting increase productivity. Collecting and analyzing the data in these processes and performing the labor with autonomous systems affect the costs positively in agriculture and is seen as one of the most effective solutions in meeting the increasing demands for food and agricultural workers (Kırkaya, 2020).

In this section, the issue of digitalization in the agriculture and food sector is discussed, and an example of an application supported by artificial intelligence in sugar beet production is presented.

2. DIGITAL FARMING, AGRICULTURE and FOOD INDUSTRY

In order to ensure digitalization in today's rapidly changing world dynamics, high technologies that are effective in every sector and field must be used (Korkusuz Polat and Baran, 2022) Events such as limited natural resources, climate change, and food waste will create pressure factors as compelling factors in meeting the demands expected to increase in the future with traditional methods used from past to present. To increase production, it is necessary to use technology to eliminate the factors that create this pressure. This means, in the most up-to-date terms, to produce with intelligent agriculture (De Clercq et al., 2018). The vehicles used at every stage of agricultural production are equipped with sensors, ensuring that the machines communicate with each other during the entire production process. With agricultural tools and fields equipped with sensors, it is aimed to maximize the yield by giving detailed information to the farmers on what field and what kind of fertilizer they should use, weather conditions, the amount of mineral and irrigation needed by the plant, the condition of the soil, and the estimated harvest time. In this way, producers have the opportunity to manage and observe the entire planting area with intelligent technology devices, minimize labor power and production input costs, and have the chance to obtain high-quality and high quantity products (Kahraman, 2017).

Agriculture, which is supported by every state in terms of its strategic importance in economic growth and development, is seen as an indispensable sector due to reasons such as feeding the country's population, contributing to national income and employment, meeting the sectoral raw material needs, and contributing to exports. It is even mentioned that among the economic development indicators of the countries, the agricultural production value of the country in question to meet its own food needs is added. (Doğan et al., 2015). Considering the share of Information and Communication Technologies (ICT) products in total exports and imports, it is seen that countries that have adapted to the Agriculture 4.0 process have high values in both exports and imports of these products. These countries have been able to increase their productivity with technology (ITB, 2018).

With this strategic importance of agriculture and the fusion of agriculture and information technologies, many new technical terms have started to be heard in daily life: such as sustainable agriculture, digital agriculture, and intelligent agriculture, precision agriculture, farm management software, and driverless (autonomous) vehicles. The most common use is smart agriculture; It includes an advanced system approach where control, electronics, computers, databases, and account information. The components of this technology include basic systems such as global positioning systems, geographic information systems, variable rate input applications, and remote sensing (Kaya, 2019).

The concept of "sustainable agriculture" refers to an economically, socially, and environmentally balanced agricultural system with the long-term protection of natural resources and ensuring their productivity. Sustainable agriculture aims to keep the economy alive, increase the quality of life of agricultural workers, and develop supportive activities by reducing the damage to the environment while increasing productivity in agriculture. The concept of sustainable agriculture should be considered as suggestions and strategies designed to solve the problems originating from industrial agriculture (Velten et al., 2015). The sustainability-themed work carried out by the United Nations Food and Agriculture Organization (FAO) ensures continuous development at the desired extent without disturbing the natural balance, where agricultural production resources are limited for the world. FAO's future work for the Sustainable Development and Sustainable Development Goals "2030 Agenda" consists of global issues given in Figure 3 (ASDG, 2017).

Figure 3. *Sustainable Development Goals for FAO 2030, More detailed information can be found in the referenced document.*

Sustainable agriculture; With the use of agricultural robots to achieve economic, social, and environmental goals, it is possible to facilitate agricultural operations and develop alternative solutions to problems that need

solution or improvement (Özgüven, 2019). Smart Agriculture practices are expected to play an essential role in overcoming these anticipated negativities. Smart Agriculture applications that came to the fore with Industry 4.0 components; reduce costs by making sustainable agriculture possible, support farmers' production activities, and offer solutions to the sustainability of food production in feeding an ever-increasing population. Examples of Agriculture 4.0 technologies can be given as drone technology, agricultural robots, irrigation automation, variable-rate fertilization systems, automatic animal milking-feeding systems, greenhouse air conditioning automation, prediction and early warning systems for pests, smart farm applications (Pakdemirli et al., 2021)

Thanks to Smart Agriculture, more efficient, productive, and sustainable agricultural production in terms of resources is possible. From the farmer's point of view, Smart Agriculture provides added value in better decision-making, more efficient business operations, and management. In this context, smart agriculture is associated with three technology areas. These; Management Information Systems, Precision Agriculture, and Agricultural Automation-Robotics. Thanks to Management Information Systems, healthy decision making is possible thanks to data collection, processing, storage, and dissemination activities necessary to fulfill the functions of a farm. At the same time, economic and environmental efficiency is ensured by managing spatial and temporal variability thanks to precision agriculture (Duman and Özsoy, 2019)

The main benefits of smart agriculture systems can be listed as follows; (ATP, 2019).

- Creating the conditions for sustainable production
- Reducing chemical input costs such as fertilizers and pesticides,
- Providing a high amount of quality products,
- Ensuring a more effective flow of information for business and breeding decisions, and
- Establishment of registration order in agriculture.

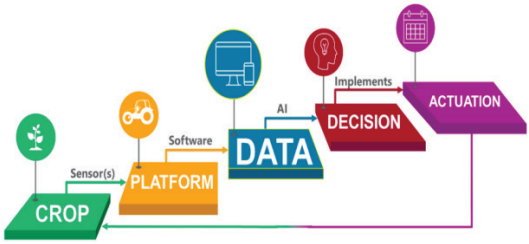

Figure 4. *Information-based management cycle for advanced agriculture*

The technologies that make smart agriculture possible and mentioned above are the components of Industry 4.0; the internet of things, cloud computing, big data, autonomous robots, and cyber-physical systems (Duman and Özsoy, 2019). Thanks to the current developments in knowledge-based management systems, smart agriculture becomes possible and enables it to grow exponentially. In Figure 4 (Saiz-Rubio and Rovira-Más, 2020), knowledge-based advanced, innovative agriculture management is modeled. In smart agriculture, producers can increase productivity and sustainability by taking advantage of objective information obtained through sensors in decision-making. With the help of robotic solutions, data-based intelligent farming techniques lay the groundwork for the sustainable agriculture of the future. This way, processes are reviewed, and crop fields are optimized while protecting the environment and saving money by improving food quality (Saiz-Rubio and Rovira-Más, 2020). Automated systems in agriculture and food can collect hundreds of data on a single food product in a matter of seconds and quickly evaluate it. For example, a system can collect and process data from hundreds of unique contents as they move rapidly on a conveyor belt; these systems can significantly reduce labor costs and waste (Di Vaio et al., 2020)

2.1. Agricultural Revolution & Agriculture 4.0

When the policies developed for agriculture are examined; Topics such as globally competitive and environmentally friendly agriculture, agricultural production, policies that support the security of supply, and dissemination of technology in agriculture are discussed. When these issues are examined; It is seen that meeting the food needs of the growing population, increasing production and efficiency, increasing the level of self-sufficiency in agricultural products, increasing agricultural incomes and providing continuity to the income provided, increasing the export of agricultural products, development of rural areas and ensuring the use of new technologies in agriculture (TCKB, 2018). When the process of industrial revolutions is examined, the aim is to provide convenience in production systems. In short, with the fourth industrial revolution-Industry 4.0, the agricultural sector has also been integrated into technology. It has passed through certain stages until its current state and has become the most advanced. Agriculture 4.0 is handled by starting from an Industry 4.0 component, especially the internet of things, and is defined as a primary sector. In this context, the studies carried out in the countryside were examined. From this point of view, the innovations in the industrial sector and the revolutions in agriculture in recent years can be listed as follows. The agricultural technology revolution started with Animal power, namely Agriculture 1.0, combustion engines defined Agriculture 2.0. By making GPS signals available to the public, precision farming has made Agriculture 3.0 possible in recent years (Marucci et al., 2017). Today, farm activities defined by Agriculture 4.0 are now connected to the cloud. Following the European agricul-

tural machinery from 2017, the next step is Agriculture 5.0 and is defined as businesses digitally integrated with robotics and some artificial intelligence of production processes (Zambon et al., 2019; Lee et al., 2015). In Figure 5. the revolutionary process in agriculture is visualized based on technology.

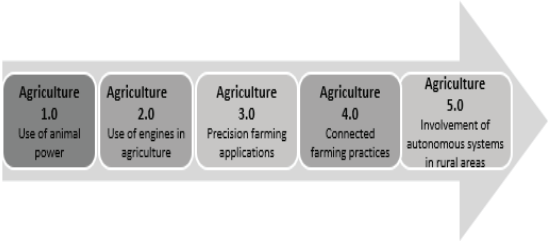

Figure 5. *Revolutionary Process in Agriculture*

The agricultural revolution is based on two key components.

✓ ***Biotechnology;*** GMO, CRSPR, Cell culture, tissue culture, etc.

✓ ***Information technologies and new generation mechanization;*** Agriculture 4.0 is the name given to this field, and it has two main components.

- *Digital agriculture;* Data collection
- *Smart farming-Precision farming/ (Smart/precision farming);* Precision Farming practices (Pakdemirli et al., 2021).

In the literature, there are many studies conducted with digital agriculture and food technologies.

With cloud-connected and camera mini uncrewed vehicles (drones), the entire farm and field can be monitored, and timely intervention can be made. This process reduces both work efficiency and costs. In addition to digitalization in the production process, innovations are also observed in production spaces. Vertical indoor agricultural production practices are becoming popular, serious investments are being made, and solutions are being sought to increase future food demand by growing plants in the desert and sea. It is aimed to increase productivity and reach the optimum production level in agriculture with an economy based on innovation and knowledge. (De Janvry and Sadoulet, 2010).

With Bosch's innovative technology, an intelligent irrigation management system has been installed for olive trees in Spain, and this system uses wireless sensors placed in trees to determine water needs. The aim is to reduce water consumption, to irrigate sensitively according to weather conditions and actual needs. Cloud-based solutions and connected microelectromechanical sensors are being developed (Kılavuz and Erdem 2019).

3. AGRICULTURE 4.0 and FOOD 4.0 TECHNOLOGIES

The concept of Industry 4.0 is a concept that expresses "together" that brings together technologies and "value chain" concepts (Lu, 2017). In this context, applying essential Industry 4.0 technologies (IoT, Artificial Intelligence, Robotics, Sensors, Blockchain, etc.) to the aforementioned sectors, similar technologies manifest themselves with practical applications under the central theme of Agriculture 4.0 and Food 4.0.

3.1. IoT and Big Data

Industry 4.0 connects all machines that can autonomously control themselves and each other along the created value chain through intelligent networks. The virtual object structure in this process is connected by the Internet of Things (IoT), and IoT brings together the concepts of "Internet" and "object" in agriculture as well as in industry. Some key features of IoT can explain this process/structure. These; interconnectivity can be expressed as object-related services, heterogeneity from various devices in the IoT, dynamism (change of device state over time), and high scalability (Zambon et al., 2019).

A large amount of data flow occurs with IoT technology, which offers new opportunities to monitor agriculture and food sector processes. Big data collected through both sensors and social media is becoming essential for these industries (Misra et al., 2020).

The connectivity of agricultural machinery, which is one of the supporting elements of digital agriculture, has an important place. Data collection and automation in agriculture through machines connected to the IoT is thought to increase yields and reduce costs for farmers. In Figure 6 (Zambon et al., 2019), Agriculture 4.0 and the virtual object structure are expressed visually (Zambon et al., 2019).

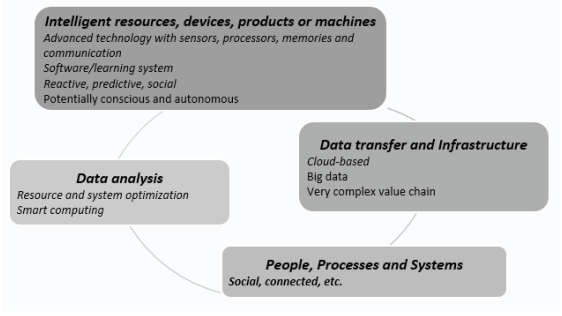

Figure 6. *Agriculture 4.0 and virtual object structure.*

Environmental conditions at different points in a farm can be measured

with IoT-based sensors. Cloud-based platforms can be used to collect and integrate this data. Artificial intelligence algorithms can work in information extraction and prediction. The farm manager can obtain such conditions, instructions, or necessary actions over the internet. All these activities are examples of applications that can be given within IoT-based monitoring and control scope as can be seen in Figure 7 (Misra et al., 2020).

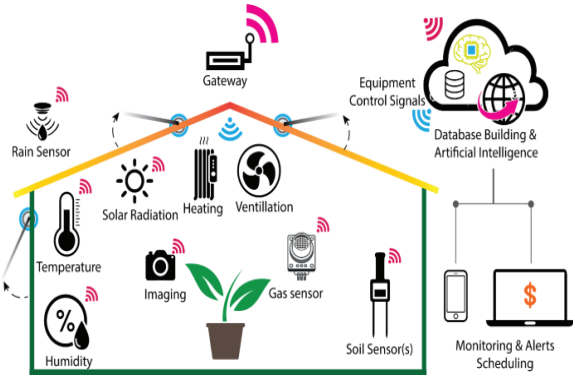

Figure 7. *IoT-based monitoring and control of greenhouse cultivation environments.*

In the greenhouse environment monitored using IoT-based sensors, Misra et al. examined the role of IoT and big data analytics in agriculture, including smart agricultural machinery and drone-based crop monitoring, in social media and supply chain modernization They discussed food quality assessment and food safety.

The data obtained through IoT, which is an important data source, can be used very effectively in many areas with the advantage of having features such as heterogeneity, diversity, redundancy and lack of structure (Korkusuz Polat and Memika, 2023).

3.2. Robotics and Sensor Technology

Robotic farming accelerates the most repetitive tasks, such as harvesting herbs and fruits or packaging. Drones and self-driving tractors enable precision farming models to be put into practice. Robots can calculate the soil and crops' exact condition or connect to satellites to figure out how much water is needed. This information is a valuable resource that allows farmers to reduce chemical inputs, machinery, and water by using information about soil, temperature, humidity, farm equipment, livestock, fertilizers, dirt, and crops planted (Di Vaio et al., 2020)

John Deere, the world's largest agricultural machinery manufacturer, can monitor crop yield, seeding, and planting, humidity, etc., through automatic sensors in the machines it produces. Data is collected. The information is then

fed back to a cloud-based interface and mobile app. Small farmers can use this app to harvest as efficiently as large agricultural conglomerates do (PC, 2017). A schematic representation of the IoT and big data framework in the agri-food sector is shown in Figure 8 (Misra et al., 2020).

3.3. Artificial Intelligence Technologies

One of the aspects that need to be precisely analyzed in the agriculture and food sector is the application of artificial intelligence to the agri-food sector, which combines modern sensory technologies with computer processing capacity. Machine learning and deep learning, computer vision processing, learning-intelligent systems, robots and software robots, natural language processing, etc. Technologies can be said to be the main ones among artificial intelligence technologies that improve agricultural product quality and retail services (Di Vaio et al., 2020).

Device sensors within an IoT network provide large volumes of data constantly flowing into a "data lake" with the help of a local physical server or cloud-based storage (i.e., distributed over the internet worldwide) with appropriate bus and data processing technologies. (Misra et al., 2020)

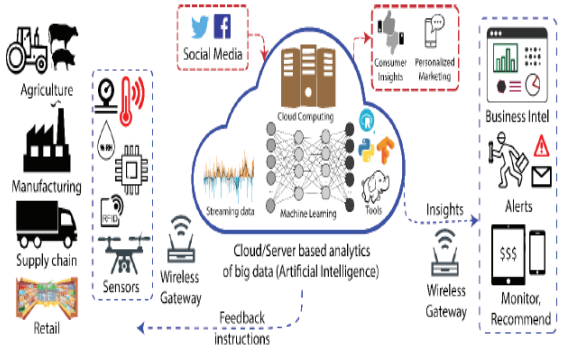

Figure 8. *A schematic representation of the IoT and big data framework in the agri-food sector (Misra et al., 2020)*

The role of artificial intelligence in the food industry is becoming increasingly important due to its ability to help save food, improve the hygiene of production areas and quickly clean more processing equipment. In short, artificial intelligence and machine learning are used in many different regions of the food industry.

Artificial intelligence applications in the food industry can be given under the following headings;

To classify food; Optical sensor-based solutions with machine learning

capabilities are among the most advanced artificial intelligence applications in the food industry. Through cameras and sensors, food is visualized according to the consumer's wishes, so consumers can order according to their preferences, save time and money in production and improve the quality of the product.

For food industry supply optimization; AI can support testing and monitoring food safety products at every stage of the supply chain.

To ensure hygiene standards; Impeccable food and beverage preparation for customers (Di Vaio et al., 2020)

3.4. Machine Learning/Image Processing Technology

One of the most common applications in agriculture, supported by vision sensors and artificial intelligence algorithms, is based on real-time visual maturity detection of products (fruits, vegetables). In this way, the harvesting process ensures the efficiency of these processes and estimates the crop load. Variable lighting conditions and identifying the right fruit in the orchard are essential issues that need to be addressed.

Different types of sensors and their combinations can be used to address these problems and various image processing techniques.

Robotic grippers, machine vision, robot carriers, and control systems developed for harvesting and collecting products without damaging them are among the application examples frequently encountered in the literature. In particular, sensors, robotic technology, and image processing technologies are mentioned intensively in determining the maturity of fruits, harvesting, and collecting them. (De-An et al., 2011; Sa et al., 2016; Yi-Chich CHIU et al., 2013; Baeten et al., 2008; Silwal et al., 2017; Gongal et al., 2015).

3.5. Blockchain Technology and Food Supply Chain

Today, instead of the old approaches in food processing and presentation to the consumer, it has become an essential issue for food safety, both to produce safer food by increasing the consumer's awareness and re-examine and re-present the food legislation of the countries. Food-related health problems, deaths, and potential risks in recent years have created great distrust among consumers and increased the sensitivity of consumers to food safety and quality, especially in developed countries (Kılavuz and Erdem, 2019). Some traditionally record on paper, while others record digitally. This means that all components cannot communicate with each other without interruption. Therefore, the system is limited to traceability capabilities, which are often described as "one step forward and one step back". Combining traceability data by sifting through hundreds or even thousands of documents during a foodborne outbreak can be slow and complex and is often not an effective

way to identify and inform action through lessons learned to prevent future episodes (Yiannas, 2018)

Technology makes it easy to simplify and integrate agricultural supply chains, improve food security, reduce risk in trade finance and promote inclusive trade. It focuses on digital technologies, above all AI and machine learning, Internet of Things (IoT), Cloud, and Blockchain, to realize the traceability of supply chains. Another use of IoT technology in the food industry is virtual IoT-based supply chain applications. The primary purpose here is to minimize the risks in the food supply chains.

Monitoring and verifying the food supply chain to understand reliability is critical to identifying and addressing worldwide disruptions in the food supply chain. The way to solve traceability problems and ensure transparency is to use blockchain technology.

Supply chain actors include the movement of each product in the supply chain, transportation and storage conditions, and all inputs and applications used on the farm (fertilizers, feed, irrigation, veterinary services, etc.). Another important aspect of this technology is that it can monitor every movement in the journey from production to sales for every registered product in the product supply chain. In this way, all consumers can observe the process transparently, risks can be followed, and it is possible to detect problematic products as soon as possible and prevent their consumption or recall them (Tripoli and Schmidhuber, 2018).

In the food industry, real-time monitoring of products during storage and transportation (critical conditions for food such as temperature, humidity, shelf life), traceability to minimize food safety risks, instant information, big data acquisition, and data analytics applications, data security, and the prevention of food hazards; as a result, cloud technology and blockchain applications in this context are essential benefits in the field.

Yiannas (2018) mentions in his study that the food supply chain is not a chain. While there is no doubt that today's food system provides consumers with a more diverse, convenient, and economical food source, it also presents new challenges.

Yiannas' Walmart example can be given as an example in this context. A study conducted by Walmart and IBM to trace sliced mangoes from South and Central America to North America has revealed the potential benefits of blockchain, highlighting the significant gap in current traceability procedures.

Verdouw et al. (2016) discussed the virtualization of the food supply chain via IoT and establishing an information systems architecture to provide defense against supply networks spanning broad geographical areas and global risks. The study states that through the integration of real-time product ob-

servations through IoT devices, supply chain virtualization will enable stakeholders to take immediate action when deviations in processes (for example, temperature fluctuations leading to changes in product quality) are observed.

With the intensive use of technology in agriculture, the increase in innovation in five different areas draws attention;

- Increasing the efficiency of the value chain (Direct delivery to the consumer, meal kits, food e-commerce, etc.).
- Drones, robots, big data and sharing platforms, and irrigation, soil, and crop technologies to increase crop productivity.
- Innovations in agrochemicals, bio-materials, and bioenergy to reduce the ecological footprint.
- Plant-based foods for sustainable protein needs.
- Indoor and vertical farming, Smart greenhouses (USB, 2017)

4. CASE STUDY: SUGAR BEET PRODUCTION

In this section, an application study was carried out with an intelligent approach in the production of sugar beet, which is the raw material of sugar, one of the basic foodstuffs. Before the application, information was given about seasonal workers and why the sugar beet plant was handled.

One of the sectors negatively affected by the global Covid-19 epidemic is agriculture. Many farmers who employ seasonal workers in our country were adversely affected by this process, and the products were left to rot in the fields. Another important disadvantage is that people leave agriculture and migrate to cities. Agricultural autonomous robots are the only solution for farmers who are faced with labor shortages.

During the epidemic, curfews, in particular, led people to buy more food than they needed, agricultural production, and food distribution. Accordingly, the mobility of seasonal farm workers and working and living conditions on a global scale came to the fore. It also showed how vital seasonal migrant farmworkers are in agriculture and the food supply chain (KA-ILO, 2020).

Those working in the sector are of great importance in global and national food supply (UN-LO, 2020). When the workers in the agricultural industry are examined, it is seen that they are employed in three different statuses. These; permanent workers, seasonal workers, and temporary workers. Seasonal workers are employed by the employer at certain times, for certain periods, or periodically during the year, depending on the seasons due to the nature of the work (Temir, 2020). About 5 million people are employed in the agricultural

sector in Turkey. Seasonal migrant agricultural workers, who generally participate in the migration process from the Eastern and Southeastern provinces of Turkey, work at certain times of the year in about 50 regions of Turkey in jobs such as soil preparation, sowing, planting, hoeing, weeding, spraying, irrigation and harvesting. Nuts, tea, fresh vegetables, tomatoes, grapes, pulses, sugar beets, onions, citrus, cotton, etc. They are essential products for seasonal agricultural labor (KA-ILO, 2020). Sugar beet, one of these products, is vital for Turkey in terms of agriculture-based industry. It is a product that has social effects and creates inputs for many sectors and provides vast employment opportunities. About 76% of sugar, one of the most basic foodstuffs, is produced from sugar cane and 24% from sugar beet. In Turkey, sugar is produced entirely from sugar beet and comes after countries such as Russia, France, the USA, and Germany, with approximately 18.9 million tons annual production. Sugar beet, which creates an essential economic added value, is an industrial plant that contributes to Turkey's agriculture and economy. It ranks second in terms of the added value it provides among industrial plants (TEPGE, 2020). In this context, sugar beet harvesting based on digitalization was carried out in the application part of the study. While vegetable harvesting and greenhouse cultivation are carried out actively at any time in Turkey, sugar beet harvest is done at certain times of the year. Sugar beet harvest is very active, especially between September-November and May-June (TEPGE, 2021).

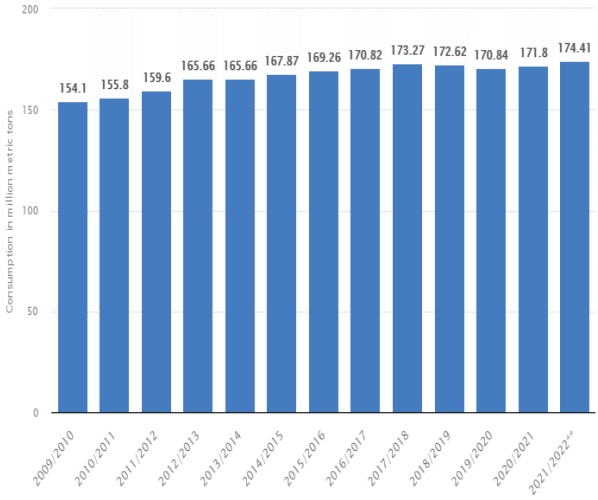

Figure 9. *Total sugar consumption worldwide 2009 to 2021.*

As can be seen from Figure 9 (Statista, 2021), world sugar consumption is increasing every year. In this context, sugar beet, one of the agricultural products with high added value, is of great importance for our country as it is for the whole world. The alternative to sugar beet in sugar production is cane sugar, and approximately 80% of the sugar produced is produced from sugar

cane. Sugar beet-producing countries; can be counted as Ukraine, Russia, Turkey, and European Union countries (TEPGE, 2020). The fact that the geography of our country is not suitable for sugar cane agriculture has highlighted sugar beet in obtaining sugar. Sugar beet is a product that is highly resistant to cold and ideal for continental climates (Koday and Yıldırım, 2021). There are ten starch-based and 33 beet-based sugar producers in our country (TEPGE, 2020; Karabina, 2021).

Table 1. *Turkey Sugar Beet and Sugar Data (thousand tons)*

	2014/15	2015/16	2016/17	2017/18	2018/19	Change (%)[1]
Sugar Beet Planting Area (1000)	2.888	2.742	3.224	3.393	2.921	-13,9
Sugar Beet Yield (kg/da)	5.824	5.837	6.076	6.234	5.969	- 3,9
Sugar Beet Production (ton)	16.743	16.023	19.593	21.149	17.436	-17,6
Sugar Production	2.058	1.976	2.559	2.770	2.273	-17,9
Sugar Consumption	2.040	2.062	2.448	2.349	2.505	6,6
Sugar Stock Change	- 153	- 41	116	424	-405	-195,5
Sugar Import	133	328	311	291	242	-16,8
Sugar Export	273	252	269	251	378	50,6

TUIK (TURKSTAT), [1]/ Data shows the change in the last two years. Market period September-August (TEGPE, 2021).

Table 1 (TEPGE, 2020) shows the sugar beet and sugar data in Turkey between the years 2014-2018. In Turkey, sugar beet farming is carried out in all regions except the Eastern Black Sea, Aegean, Mediterranean coastline, and Southeastern Anatolia Region. According to TUIK data; In 2019, sugar beet was planted on a total of 3.1 million decares in Turkey. Compared to the previous production period, Turkey's sugar beet cultivation areas increased by 7.4% in the 2019/20 production areas. In Turkey's 2019/20 production period, sugar beet production was 18.1 million tons, rising by 3.5% compared to the previous production period. The most important reason for this increase is

considered to be the increase in the number of farmers producing sugar beet and the increase in the production area accordingly. With a population of approximately 83 million, Turkey is a vital sugar consumer. Turkey's total annual sugar and sweetener consumption is around 3 million tons. Beet sugar constitutes 2.7-2.9 million tons of this. According to TUIK data, the total yearly sugar consumption per capita in Turkey in the 2018/19 market period is 30.5 kg (TEPGE, 2020).

Only a few start-up companies worldwide are mainly in the research phase of applications for land and air vehicles that can harvest and communicate with each other. At the same time, there is a need for a data set on the development of agricultural products in our country.

4.1. Case Study Stage#1; Thanks to the OPEN CV Python program, which sugar beets were ripe and ready for harvesting was determined. Thanks to the sugar beet leaf images uploaded to the system, a data set was created, and it was determined whether the product was ripe or not by comparison. Which beet will be collected from which station was determined with the help of crewless aerial vehicles (drone). Figure 10 shows sugar beet leaf images loaded into the system.

4.2.Case Study Stage#2; 0-1 integer programming was used in order to find the optimal picking time of the ripe sugar beets whose locations were determined. In this way, it has been determined whether land vehicles collect sugar beets or not. It has been selected by which land vehicle the beets within the range will be collected. In Turkey, sugar beet is planted at a distance of 45 cm between rows and is generally singled out at a distance of 20-25 cm. 8000 plants in 1 decare give the best results in trials" (UPEK, 2021). Sugar beets were placed in the problem regarding the study titled "Determination of yield and quality characteristics of some sugar beet varieties in ecological conditions" by Şahiner in 2020. While determining the harvest time, the study of Sefaoğlu et al. was taken as a reference (Sefaoğlu et al., 2016).

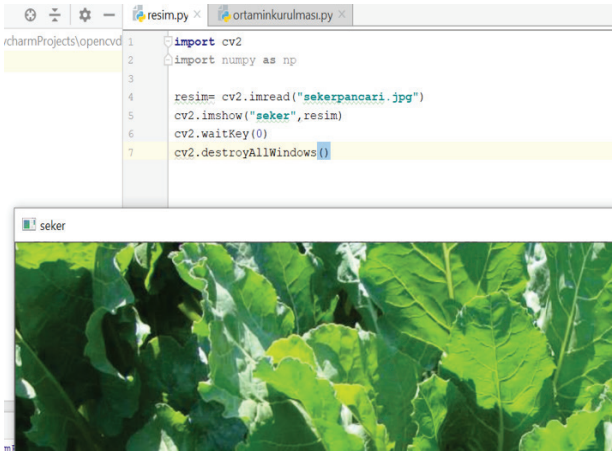

Figure 10. *Sugar beet leaf images uploaded to the system/introducing the image to the system*

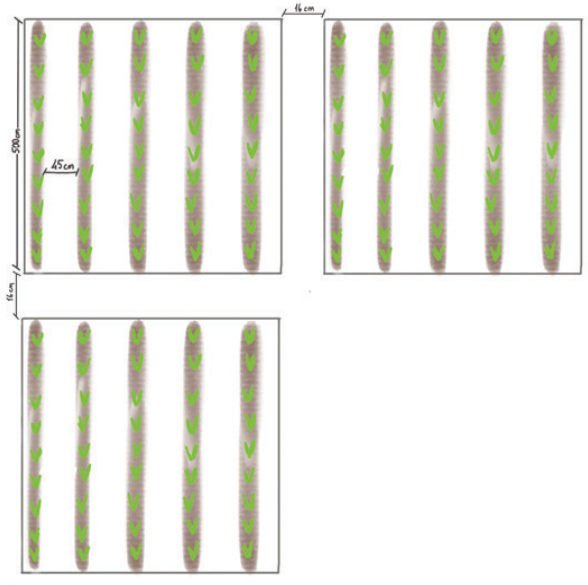

Figure 11. *Ideal dimensions for planting sugar beet.*

In this study, the distance between rows was 45 cm, and between rows was 16 cm. The plots are 5 m long and consist of 5 rows. The study was calculated on 30 parcels, considering three different harvest times for ten other sugar beet species. The sugar beet distributions are as given in Figure 12.

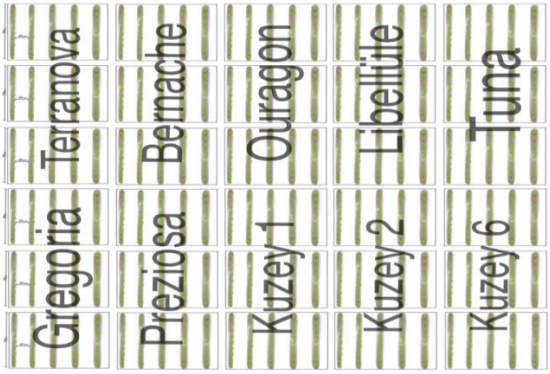

Figure 12. *Sugar beet distributionsTwo different vehicles were assigned for the collection; vehicle 1, Terranova, Gregoria, Bernache, Preziosa, Ouragon, was responsible for beets. Vehicle 2; North 1 was held accountable for Libellüle, North 2, Danube, and North 6. Lingo (LINGO 19.0 - Optimization Modeling Software for Linear, Nonlinear, and Integer Programming) inputs and outputs prepared for Harvest 1 are as given in Figure 13.*

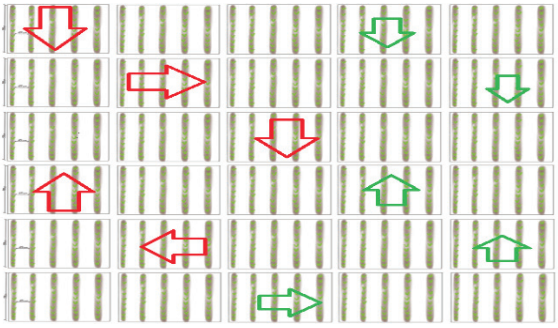

Figure 13. *Lingo inputs and outputs prepared for Harvest 1.*

The areas marked in red show the sugar beets that have come to harvest for Vehicle 1. The areas marked in green show the sugar beets that have come to harvest time for Vehicle 2. The station numbers are given in order from top to bottom. The following Table 2 and 3 have been created by calculating the multiples of 16, taking into account the 16 cm parcel spacing between the stops. For ease of operation, only the coefficient has been taken.

Table 2. *Stops that Vehicle 1 should stop by*

	Stop1 (1)	Stop4 (2)	Stop8 (3)	Stop11 (4)	Stop15 (5)
Stop 1 (1)	0	3	2	5	4
Stop 4 (2)	3	0	3	2	3
Stop 8 (3)	2	3	0	2	2
Stop 11 (4)	5	2	2	0	3
Stop 15 (5)	4	3	2	3	0

Tablo 3. *Stops that Vehicle 2 should stop by*

	Stop 18 (1)	Stop 19 (2)	Stop 22 (3)	Stop 26(4)	Stop 29 (5)
Stop 18 (1)	0	6	3	6	3
Stop 19 (2)	6	0	3	2	5
Stop 22 (3)	3	3	0	4	2
Stop 26(4)	6	2	4	0	3
Stop 29 (5)	3	5	2	3	0

Lingo entries for Vehicle 1;

min=3*x12+2*x13+5*x14+4*x15+3*x21+3*x23+2*x24+3*x25+2*x-31+3*x32+2*x34+2*x35+5*x41+2*x42+2*x43+3*x45+4*x51+3*x-52+2*x53+3*x54;

x21+x31+x41+x51=1;

x12+x13+x14+x15=1;

……..

x51+x52+x53+x54=1;

x12+x21<=1;

x23+x32<=1;

……

x45+x54<=1;

@BIN(x12);

@BIN(x21);

……

@BIN(x25);

……..

@BIN(x54);

Lingo output;

Route: Stop 1 → Stop 8 → Stop 15 → Stop 11 → Stop 4

Similar operations were performed for the other vehicles. Figure 14 and Figure 15 show Lingo inputs and outputs for those.

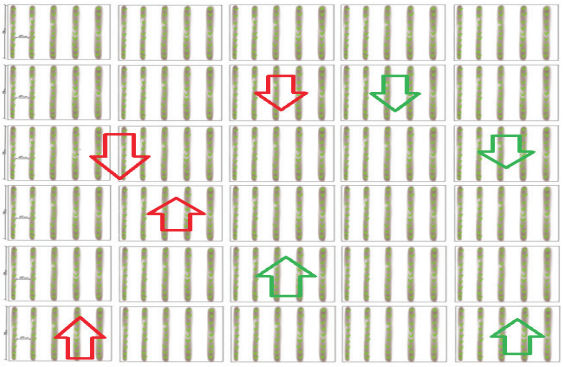

Figure 14. *Lingo inputs and outputs prepared for Harvest 2*

Assumes for the next processes

Assume# 1: It was assumed that different types of sugar beets mature simultaneously in adjacent plots during the 2nd harvest, which reduced the number of stops. The Terranova and Bernache beets in plots 3 and 9 are ready for harvest at the 2nd harvest.

Assume#2: It was assumed that the North 2 sugar beets were not mature at this harvest, which would reduce the number of stalls.

3. Harvest

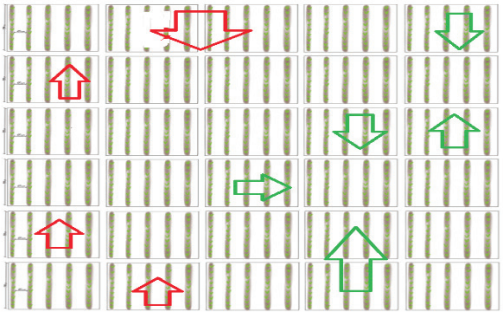

Figure 15. *Lingo inputs and outputs prepared for Harvest 3*

For vehicle 1, the number of stops has decreased as stops 7 and 13 are next.

Table 4 and Table 5 shows vehicle 1 and vehicle 2 stops.

Table 4. *Stops that Vehicle 1 should stop by*

	Stop 2 (1)	Stop 5 (2)	Stop 7,13 (3)	Stop 12 (4)
Stop 2 (1)	0	3	2	5
Stop 5 (2)	3	0	5	2
Stop 7 (3)	2	5	0	5
Stop 12 (4)	5	2	5	0

Route: Stop 7,13 → Stop 12 → Stop 5 → Stop 2

Table 5. *Stops that Vehicle 2 should stop by*

	Stop16 (1)	Stop21 (2)	Stop23,24(3)	Stop25 (4)	Stop28 (5)
Stop 16 (1)	0	2	2	5	2
Stop 21 (2)	2	0	2	3	2
Stop23,24(3)	2	2	0	6	3
Stop 25 (4)	5	3	6	0	3
Stop 28 (5)	2	2	3	3	0

Route: Stop 25→ Stop 21→ Stop 23,24→ Stop16→ Stop28

4.3. Case Study Stage#3-Suggestion: Harvest time of the sugar beets can be collected as a database set. The number of the stall where they were collected, the number of beets at the booth, the collection time of the farthest beet at the stall (min), the time spent at the kiosk, the date of harvest, the amount of precipitation in that period (mm), the highest temperature, the lowest temperature. Average temperature, relative humidity %, a library consisting of sugar beet yield can be created. It is a stage that sheds light on harvest optimization in the following years.

"When the average temperature is lower than ten and the sugar beet yield is more than 1250, which beet species can be grown" and the harvest time can be easily filtered.

4.4.Case Study Stage#4; The Results of the Application

In the study, necessary adaptations were made on the optimal harvesting of sugar beets for 10 different sugar beet species for 3 harvest periods without the need for any seasonal workers.

As a result of the application study, it was seen that the sugar beets with the highest yield in the 2nd harvest were Gregoria, Ouragan, Libellüle, North 6, North 1, and the sugar beets with the highest yield in the 3rd harvest were Terranova, Bernache, Preziosa, North 2, Danube.

In addition, with the application study, it was aimed to establish a database where many questions such as which sugar beet species were grown more efficiently in which harvest period, how it was affected by climatic conditions, how it was affected by the temperature difference.

Considering Turkey in particular, it is among the expected targets to contribute to the digital library describing the development of agricultural products, which is tried to be developed, and to shed light on the optimization of agriculture in the future. Precautions can be taken by predicting how the beet will react to climate changes in future harvests.

This case study has two main expectations: The first is to analyze and record which sugar beet is ripe, thanks to the unmanned aerial vehicle (like drone) image processing technology. The other is to determine the route of two land vehicles with, which is one of the optimization problem solving methods, and to calculate the harvesting times as soon as possible. As a result of the calculations, it was seen that a total of 46.14 seconds for Harvest 1, a total of 41.74 seconds for Harvest 2, and a total of 48.28 seconds for Harvest 3 were sufficient. (While determining the speed of the land vehicle, the semi-autonomous Ropa Tiger 6s on the market was taken as an example. Its speed is 8.4 kilometers per hour.)

After the programming and routing processes results can be summarized in Table 6 and Table 7.

Table6. *Three Harvest results with the two vehicles.*

	1. vehicle	2. vehicle
Harvest 1	19,8 sn	26,34 sn
Harvest 2	22 sn	19,74 sn
Harvest 3	26,34 sn	21,94 sn

Table 7: *Sugar ratios by the harvests.*

Sugar ratio (yield)	Harvest 1	Harvest 2	Harvest 3
Terranova	1059	1264	1290
Gregoria	930	1120	1029
Bernache	949	1135	1136
Preziosa	1063	1171	1173
Ouragan	936	1183	1092
Kuzey 1	968	1034	956
Libellüle	879	1270	1106
Kuzey 2	799	---	1092
Tuna	1055	1287	1323
Kuzey6	891	1270	1118

As a result of the measurements, it was found which sugar beet species was the most productive at which harvest time.

5. EVALUATION

Today, with the effect of the "Industry 4.0" revolution, the agriculture sector has also been affected by the digitalization process in the industrial sector. It is estimated that the countries that do not keep up with the technologies in agriculture will face difficulties in terms of food, especially with the prediction that the demand for food will increase by approximately 70% despite the needs of the rapidly increasing world population. It is thought that countries that cannot follow the technology in the field of food and agriculture will be condemned to buy food from outside.

In order to meet the increasing need for food over time, it has become imperative to approach the agricultural sector more innovatively and professionally. It is seen that the innovations made or being made for the food and agriculture sector have the potential to fundamentally change the usual working style of this sector. It is expected that food safety can be ensured by increasing food supply with innovations in fields such as fertilization and irrigation, and developments in smart applications, robot technologies, genetics and biology will also make positive contributions to the sector by changing consumption habits and working styles.

Smart agriculture is a technique that minimizes the damage to the environment by using the resources at an autopimum level in order to increase the product and soil management with the product and soil management in order to increase the agricultural production. In this context, it is aimed to abandon conventional agriculture and implement an application form that handles the

land with a non-homogeneous variable approach. The main element aimed here is to use the inputs applied in agricultural production at the time, place and amount when needed.

Thanks to digitalization, data obtained with smart tools is analyzed. These smart tools facilitate aquaculture activities by analyzing in detail and in real time, what amount and what kind of fertilizers should be applied to where, weather conditions, minerals needed by plants and irrigation process, soil condition, pest control, estimated harvest time. The aim of these applications; is to maximize agricultural productivity compared to traditional methods.

Traditional farming methods have become inadequate today and providing a sustainable future in agriculture is possible with digital agriculture.

Thanks to digital agriculture;

- Saving labor and time,
- Increasing sensitivity to the environment
- Increase in production quantity and quality,
- Contribution to the economy and
- During the Pandemic, it is aimed to eliminate the labor-related problems experienced in the agriculture and food sector, as in every sector.

REFERENCES

PM-Population Matters 2020/ (populationmatters.org). https://populationmatters.org/population-numbers?gclid=CjwKCAiAt9z-BRBCEiwA_bWv-InxHIKyPiPfm-m1uycsZsNrqnAXCGo0P16WSjbL_FNLr0OYBK2FrxoCnGwQAvD_BwE%20abgerufen (accessed Nov 07, 2021).

Grain 2020/(grain.org). https://www.grain.org/article/entries/5102-food-sovereignty-5-steps-to-cool-the-planet-and-feed-its-people abgerufen (accessed Nov 25, 2021).

Kaya, M. Ağrı'nın Kalkınması İçin Akıllı Tarım (Tarım 4.0) Önerisi, Akademikbakış Dergis. [Online], 2019, 75, 130-156 https://dergipark.org.tr/tr/download/article-file/927557 (accessed Nov 30, 2021).

Kırkaya, A. Akıllı Tarım Teknolojileri Uygulamaları. Gebze Technical University - Hektaş R&D Center [Online] 2020 https://www.researchgate.net/publication/339029285_Akıllı_Tarım_Teknolojılerı_Uygulamaları (accessed Nov 29, 2021).

Korkusuz Polat., T; Baran, E. Classification of Industry 4.0 for Total Quality Management: A Review (2022). Sustainability 2022, 14(6), 3329; https://doi.org/10.3390/su14063329

De Clercq, M.; Vats, A.; Biel, A.; Collaboration Wyman, O. Agriculture 4.0: The Future of Farming Technology, 2018, World Government Summit https://www.oliverwyman.com/content/dam/oliver-wyman/v2/publications/2021/apr/agriculture-4-0-the-future-of-farming-technology.pdf (accessed Nov 22, 2021).

Türkiye'nin endüstri 4.0 Platformu, Kahraman, H., Endüstri 4.0'la Birlikte Gelen Akıllı Tarım http://www.endustri40.com/endustri-4-0la-birlikte-gelen-akilli-tarim/ (accessed Nov 17, 2021).

Doğan, Z.; Arslan, S.; Berkman, A. N. Türkiye'de Tarım Sektörünün İktisadi Gelişimi ve Sorunları: Tarihsel Bir Bakış, Niğde Üniversitesi İİBF Dergisi [Online] 2015, 8(1) 29-41 https://dergipark.org.tr/en/download/article-file/185141 (accessed Nov 10, 2021).

ITB- İzmir Ticaret Borsası, Saygılı, F.; Kaya, A. A.; Tunalı Çalışkan, E.; Erdölek Koza, E. Report; Türk Tarımının Global Entegrasyonu ve Tarım 4.0, 2019 ISBN 978-605-137-710-0). https://itb.org.tr/Duyuru/371-turk-tarimin-global-entegrasyonu-ve-tarim-40 (accessed Sep 10, 2021).

Velten, S.; Leventon, J.; Jager, N.; Newig, J.; What Is Sustainable Agriculture? A Systematic Review Sustainability [Online] 2015, 7, 7833-7865 https://www.mdpi.com/2071-1050/7/6/7833/htm (accessed Sep 01, 2021).

ASDG, Report; The 2030 Agenda And The Sustainable Development Goals: The Challenge For Aquaculture Development And Management, Rome, 24–27 October 2017, Page; 19, ISBN 978-92-5-109928-5 https://www.fao.org/3/i7808e/i7808e.pdf (accessed Sep 07, 2021).

Özgüven, M. M. Tarım Robotlarının Sürdürülebilir Tarıma Katkıları, 3. Uluslararası

ÜNİDOKAP Karadeniz Sempozyumu "Sürdürülebilir Tarım ve Çevre" 21-23 Haziran 2019, ISBN: 978-605-80568-1-7

Pakdemirli, B.; Biricik, N.; Aslan, İ.; Sönmez, B. & Gezici, M. Türk Tarımında Dijital Teknolojilerin Kullanımı ve Tarım-Gıda Zincirinde Tarım 4.0. Toprak Su Dergisi, [Online] 2021, 10 (1), 78-87 https://dergipark.org.tr/tr/pub/topraksu/issue/57793/898774 (accessed Oct 20, 2021).

Duman, B. ve Özsoy, K. Endüstri 4.0 Perspektifinde Akıllı Tarım (Smart Agriculture in Industry 4.0 Perspectıve), 4th International Congress On 3d Printing (Additive Manufacturing) Technologies and Digital Industry, 11-14 Nisan 2019, ISBN: 978-975-96797-3-6

ATP- Akıllı Tarım Platformu, Report; Türkiye'de Akıllı Tarımın Mevcut Durum Raporu 2019, Demirel Atasoy, Z. http://www.tarmakbir.org/haberler/atp/atprapor.pdf (accessed Nov 24, 2021).

Saiz-Rubio, V. and Rovira-Más, F. From Smart Farming towards Agriculture 5.0: A Review on Crop Data Management. Agronomy 10, 2, 2020, 207, 1-21, doi:10.3390/agronomy10020207

Di Vaio, A.; Boccia, F.; Landriani, L. and Palladino. R., Artificial Intelligence in the Agri-Food System: Rethinking Sustainable Business Models in the COVID-19 Scenario, Sustainability, 12, 4851, 2020; doi:10.3390/su12124851

TCKB-T.C. Kalkınma Bakanlığı On Birinci Kalkınma Planı (2019-2023), Report; Tarım ve Gıdada Rekabetçi Üretim, Özel İhtisas Komisyonu Raporu Ankara 2018, https://www.sbb.gov.tr/wp-content/uploads/2020/04/Tarim_ve_Gidada-RekabetciUretimOzelIhtisasKomisyonuRaporu.pdf (accessed Nov 30, 2021).

Marucci, A.; Colantoni, A.; Zambon, I.; Egidi, G. Precision farming in hilly areas: The use of network RTK in GNSS technology. Agriculture 2017, 7, 60. https://www.mdpi.com/search?authors=Marucci&journal=agriculture (accessed Nov 30, 2021).

Zambon, I.; Cecchini, M.; Egidi, G.; Saporito, M. G.; Colantoni, A. Revolution 4.0: Industry vs. Agriculture in a Future Development for SMEs. Processes 2019, 7, 36. https://www.readcube.com/articles/10.3390%2Fpr7010036 (accessed Nov 29, 2021).

Lee, J.; Bagheri, B.; Kao, H.-A. A Cyber-Physical Systems architecture for Industry 4.0-based manufacturing systems. Manuf. Letters. 2015, 3, 18–23. https://www.sciencedirect.com/science/article/pii/S221384631400025X (accessed Nov 25, 2021).

De Janvry, A. and Sadoulet, E. Agricultural Growth and Poverty Reduction. The World Bank Research Observer. World Bank 2009, Volume 25, Issue 1. pp.1-20. https://openknowledge.worldbank.org/bitstream/handle/10986/4432/wbro_25_1_1.pdf?sequence=1&isAllowed=y (accessed Nov 02, 2021).

Kılavuz, E.; Erdem, İ. Agrıculture 4.0 Applications In The World And Transformation of Turkish Agriculture, Social Sciences (NWSASOS), 14 (4): 133-157, Doi:10.12739/NWSA.2019.14.4.3C0189.

Lu, Y. Industry 4.0: A survey on technologies, applications and open research issues. Journal of Industrial Information Integration 2017, 6, 1–10. https://www.sciencedirect.com/science/article/pii/S2452414X17300043 (accessed Oct 29, 2021).

Misra, N. N.; Dixit, Y.; Al-Mallahi, A.; Bhullar, M. S. ; Upadhyay, R; Martynenko, A. IoT, big data and artificial intelligence in agriculture and food industry. , IEEE Internet of Things Journal. 2020, pp 99: 1-1. https://ieeexplore.ieee.org/document/9103523 (accessed Oct 27, 2021).

Korkusuz Polat, T.; Memika, T., Internet of Things upported Airport Boarding System and Evaluation with Fuzzy. Intelligent Automation & Soft Computing. 2023, *35*(3), 2687-2702. https://doi.org/10.32604/iasc.2023.026955

PC-PCMag, How to Build a Business-Ready Internet of Things: Use Cases. Marvin, R. 2017, https://in.pcmag.com/feature/113349/how-to-build-a-business-ready-internet-of-things-use-cases (accessed Oct 27, 2021).

De-An, Z.; Jidong, L.; Wei, J.; Ying, Z.; Yu, C. Design and control of an apple harvesting robot, Biosystems Engineering, Volume 110, Issue 2, 2011, Pages 112-122. https://doi.org/10.1016/j.biosystemseng.2011.07.005 (accessed Oct 07, 2021).

Sa, I.; Ge, Z.; Dayoub, F.; Upcroft, B; Perez, T.; McCool, C. DeepFruits: A Fruit Detection System Using Deep Neural Networks. Sensors. 2016; 16 (8):1222. https://doi.org/10.3390/s16081222

Yi, C. C.; Suming, C.; Jia, F. L. Study of an Autonomous Fruit Picking Robot System in Greenhouses, Engineering in Agriculture, Environment and Food, Volume 6, Issue 3, 2013, Pages 92-98. https://doi.org/10.1016/S1881-8366(13)80017-1

Baeten, J.; Donné, K.; Boedrij, S.; Beckers, W.; Claesen, E. Autonomous fruit picking machine: A robotic apple harvester. 6th International Conference on Field and Service Robotics - FSR 2007, Jul 2007, Chamonix, France. ffinria-00194739f. https://hal.inria.fr/file/index/docid/194739/filename/fsr_21.pdf (accessed Nov 29, 2021).

Silwal, A.; Davidson, J. R; Karkee, M.; Mo, C.; Zhang, Q.; Lewis, K. Design, integration, and field evaluation of a robotic apple harvester. Journal of Field Robotics, vol. 34, no. 6, pp. 1140-1159, 2017. Doi: 10.1002/rob.21715.

Gongal, A.; Amatya, S.; Karkee, M.; Zhang, Q.; Lewis, K. Sensors and systems for fruit detection and localization: A review. Computers and Electronics in Agriculture Volume 116, August 2015, Pages 8-19. https://www.sciencedirect.com/science/article/pii/S0168169915001581 (accessed Nov 29, 2021).

Yiannas, F. A New Era of Food Transparency Powered by Blockchain, Innovations/Blockchain for Global Development, 12, issue 1-2, 2018, p. 46-56. https://direct.mit.edu/journals/search-results?page=1&q=A%20New%20Era%20of%20Food%20Transparency%20Powered%20by%20Blockchain%2C%20Innovations%2FBlockchain%20for%20Global%20Development&fl_SiteI-

D=1000001&allJournals=1 (accessed Nov 29, 2021).

Tripoli, M. And Schmidhuber, J. Emerging Opportunities for the Application of Blockchain in the Agri-food Industry. FAO and ICTSD: Rome and Geneva. Licence: CC BY-NC-SA 3. https://www.fao.org/3/ca1335en/CA1335EN.pdf (accessed Nov 09, 2021).

Verdouw, C. N.; Wolfert, J.; Beulens, A. J. M.; and Rialland, A. Virtualization of food supply chains with the internet of things. *Journal of Food Engineering,* vol. 176, pp. 128-136, 2016. https://www.researchgate.net/publication/285549643_Virtualization_of_food_supply_chains_with_the_internet_of_things (accessed Nov 09, 2021).

USB-University of Stellenbosch Business School, Synthesis report-2017; The future of the Western Cape agricultural sector in the context of the Fourth Industrial Revolution. https://bpcwpdev02.belpark.sun.ac.za/wp-content/uploads/2018/07/THE-FUTURE-OF-THE-WC-AGRICULTURAL-SECTOR-IN-THE-CONTEXT-OF-4IR-FINAL-REP.pdf (accessed Nov 17, 2021)

KA-ILO-Kalkınma Atölyesi-Uluslararası Çalışma Örgütü Türkiye Ofisi. Zırh, B. C.; Karakılıç, İ. Z.; Çetinkaya, Ö.; Ayaeş, S.; Özsoy, A. and Karabıyık, E. Report; Korona Virüs Salgınının Mevsimlik Gezici Tarım İşçileri ve Onların Çocukları ile Bitkisel Üretime Olası Etkisi 2020. https://www.ilo.org/wcmsp5/groups/public/---europe/---ro-geneva/---ilo-ankara/documents/publication/wcms_743368.pdf (accessed Nov 17, 2021)

UN-LO, United Nations, Labor Organization. Policy Brief: The World of Work and COVID-19, 2020. https://www.un.org/sites/un2.un.org/files/the_world_of_work_and_covid-19.pdf (accessed Nov 09, 2021).

Temir, M. Özel Hukuk Anabilim Dalı; Türk İş ve Sosyal Güvenlik Hukukunda Tarımda Çalışanlar. Yüksek Lisans Tezi, T.C. Ankara Üniversitesi Sosyal Bilimler Enstitüsü, Ankara, 2020.

TEPGE-Tarım ve Orman Bakanlığı Tarımsal Ekonomi ve Politika Geliştirme Enstitüsü. Şentürk, Ö. Ürün Raporu-Şeker Pancarı, 2020. https://arastirma.tarimorman.gov.tr/tepge/Belgeler/PDF%20%C3%9Cr%C3%BCn%20Raporlar%C4%B1/2020%20%C3%9Cr%C3%BCn%20Raporlar%C4%B1/%C5%9Eeker%20Pancar%C4%B1%20%C3%9Cr%C3%BCn%20Raporu%202020-328%20TEPGE.pdf (accessed Oct 09, 2021).

TEGPE-Tarımsal Ekonomi ve Politika Geliştirme Enstitüsü. Tarım Ürünleri Piyasaları- Şeker Pancar, Ocak 2021. https://arastirma.tarimorman.gov.tr/tepge/Belgeler/PDF%20Tar%C4%B1m%20%C3%9Cr%C3%BCnleri%20Piyasalar%C4%B1/2021-Ocak%20Tar%C4%B1m%20%C3%9Cr%C3%BCnleri%20Raporu/%C5%9Eeker%20Pancar%C4%B1,%20Ocak-2021,%20Tar%C4%B1m%20%C3%9Cr%C3%BCnleri%20Piyasa%20Raporu%20Haz%C4%B1r.pdf (accessed Oct 09, 2021).

Statista-Statista.com. Total sugar consumption worldwide from 2009/2010 to 2020/2021 (in million metric tons), Published by M. Shahbandeh, May 27, 2021. https://www.statista.com/statistics/249681/total-consumption-of-su-

gar-worldwide/ (accessed Oct 29, 2021).

Koday, Z. and Yıldırım, K. Erzurum ve Çevresinde Şeker Pancarı Tarımı ve Şeker Sanayi. Doğu Esintileri, Sayı 15, 121 - 147, 2021. https://dergipark.org.tr/tr/download/article-file/1851613 (accessed Oct 02, 2021).

Karabina, K. Report Name: Sugar Annual, Date: April 16, 2021, Report Number: TU2021-0020, https://apps.fas.usda.gov/newgainapi/api/Report/DownloadReportByFileName?fileName=Sugar%20Annual_Ankara_Turkey_04-15-2021.pdf (accessed Oct 02, 2021).

UPEK- S.S. Uşak Pancar Ekicileri Kooperatifi. http://usakpancar.com.tr/#bi%CC%87lgi%CC%87%20bankasi%20/Kooperatif/Sayfa/1033 (accessed Oct 02, 2021).

Şahiner, A. And Demir, İ. Kırşehir Ekolojik Koşullarında Bazı Şeker Pancarı Çeşitlerinin Verim ve Kalite Özelliklerinin Belirlenmesi. Manas Journal of Agriculture Veterinary and Life Sciences Cilt 10, Sayı 2, 71 - 75, 28.12.2020. https://dergipark.org.tr/tr/pub/mjavl/issue/58569/808606 (accessed Oct 02, 2021).

Sefaoğlu, F.; Kaya, C. & Karakuş, A. Farklı Tarihlerde Hasat Edilen Şeker Pancarı Genotiplerinin Verim ve Verim Unsurlarının Belirlenmesi. Tarla Bitkileri Araştırma Enstitüsü Dergisi Cilt 25, Sayı ÖZEL SAYI-2, 61-66, 31.12.2016. https://dergipark.org.tr/tr/pub/tarbitderg/issue/26737/281846 (accessed Oct 02, 2021).

LINGO 19.0-Optimization Modeling Software for Linear, Nonlinear, and Integer Programming

OPEN CV Python program

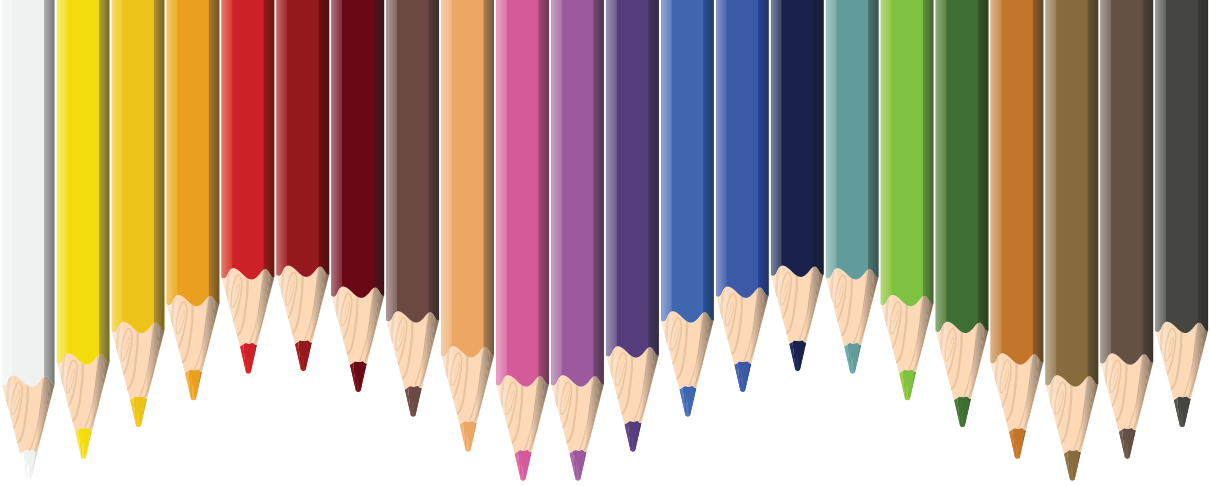

Chapter 17

BRAIN-COMPUTER INTERFACE SYSTEM WITH THE MOST COST-EFFECTIVE EEG DEVICE

***Mesut MELEK*[1]**

1 Gümüşhane University, Electronics and Automation Department, Gumushane / Turkey, e-mail: mesutmelek@gumushane.edu.tr, Orcid No: 0000-0002-7152-7788

I. Introduction

Nowadays, technological devices are an integral part of our lives and even play a vital role in many places. An electroencephalography (EEG) signal is produced by the electrical activity of hundreds of millions of neurons in the brain. This signal contains much information about brain activity and is a voltage-type signal that changes over time [1]–[4] . The brain is also a very important and mysterious organ of the human body, and for this reason, its research value is always high. EEG signals are used in many areas [5]. Additionally, various studies are available to facilitate its application in clinical studies and practical use. In most of these invasive techniques, electrodes are placed around the skull. The disadvantage of this is that the signals are read through the thick bone of the skull and therefore the signals are attenuated [6]. The amplitude of raw electrical data obtained with these methods is measured in microvolts (uV). The EEG device consists of several electrodes that are placed on the scalp according to a certain standard and record the electrical activity occurring in different parts of the brain. The sampling frequency of these devices varies between 128-1024 Hz. Researchers are working in depth to reduce the cost of these devices. In addition to cost, the comfort of these devices is also an important issue [7].

One of the most popular areas of using EEG is in noninvasive brain-computer interface (BCI) systems [8] [9]. EEG-based noninvasive BCI technology is a method of human-computer interaction. Human beings can communicate with their environment independently of their peripheral nerves and muscle tissues, that is, interaction between the human brain and computers or other peripheral devices can occur, and thus they can control the environment without using any muscles.

When we look at the usage areas of BCI systems, it seems that they serve many areas. Emotion detection, digital marketing, customer surveys, etc. It opens a new era of progress by being used in many areas such as. The brain's response and neural activity to colors, design, texture, and other customer-focused features have been studied in depth. On the other hand, a product can now be designed and released later. When all of these come together, it is predicted that a revolution will be created in the mentioned areas. It is currently being used, albeit in a small way, as an important mechanism in the renewal of commercial lie detection solutions, and efforts are ongoing to make such applications accessible to everyone soon [10].

The first reason for the emergence of BCI systems, that is, helping disabled people, has also provided great benefits in the field of health. For example, BCI systems designed for people with paralysis related to motor functions, interactive platforms for people with severe motor dysfunction, controllable wheelchairs based on EEG signals, and BCI systems based on Visual Evoked

Potential (VEP) signals can be listed. BCI also has great potential for reliable monitoring of a person's mental state, classification of stress, and studying patients suffering from post-traumatic experiences, depression, and anxiety, or in a qualitative study of their rehabilitation during motor functions.

BCI systems are currently the only promising means of communication between two people without any special physical movement [11]. Although these systems were introduced a long time ago, they are not yet offered to users actively and reliably, and the work is still ongoing. Even though technology has come so far today, users still control a smartphone or a computer using their muscles [12]. The real reason why BCI technology cannot market its segment is the difficulties and differences in real-world problems. For this, existing approaches and methods should be reviewed and it is very important to test new ideas and methodologies. The aim is to do things by thinking only. In conclusion, BCI systems deserve to be a complex and important part of the human body.

The realization of BCI systems is thanks to artificial intelligence. Artificial intelligence and machine learning have made great strides in the last few years, realizing many events that were once the subject of science fiction movies. Artificial intelligence has not only affected the work of researchers. By extending from researchers' laboratories to the real life of human beings, artificial intelligence has tremendously made human life much easier and greatly improved the quality of life [13] [14].

Researchers working on BCI systems, after passing the obtained EEG signals through pre-processing stages such as filtering and normalization, extract the signal features in time and frequency space and then classify them. The ultimate goal, as mentioned, is to bring about the desired change in the user's environment. It is quite common to use Fourier transform (FT) based methods for feature extraction. Machine learning methods such as support vector machine (SVM) [15] and artificial neural networks [16] are widely used as classification methods. Of course, in recent years, deep learning methods have affected BCI systems, as in all areas.

In this study, two different problems each one having two classes were addressed by using classical machine learning methods. For this, the Mindbigdata dataset [17] was used. In this dataset, candidates were asked to think of numbers between 0-9, thus a 10-class dataset was obtained. Then, the subjects were asked to think about different things, and in this way, the 11th class was recorded. this class is labeled -1. This experiment was conducted with four different cost-effective EEG devices. In this study, signals recorded with the MindWave (MW) headset [18], known as the most cost-effective device with a single electrode, were discussed. In the first step, classes 0 and 1 were classified with 30 different classifiers, and in the second step, all numbers

were classified against class -1. For this, the recorded two-second signal was first passed through a 4th-degree Butterworth filter, and the basic 5 frequency bands of the EEG signal were reached with wavelet transform. Then, features were obtained from each frequency band with 7 different statistical methods and were classified.

The rest of the study will be as follows: Section 2 describes the material and method. In this section, the dataset used in the study and the steps in machine learning will be presented in detail. The results obtained will be given in Section 3. The best methods will be discussed by measuring the results of the methods used with different metrics. Finally, the conclusion will be given in the last section, that is section 4.

II. Materıals and methods

a) Dataset

An 11-class EEG signal was recorded in the Mindbigdata [17] dataset, which was last updated in January 2023. In this dataset, candidates were asked to look at digits 0-9 separately and think about them. This time is approximately 2 seconds for all digits. The procedures were repeated with 4 different cost-effective EEG devices. The list of these devices and the number of signals obtained separately for each digit from each device are given in Table 1. As can be seen in the Table, EEG devices with electrode arrays arranged according to the standard 10-20 system were used to collect the data set. These devices are NeuroSky MindWave, Emotiv EPOC, Interaxon Muse, and Emotiv Insight. The signals obtained are raw signals and have not been subjected to any preprocessing. Additionally, signals are not separated as train and test sets. As seen in the table, one of the classes is labeled with the number –1. Signals of this class are random actions that are not related to thinking or seeing numbers.

This study discussed signals recorded with the MindWave (MW) device, known as the single-electrode and most cost-effective EEG device. The distribution of signals in this device is given in Table 2. MindWave is a cost-effective EEG device with a single electrode and a sampling frequency of 512 Hz. This device, which costs around $130 [18], records on the FP1 channel. The location of this channel is shown in Figure 1.

Tablo 1. Distribution of the signals per device and digit

Device/Digit	0	1	2	3	4	5	6	7	8	9	-1	Total
MindWave (MW)	5,531	5,498	5,517	5,416	5,381	5,568	5,476	5,552	5,545	5,450	12,701	67,635
EPOC (EP)	91,224	88,914	90,930	92,652	88,886	91,994	91,322	88,718	91,728	91,882	2,226	910,476
Muse (MU)	11,904	11,632	11,920	11,832	11,536	12,052	12,368	12,080	12,208	11,988	44,412	163,932
Insight (IN)*	6,305	6,740	6,535	6,605	6,620	6,460	6,425	6,470	6,590	6,500	0	65,250

Tablo 2. Distribution of the signals per digit in MW headset

Digit	0	1	2	3	4	5	6	7	8	9	-1	Total
number of signals	5.531	5.498	5.517	5.416	5.381	5.568	5.476	5.552	5.545	5.450	12.701	67.635

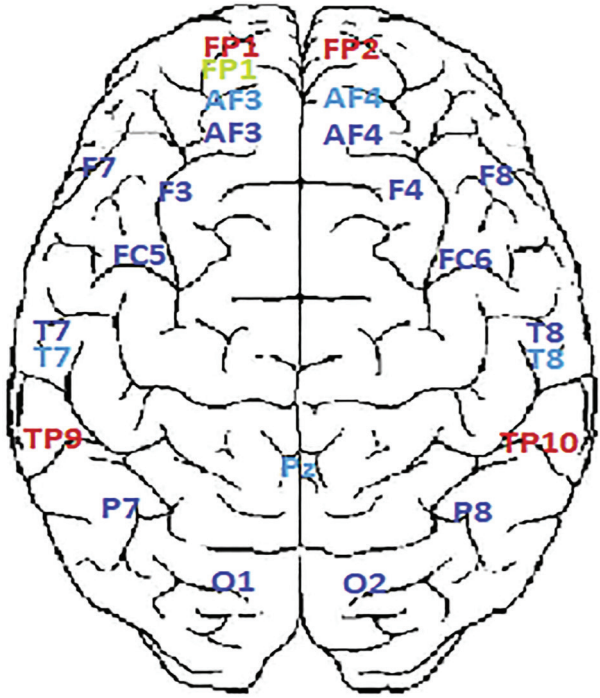

Figure 1. Channel locations [19]

b) Wavelet transform

Many of the signals in our lives are not static, that is, the properties of the signals change over time and do not remain constant. Time-frequency analysis is widely used to notice how a signal changes over any time interval, in other words, it is used to localize events. The traditional way of time-frequency analysis is the Short-Time Fourier Transform (STFT). For this, the Fourier transform of the signal is taken over short windows, and the spectrogram graph is obtained. STFT has limitations in resolutions due to Heisenberg's uncertainty principle. Improvement in time resolution leads to poorer frequency resolution and vice versa, improvement in frequency resolution leads to poorer time resolution. To avoid this problem, wavelet transform takes advantage of the property of low-frequency signals to spread over time and high-frequency bursts occurring in short intervals [20].

The wavelet transform has a wavelet and makes use of variable window sizes. Wavelet analysis is generally applied in two ways: Continuous Wavelet Transform (CWT) and Discrete Wavelet Transform (DWT). DWT is one of the frequently used methods in EEG signals and especially in BCI systems.

DWT decomposes the signal into two;

1- average or low pass signal using a scaling function

2- difference or high pass signal using wavelet function [20]

Conventional DWT repeatedly decomposes the low pass signal to the desired decomposition level with the same scaling and wavelet functions, so that the desired frequency range can be easily reached. The traditional frequency bands in the EEG signal are as follows; theta (0-4), delta (4-8), alpha (8-12), beta (12-30), and gamma (30-50) [21]. To reach these frequency bands and since the sampling frequency of the signals in this study was specified as 512 Hz, DWT decomposition was performed 7 times in this study.

c) Comprehensive performance measure; normalized area of general polygon (NAoGP)

There are many parameters such as accuracy rate, sensitivity, specificity, and kappa value to evaluate the performance of classification systems. However, many times, a system cannot show superiority over other systems in all parameters. In other words, while the system reaches higher values in a few parameters, it lags behind the other system in a few other parameters, thus making comparisons between two or more systems impossible. To eliminate this problem, we proposed the NAoGP value in our previous work [22] [23] The NAoGP value summarizes all parameters obtained for any classification system into a single value. In this study, 3 parameters were calculated to make comparisons between classifiers; These are accuracy rate, specificity, and sensitivity parameters. To calculate the NAoGP value, we created a triangle and summarized these three parameters into a single value.

III. Results

As mentioned, a classification process was performed on the Mindbigdata dataset in this study. In this data set, signals recorded with the Mindwave EEG device at a frequency of 512 Hz were considered. The subjects were asked to look at and think about the numbers 0-9. Then, they were asked to perform other operations, and an 11-class data set was prepared. The length of the signals is 2 seconds. In the first stage of this study, signals were classified by looking only at the numbers 0 and 1. Signals were passed through a 4th-order

Butterworth filter and 7-stage DWT was applied. 8 different statistical values were obtained from five EEG bands. These are mean, variance, skewness, kurtosis, Wavelet entropy based on Shannon, mean of power spectrum density, root mean square, and Trapezoidal numerical integration. Thus, a total of 40 features were obtained from each 2-second signal. Then, these features were classified with 30 different classifiers. As mentioned, the sensitivity, specificity, and accuracy rate as well as the NAoGP value were calculated for each classifier. These results are given in Table 3. In addition, for easier comparison of the results, the accuracy rates and NAoGP values are presented graphically in Figure 2. Sensitivity shows the ratio of the number of correctly detected samples in class 0 to the total number and specificity is the ratio of the number of correctly detected samples to the total number in class 1.

As seen, Classifier 19, namely Ensemble boosted tree, has the highest accuracy rate compared to other classifiers with an accuracy rate of 51.70. Considering the responses of the systems to the classes, that is, sensitivity and specificity, the NAoGP value of this classifier is also higher than other systems. When looking at the accuracy rate, the second successful system is the 23rd Classifier, that is Ensemble RUSboosted trees with 51.60. However, the NAoGP value shows the second successful system is Logistic regression.

Tablo 3. Classification results of class 0 and class 1

Order	Classifier	Sensitivity%	Specificity%	ACC%	NAoGP
1	Tree fine tree	44.00	57.80	50.90	0.2575
2	Tree medium tree	42.00	61.00	51.50	0.2622
3	Tree course tree	44.40	58.60	51.50	0.2635
4	Logistic regression	54.70	48.20	51.50	0.2645
5	Naïve bayes gaussian	87.80	13.00	50.50	0.2077
6	Naïve bayes kernel	65.00	36.40	50.80	0.2506
7	Svm-linear	57.20	45.00	51.10	0.2599
8	Svm-quadratic	53.20	47.80	50.50	0.2548
9	Svm-cubic	38.00	60.00	50.50	0.2410
10	Svm-fine gaussian	39.30	62.80	51.00	0.2558
11	Svm-medium gaussian	53.40	47.60	50.50	0.2547
12	Svm-coarse gaussian	60.50	41.50	51.10	0.2574
13	Knn-fine knn	50.90	50.10	50.50	0.2550
14	Knn-Medium knn	64.80	35.90	50.40	0.2467
15	Knn-course knn	59.60	39.40	49.60	0.2420
16	Knn-cosine knn	64.60	37.60	51.10	0.2550
17	Knn-cubic knn	65.10	36.70	51.00	0.2527
18	Knn-whited knn	52.30	48.60	50.50	0.2546
19	Ensemble-boosted tree	52.10	51.30	51.70	0.2673
20	Ensemble-bagged tree	57.00	43.30	50.20	0.2501

21	Ensemble-subspace discriminant	56.60	45.70	51.20	0.2608
22	Ensemble-subspace knn	54.40	44.70	49.60	0.2449
23	Ensemble-RUSboosted trees	42.20	61.10	51.60	0.2636
24	Neural-network narrow	52.00	48.30	50.10	0.2512
25	Neural-network medium	51.30	49.10	50.20	0.2520
26	Neural-network wide	50.00	51.00	49.50	0.2517
27	Neural-network biyalered	50.10	50.40	50.30	0.2527
28	Neural-network trailered	50.20	50.10	50.20	0.2517
29	Kernal-svm kernel	54.20	47.50	50.80	0.2580
30	Kernal-logistic regression Kernel	51.50	48.40	50.00	0.2496

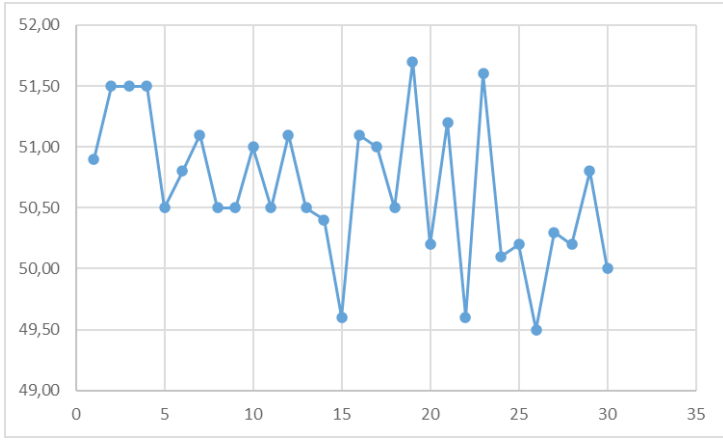

(a)

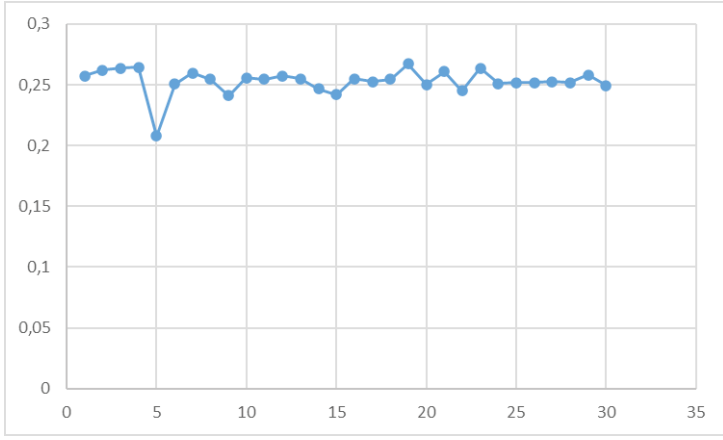

(b)

Figure 2. (a) Accuracy rate of 30 different classifiers, (b) NAoGP value of 30 different classifiers

In the second stage, all digits were classified against other thought (-1 class) signals. The accuracy rates of the classifiers are given in Table 4 in decreasing order. As it turns out, the most successful system, in terms of accuracy, is the Neural network-Narrow classifier. Although the accuracy rate of this system is 97.40, the NAoGP value is lower than Neural network-biased and Neural network-trialered, and according to this value, these two systems are the most successful. Also, for easier comparison of the results, the accuracy rates and NAoGP values are presented graphically in Figure 3. Sensitivity shows the ratio of the number of correctly detected samples in class -1 to the total number and specificity is the ratio of the number of correctly detected samples to the total number in class 0-9.

Table 4. Classification results of class 0-9 versus class -1

Order	Classifier	Sensitivity%	Specificity%	ACC%	NAoGP
1	Neural-network narrow	92.20	98.50	97.40	0.9219
2	Neural-network biyalered	92.50	98.40	97.30	0.9226
3	Neural-network trailered	92.50	98.40	97.30	0.9226
4	Neural-network medium	92.00	98.20	97.10	0.9168
5	Svm-quadratic	88.60	98.60	96.80	0.8952
6	Neural-network wide	90.10	98.00	96.50	0.8994
7	Svm-medium gaussian	84.70	98.80	96.10	0.8668
8	Ensemble-bagged tree	86.90	98.00	95.90	0.8749
9	Ensemble-boosted tree	85.40	97.70	95.40	0.8604
10	Logistic-regression	83.90	98.10	95.40	0.8531
11	Svm-coarse gaussian	81.10	98.50	95.20	0.8362
12	Svm-linear	82.50	98.20	95.20	0.8435
13	Tree-fine tree	83.10	97.00	94.40	0.8354
14	Knn-Medium knn	78.80	97.70	94.20	0.8108
15	Knn-whited knn	77.00	98.10	94.20	0.8016
16	Knn-cosine knn	83.60	96.50	94.10	0.8338
17	Ensemble-subspace discriminant	77.10	97.70	93.80	0.7976
18	Tree-medium tree	78.90	97.30	93.80	0.8068
19	Ensemble-RUSboosted tree	90.60	94.60	93.80	0.8648
20	Knn-course knn	73.20	98.40	93.60	0.7755
21	Knn-cubic knn	76.00	97.60	93.60	0.7889
22	Tree-course tree	71.20	97.30	92.40	0.7499
23	Knn-fine knn	76.40	95.80	92.20	0.7732
24	Ensemble-subspace knn	61.20	95.00	88.60	0.6551
25	Naïve-bayes gaussian	70.70	92.80	88.60	0.7016
26	Svm-cubic	89.10	88.30	88.50	0.7856
27	Naïve-bayes kernel	89.50	86.00	86.70	0.7638
28	Kernal-svm kernel	42.90	94.40	84.70	0.5226
29	Kernal-logistic regression kernel	42.50	94.30	84.50	0.5189
30	Svm-fine gaussian	4.00	100.00	82.00	0.2976

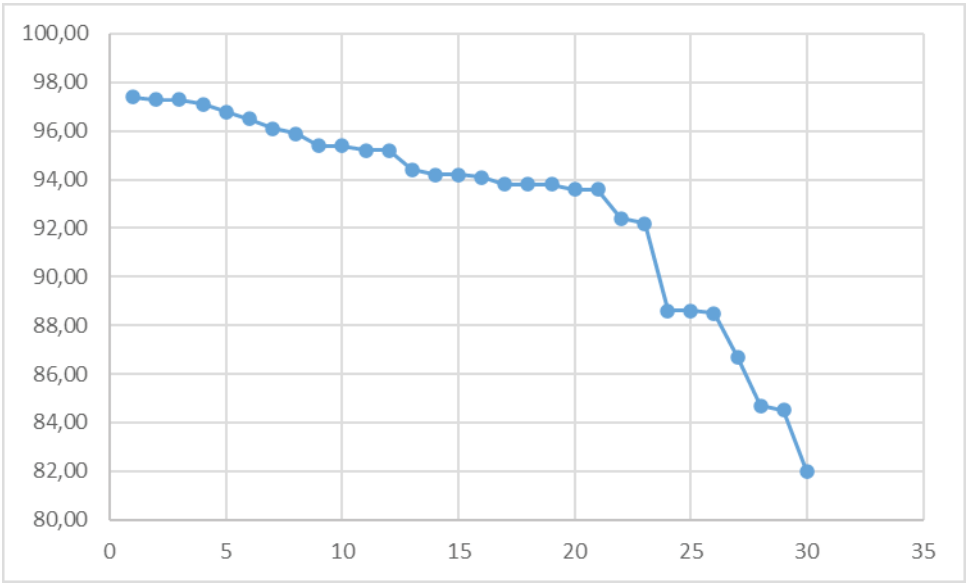

(a)

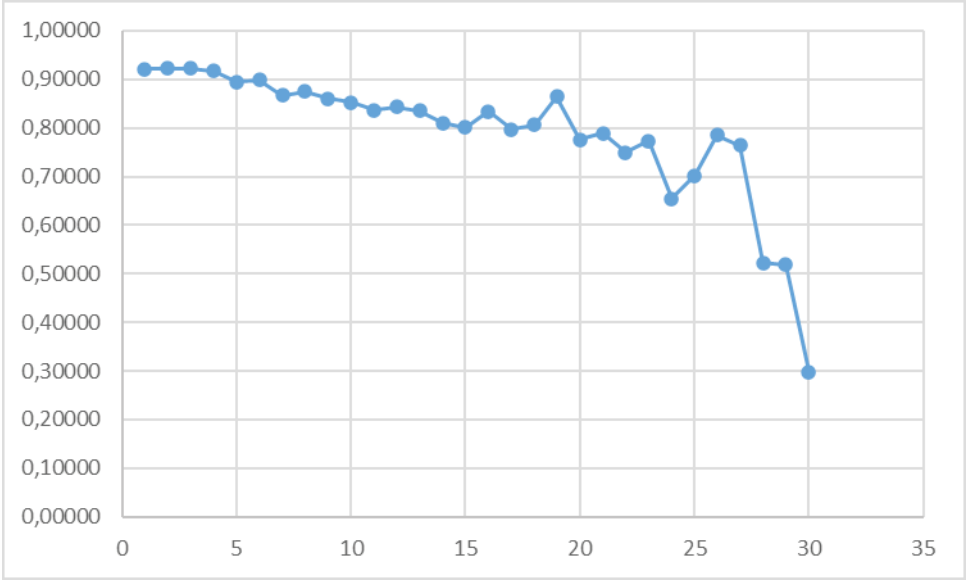

(b)

Figure 3. (a) Accuracy rate of 30 different classifiers, (b) NAoGP value of 30 different classifiers

IV. Conclusion

Many important studies have been carried out on BCI systems so far. These systems have been studied for years, but BCI systems face major problems in the implementation phase (Moore, 2003). These systems are used only in training and meditation during the application phase and are limited to these two areas. One of the reasons for this is that the affordable EEG device manufacturers mentioned earlier only promote these devices for use in meditation. The reason for this is that EEG signal classification studies are limited to a small number of classes and the majority of them belong to the binary classification problem, and also the results obtained from EEG classification are based on completely different stimuli [19].

BCI systems are taking the first steps in their development. The purpose of these systems is to restore the lost function of the disabled person and compensate for disconnections in the nervous system by creating an electronic "neural bypass"[24] [25]. Although these systems originally emerged to restore the functional wrist and finger movement of a paralyzed person, today they seem essential to serve as a part of the human body in many areas. These systems already promise to provide numerous benefits to their users in various daily applications with smart technology, telepresence, medical advances, neuroeconomics and smart environment, education and self-regulation, security, and authentication.

In the presented study, a BCI system based solely on thought and without any triggering (Visual evoked potential (VEP)) was presented. As mentioned, user comfort is very important in these systems. Studies have shown that much faster and more accurate systems are available. However, since most of these studies use VEP, they cause the user to suffer from eye diseases after a while. For this reason, it is very important to expand BCI systems based solely on thought, such as the presented study.

V. References

[1] X. Chai, Q. Wang, Y. Zhao, X. Liu, O. Bai, and Y. Li, "Unsupervised domain adaptation techniques based on auto-encoder for non-stationary EEG-based emotion recognition," *Comput Biol Med*, vol. 79, pp. 205–214, Dec. 2016, doi: 10.1016/J.COMPBIOMED.2016.10.019.

[2] Y. Shin, S. Lee, M. Ahn, H. Cho, S. C. Jun, and H. N. Lee, "Noise robustness analysis of sparse representation based classification method for non-stationary EEG signal classification," *Biomed Signal Process Control*, vol. 21, pp. 8–18, Aug. 2015, doi: 10.1016/J.BSPC.2015.05.007.

[3] S. Pattnaik, M. Dash, and S. K. Sabut, "DWT-based feature extraction and classification for motor imaginary EEG signals," *2016 International Conference on Systems in Medicine and Biology, ICSMB 2016*, pp. 186–201, Apr. 2017, doi: 10.1109/ICSMB.2016.7915118.

[4] M. Soleymani, S. Asghari-Esfeden, Y. Fu, and M. Pantic, "Analysis of EEG Signals and Facial Expressions for Continuous Emotion Detection," *IEEE Trans Affect Comput*, vol. 7, no. 1, pp. 17–28, Jan. 2016, doi: 10.1109/TAFFC.2015.2436926.

[5] Negin MELEK, "Comparison of EEG and EOG signals in classification of sleep stages," *Pamukkale Univ Muh Bilim Derg. 2*, vol. 29, no. 6, pp. 607–616, 2023.

[6] B. A. Taheri, R. T. Knight, and R. L. Smith, "A dry electrode for EEG recording," *Electroencephalogr Clin Neurophysiol*, vol. 90, no. 5, pp. 376–383, May 1994, doi: 10.1016/0013-4694(94)90053-1.

[7] M. Maleki, N. Manshouri, and T. Kayikcioglu, "Brain-computer Interface Systems for Smart Homes - A Review Study," *Recent Advances in Electrical & Electronic Engineering (Formerly Recent Patents on Electrical & Electronic Engineering)*, vol. 14, no. 2, pp. 144–155, Jul. 2020, doi: 10.2174/2352096513999200727175948.

[8] D. Wu, J. T. King, C. H. Chuang, C. T. Lin, and T. P. Jung, "Spatial Filtering for EEG-Based Regression Problems in Brain-Computer Interface (BCI)," *IEEE Transactions on Fuzzy Systems*, vol. 26, no. 2, pp. 771–781, Apr. 2018, doi: 10.1109/TFUZZ.2017.2688423.

[9] Z. Jin, G. Zhou, D. Gao, and Y. Zhang, "EEG classification using sparse Bayesian extreme learning machine for brain–computer interface," *Neural Comput Appl*, vol. 32, no. 11, pp. 6601–6609, Jun. 2020, doi: 10.1007/S00521-018-3735-3/FIGURES/4.

[10] J. P. Rosenfeld, M. Soskins, G. Bosh, and A. Ryan, "Simple, effective countermeasures to P300-based tests of detection of concealed information," *Psychophysiology*, vol. 41, no. 2, pp. 205–219, Mar. 2004, doi: 10.1111/J.1469-8986.2004.00158.X.

[11] H. Si-Mohammed *et al.*, "Towards BCI-Based Interfaces for Augmented Reality: Feasibility, Design and Evaluation," *IEEE Trans Vis Comput Graph*, vol.

26, no. 3, pp. 1608–1621, Mar. 2020, doi: 10.1109/TVCG.2018.2873737.

[12] C. Guger, G. Edlinger, W. Harkam, I. Niedermayer, and G. Pfurtscheller, "How many people are able to operate an EEG-based brain-computer interface (BCI)?," *IEEE Transactions on Neural Systems and Rehabilitation Engineering*, vol. 11, no. 2, pp. 145–147, Jun. 2003, doi: 10.1109/TNSRE.2003.814481.

[13] C. Bhargava and P. K. Sharma, "Statistical and intelligent reliability analysis of multi-layer ceramic capacitor for ground mobile applications using Taguchi's approach," *International Journal of Quality and Reliability Management*, vol. 39, no. 10, pp. 2273–2285, Nov. 2022, doi: 10.1108/IJQRM-09-2020-0316/FULL/PDF.

[14] P. Narayanan *et al.*, "Analysis and design of fuzzy-based manoeuvring model for mid-vehicle collision avoidance system," *J Ambient Intell Humaniz Comput*, vol. 12, no. 10, pp. 9909–9922, Oct. 2021, doi: 10.1007/S12652-020-02737-X/TABLES/9.

[15] N. Manshouri and T. Kayikcioglu, "A Comprehensive Analysis of 2D&3D Video Watching of EEG Signals by Increasing PLSR and SVM Classification Results," *Comput J*, vol. 63, no. 3, pp. 425–434, Mar. 2020, doi: 10.1093/COMJNL/BXZ043.

[16] Y. Gu, Z. Liang, and S. Hagihira, "Use of Multiple EEG Features and Artificial Neural Network to Monitor the Depth of Anesthesia," *Sensors (Basel)*, vol. 19, no. 11, Jun. 2019, doi: 10.3390/S19112499.

[17] D. Vivancos and F. Cuesta, "MindBigData 2022 A Large Dataset of Brain Signals," Dec. 2022, Accessed: Dec. 20, 2023. [Online]. Available: https://arxiv.org/abs/2212.14746v1

[18] "MindWave." Accessed: Dec. 20, 2023. [Online]. Available: https://store.neurosky.com/pages/mindwave

[19] A. Shankhdhar, P. K. Verma, P. Agrawal, V. Madaan, and C. Gupta, "Quality analysis for reliable complex multiclass neuroscience signal classification via electroencephalography," *International Journal of Quality and Reliability Management*, vol. 39, no. 7, pp. 1676–1703, Jul. 2022, doi: 10.1108/IJQRM-07-2021-0237/FULL/PDF.

[20] N. Bajaj and N. Bajaj, "Wavelets for EEG Analysis," *Wavelet Theory*, Nov. 2020, doi: 10.5772/INTECHOPEN.94398.

[21] N. Manshouri, M. Maleki, and T. Kayikcioglu, "An EEG-based stereoscopic research of the PSD differences in pre and post 2D&3D movies watching," *Biomed Signal Process Control*, vol. 55, p. 101642, Jan. 2020, doi: 10.1016/J.BSPC.2019.101642.

[22] M. Melek, N. Manshouri, and T. Kayikcioglu, "An automatic EEG-based sleep staging system with introducing NAoSP and NAoGP as new metrics for sleep staging systems," *Cogn Neurodyn*, vol. 15, no. 3, pp. 405–423, Jun. 2021, doi: 10.1007/S11571-020-09641-2/TABLES/22.

[23] M. Melek and N. Melek, “Roza: a new and comprehensive metric for evaluating classification systems,” *Comput Methods Biomech Biomed Engin*, vol. 25, no. 9, pp. 1015–1027, 2022, doi: 10.1080/10255842.2021.1995721.

[24] G. Sharma, N. Annetta, D. A. Friedenberg, and M. Bockbrader, “Advances in BCI: A Neural Bypass Technology to Reconnect the Brain to the Body,” pp. 9–20, 2017, doi: 10.1007/978-3-319-64373-1_2.

[25] P. K. Sharma, C. Bhargava, and K. Kotecha, “Sustainability Analysis of a ZnO-NaCl-Based Capacitor Using Accelerated Life Testing and an Intelligent Modeling Approach,” *Sustainability 2021, Vol. 13, Page 10736*, vol. 13, no. 19, p. 10736, Sep. 2021, doi: 10.3390/SU131910736.